



A DFT STUDY OF VITAMIN B₁₂ DERIVATIVES

BY

POOMANI PENNY GOVENDER

Student Number: 407701

Thesis in fulfillment of the requirement for the degree

DOCTOR OF PHILOSOPHY

in

CHEMISTRY

in the

FACULTY OF SCIENCE

of the

UNIVERSITY OF THE WITWATERSRAND

Supervisor : Prof HM Marques
Co-Supervisor : Dr CB Perry

DECLARATION

I hereby declare that this thesis, which I herewith submit for the research qualification

DOCTOR OF PHILOSOPHY

to the University of the Witwatersrand, School of Chemistry, is, apart from the recognised assistance of my supervisors, my own work and has not previously been submitted by me to another institution to obtain a research diploma or degree.

_____ on this ____ day of _____
(Candidate)

_____ on this ____ day of _____
(Supervisor)

_____ on this ____ day of _____
(Co-supervisor)

DEDICATION

To my parents for their overwhelming guidance in spirit and prayer.

To my dogs, Macgyver and Kodie, who had their walks sacrificed on many occasions
because I needed dedicated time to complete my studies.

ACKNOWLEDGEMENTS

I extend a sincere thanks to the following people who assisted me during this study:

My academic supervisors, Professor H.M. Marques and Dr C.B. Perry for their excellent advice and guidance.

My line manager, Professor B.B. Mamba, for ensuring me time off to complete my studies as soon as possible and for offering encouragement and advice at all times.

Professor R.W.M. Krause (now at Rhodes University) for his encouragement, and for making a financial contribution from the Nanoscience Centre towards purchasing extra hardware for the Wits cluster.

Dr I. Navizet, postdoctoral fellow in the School of Chemistry at the University of the Witwatersrand, who offered words of encouragement, advice on my project, showed me how to perform and interpret TD-DFT calculations, proofread Chapter 2 and guided me on Chapter 9.

Professor D. Joubert, from the School of Physics at the University of the Witwatersrand, who proofread and offered suggestions on Chapter 2.

My parents, who always phoned and offered words of encouragement and overwhelming support.

Aunt Silvie, who despite fighting her own battles, always made the effort to phone and offer her support and advice.

I would also like to extend thanks for the following:

Financial support from the NRF-Thuthuka program and the URC-University of Johannesburg.

The Centre of High Performance Computing (CHPC) for the unlimited use of their clusters and technical assistance throughout this study.

ABSTRACT

Density functional theory (DFT) and time dependent-DFT (TD-DFT) was applied to investigate the geometric and electronic properties of cobalamin (Cbl) models. Model compounds of the type, $[B-(Co(III)(L)_4-X)-Y]^{n+}$ were used, where B and Y were comprised of the alpha (α) and β axial ligands, $(L)_4$ represented the equatorial ligand(s) and X was either hydrogen or a substituent of electron donating or withdrawing character, quantified by the Hammett constant (σ_p), at C₁₀ of the corrin. All calculations were conducted in the gas phase or implicit solvent medium at the BP86/6-31+G(d,p) level of theory. High-resolution crystal structures of B₁₂, extracted from the Cambridge Crystal Structural Database (CCSD), were used as the source of initial coordinates.

DFT was used to explore the *trans* influence of the lower (α) axial ligand, the *cis* influence of various equatorial ligands and the *cis* influence of a substituted corrin ring at the C₁₀ position on the Gibbs free energy (ΔG) and bond dissociation energies (BDEs) of the Co(III)–C _{β} bond. Other geometric parameters such as ring distortion, axial bond lengths, equatorial bond lengths and partial charges on the Co metal centre, donor atom of the upper and lower axial ligands as well as the N-donor atoms of the macrocyclic ring are documented and discussed.

The use of a broad range of alpha (α) ligands in the cobalamin models from charged and neutral N-donor ligands (NH₃, NH₂⁻, NH²⁻, NH₂F, NHF⁻, NF²⁻, NH₂CH₃, NHCH₃, NH(CH₃)₂, N(CH₃)₃), to naturally occurring amino acids or realistic models of their metal-coordinating side chains (methanethiol, dimethylsulfide, cysteine, methanethiolate, glycine, *p*-aminopyridine, imidazole, histidine, acetate, 2-propanol, serine and tyrosine), provided significant information on the *trans* influence of these ligands on the BDE of the Co(III)–C bond (upper axial ligand). The ligands NH₃, NH₂⁻, NH²⁻, NH₂F, NHF⁻, NF²⁻, NH₂CH₃, NHCH₃, were used to explore electronic

effects while NH_3 , NH_2CH_3 , $\text{NH}(\text{CH}_3)_2$, and $\text{N}(\text{CH}_3)_3$ were used to investigate steric effects. The naturally occurring amino acids or their models focused primarily on exploring why nature chooses an N-donor ligand such as histidine or imidazole instead of an S-donor or O-donor ligand that is also readily available from protein side chains.

As the basicity of the α ligand increased in the series $\text{NH}_2\text{F} < \text{NH}_3 < \text{CH}_3\text{NH}_2 < (\text{CH}_3)_2\text{NH} < (\text{CH}_3)_3\text{N} < \text{NH}\text{F}^- < \text{NHCH}_3^- < \text{NH}_2^- < \text{NF}^{2-} < \text{NH}^{2-}$ (as assessed by the proton affinities) a normal *trans* influence was observed between the axial ligands. While the Co(III)–C bond was observed to increase in length, the Co(III)– N_α bond length decreased. The weakening of the Co(III)–C bond was paralleled by the decrease in the Co(III)–C BDE.

On the other hand, as the steric bulk of the α ligand (NH_3 , NH_2CH_3 , $\text{NH}(\text{CH}_3)_2$, and $\text{N}(\text{CH}_3)_3$) increased (assessed by the molar volume and Tolman cone angle), an inverse *trans* influence (in other words, simultaneous lengthening or shortening) between the upper and lower axial bonds was observed. The Co(III)–C bond showed a marginal increase in length while the Co(III)– N_α bond length steadily increased as the molar volume of the α ligand increased. Interestingly, the large difference in the Co– N_α bond length from the 5-coordinate to the 6-coordinate complex (later referred to as $\Delta\text{Co–N}_{\alpha(5c-6c)}$), paralleled the decrease of the Co(III)–C BDEs.

It also became evident from calculations with the amino acids posing as α ligands that the nature of the α ligand (assessed by the absolute chemical hardness (η) of the ligand, with the greater the η value the harder the ligand) plays a major role in the labilisation of the organometallic bond. As the η of the α ligand increased, the Co(III)–C BDE increased. The *trans* influence of the α ligands resulted in the strengthening (hard ligand) and weakening (soft ligand) of the Co(III)–C bond, as was affirmed by the electron density at the bond critical point (bcp) of the Co(III)–C bond. The N-donor ligands (described as having an intermediate character as the η -

values were between the hard and soft ligands) were found to be catalytically suitable (31.89 – 32.45 kcal mol⁻¹), rather than the soft and hard donor ligands. The *trans* influence of the latter two ligands on the upper axial bond revealed a weakly and strongly bound alkyl group to the Co metal centre, giving Co(III)–C BDEs values of 29.39–32.27 kcal mol⁻¹ and 32.54–34.96 kcal mol⁻¹, respectively.

In addition to the corrin macrocycle, other equatorial ligands like cobaloxime, corrole, porphyrin, methylcobalt(III) pentaamine, [14-ane]N₄, [15-ane]N₄ and [16-ane]N₄ were used in calculations to explore the *cis* influence on the labilisation of the Co(III)–C bond. These ligands included saturated and unsaturated cyclic rings. The results showed that the flexibility of the ring increased as the size of the equatorial ligand increased and thus affected the displacement of the Co(III) metal centre from the defined mean plane. This subsequently affected the strength of the organometallic bond, which paralleled the BDEs.

The hydrogen atom at C₁₀ of the corrin ring was substituted by electron donating (CH₃, OH and NH₂) or –withdrawing groups (NO, NO₂, CN, COOH and Br) and the *cis* influence of these groups on the organometallic bond was investigated. A normal *trans* influence between the axial ligands was observed. As the electron density from the substituents increased towards the ring, the Co(III)–C bond strengthened and the Co(III)–N_α bond weakened. The increased electron density from the C₁₀ substituents influenced the contraction of the Co–N_α bond length. The greater difference in contraction of the Co–N_α bond length from the 5-coordinate to the 6-coordinate complex ($\Delta\text{Co-N}_{\alpha(5c-6c)}$) resulted in lower Co(III)–C BDEs.

The TD-DFT method was used to generate both the absorption and circular dichroism (CD) spectra where the vertical electronic excited states of Co(III) cobalamin species that differ with respect to their upper axial ligand, including FCbl, ClCbl, BrCbl, SeCNCbl and CH₃Cbl were calculated. The *cis* influence for each of the species was analysed within the framework of TD-DFT to assign the major spectral

features, in other words, the α/β , D/E and γ bands in the predicted UV-visible spectra. These studies reveal that the “typical” and “atypical” absorption exhibit a high degree of σ -donation from the β -ligand to the Co(III) metal centre and the subsequent destabilisation of the corresponding d-orbitals of Co. Furthermore, as the donor ability of the β ligand increased, the contributions from the antibonding d_z^2 orbital to the HOMO increased, leading to a strong Co(III)–N $_{\alpha}$ σ -antibonding interaction, which is consistent with the observed lengthening of the same bond from FCbl, ClCbl, BrCbl, SeCNCbl to CH₃Cbl.

TABLE OF CONTENTS

<u>Section</u>	<u>Page</u>
Declaration	i
Dedication	ii
Acknowledgements	iii
Abstract	v
Table of Contents	ix
List of Tables	xiii
List of Figures	xviii
List of Abbreviations	xxvi
CHAPTER 1: INTRODUCTION	- 1 -
1.1 Background.....	- 1 -
1.2 Vitamin B ₁₂	- 2 -
1.3 Objectives of the study.....	- 6 -
CHAPTER 2: THEORETICAL TOOLS FOR BIOINORGANIC SYSTEMS	- 9 -
2.1. Computational Methods.....	- 9 -
2.1.1 Molecular Mechanics.....	- 9 -
2.1.2 Quantum Mechanical (QM) Methods.....	- 10 -
2.1.2.1 Ab Initio Methods.....	- 12 -
2.1.2.2 Semi-Empirical Method.....	- 19 -
2.1.3 Density Functional Theory	- 20 -

2.1.4	TD-DFT	- 39 -
2.1.5	Current Study.....	- 39 -
CHAPTER 3: LITERATURE REVIEW		- 41 -
3.1	Steric and Electronic Effects.....	- 41 -
3.2	Bond Dissociation Energies	- 47 -
3.3	Structural and Electronic Properties of the Co–Corrin Macrocycle	- 58 -
3.4	A Free Coenzyme Complex versus a Coenzyme Complex Embedded in Protein.....	- 59 -
3.5	Is DFT the Answer?	- 60 -
3.6	The Truhlar Group Functionals	- 60 -
3.6.1	Meta-GGA Exchange Functional	- 62 -
3.6.2	Meta-GGA Correlation Functional.....	- 63 -
3.6.3	Hybrid Meta Functional.....	- 64 -
3.7	Summary	- 66 -
CHAPTER 4: COMPUTATIONAL DETAILS		- 69 -
4.1	Software	- 69 -
4.1.1	Gaussian 09 Computer Program.....	- 69 -
4.1.2	Gaussview 5.0.8.....	- 70 -
4.1.3	AIMALL(version 10.05.04 and 12.06.03 professional)	- 70 -
4.1.4	ChemCraft.....	- 70 -
4.2	Hardware.....	- 70 -
CHAPTER 5: INFLUENCE OF THE ALPHA LIGAND: PART 1		- 72 -
5.1	Introduction.....	- 72 -
5.2	Model Structures	- 75 -
5.3	Results and Discussion	- 80 -
5.3.1	Relaxed Conditions.....	- 80 -

5.3.2	Restricted Conditions.....	- 120 -
5.4	Conclusion	- 137 -

**CHAPTER 6: TRANS INFLUENCE OF THE ALPHA LIGAND:
PART 2 - 139 -**

6.1	Introduction.....	- 139 -
6.2	Model Structures	- 142 -
6.3	Method	- 144 -
6.4	Results and Discussion	- 144 -
6.5	Conclusion	- 163 -

**CHAPTER 7: CIS INFLUENCE: THE EFFECT OF THE EQUATORIAL
MACROCYCLE - 165 -**

7.1	Introduction.....	- 165 -
7.2	Model Structures and Method	- 167 -
7.3	Gas Phase: Results and Discussion.....	- 169 -
7.4	Solution Phase: Universal Solvation Model	- 187 -
7.4.1	Solvent Phase: Results and Discussion	- 188 -
7.5	Conclusions.....	- 210 -

**CHAPTER 8: CIS INFLUENCE: SUBSTITUTION ON CORRIN'S
C₁₀ - 212 -**

8.1	Introduction.....	- 212 -
8.2	Model Structures and Method.....	- 216 -
8.3	Results and Discussion	- 218 -
8.4	Conclusions.....	- 229 -

CHAPTER 9:	AN INVESTIGATION INTO THE CIS INFLUENCE IN COBALT CORRIN MODELS, $[\text{NH}_3\text{-(Co(III)(CORRIN))}\text{-R}]^{\text{n+}}$, WHERE R = F, Cl, Br, SECN OR CH₃ BY DFT AND TD-DFT STUDIES	- 231 -
9.1	Introduction.....	- 231 -
9.2	Model Structures	- 235 -
9.3	Method	- 237 -
9.4	Results and Discussion	- 237 -
9.5	Conclusions.....	- 257 -
CHAPTER 10:	OVERALL CONCLUSIONS	- 258 -
APPENDIX 1:	DATA FOR CHAPTER 2	- 264 -
APPENDIX 2:	DATA FOR CHAPTER 5	- 265 -
APPENDIX 3:	DATA FOR CHAPTER 6	- 271 -
APPENDIX 4:	DATA FOR CHAPTER 7	- 272 -
APPENDIX 5:	DATA FOR CHAPTER 8	- 284 -
APPENDIX 6:	DATA FOR CHAPTER 9	- 286 -
REFERENCES		- 287 -

LIST OF TABLES

Table 2.1:	Zeta values	- 15 -
Table 4.1:	Hardware parameters	- 71 -
Table 5.1A:	Geometric parameters, ΔG and BDE for homolysis of the Co(III)–C $_{\beta}$ bond in models A, B and D.....	- 81 -
Table 5.1B:	Geometric parameters, ΔG and BDE for homolysis of the Co(III)–C $_{\beta}$ bond in model C	- 82 -
Table 5.1C:	α ligands used to explore electronic and steric effects in model C.....	- 82 -
Table 5.2:	BP86/Corrin:- Topological properties of the electron density (ρ) at the bcp (au) of Co(III)–CH $_3$, Co(III)–N $_{\alpha}$ and Co(II)–N $_{\alpha}$	- 85 -
Table 5.3:	Mulliken and APT partial charges (e) for the corrin model C.....	- 87 -
Table 5.4:	Torsion angles of cobaloxime, corrole, corrin and porphyrin.....	- 101 -
Table 5.5A:	Mulliken and APT charges (e) for model complexes A – D ...	- 103 -
Table 5.5B:	NBO and BADER charges (e) for model complexes A – D ...	- 104 -
Table 5.6:	Bond lengths (\AA) for N $_{\text{eq}}$ donors in the Co(III) models.....	- 110 -
Table 5.7A:	Topological properties of the electron density (ρ) at the bcp (au) of Co(III)–CH $_3$ and Co(III)–NH $_3$ in the [NX $_3$ –(Co(III)(L) $_4$)–CH $_3$] $^{n+}$ model with (L) $_4$ = cobaloxime and corrole.....	- 117 -
Table 5.7B:	Topological properties of the electron density (ρ) at the bcp (au) of Co(III)–CH $_3$ and Co(III)–NH $_3$ in the [NX $_3$ –(Co(III)(L) $_4$)–CH $_3$] $^{n+}$ model with (L) $_4$ = corrin and porphyrin.....	- 118 -

Table 5.8:	Geometric parameters, ΔG and BDE for the homolysis of the Co(III)–C $_{\beta}$ bond in cobaloxime.....	122 -
Table 5.9:	Geometric parameters, ΔG and BDE for the homolysis of the Co(III)–C $_{\beta}$ bond in corrole.....	123 -
Table 5.10:	Geometric parameters, ΔG and BDE for the homolysis of the Co(III)–C $_{\beta}$ bond in corrin.....	124 -
Table 5.11:	Geometric parameters, ΔG and BDE for the homolysis of the Co(III)–C $_{\beta}$ bond in porphyrin.....	125 -
Table 5.12A:	Mulliken and APT partial charges (e) for the corrin model	130 -
Table 5.12B:	NBO and Bader partial charges (e) for the corrin model.....	131 -
Table 5.13A:	Topological properties of the electron density (ρ) at the bcp of Co(III)–CH $_3$ for the corrin complex.....	133 -
Table 5.13B:	Topological properties of the electron density (ρ) at the bcp of Co(III)–NH $_3$ for the corrin complex.....	134 -
Table 5.14:	Torsion and N $_{\alpha}$ –Co(III)–C $_{\beta}$ ($^{\circ}$) angles for the corrin model at the restricted Co(III)–N $_{\alpha}$ bond length of 1.9 Å	135 -
Table 6.1:	Geometric parameters for corrin BP86/6-31+G(d,p) with a change in the types of α -ligands	145 -
Table 6.2:	Topological properties of the electron density (ρ) (au) at the bcp of Co(III)–CH $_3$, Co(III)–B $_{\alpha}$ and Co(II)–B $_{\alpha}$ for model complexes A – M with soft, hard and intermediate (interm.) ligands.....	146 -
Table 6.3A:	Mulliken and APT partial charges (e) for model complexes A – M.....	147 -
Table 6.3B:	NBO and Bader partial charges (e) for model complexes A – M.....	148 -
Table 7.1A:	BP86 and M06L:-Energies (kcal mol $^{-1}$) and geometric parameters for models A – H.....	171 -
Table 7.1B:	B3LYP and PBE1PBE:-Energies (kcal mol $^{-1}$) and geometric parameters for models A – H.....	172 -

Table 7.2A:	BP86:- Topological properties of the electron density at the bcp of Co(III)–CH ₃ and Co(III)–NH ₃ for model complexes A – H	179 -
Table 7.2B:	M06L: Topological properties of the electron density at the bcp of Co(III)–CH ₃ and Co(III)–NH ₃ for model complexes A – H	180 -
Table 7.2C:	Summary of factors that may influence the Co(III)–C _β BDEs.....	180 -
Table 7.3:	APT, NBO and Bader partial charges for models A – H for BP86 and M06L.....	183 -
Table 7.4:	Solvent relative permittivity(ε) values.....	187 -
Table 7.5:	BP86:Co(III)–C _β ΔG and BDE (kcal mol ⁻¹)for models A – H in gas and solution phase	189 -
Table 7.6:	BP86: Geometric parameters for models A – H in gas and solution phase	190 -
Table 7.7:	BP86: ΔΔG _{solv} for models A – H in various solvents.....	193 -
Table 7.8:	BP86: BDE _{solv} for models A – H in gas phase and various solvents	194 -
Table 7.9:	Average N _{eq} –Co–C _β bond angles (°) and Co(III)–C _β BDEs (kcal mol ⁻¹) for models A – D in both gas and solution phase	198 -
Table 7.10:	Average N _{eq} –Co–C _β bond angles (°), average angle of ring distortion (ω _{avg} /°) and Co(III)–C _β BDEs (kcal mol ⁻¹)for models A – D in both gas and solution phase.....	199 -
Table 8.1:	Hammett substituent constant (σ _p) values	213 -
Table 8.2:	Geometric parameters and ΔG and BDEs for the homolysis of the Co(III)–C _β bond.....	219 -
Table 8.3:	NBO partial charges of atoms in the model complex, [NH ₃ –(Co(III)(corrin-X))–CH ₃] ⁺	225 -

Table 8.4:	Topological properties of the electron density of the Co(III)–C _β and Co(III)–N _α bonds- 226 -
Table 9.1:	TD-BP86 vertical electronic excitation energies (E), the corresponding oscillator strengths (f), and description of dominant configurations for the [Im–(Co(III)(corrin))–Cl] ⁺ complex.....- 241 -
Table 9.2:	TD-BP86 vertical electronic excitation energies (E), the corresponding oscillator strengths (f), and description of dominant configurations for the [Im–(Co(III)(corrin))–Br] ⁺ complex.....- 242 -
Table 9.3:	TD-BP86 vertical electronic excitation energies (E), the corresponding oscillator strengths (f), and description of dominant configurations for the [Im–[Co(III)(corrin)]–F ⁺] complex.....- 245 -
Table 9.5:	TD-BP86 vertical electronic excitation energies (E), the corresponding oscillator strengths (f), and description of dominant configurations for the Im–[Co(III)(corrin)]–CH ₃ ⁺ complex- 256 -
Table A2.1:	Torsion angles (°) for Cobaloxime- 266 -
Table A2.2:	Torsion angles (°) for Corrole.....- 266 -
Table A2.3:	Torsion angles (°) for Corrin- 267 -
Table A2.4:	Torsion angles (°) for Porphyrin.....- 267 -
Table A2.5:	Mulliken and APT partial charges (e) for cobaloxime at restricted Co–N _α bond lengths.....- 268 -
Table A2.6:	Mulliken and APT partial charges (e) for corrole at restricted Co–N _α bond lengths.....- 269 -
Table A2.7:	Mulliken and APT partial charges (e) for porphyrin at restricted Co–N _α bond lengths.....- 270 -
Table A3.1:	IP and EA values in kcal mol ⁻¹- 271 -
Table A4.1:	BP86 Thermochemical data for gas phase.....- 272 -

Table A4.2:	M06L Thermochemical data for gas phase	272 -
Table A4.3:	B3LYP Thermochemical data for gas phase	273 -
Table A4.4:	PBE1PBE Thermochemical data for gas phase.....	273 -
Table A4.5(A):	M06L: ΔG and BDE of Co(III)-C $_{\beta}$ bonds for models A – H in gas and solution phase	274 -
Table A4.5(B):	M06L: Geometrical parameters for models A – H in gas and solution phase.....	275 -
Table A4.6(A):	B3LYP: ΔG and BDE for Co(III)-C $_{\beta}$ bonds in models A – H in gas and solution phase	276 -
Table A4.6(B):	B3LYP: Geometrical parameters for models A – H in gas and solution phase.....	277 -
Table A4.7(A):	PBE1PBE: ΔG and BDE for Co(III)-C $_{\beta}$ bonds in models A – H in gas and solution phase	278 -
Table A4.7(B):	PBE1PBE: Geometrical parameters for models A – H in gas and solution phase	279 -
Table A4.8:	$\Delta\Delta G_{\text{solv}}$ for BP86, M06L, B3LYP and PBE1PBE for models A – H.....	280 -
Table A4.9:	BDE $_{\text{solv}}$ for BP86, M06L, B3LYP and PBE1PBE for models A – H for all solvents	281 -
Table A4.10:	N $_{\text{eq}}$ -Co-C $_{\beta}$ bond angles ($^{\circ}$) for models A – D in both gas and solution phase.....	282 -
Table A4.11:	Torsion angles ($^{\circ}$) for models E – H in both the gas and solution phase	283 -
Table A5.1:	GAS PHASE: Geometrical parameters and energies for M06L	284 -
Table A5.2:	GAS PHASE: Geometrical parameters and energies for B3LYP	284 -
Table A5.3:	GAS PHASE: Geometrical parameters and energies for PBE1PBE.....	285 -

LIST OF FIGURES

Figure 1.1:	The Cobalamin framework with standard numbering format	- 3 -
Figure 1.2:	A simplified representation of AdoCbl	- 4 -
Figure 1.3:	Truncated corrin framework of the type $[Y-(Co(III)(L)_4)-R]^{n+}$	- 7 -
Figure 2.1:	A typical potential energy surface (PES) illustration with two degrees of freedom within the molecule.	- 10 -
Figure 2.2:	STO calculation of a simple one electron, one dimension system showing an exponential relationship between the radius and wavefunction.....	- 15 -
Figure 2.3:	GTO (black) calculation versus STO of a one electron system	- 16 -
Figure 2.4:	Wavefunction of STO (red) versus GTO (black) versus STO-3G (blue) of a one electron system.....	- 17 -
Figure 3.1:	Molecular structure of model cobalamins with a change in R and Y, as used in the study by Kozłowski <i>et al.</i>	- 42 -
Figure 3.2:	Illustrative trends of relative energies of Im-[Co(III)corrin]-Me in the presence and absence of an electrostatic environment. A and B represents the Co-R and Co-Y bonds, respectively. A (blue line) and A' (green line) correspond to the elongation of the Co-R bond while B (purple line) and B' (red line) correspond to simultaneous elongation of both the Co-R and Co-Y bonds.....	- 44 -
Figure 3.3:	Homolytic activation of the Y-(Co(III)corrin)-R cobalamin model.	- 48 -
Figure 3.4:	Models used by Dolker <i>et al.</i> to calculate Co-C BDE. QM in red, MM in black (redrawn from reference 13).....	- 54 -

Figure 3.5:	Models for frequency (6) and solvent effects (7). R is a Me or an Ado group, dependent on the cobalamin modelled (reproduced from reference 13).....	56 -
Figure 5.1:	Model structure of the type $[\text{NX}_3\text{-(Co(III)(L)}_4\text{)-CH}_3]^{\text{n}+}$.	76 -
Figure 5.2:	Models A–D showing the equatorial ligands, (L) ₄ .	76 -
Figure 5.3:	Crystal field description of the low spin and high spin states for Co(III) and Co(II) complexes.	79 -
Figure 5.4:	The change in length of the Co(III)–C _β and Co(III)–N _α bond versus the calculated proton affinity values (kcal mol ⁻¹) in the corrin model.....	83 -
Figure 5.5:	Proton affinity values (kcal mol ⁻¹) of the α axial ligand versus ΔG (●) and BDE (▲) (kcal mol ⁻¹) of the Co–C _β bond for A) corrin and B) porphyrin model systems.	90 -
Figure 5.6:	A) Co(III)–N _α and B) Co(II)–N _α bond lengths (Å) are plotted against ΔG (●) and BDE (▲) (kcalmol ⁻¹) of the Co–C _β bond for the corrin model.	91 -
Figure 5.7:	The Co(III)–C _β ΔG (●) and BDE (▲) (kcalmol ⁻¹) as a function of ΔCo–N _{α(5c-6c)} bond length (Å) for the corrin model.	93 -
Figure 5.8:	Numbering format used for measurement of torsion angles (ω ₁ - ω ₈) for models A – D.	96 -
Figure 5.9A:	Cobaloxime: Co(III) and Co(II) species with α ligands, 1=NH ₃ ; 2=NH ₂ CH ₃ ; 3=NH(CH ₃) ₂ ; 4=N(CH ₃) ₃ and 5=NH ₂ ⁻ .	97 -
Figure 5.9B:	Corrole: Co(III) and Co(II) species with α ligands, 1=NH ₃ ; 2=NH ₂ CH ₃ ; 3=NH(CH ₃) ₂ ; 4=N(CH ₃) ₃ and 5=NH ₂ ⁻	98 -
Figure 5.9C:	Corrin: Co(III) and Co(II) species with α ligands, 1=NH ₃ ; 2=NH ₂ CH ₃ ; 3=NH(CH ₃) ₂ ; 4=N(CH ₃) ₃ ; 5=NH ₂ ⁻ and 6=NH ²⁻	99 -

Figure 5.9D: Porphyrin: Co(III) and Co(II) species with α ligands, 1= NH_3 ; 2= NH_2CH_3 ; 3= $\text{NH}(\text{CH}_3)_2$; 4= $\text{N}(\text{CH}_3)_3$ and 5= NH_2^-	100 -
Figure 5.10: Partial charges (e) for: A) Mulliken; B) APT; C) NBO and D) Bader on the Co atom versus BDE (kcal mol^{-1}) of the Co(III)- C_β bond for the corrin model.....	106 -
Figure 5.11: Partial charges (e) for: A) Mulliken; B) APT; C) NBO and D) Bader on the N_α atom versus BDE (kcal mol^{-1}) of the Co(III)- C_β bond for the corrin model.....	108 -
Figure 5.12: A plot of the Co(III)- C_β bond length (\AA) with its associated BDE (kcal mol^{-1}) for models with a change in $(\text{L})_4$ and α ligands A) NH_2^- (charged ligand) and B) NH_3 (neutral ligand).	111 -
Figure 5.13: Corrole model where the Co(III) ion is identified 0.037 \AA above the mean plane defined through the N_{eq} donors.	114 -
Figure 5.14: The distance of the Co(III) ion from the macrocyclic mean plane (\AA) is plotted against the Co(III)- C_β BDE (kcal mol^{-1}) for A) corrole and B) porphyrin.	115 -
Figure 5.15: The distance of the Co(III) ion from the macrocyclic mean plane is plotted against the Co(III)- C_β (\bullet) bond length (\AA) and its associated BDE (\blacktriangle) (kcal mol^{-1}) for the corrin model.....	119 -
Figure 5.16: Co(III)- N_α restricted bond lengths (\AA) for Co(III) complex and Co(II)- N_α for Co(II) species.....	120 -
Figure 5.17: Co(III)- C_β ΔG (\bullet) and BDE (\blacktriangle) (kcal mol^{-1}) of the corrin model as a function of the A) Co(III)- C_β and B) Co(III)- N_α bond length (\AA).	128 -
Figure 5.18: Corrin model depicting the decrease of the Co(III)- C_β bond length (\AA) as a function of the attractive charge (e) between the Co metal centre and β ligand.	132 -
Figure 6.1: Structures of the α -ligands used to investigate <i>trans</i> influences.....	140 -
Figure 6.2A: Corrin models A – M with a change in the α -ligands.	142 -

Figure 6.2B:	Sketch of the corrin models A – M with a change in the α -ligands.	143 -
Figure 6.3:	Proton affinities (kcal mol^{-1}) is plotted against the Co(III)-C_β BDEs (kcal mol^{-1}) for models A – M.	150 -
Figure 6.4:	The dependence of the homolysis of the Co(III)-C_β BDE (kcal mol^{-1}) as a result of the electron density at the bcp of the Co(III)-C_β bond.	151 -
Figure 6.5:	A) Absolute chemical hardness (eV) and B) the change in the lower axial bond length from the 5- to the 6-coordinate complex (\AA) is plotted against the Co(III)-C_β BDE (kcal mol^{-1}).	153 -
Figure 6.6:	The shift of the Co metal centre (\AA) in the Co(II) and Co(III) complexes respectively, versus the change in A) Co(II)-B_α bond length (\AA) and B) Co(III)-C_β (\bullet) and Co(III)-B_α (\blacktriangle) bond lengths (\AA).	155 -
Figure 6.7:	The Co(III)-C_β BDE (kcal mol^{-1}) is plotted against the absolute chemical hardness (η) (eV) of α ligands in cobalamin models where oxygen is both neutral and negatively charged.	157 -
Figure 6.8:	Proton affinity is plotted against the Co(III)-C_β bond length for A) aliphatic and aromatic α ligands and B) aromatic α ligands only.	159 -
Figure 6.9:	A correlation of the homolysis of the Co(III)-C_β BDE (kcal mol^{-1}) against A) absolute chemical hardness (eV) and B) $\Delta\text{Co-B}_{\alpha(5c-6c)}$ (\AA).	160 -
Figure 6.10:	The dependence of the Co(III)-C_β BDE (kcal mol^{-1}) as a function of the electron density (au) at the bcp of the Co(III)-C_β bond.	161 -
Figure 6.11:	The inverse relationship of the electron densities at the bcp's of the Co(III)-C_β and Co(III)-B_α bonds for A) neutral O, S	

	and anionic S donors and B) aliphatic and aromatic N and anionic O donors.....	162 -
Figure 7.1:	Model complexes A – H where the α and β axial ligands remain constant while the equatorial ligands are varied.	168 -
Figure 7.2:	A) BP86 (●) and B) M06L (▲): ΔG and BDE (kcal mol ⁻¹) trends for the Co(III)–C $_{\beta}$ bond in models A – H.....	173 -
Figure 7.3:	A) BP86 (●) and B) M06L (▲): Bond lengths (Å) for Co(III)–C $_{\beta}$ is plotted against Co(III)–N $_{\alpha}$ for models A – H.....	174 -
Figure 7.4:	BP86: Co(III)–C $_{\beta}$ bond length (Å) is plotted against the Co(III)–C $_{\beta}$ BDE (kcal mol ⁻¹) for models A – H.....	175 -
Figure 7.5:	BP86: The change in the lower axial bond length, $\Delta\text{Co-N}_{\alpha(5c-6c)}$, (Å) is plotted against the Co(III)–C $_{\beta}$ BDE (kcal mol ⁻¹) for models A – H.	176 -
Figure 7.6:	BP86: Electron density (au) at bcp of A) Co(III)–C $_{\beta}$ and B) Co(III)–N $_{\alpha}$ bond lengths (Å) for models A – H.....	178 -
Figure 7.7:	Correlation of the Co(III)–C $_{\beta}$ BDE (kcal mol ⁻¹) with its associated bond length (Å) and $ V(r) /G(r)$ value.	181 -
Figure 7.8:	BP86: Correlation of the APT partial charges on Co(III) and N $_{\alpha}$ for models A – H.	184 -
Figure 7.9:	BP86: Correlation of the NBO partial charges on Co(III) and N $_{\alpha}$ for models A – H.	185 -
Figure 7.10:	BP86: Correlation of the Bader partial charges on Co(III) and N $_{\alpha}$ for models A – H.	186 -
Figure 7.11:	SMD method describing a solute-solvent interaction.	188 -
Figure 7.12:	Co(III)–C $_{\beta}$ BDEs (●) and Co(III)–C $_{\beta}$ BDE _{solv} (▲) (kcal mol ⁻¹) trends as a function of the Co(III)–C $_{\beta}$ and Co(III)–N $_{\alpha}$ bond lengths (Å) for models A – D and E – H in MeOH.....	196 -
Figure 7.13:	The N _{eq} –Co–C $_{\beta}$ bond angle versus Co(III)–C $_{\beta}$ BDE for models A – D in the gas phase.	200 -

Figure 7.14:	The change in the Co(III)–C _β BDE as a function of the ρ-value at the bcp of the Co(III)–C _β bond for models A – D in the gas phase.....	201 -
Figure 7.15:	Movement of the equatorial ligand in the pre- (Co(III)) and post (Co(II)) homolysis complexes of the type [NH ₃ –(Co(III)(L ₄))–CH ₃] ⁿ⁺ from the Neq defined mean plane.	204 -
Figure 7.16:	Movement of the equatorial ligand in the pre- (Co(III)) and post (Co(II)) homolysis complexes of the type [NH ₃ –(Co(III)(L ₄))–CH ₃] ⁿ⁺ from the N _{eq} defined mean plane.	204 -
Figure 7.17:	For model E, the Co(III)–C _β BDE (kcal mol ⁻¹) is plotted as a function of the relative permittivities for polar aprotic, polar protic and non-polar solvents.	205 -
Figure 7.18:	The change in the Co(III)–C _β BDE (kcal mol ⁻¹) as a function of the the ε of the solvents and the distortion of the N _{eq} –Co–C _β (in °) in models F (●) and H (▲).	207 -
Figure 7.19:	The change in the Co(III)–C _β BDE (kcal mol ⁻¹) as a function of the A) Co(III) shift from the mean plane (Å) and B) the ε of the solvents in model G.....	209 -
Figure 8.1:	Representation of the corrin macrocycle used for calculations in complexes of the type, [NH ₃ –(Co(III)(corrin-X))–CH ₃] ⁺	212 -
Figure 8.2:	A linear relationship between log k vs log K is shown for a set of meta- and para-substituents on benzoic acids (redrawn from references 299 and 300).....	214 -
Figure 8.3:	Cobalamin model of the type: [NH ₃ –(Co(III)(corrin-X))–CH ₃] ⁺ where X in A=NO, B=NO ₂ , C=CN, D=COOH, E=Br, F=H, G = CH ₃ , H = OH and I=NH ₂	217 -

- Figure 8.4: The Co(III)–N_α bond length is plotted as a function of the
A) Hammett constant (σ_p) and B) Co(III)–C_β bond length (Å).- 220 -
- Figure 8.5: A schematic representation of the normal *trans* effect as a
result of the electron donation increasing towards the
macrocyclic equatorial ligand.....- 221 -
- Figure 8.6: Vibrational analysis of the Co(III)–C_β bond (●) and C_β–H
symmetric stretch (▲) against the Hammett constant (σ_p) of
the C₁₀ substituent in the [NH₃–(Co(III)(corrin-X))–CH₃]ⁿ⁺
complex.- 222 -
- Figure 8.7: The Co(III)–C_β bond length (Å) is plotted as a function of the
 ΔG (●) and BDE (▲) (kcal mol⁻¹) for the homolysis of the
Co(III)–C_β bond (Å).....- 223 -
- Figure 8.8: Trends in ΔG (●) and BDE (▲) (kcal mol⁻¹) for the
homolysis of the Co(III)–C_β bond in the
[NH₃–(Co(III)(corrin-X))–CH₃]⁺ complex as A) the Co–N_α
bond length (Å) varies from the 6-coordinate to the
5-coordinate species and B) the σ_p of the C₁₀ substituent is
varied.- 224 -
- Figure 8.9: NBO partial charge on Co(III) (●) and N_α (▲) atoms as a
function of the Hammett constant.- 227 -
- Figure 8.10: NBO partial charge on the equatorial N donors A) N₁, B) N₂,
C) N₃ and D) N₄ as a function of the Hammett constant.- 228 -
- Figure 9.1: "Typical" (H₂OCbl⁺) vs "atypical" (SCNCbl) absorption
spectra of cobalamins.- 233 -
- Figure 9.2: Models A – E of the type, [Im–(Co(III)(corrin))–R]ⁿ⁺, used in
the DFT and TD-DFT calculations.....- 236 -
- Figure 9.3: Comparisons of distinctive spectral features in simulated and
experimental absorption spectra for models A, B and C in
vacuo and methanol. The electromagnetic spectrum was
obtained from reference 332.....- 239 -

Figure 9.4:	Natural Transition orbitals for the main transition bands α and band A for ClCbl in vacuo.....	243 -
Figure 9.5:	Natural Transition orbitals for the main transition bands α and band A for BrCbl in vacuo.....	244 -
Figure 9.6:	MO diagram of the 3 highest occupied orbitals and the 3 lowest unoccupied orbitals.	246 -
Figure 9.7:	Isosurface plots for frontier molecular orbitals in the complex [Im-(Co(III)(corrin))-F] ⁺	247 -
Figure 9.8:	Isosurface plots for frontier molecular orbitals in the complex [Im-(Co(III)corrin)-Cl] ⁺	248 -
Figure 9.9:	Isosurface plots for frontier molecular orbitals in the complex [Im-(Co(III)corrin)-Br] ⁺	249 -
Figure 9.10:	Simulated electronic absorption (black and red line) spectra of [Im-(Co(III)(corrin))-SeCN] ⁺ based on 30 first singlet excited states. The black and red line corresponds to a Doppler broadening with a width at half peak of 9 and 20 nm, respectively. The electromagnetic spectrum was obtained from reference 332.	251 -
Figure 9.11:	Natural Transition orbitals for the main transition bands α and band A for SeCNCbl in vacuo.....	253 -
Figure 9.12:	Simulated electronic absorption (black and red line) spectra of [Im-(Co(III)(corrin))-CH ₃] ⁺ based on 30 first singlet excited states. The black and red line corresponds to a Doppler broadening with a width at half peak of 9 and 20 nm, respectively. The electromagnetic spectrum was obtained from reference 332.	255 -
Figure 9.13:	Natural Transition orbitals for the main transition bands α and band A for CH ₃ Cbl in vacuo.	257 -

LIST OF ABBREVIATIONS

ΔG	Gibbs free energy
ACF	Adiabatic connection formula
Ado	Adenosyl
AdoCbl	Adenosylcobalamin
AIM	Atoms in Molecules
APT	Atomic polar tensor
B3LYP	Becke three-parameter hybrid exchange functional with Lee-Yang-Parr exchange-correlation
bcp	bond critical point
BDE	Bond dissociation energy
Bzm	Benzimidazole
CPCM	Conductor polarizable continuum model
DFT	Density functional theory
DMB	5,6-dimethylbenzimidazole
Et	Ethyl
EXAFS	Extended X-ray absorption fine structure
GGA	Generalised gradient approximation
GUI	Graphical user interface
HF	Hartree Fock
Im	Imidazole
Imm	Imidazolate
IMOMM	Intergrated molecular orbital molecular mechanics approach
iProp	<i>isopropyl</i>
LDA	Local density approximation
LSD	Low spin density
LSDA	Local spin density approximation
Me	Methyl
MeCbl	Methylcobalamin
MM	Molecular mechanics
MP2	Moller Plesset 2
MST	Miertus-Scrocco-Tomasi
NBO	Natural bond orbitals
NPA	Natural population analysis
PES	Potential energy surface
QM/MM	Quantum mechanics/molecular mechanics
QTAIM	Quantum Theory of Atoms in Molecules
SMD	Universal solvent model density

tBut	<i>tert</i> -Butyl
TDDFT	Time dependent density functional theory
THF	Tetrahydrofuran
ZPE	Zero-point energy
ρ	Electron density

CHAPTER 1

INTRODUCTION

1.1 BACKGROUND

Theoretical science, observational science, experimental science and computational science are only four endeavours that currently contribute to the world of Science.¹ Traditionally, the first three have always been an acceptable approach towards the fundamental growth of science while computational science, sometimes within the discipline of Chemistry, referred to as computational chemistry or molecular modelling, is fairly new and only made its debut in the early 1950s.²

Computational chemistry allows chemists to study and solve complex, challenging or unobserved chemical phenomena by running calculations on computers based on computer science and mathematical techniques. However, merely defining this particular science lends no credence to its power as a recently acquired analytical tool. The synergy between the experimental and theoretical communities has vastly accelerated progress in many areas such as materials science, environmental science, the life sciences, as well as medicine.^{1,3} The areas computationally investigated in material science include nanotechnology, biopolymers and crystallography; while in the environmental sciences, conditions such as reaction kinetics and mechanisms, thermodynamics and structure-property-activities of compounds that are most important to the environment, have been explored. Molecular biology researchers trained in computational chemistry have made significant inroads into the life science arena covering sub-domains such as molecular biology, genomics and proteomics whereas to date medicine is one particular topic that has, and still is, taking significant advantage of computational chemistry to explore the field of medicinal chemistry, namely pharmacology.¹

Computational methods have made a remarkable impact across the board in science. While computational models cannot replace the laboratory, they have become an integral part of the overall search for scientific knowledge. Researchers can use computational techniques to accomplish a number of goals in, for example, making observations, conducting experiments, and creating or testing new theories, by performing calculations on large, high-powered computers (referred to as high powered computing) or through supercomputing.^{2,4} Delicate experimentation that may include unknown or even dangerous molecules can be incorporated easily into a computational scheme to make a qualitative or approximate quantitative assessment.² Finally, key issues such as designing molecules, exploring structure geometries and being able to investigate properties that are experimentally difficult to access, become a reality through this scientific tool.

1.2 VITAMIN B₁₂

For decades, the synthesis and chemistry of vitamin B₁₂ (formally known as cyanocobalamin)^{5,6} and its cofactors (derivatives of vitamin B₁₂) have been extensively studied.⁷ The coenzymes of B₁₂ and its coenzymes, see **Figure 1.1**, are unique and of great biological importance among known natural products due to their organometallic (Co–C) bond.⁸⁻¹⁰

Current studies have revealed this macrocyclic biomolecule to play a role in understanding particular topics such as pharmacology (target drug delivery) and enzymatic activities, metabolism pathways and processes.¹¹ The key to the enzymatic activity of the cobalamins lies in the stable covalent Co–C bond¹²⁻¹⁴ making further exploration of this organometallic bond a necessity.

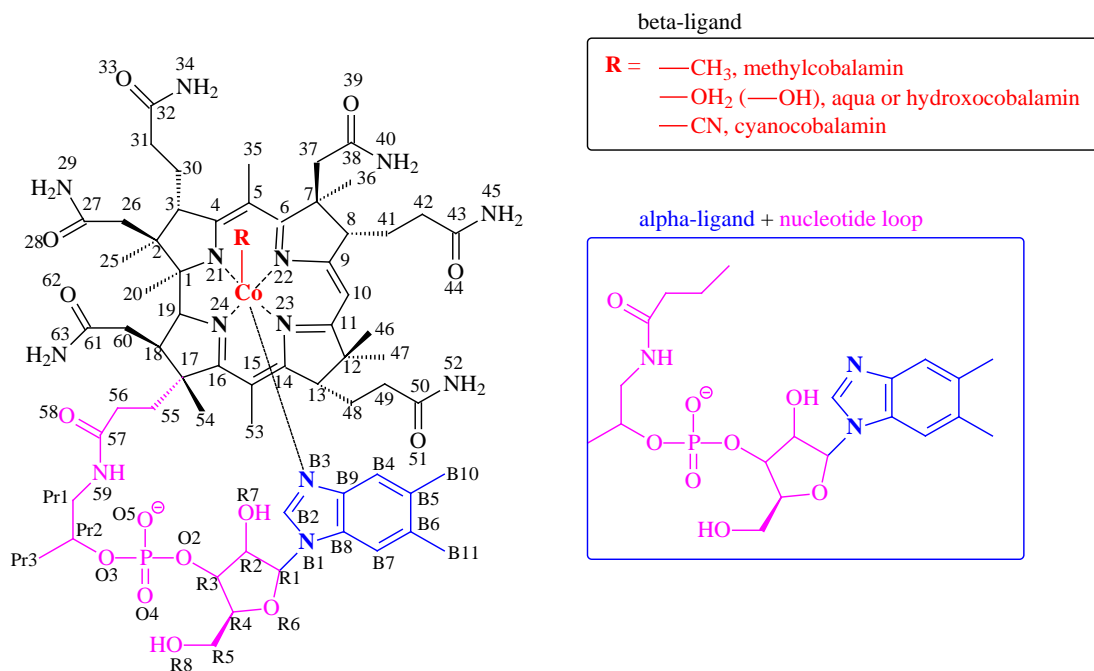


Figure 1.1: The Cobalamin framework with standard numbering format

The two biologically active forms of cobalamins are adenosylcobalamin (AdoCbl) with R= 5-deoxyadenosyl and methylcobalamin (MeCbl) with R=methyl.^{6,15} Both of these coenzymes are products of cyanocobalamin hydrolysis. AdoCbl deficiency results in neurological degeneration while MeCbl deficiency is responsible for megaloblastic anaemia.

A close inspection of these two cobalamin analogues, MeCbl and AdoCbl, using X-ray diffraction methods, reveals an octahedral environment with a d^6 low spin cobalt (III) ion in its ground state, with four equatorial positions occupied by the nitrogen atoms of a corrin ring in an approximately planar framework. Seven amide chains are placed on the periphery of the corrin ring, with a nucleotide loop connecting one of these chains to the lower-axial (α) ligand, which is 5,6-dimethylbenzimidazole (DMB) while the *trans* axial ligand (β ligand) position is occupied by the 5'-deoxyadenosyl alkyl group, **Figure 1.2**.^{9,16,17}

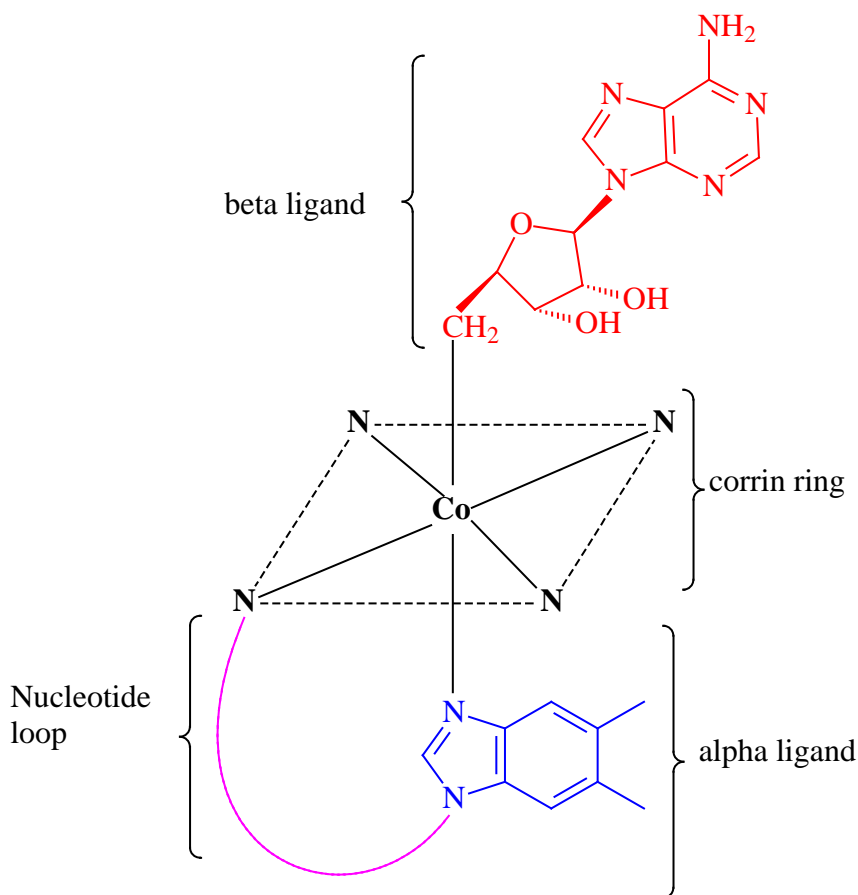


Figure 1.2: A simplified representation of AdoCbl

Although AdoCbl and MeCbl share a similar structural framework with differences only in the “R” substituent; in an enzymatic environment these two cofactors catalyze different reactions. MeCbl undergoes a heterolytic cleavage of its Co–C bond to yield a methyl cation and cob(I)alamin species¹⁸ while AdoCbl undergoes a homolytic^{12,19-23} breaking of the Co–C bond, producing a 5-deoxyadenosyl radical and cob(II)alamin fragment.²⁴ The Co–C bond is a water-stable organometallic bond¹² and enzymes that bind and utilise the coenzyme must act to overcome the inherent kinetic inertness of the organometallic bond.²⁵ The Co–C dissociation enthalpy is $31.4 \pm 1.5 \text{ kcal mol}^{-1}$ for AdoCbl in solution and the thermal homolysis rate at 25°C is only $10^{-9\pm 1} \text{ s}^{-1}$.⁸ In AdoCbl dependent enzymes, this rate increases by a factor of $10^{12\pm 1} \text{ s}^{-1}$, implying a $\sim 15 \text{ kcal mol}^{-1}$ destabilisation of the Co–C bond.^{8,26,27}

This key fact further emphasises the point that reactivity of the cobalamins lies in the region of the Co–C bond, and precise knowledge of the factors inducing, triggering, or controlling (selectively permitting)²⁸ the strength²⁹ of this bond is important.^{12,14,30} As a further advantage, being able to control the destined cleavage of the Co–C bond will help to inhibit abiological side reactions.³¹

Since the discovery of vitamin B₁₂ in the early 1930s by Whipple, Minot and Murphy, an impressive amount of experimental research has been conducted on coenzymes of vitamin B₁₂.³² In studies commenced during the latter part of the 20th century computational chemistry methodology was used to complement some of the experimental data. This type of research also serves as guidance to the experimental research mentioned earlier. In an attempt to understand the true behaviour of cobalamins and the mysterious cleavage of the organometallic bond, many computational studies have appeared in the literature on vitamin B₁₂ analogues or models thereof. Some of the discussions surrounding the cause for the labilisation of the organometallic bond include: steric and electronic *trans* effects due to a very bulky or nucleophilic α ligand causing a mechano-chemical triggering effect;^{6,20,33-37} the corrin ring interacting with its side chains;^{38,39} twisting of the α ligand about the Co–N_{ax} bond;⁴⁰ pulling or tilting of the β ligand (ado group)^{41,42} and the protein favouring the dissociated state over its ground state.^{28,43} However, some of these hypotheses became questionable once crystal structures of B₁₂-dependent enzymes gave an indication that there was no significant structural distortion of the corrin moiety in the substrate free enzymes.^{44,45}

Density Functional Theory (DFT) methods have been used widely for biochemical applications and more recently for the theoretical exploration of the cobalamins,^{6,9,14,17,46} but no definitive conclusion has been reached as to what intrinsic factor(s) is responsible for the easy labilisation of the Co–C bond. Several explanations have been suggested but none have explained the experimental data satisfactorily. The initial probe into the cobalamin organometallic bond gave rise to

the suggestion that its homolytic breaking was due to steric distortion of the protein-bound coenzyme (upward corrin distortion) while any electronic effects were of minor importance.⁴⁷ However, recent literature has indicated that electronic factors cannot be ignored.^{4,48-52}

1.3 OBJECTIVES OF THE STUDY

DFT was used as the method of elucidation as it has already proven its superiority in describing the electronic structure of atoms, molecules, clusters, surfaces and solids, and is successfully reigning supreme as a universal language for electronic structure theory across the disciplines of organic chemistry, inorganic chemistry, surface chemistry, materials science and physics.^{25,53}

As the available computer power directly affects the type of moiety under investigation, calculations were performed on truncated structures (see **Figure 1.3**) of the type $[Y-(Co(III)(L)_4)-R]^{n+}$ where L_4 is the equatorial ligand.^{54,55,56} In the model system, all seven attached side chains to the corrin ring were converted into hydrogen with a change in both the $\alpha(Y)$ and $\beta(R)$ axial ligands while the nucleotide loop was completely removed (this is otherwise referred to as a naked corrin). This type of truncated model with changes made to the α and β ligands has been extensively used.^{6,9,48,57-61}

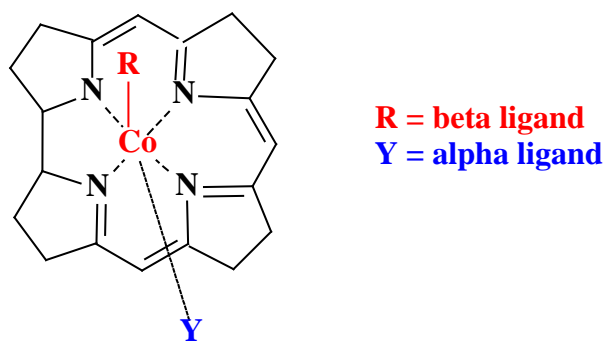


Figure 1.3: Truncated corrin framework of the type $[\text{Y}-(\text{Co}(\text{III})(\text{L})_4)-\text{R}]^{\text{n}+}$

In this study, various steric and electronic effects were investigated by focusing on the Gibbs free energy (ΔG) and bond dissociation energy (BDE) of the homolysis reaction. As the direction of any spontaneous change always drives towards a lower ΔG , the results obtained were used to explore why the Co–C bond is labilised in the cobalt corrins.

After the presentation of the theoretical tools and literature review (Chapters 2 and 3) and the computational details (Chapter 4), the principal results are collated and outlined as follows:

- The *trans* influence, which is the influence of the α ligand on the properties of the β ligand, is explored. Cobalamin model systems of the type given in **Figure 1.3** were used, where Y was chosen between a range of α ligands and $\text{R}=\text{CH}_3$. The α ligand substituents of different proton affinities were used to monitor the effect on bond lengths between Co and the α and β ligands and the equatorial nitrogens, as well as R–Co–Y bond angles together with N–Co–N–C torsional angles of the macrocyclic ring and finally the ΔG and BDE of the Co–C homolysis reaction. The results for the *trans* influence of the α axial ligands are presented and discussed in Chapters 5 and 6.
- The *cis* influence, or the influence of the equatorial ring on the properties of the β ligand, was explored by changing the equatorial ligands, moving from saturated (containing σ bonds only) models to unsaturated (containing a

mixture of σ and π bonds) models with macrocyclic rings, in both gas and a simulated solution phase. These models are further described in Chapter 7 (see **Figures 7.1** and **7.4**) together with a discussion of the results obtained. Various functionals such as BP86, M06L, B3LYP and PBE1PBE at the 6-31+G(d,p) level of theory were used and comparisons drawn between them.

- The *cis* influence (thermodynamic) on the Co–C bond in substituted corrins was explored by analysing the geometric parameters, ΔG , BDEs and atomic charges. Electron withdrawing and electron donating groups such as NO; COOH; NO₂; Br; CN; OH; NH₂ and CH₃ were substituted on C₁₀ (see **Figure 1.1**) of the corrin macrocycle. The data are highlighted and discussed in Chapter 8.
- Absorption spectra of vitamin B₁₂ analogues obtained by the means of time dependent-DFT (TD-DFT) calculations on cobalamin models were carried out. The influence of changing the β axial ligand (R=F, Cl, Br, SeCN and CH₃) while the α axial ligand (X = imidazole) remained constant, was examined. All of the data obtained are presented and discussed in Chapter 9.

Finally, Chapter 10 concludes and highlights the findings of the study undertaken, the extent to which the objectives of the study have been fulfilled and some recommendations, if any, for possible future studies.

CHAPTER 2

THEORETICAL TOOLS FOR BIOINORGANIC SYSTEMS

Computational chemistry calculations are always based on one of two types, namely, classical physics or quantum physics.⁴ Molecular Mechanics (MM) is an example of the former while *ab initio*, semi-empirical, and Density Functional Theory (DFT) methods fall into the latter category.

2.1. COMPUTATIONAL METHODS

2.1.1 MOLECULAR MECHANICS

MM is a computational method employed to elucidate, by calculation, equilibrium conformations (minimal energy state) of large molecules by its potential energy surface, see **Figure 2.1**. The potential energy surface mathematically links the molecular structure and its resultant energy.^{62,63}

MM methods calculate the behaviour of the atomic composition (nuclei only), viewed as a collection of masses of a molecule interacting with each other via interatomic forces, and such interactions are usually, but not always, taken to be harmonic. The behaviour of electrons is excluded from this calculation. Because of this simplification MM methods are relatively fast and practically better to employ for macromolecular structures as opposed to quantum mechanical methods.⁶⁴ This method is used for geometry optimization prior to further calculations in order to ensure the molecule is in its ground state so that comparisons can be made between the experimental and calculated results. Although MM is useful for studying large

biomolecules, important chemical processes such as chemical reactions or predicting the reactivity of molecules cannot be explored as MM methods do not deal directly with electron density.¹

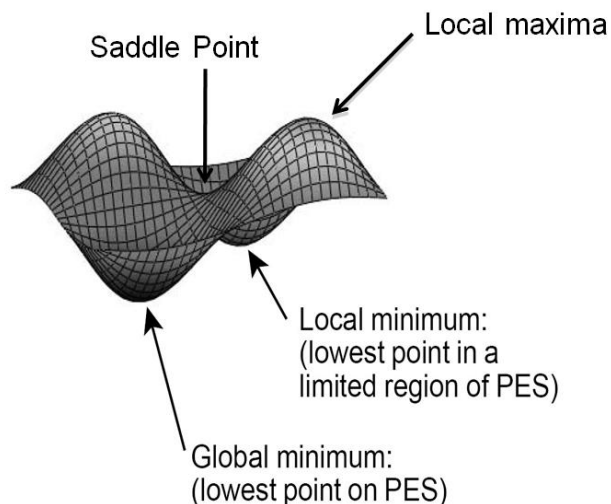


Figure 2.1: A typical potential energy surface (PES) illustration with two degrees of freedom within the molecule.

Each point in the figure above corresponds to the specific values of the two structural variables representing a particular molecular structure. Height of the surface at a particular point corresponds to the energy of that structure.⁶³

2.1.2 QUANTUM MECHANICAL (QM) METHODS

As the name suggests, QM (electronic structure) methods employ the laws of quantum mechanics as a basis for their computations. QM methods cover calculations of transition states or mechanistic pathways as well as the exploration of molecular geometries influenced by polarization effects or unusual electron densities.⁶² The ultimate goal of Molecular QM lies in solving the nonrelativistic,

time independent Schrödinger equation, with the specific aim of calculation of the electronic structures of atoms and molecules.^{63,65,66}

By combining the classical differential equation describing the profile of a simple harmonic standing wave and de Broglie's relation between matter and waves, Schrödinger postulated the well known energy (E) relationship of the time-independent wave equation:^{63,67,68}

$$\left[-\frac{\hbar^2}{8\pi^2} \sum_i \frac{1}{m_i} \left(\frac{\partial^2}{\partial x_i^2} + \frac{\partial^2}{\partial y_i^2} + \frac{\partial^2}{\partial z_i^2} \right) + V(r) \right] \cdot \Psi(r) = E \cdot \Psi(r) \quad 2.1$$

which approximates the form of the spatial wavefunction, $\Psi(r)$, associated with any set of particles having masses m_i , by analyzing the way in which it is perturbed by the potential field $V(r)$ in which the particles are in motion, where r represents the set of component vectors describing the x , y and z coordinates of each particle.

Equation 2.1 can also be expressed in its abbreviated form:⁶⁷

$$\hat{H}\Psi = E\Psi \quad 2.2$$

where the Hamiltonian \hat{H} is a differential operator representing the total energy.⁶⁷

The Hamiltonian in equation 2.3 is the sum of the kinetic energy (\hat{T}) and the potential energy (\hat{V}) operators:

$$\hat{H} = \hat{T} + \hat{V} \quad 2.3$$

where

$$\hat{T} = \left[-\frac{\hbar^2}{8\pi^2} \sum_i \frac{1}{m_i} \left(\frac{\partial^2}{\partial x_i^2} + \frac{\partial^2}{\partial y_i^2} + \frac{\partial^2}{\partial z_i^2} \right) \right] \quad 2.4$$

and

$$\hat{V} = \sum_i \sum_{<j} \left(\frac{e_i e_j}{r_{ij}} \right) \quad 2.5$$

and where the sums are across all particles i (nuclei and electrons) with masses m_i in equation 2.4, and all distinct pairs of particles i and j with electric charges e_i and e_j , separated by a distance r_{ij} in equation 2.5.

In order to solve equation 2.2, we need to make some approximations. The first one is the Born-Oppenheimer (clamped-nuclei) approximation, which allows the uncoupling of the electron and nuclei motion, due to the big difference of mass. This allows a PES to be defined where the nuclei move. The resolution of the system then shifts to solve equation 2.2 for the electronic part, $\hat{H}\Psi_i = E\Psi_i$, where Ψ_i is an electronic wavefunction. The second approximation is that Ψ_i can be deconstituted into a mathematic combination of known functions: $\Psi_i \simeq \Psi_i^\Omega = \sum_\mu C_\mu \chi_\mu$. Finally, the third approximation is the orbitals approximation where the φ_i (electronic configuration) is a combination of mono-electronic spin orbitals, written in the form of a determinant, χ_μ . Obtaining solutions to equation 2.2 will correspond to different stationary states of the particle (molecule). Ultimately, the one with the lowest energy is described as the ground state of the molecule.⁶³

2.1.2.1 AB INITIO METHODS

Ab initio (meaning from the beginning or “from scratch”)^{1,53} methods are fairly popular due to their independence from experimental data. Unlike the semi-empirical method of calculation where experimental parameters are mandatory in their computations, *ab initio* methods irrespectively produce precise and accurate results that can be satisfactorily compared to experimental data.⁴ The *ab initio* molecular orbital method is based purely on a mathematical model and its primary function is to

interpret and predict the properties of atomic and molecular systems at the electronic level. This method is based exclusively on the laws of quantum mechanics and on the values of physical constants such as the speed of light, the masses and charges of electrons and nuclei and Planck's constant.^{1,69}

The key to a qualitative calculation depends on choosing an appropriate basis set for the calculation as well as the computational method to be used. Knowing the molecule under investigation and having a clear objective for the calculation will aid in choosing the most suitable basis set. However, a significant disadvantage to this method is the size limitation of the molecule under investigation because of the amount of time required for a calculation.

2.1.2.1.1 Basis set

One of the approximations used is to describe the molecular orbitals of polyatomic species as linear combinations of atomic orbitals (LCAO) giving:^{1,63}

$$\Psi = \sum_{\mu} c_{\mu} \chi_{\mu} \quad 2.6$$

where c_{μ} is the molecular orbital expansion coefficient, and χ_{μ} is the basis function of the atomic orbital. A basis set is the choice of the set of basis functions (explained further in the next section) used for the calculation. For a given basis set (χ_{μ}), the wavefunction Ψ , corresponding to the lowest energy in the Schrödinger equation, can be obtained by varying the coefficient c_{μ} . The obtained energy is always higher than the true energy minimum. The larger the basis is, the lower the energy. However, at some point the energy will not decrease significantly despite further increasing the size of the basis set, which means that the best single determinant wavefunction has been reached. Once this occurs, any further change to the wavefunction will not alter the energy.

The number of atomic orbitals, χ_{μ} , determines the quality of the molecular orbital, Ψ . A large molecular system means a large number of electrons and therefore a large number of atomic integrals will be required. Because of this, fast computers with a large amount of memory become essential.

There are two types of atomic basis functions (formulas) commonly used to represent the wavefunction, namely Slater-type atomic orbitals (STOs) and Gaussian-type atomic orbitals (GTOs).¹

(a) STOs^{4,70}

The use of STOs in practical molecular orbital calculation has been limited to small molecules due to their complexity for a many-particle system.^{1,71} The STO is expressed according to the simplified formula for the one electron system,

$$STO = \left(\frac{\zeta^3}{\pi}\right)^{0.5} e^{-\zeta r} \quad 2.7$$

Where ζ (for published values from literature, see **Table 2.1**) equals the value of the basis set; π is the π constant; and r represents the radius. The normalized STO formula used in extended Huckel theory is provided in Appendix 1: A1.1.

Table 2.1: Zeta values⁴

Atom	Zeta value for 1s orbital	Zeta value for 2s and 2p orbitals
H	1.24	
He	1.69	
Li	2.69	0.80
Be	3.68	1.15
B	4.68	1.50
C	5.67	1.72
N	6.67	1.95
O	7.66	2.25
F	8.56	2.55
Ne	9.64	2.88

By using equation 2.7, one observes the wavefunction to exponentially decrease as the electron is found to move further away from the nucleus^{1,3}, see **Figure 2.2**.

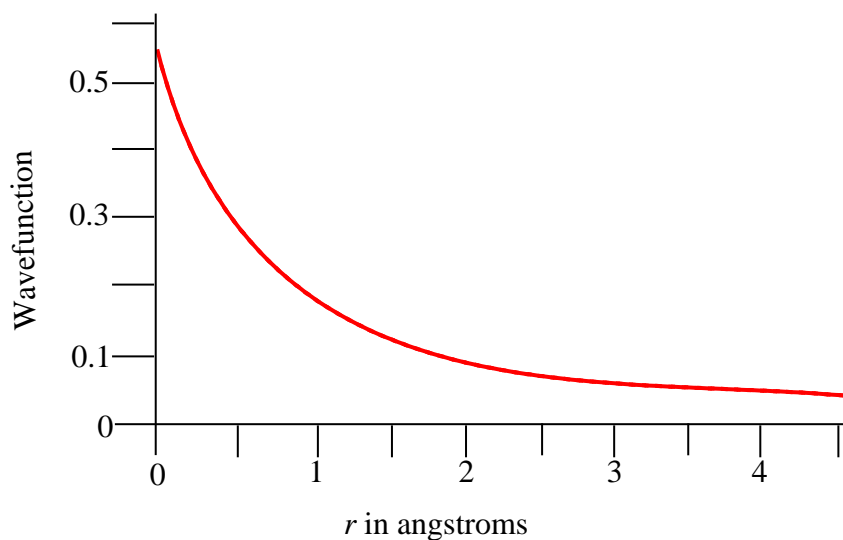


Figure 2.2: STO calculation of a simple one electron, one dimension system showing an exponential relationship between the radius and wavefunction.¹

(b) GTOs^{1,3,62,71}

As STO calculations are limited to small molecular systems, the GTO formula was developed for larger molecular systems. Almost all *ab initio* codes employ GTO basis sets.

The simplified GTO formula (see Appendix 1, A1.2 for the general functional form of a normalized GTO in atom-centred Cartesian coordinates) is expressed as

$$GTO = \left(\frac{2\alpha}{\pi}\right)^{0.75} e^{-\alpha r^2} \quad 2.8$$

This mathematical formula is similar to that of the STO except for the zeta constant (ζ) being replaced by α (α),* and which has a basis set value of 0.4166. By correctly using the value for α in equation 2.8, the following graph, (**Figure 2.3**), is obtained.⁴

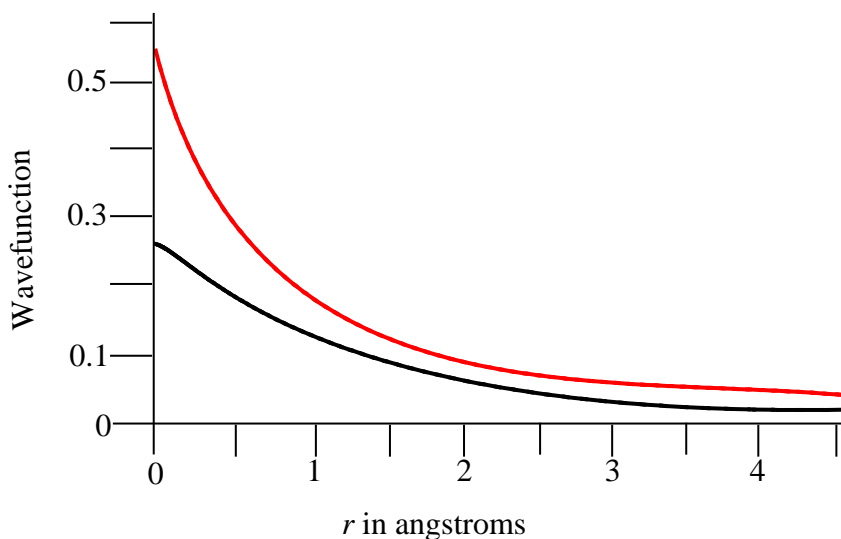


Figure 2.3: GTO (black) calculation versus STO of a one electron system.¹

* Values of constants for the GTO basis sets can be obtained from <http://www.emsl.pnl.gov/forms/basisform.html>.

Assuming the STO calculation to be correct, **Figure 2.3** shows a discrepancy between 0–1 angstroms for the GTO calculation. This discrepancy would make it difficult to predict the location of an electron when it is close to the nucleus. In order to address this problem of the GTO approximation, several Gaussian probability functions (each having its own α and contraction coefficient value) have been introduced, where each function contributes towards the final solution. **Figure 2.4** (STO-3G graph) illustrates the outcome to the GTO approximation when three Gaussian probability functions are introduced into the calculation.

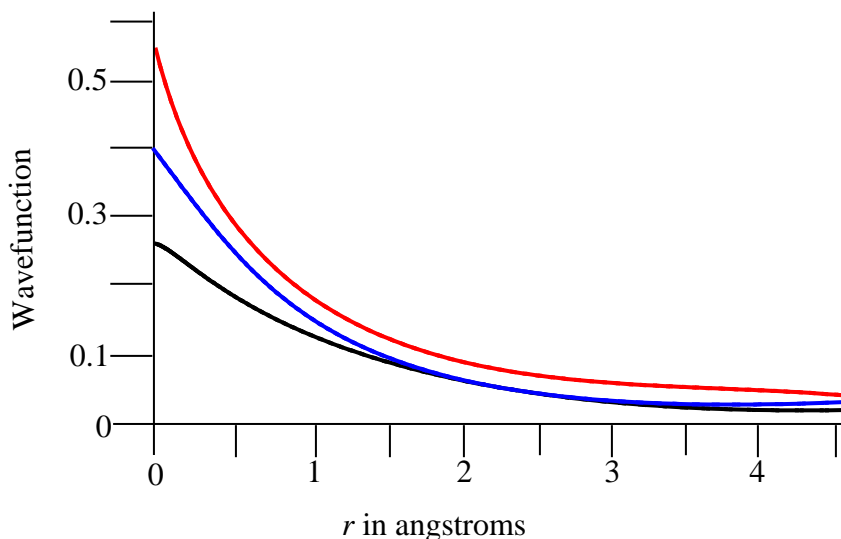


Figure 2.4: Wavefunction of STO (red) versus GTO (black) versus STO-3G (blue) of a one electron system[†].

Although the graphical results obtained for both the STO and STO-3G[†] cannot be superimposed over each other, the margin of difference between the two is very small compared to the difference between the STO and GTO calculations. However, further improvement can be achieved by increasing the number of Gaussian probability functions used in the GTO basis sets.

[†]Example of a minimal basis set which is further explained in the section on minimal basis sets

All currently available software has an accessible range of pre-defined basis sets, which are classified by the number and types of functions they contain. There are four categories of which only a few are commonly used in *ab initio* molecular orbital calculations. The four classes are:

Minimal Basis Sets^{1,63}

Although this basis set produces a quantitative result, it is rarely used for any serious research purposes and even then only for quick qualitative checks for one or more molecular properties. This particular basis set classes all electrons as equally important and contains the minimum number of basis functions needed for each atom. The STO-3G and STO-6G basis set make up this group. For STO-3G and STO-6G, a combination of three and six Gaussian functions, respectively, approximate the STO basis set.

Split Valence Basis Sets^{1,63}

As the name suggests, the valence electrons receive more attention in this calculation since they are involved in chemical reactions and bonding. However, the behaviour of the core electrons is touched upon when making approximations during calculations of the behaviour of the valence electrons. Examples of these basis sets are the 3-21G, 4-31G and 6-31G basis sets.

The split valence basis set allows orbitals to change their size but not their shape. Considering the 3-21G basis set, the valence (outer) shell is split into an *inner* or firmly held part which is expanded in terms of two primitive Gaussian functions, and an *outer* more diffuse part which is written in terms of one primitive Gaussian function, denoted as 3-21G.

Polarized Basis Sets^{1,63}

Electron configuration is used to describe the location of an electron in an atom. However an electron may on occasion move into a higher energy level and the effect of polarization takes this into account. This polarization gives a more accurate location of the electron and where the electron can exist. In most instances an asterisk, “*” on the orbital name is used to indicate a polarized basis set. For example, a 4-31G* and 4-31G(d) basis set is one and the same thing. This example is also described as a polarized split-valence basis set. Perhaps the most commonly used polarized basis set is the 6-31G*/ 6-31G(d) where d functions are added to heavy atoms (all atoms excluding hydrogen and helium) and the 6-31G**/ 6-31G(d,p), which adds Gaussian type p functions to hydrogen or helium atoms in addition to d functions on heavy atoms.

DiffuseBasis Sets^{1,63}

In a small particle system, the probability of finding an electron close to the nucleus is quite high. However, as the atomic radius of an atom gradually increases, so pinpointing the exact location of an electron becomes more difficult since our knowledge of position is limited by the constraints of the Uncertainty Principle. But in systems involving anions and atoms in excited states, diffuse basis sets can be used to extend the distance away from the nucleus for search of the electrons. These basis sets are indicated by a “+” symbol such as 6-31+G(d) or a “++” symbol indicating double diffusion, 6-31++G(d). In the former basis set a diffuse function is added to the heavy atoms while the latter add diffuse functions to both the heavy atoms and hydrogens. This is also a typical example of a polarized diffuse split valence basis set.

2.1.2.2 SEMI-EMPIRICAL METHOD

This method bridges the gap between MM and *ab initio* calculations. Although semi-empirical methods are quantum mechanical in nature they differ from *ab initio*

calculations because of the essential need for empirical parameters from an experiment prior to running a calculation.⁷² This method also addresses the accuracy setback and computing time disadvantage experienced in MM and *ab initio* calculations, respectively, by making several assumptions and ignoring non-valence electrons. This alteration in the method involves parameterization (using empirical parameters) of calculations to fine tune accuracy and simplifying the mathematics which causes a reduction in computing time for the calculations.

Unfortunately, this method also has some limitations; molecules that do not have suitable empirical parameters cannot be investigated, and the quicker computation time (as a result of only valence electrons being considered in the calculation) affects the accuracy of the semi-empirical method. Semi-empirical methods also tend to perform very poorly for chemical systems that may contain hydrogen bonding, transition structures or molecules that contain atoms that are inadequately (or not at all) parameterized.^{1,70}

2.1.3 DENSITY FUNCTIONAL THEORY

DFT, classed as an *ab initio* method, is another electronic structure method. DFT is most attractive among these methods because in its model structure it includes the effects of electron correlation by accounting for inter-electron interaction.^{1,63} This method focuses on determining the electron density (physical characteristic) of a molecule in order to reach some conclusions about molecular properties. It has the added ability of performing calculations that contain metals as part of the molecule framework, which is a matter of great importance for this study as it will be expanded on later.

DFT methods help to address the two major criticisms that *ab initio* methods incur. Firstly, all data abstracted from an *ab initio* calculation is completely dependent on the determination of the wavefunction, a characteristic that is complicated and

problematic as it cannot be measured physically and only exists as a mathematical entity. Secondly, the effect of electron correlation is absent from native *ab initio* calculations.⁶⁵ However, the wavefunction has served well in making probable predictions to the location of an electron in a molecule and in depicting the energy of the molecule together with other actual properties of the molecule. For many years the computational chemist has tried to determine the energy and derivative properties of atoms and molecules from actual existing properties of atoms and molecules. Thomas and Fermi (1927) found a direct relationship between the electron density of a molecule and the wavefunction of a many-electron molecule.^{1,65,73} It was this key relationship that prompted Hohenberg and Kohn (1964) to prove that electron density is the only requirement for the exploration of molecular properties of a system, in turn establishing the platform for DFT methods.^{1,74} The core DFT methods then focused on modelling the electron correlation via general functionals of the electron density.^{63,71}

2.1.3.1 Functionals

A functional is defined as a function of a function. Mathematically, a function can be denoted as:

$$y = f(x) \tag{2.9}$$

where f is a function of the variable x . A functional F , is a function mapping a function f to a scalar y as $y = F[f]$ and this function f becomes the input for the functional F making it a function of a function.^{1,3,63}

Similarly, electron density, $\rho(x, y, z)$, is a function of three variables, namely the x , y and z positions of the electrons, regardless of the number of electrons. The electron density then becomes a functional for the determination of a molecule's energy (equation 2.10). In essence, the aim of DFT is to find the value of the functional, F .

This method poses a great advantage over *ab initio* methods in that the calculation remains uncomplicated regardless of the increase of electrons in a molecular system.

$$\text{Energy} = F[\rho] \quad 2.10$$

As all modern day density functional theories stem from the Hohenberg-Kohn theorems, it is imperative to look at the history of the beginnings of DFT and how its foundation was cemented after Thomas and Fermi's discovery which demonstrated that DFT is a legitimate quantum chemical tool.³

2.1.3.2 Hohenberg-Kohn: Theorem 1^{3,65,71}

“The external potential $V_{ext}(\vec{r})$ is (to within a constant) a unique functional of $\rho(\vec{r})$; since, in turn $V_{ext}(\vec{r})$ fixes \hat{H} we see that the full many particle ground state is a unique functional of $\rho(\vec{r})$.”⁷⁴

This theorem provides proof of the 1:1 relationship between electron density and the Hamiltonian operator, \hat{H} . Since integration of the density quantifies the number of electrons (N) the only unknown is the external potential (V_{ext}), being the potential created by the nuclei and dependent on their charges and position.^{3,65} In order to prove that the ground state density (ρ_0) determines the external potential, an assumption to the contrary must be made, leading to the generation of an impossible result, a “*reductio ad absurdum*”.

Therefore, consider the following assumption: two different external potentials V_1 and V_2 (differing by more than a constant) produce the same electron density linked to the corresponding non-degenerate ground states $\rho(\vec{r})$ of N particles. V_1 and V_2 appear in different Hamiltonian operators, \hat{H}_1 and \hat{H}_2 , where the only difference is in the external potential: $\hat{H}_1 = \hat{T} + \hat{V}_{ee} + V_1$ and $\hat{H}_2 = \hat{T} + \hat{V}_{ee} + V_2$. Each Hamiltonian is associated with different ground state wave functions, Ψ_1 and Ψ_2 and

corresponding ground state energies, E_1 and E_2 where $E_1 \neq E_2$. According to the variational principle of molecular orbital theory, the expectation value of \hat{H}_1 over the trial wavefunction Ψ_2 must be higher than the ground-state energy of E_1 , as shown in equation 2.11.

$$E_1 < \langle \Psi_2 | \hat{H}_1 | \Psi_2 \rangle = \langle \Psi_2 | \hat{H}_2 | \Psi_2 \rangle + \langle \Psi_2 | \hat{H}_1 - \hat{H}_2 | \Psi_2 \rangle \quad 2.11$$

Alternatively, because the only difference in the Hamiltonian operators is the external potential

$$E_1 < E_2 + \langle \Psi_2 | \hat{T} + \hat{V}_{ee} + V_1 - \hat{T} - \hat{V}_{ee} - \hat{V}_2 | \Psi_2 \rangle \quad 2.12$$

which then yields

$$E_1 < E_2 + \int \rho(\vec{r}) \{V_1 - V_2\} d\vec{r} \quad 2.13$$

As there is no distinction between 1 and 2, the indices in the expression for 2.13 can be interchanged to produce another valid expression.

$$E_2 < E_1 + \int \rho(\vec{r}) \{V_2 - V_1\} d\vec{r} \quad 2.14$$

Adding equations 2.13 and 2.14 produces the following contradiction.

$$E_1 + E_2 < \int \rho(\vec{r}) \{V_1 - V_2\} d\vec{r} + \int \rho(\vec{r}) \{V_2 - V_1\} d\vec{r} + E_2 + E_1$$

$E_1 + E_2 < \int [V_1 - V_2 + V_2 - V_1] \rho(\vec{r}) d\vec{r} + E_2 + E_1$, assuming that the ground state densities linked to Ψ_1 and Ψ_2 were the same, the sum of the integrals must equal zero to yield,

$$E_1 + E_2 < E_2 + E_1 \quad 2.15$$

This conclusion is impossible and therefore proves the initial assumption of two different external potentials yielding the same ground state electron density as incorrect. So, it can be stated that the non-degenerate ground-state density uniquely specifies the external potential V_{ext} which directly relates to the Hamiltonian and in turn the wavefunction.^{3,65}

Because the complete ground state energy E_0 is a functional of the ground state electron density ρ_0 , the equation (see 2.16), can be written to show the dependency of the individual components on the ground state density as well.

$$E_0[\rho_0] = T[\rho_0] + E_{ee}[\rho_0] + E_{Ne}[\rho_0] \quad 2.16$$

Equation 2.16 can be further manipulated by separating the potential energy (E_{Ne} , due to the nuclei-electron attraction), that is dependent on the actual system (equation 2.17), from those variables independent of N , R_A and Z_A , equation 2.18.

$$E_{Ne}[\rho_0] = \int \rho_0(\vec{r}) V_{Ne} d\vec{r} \quad 2.17$$

$$E_0[\rho_0] = \underbrace{\int \rho_0(\vec{r}) V_{Ne} d\vec{r}}_{\text{System dependent}} + \underbrace{T[\rho_0] + E_{ee}[\rho_0]}_{\text{System independent (universal functionals)}} \quad 2.18$$

System dependent System independent
(universal functionals)

The independent quantities can be collated into the Hohenberg-Kohn functional giving

$$E_0[\rho_0] = \int \rho_0(\vec{r}) V_{Ne} d\vec{r} + F_{HK}[\rho_0] \quad 2.19$$

Once any density value is substituted into the Hohenberg-Kohn functional the following result is achieved.

$$F_{HK}[\rho] = T[\rho] + E_{ee}[\rho] = \langle \Psi | \hat{T} + \hat{V}_{ee} | \Psi \rangle \quad 2.20$$

Equation 2.20 indicates that the sum of the kinetic energy and the electron-electron repulsion operator with the ground state wavefunction (associated with the lowest energy) is linked to the input density. The attraction of this functional is its independence from the molecular system and its application to either simple atoms or complex molecules. Although Theorem 1 concluded that the ground state density was sufficient to determine all properties under investigation for a molecular system, there was no assurance that the predicted density actually is the ground state density being sought, prompting Hohenberg and Kohn's need for a second theorem.

2.1.3.3 Hohenberg-Kohn: Theorem 2^{3,65}

" $F_{HK}[\rho]$, the functional that delivers the ground state energy of the system, delivers the lowest energy if and only if the input density is the true ground state density, ρ_0 ."^{65,74}

In a similar fashion to molecular orbital theory, Hohenberg and Kohn showed that the density also obeys a variational principle:

$$E_0 \leq E[\rho'] = T[\rho'] + E_{Ne}[\rho'] + E_{ee}[\rho'] \quad 2.21$$

As previously mentioned, any trial density $\rho'(\vec{r})$ defines its own Hamiltonian \hat{H} , and in turn its own wavefunction Ψ' . That being the case, the following equation is obtained,

$$\langle \Psi' | \hat{H} | \Psi' \rangle = T[\rho'] + V_{ee}[\rho'] + \int \rho'(\vec{r}) V_{ext} d\vec{r} = E[\rho'] \geq E_0[\rho_0] = \langle \Psi_0 | \hat{H} | \Psi_0 \rangle \quad 2.22$$

In principle, this simply means that a trial density $\rho'(\vec{r})$ which provides a minimum energy as calculated by equation 2.19, will produce an answer that is the exact ground state density. Herein, lies the problem. How does one go about rationally choosing a trial density for this purpose? The challenge lies in the nature of the functional itself. So far, Hohenberg and Kohn have shown a sequential move from $\rho \rightarrow V_{ext} \rightarrow \hat{H} \rightarrow \Psi \rightarrow E$, however, no suggestion is made to use the density as an argument in a chemical expression independent of the wavefunction that will still give the ground state energy. As long as the Hamiltonian and the wavefunction are involved, solving the Schrödinger equation will always have to be the final outcome, in turn retaining the complexity of the energy calculation and defeating the purpose of DFT.

Up to this point Hohenberg and Kohn used the Thomas-Fermi theorem to theoretically develop DFT while providing no prescription on how to construct or approximate a proper functional for the calculation. A year later, in 1965, Kohn and Sham decided to rectify this by adapting the DFT model into a practical version to help solve this dilemma.

2.1.3.4 The Kohn-Sham Approach^{1,63,65,71,73}

While Kohn and Sham were proposing suggestions on how to approach the unknown universal functionals previously mentioned in equation 2.18, they realized that most problems with direct density functionals stemmed from the determination of the kinetic energy. Since orbital approaches such as the Hartree-Fock method are known to accurately determine the kinetic energy, this prompted Kohn and Sham to use the same principle for their model.

Kohn and Sham adapted the model of a fictitious system from a set of orbitals of non-interacting electrons with the same ground state electron density as a real system of interacting electrons. Since density determines the position and atomic numbers of the nuclei, these quantities should be identical in both the real and fictitious

environment. This fictitious environment of non-interacting electrons was proposed as it would allow a major part of the kinetic energy to be calculated with good accuracy. By using this method most of the information would be computed exactly, leaving only a small part of the total energy to be determined by an approximate functional.

It would be a great advantage to look at some fundamental knowledge that will help to understand the Kohn-Sham (KS) equations that are discussed later on. Defining the ground state energy of an atomic or molecular system for N -electrons leads to the expression where

$$E_0 = \min_{\rho \rightarrow N} (F[\rho] + \int \rho(\vec{r}) V_{Ne} d\vec{r}) \quad 2.23$$

with the universal functional $F[\rho]$ being composed of the following energy contributions.

$$F[\rho(\vec{r})] = T[\rho(\vec{r})] + J[\rho(\vec{r})] + E_{ncl}[\rho(\vec{r})] \quad 2.24$$

where

$T[\rho(\vec{r})]$ is the kinetic energy of the electrons,

$J[\rho(\vec{r})]$ is the electron-electron repulsive (Coulombic) energy and

$E_{ncl}[\rho(\vec{r})]$ is the non classical energy due to self-interaction correction, exchange (antisymmetry) and electron correlation effects.

Of these energies, only $J[\rho]$ is known. Furthermore, in the Hartree-Fock model the wavefunction was built on a single Slater determinant Φ_{SD} constructed from N spin orbitals and used as an approximation to the true N -electron wavefunction. On the other hand, for a fictitious system of N non-interacting electrons moving in the effective potential V_{HF} , the Φ_{SD} can also be looked upon as an exact wavefunction leading to the following kinetic energy expression,

$$T_{HF} = -\frac{1}{2}\sum_i^N \langle \chi_i | \nabla^2 | \chi_i \rangle \quad 2.25$$

The chosen HF spin orbitals χ_i are expected to produce a minimum value for E_{HF} , provided that χ_i remains orthonormal[‡].

$$E_{HF} = \min_{\Phi_{SD \rightarrow N}} \langle \Phi_{SD} | \hat{T} + \hat{V}_{Ne} + \hat{V}_{ee} | \Phi_{SD} \rangle \quad 2.26$$

This kinetic energy expression for a non-interacting system is exploited in order to calculate the major part of the kinetic energy for a real system of interacting electrons. Once it is known that the exact wavefunction of non-interacting fermions[§] are Slater determinants it becomes possible to set up a fictitious system with a Hamiltonian whereby an effective local potential $V_s(\vec{r})$ is introduced without the description for electron-electron interactions.

$$\hat{H}_s = -\frac{1}{2}\sum_i^N \nabla_i^2 + \sum_i^N V_s(\vec{r}_i) \quad 2.27$$

Using different variable notations (Θ_S and φ) in order to distinguish from HF theory, we can express the Slater determinants (Θ_S) for the ground state wavefunction, determine the spin orbitals (φ) and indicate the one-electron Kohn-Sham operator by the respective equations.

$$\Theta_S = \frac{1}{\sqrt{N!}} \begin{vmatrix} \varphi_1(\vec{x}_1) & \varphi_2(\vec{x}_1) & \dots & \varphi_N(\vec{x}_1) \\ \varphi_1(\vec{x}_2) & \varphi_2(\vec{x}_2) & \dots & \varphi_N(\vec{x}_2) \\ \vdots & \vdots & & \vdots \\ \varphi_1(\vec{x}_N) & \varphi_2(\vec{x}_N) & \dots & \varphi_N(\vec{x}_N) \end{vmatrix} \quad 2.28$$

[‡] Two vectors which are orthogonal and of length 1 are said to be orthonormal.

[§] Particles such as electrons with spin = $\frac{1}{2}$ and with an antisymmetric wavefunction.

$$\hat{f}^{KS} \varphi_i = \varepsilon_i \varphi_i \quad 2.29$$

$$\hat{f}^{KS} = -\frac{1}{2} \nabla^2 + V_S(\vec{r}) \quad 2.30$$

These orbitals of the fictitious system are classified as the Kohn-Sham orbitals. Finally, in choosing the effective potential V_S for which an electron density, generated from the fictitious system, exactly equals the ground state density of the real system, this firmly establishes a link between the two systems as Kohn and Sham set out to do, shown in equation 2.31.

$$\rho_S(\vec{r}) = \sum_i^N \sum_s |\varphi_i(\vec{r}, s)|^2 = \rho_0(\vec{r}) \quad 2.31$$

Adapting equation 2.25 to best solve for the kinetic energy of the artificial system by using the electron density of the real system gives

$$T_S = -\frac{1}{2} \sum_i^N \langle \varphi_i | \nabla^2 | \varphi_i \rangle \quad 2.32$$

Although both systems share the same density, Kohn and Sham anticipated that their kinetic energies would differ and accounted for this by introducing the following contributions to the functionals.

$$F[\rho(\vec{r})] = T_S[\rho(\vec{r})] + J[\rho(\vec{r})] + E_{XC}[\rho(\vec{r})] \quad 2.33$$

The new term E_{XC} , the *exchange-correlation energy*, is further defined by the following expression,

$$E_{XC}[\rho] \equiv (T[\rho] - T_S[\rho]) + (E_{ee}[\rho] - J[\rho]) = T_C[\rho] + E_{ncl}[\rho] \quad 2.34$$

where

T_C is the correction to the kinetic energy deriving from the interacting nature of the electrons and

E_{ncl} represents all non-classical corrections to the electron-electron repulsion energy.

E_{XC} signifies a collection of the effects of quantum mechanical exchange and correlation, the correction for the classical self-interaction energy and the difference in kinetic energy between the fictitious non-interacting system and the real system.

Before going on to solve for the ground state energy, equation 2.33 is rewritten into the energies of the interacting real system with an emphasis on the orbital dependency as indicated in equations 2.31 and 2.32, respectively, giving

$$\begin{aligned}
 E[\rho(r)] &= T_S[\rho] + J[\rho] + E_{XC}[\rho] + E_{Ne}[\rho] \\
 &= T_S[\rho] + \frac{1}{2} \iint \frac{\rho(\vec{r}_1)\rho(\vec{r}_2)}{r_{12}} d\vec{r}_1 d\vec{r}_2 + E_{XC}[\rho] + \int V_{Ne}\rho(\vec{r})d\vec{r} \\
 &= -\frac{1}{2} \sum_i^N \langle \varphi_i | \nabla^2 | \varphi_i \rangle + \frac{1}{2} \sum_i^N \sum_j^N \iint |\varphi_i(\vec{r}_1)|^2 \frac{1}{r_{12}} |\varphi_j(\vec{r}_2)|^2 d\vec{r}_1 d\vec{r}_2 + E_{XC}[\rho(\vec{r})] - \\
 &\quad \sum_i^N \int \sum_A^M \frac{Z_A}{r_{1A}} |\varphi_i(\vec{r}_1)|^2 d\vec{r}_1
 \end{aligned} \tag{2.35}$$

From here, the variational principle is applied under the constraint of $\langle \varphi_i | \varphi_j \rangle = \delta_{ij}$ in order to work out what condition must be fulfilled by the orbitals (φ_i) to minimize the energy expression. This leads to the following equation:

$$\begin{aligned}
 &\left(-\frac{1}{2} \nabla^2 + \left[\int \frac{\rho(\vec{r}_2)}{r_{12}} d\vec{r}_2 + V_{XC}(\vec{r}_1) - \sum_A^M \frac{Z_A}{r_{1A}} \right] \right) \varphi_i \\
 &= \left(-\frac{1}{2} \nabla^2 + V_{eff}(\vec{r}_1) \right) \varphi_i = \varepsilon_i \varphi_i
 \end{aligned} \tag{2.36}$$

where, M is equal to the number of nuclei and Z_A the charges of the nuclei.

Comparing equation 2.36 with the one-electron Kohn-Sham operator equation, that is, equations 2.29 and 2.30 respectively, we see that V_{eff} here is the same as V_S from equation 2.30.

$$V_S(\vec{r}) \equiv V_{eff}(\vec{r}) = \int \frac{\rho(\vec{r}_2)}{r_{12}} d\vec{r}_2 + V_{XC}(\vec{r}_1) - \sum_A^M \frac{Z_A}{r_{1A}} \quad 2.37$$

Finally, when we know the mixture of contributions in equation 2.37, the potential V_S can then be inserted into the one-particle equations which leads us to iteratively determine the KS orbitals (equations 2.28–2.30), the ground state density (equation 2.31) and lastly the ground state energy by using equation 2.33.

Special mention should be made of V_{XC} , the potential due to the exchange-correlation energy E_{XC} . Although there is a dilemma on how this energy should be expressed it is merely defined as the functional derivative of E_{XC} with respect to ρ as follows:

$$V_{XC} \equiv \frac{\partial E_{XC}}{\partial \rho} \quad 2.38$$

In summary, the Kohn-Sham approach is, in principle, exact whereas the HF model, which begins with an approximation to the wavefunction, does not allow the determination of a true solution. In the KS approach an approximation is made only when the E_{XC} and V_{XC} require solving. This ultimately leads to the challenging goal of DFT, or rather, to find the best approximations to these two quantities.

2.1.3.5 DFT models

DFT functionals are divided into three classes:

- (i) Local Density
- (ii) Gradient Corrected
- (iii) Hybrid

(i) Local Density^{65,71}

The critical assumption of the Local Density Approximation (LDA) is that for a gaseous molecular system with many electrons, the local density should be treated as a uniform electron gas. The exchange energy of an electron (ϵ_X) for a uniform electron gas is given by equation 2.39** below.

$$E_X^{LDA}[\rho] = -C_X \int \rho^{4/3}(r) dr$$

$$\epsilon_X^{LDA}[\rho] = -C_X \rho^{1/3} \quad 2.39$$

Where C_X is a numerical constant.

The correlation between electrons of the same (parallel) spin is different from that between electrons of opposite spin. By definition, the exchange energy is a sum of contributions by the α and β spin densities since the exchange energy only involves electrons of parallel spin. In cases where the α and β densities are unequal, LDA (where the sum of the densities is raised to the 4/3 power) has been replaced by the Local Spin Density Approximation (LSDA), calculated by the sum of the individual densities raised to the 4/3 power, as shown in equation 2.40.

$$E_X^{LSDA}[\rho] = -2^{1/3} C_X \int [\rho_\alpha^{4/3} + \rho_\beta^{4/3}] dr$$

$$\epsilon_X^{LSDA} = -2^{1/3} C_X [\rho_\alpha^{1/3} + \rho_\beta^{1/3}] \quad 2.40$$

Revising this equation to represent the total density and the spin polarization ζ leads to the following.

** Derived with information from the Thomas-Fermi-Dirac method

$$\varepsilon_X^{LSDA}[\rho] = -\frac{1}{2}C_X\rho^{1/3}[(1 + \zeta)^{4/3} + (1 - \zeta)^{4/3}] \quad 2.41$$

$$\zeta = \frac{\rho_\alpha - \rho_\beta}{\rho_\alpha + \rho_\beta}$$

When dealing with closed-shell systems, (a common occurrence), where there are an even number of electrons divided into pairs of opposite spin, LSDA=LDA with the approximations used interchangeably. In the general case (with open-shell systems) equations 2.39 and 2.40 will need to be used.

Another method (denoted as the X_α method) which contributes to LDAs is proposed by Slater, which accordingly neglects the correlation energy, making the exchange expression read as follows.

$$\varepsilon X_\alpha[\rho] = -\frac{3}{2}\alpha C_X\rho^{1/3} \quad 2.42$$

The current value used for α is $\alpha = \frac{3}{4}$, which is different from that of the original method where $\alpha = 1$, since the current value has shown a better agreement for both atomic and molecular systems. This exchange functional is frequently referred to as the Slater exchange when the electron density is raised to the 4/3 power or 1/3 power for the energy density.

On the other hand, highly accurate Monte Carlo simulations have been used to determine the correlation energy ε_C of a homogenous electron gas for different densities. However, in order to make use of these results in DFT calculations, a suitable analytical interpolation expression is required. Vosko, Wilk and Nusair (VWN)⁷⁵ developed such an expression (shown in equation 2.43) which is fairly widely used and considered to be an accurate fit.

$$\varepsilon_c^{VWN}(r_S, \zeta) = \varepsilon_c(r_S, 0) + \varepsilon_a(r_S) \left[\frac{f(\zeta)}{f''(0)} \right] [1 - \zeta^4] + [\varepsilon_c(r_S, 1) - \varepsilon_c(r_S, 0)] f(\zeta) \zeta^4$$

$$f(\zeta) = \frac{(1 + \zeta)^{4/3} + (1 - \zeta)^{4/3} - 2}{2(2^{1/3} - 1)}$$
2.43

$\zeta = 0 = \text{unpolarised}$; $\zeta = 1 = \text{spin polarised}$

Functionals $\varepsilon_c(r_S, \zeta)$ and $\varepsilon_a(r_S)$ are parameterized according to the following equation:

$$\varepsilon_{c/a}(x) = A \left\{ \ln \frac{x^2}{X(x)} + \frac{2b}{Q} \tan^{-1} \left(\frac{Q}{2x+b} \right) - \frac{bx_0}{X(x_0)} \left[\ln \frac{(x-x_0)^2}{X(x)} + \frac{2(b+2x_0)}{Q} \tan^{-1} \left(\frac{Q}{2x+b} \right) \right] \right\}$$
2.44

where:

$$x = \sqrt{r_S}$$

$$X(x) = x^2 + bx + c$$

$$Q = \sqrt{4c - b^2}$$

Parameters A , x_0 , b and c are fitting constants and are different for $\varepsilon_c(r_S, 0)$, $\varepsilon_c(r_S, 1)$ and $\varepsilon_a(r_S)$.

In 1992, Perdew and Wang modified $\varepsilon_{c/a}(r_S)$, shown in equation 2.45, and used it in the PW91 functional.⁶⁵

$$\frac{\varepsilon_c^{PW91}}{a}(x) = -2a\rho(1 + \alpha x^2) \ln \left(1 + \frac{1}{2a(\beta_1 x + \beta_2 x^2 + \beta_3 x^3 + \beta_4 x^4)} \right)$$
2.45

LSDA methods work well for determining molecular properties such as optimized structures, harmonic frequencies or charge moments. They are comparable to wave

mechanics HF approximations and sometimes produce better results. However, LSD approximation generally underestimates the exchange energy by ~10%, which in turn affects bond energies while overestimating electron correlation by a factor close to 2 and thus overestimating bond strengths.^{65,71}

(ii) Gradient Corrected Methods^{65,71}

Simply expressed, this method is the calculation of the electron density linked with a gradient^{††} correction factor. The gradient factor accounts for the non-uniformity of the electron density, and the method is therefore known as the Gradient Corrected method, the Generalised Gradient Approximation (GGA) method or a semi-local method. A generic representation of this method would be

$$E_{XC}^{GGA}[\rho_\alpha, \rho_\beta] = \int f(\rho_\alpha, \rho_\beta, \nabla\rho_\alpha, \nabla\rho_\beta) d\vec{r} \quad 2.46$$

This method is considered to be an improvement over the LSDA approach due to its non-uniform system. There have been many alterations, modifications and corrections to either the exchange or correlation functionals. Here follows the most common ones used in theory or practice.

1. Perdew and Wang (PW86)⁷⁶ proposed these modifications to the LSDA exchange expression to give,

$$E_X^{PW86} = \varepsilon_X^{LDA} (1 + ax^2 + bx^4 + cx^6)^{1/15} \quad 2.47$$

where:

$$x = \frac{|\nabla\rho|}{\rho^{4/3}} = \text{dimensionless gradient variable}$$

^{††} A function that measures the rate of change of some property and usually denoted ∇

a, b and $c =$ suitable constants

- Becke's⁷⁷ correction (B or B88) is for the LSDA exchange energy which has the correct $-r^{-1}$ asymptotic behaviour for the energy density but not for the exchange potential.

$$\begin{aligned}\varepsilon_X^{B88} &= \varepsilon_X^{LDA} + \Delta\varepsilon_X^{B88} \\ \Delta\varepsilon_X^{B88} &= -\beta\rho^{1/3} \frac{x^2}{1+6\beta x \sinh^{-1} x}\end{aligned}\quad 2.48$$

x is defined in equation 2.47 and the β parameter is determined by fitting to known atomic data.

- Another Perdew and Wang proposal regarding an exchange functional similar to B88 which must be used in connection with the PW91 correlation functional given in equation 2.49, where a_{1-5} and b again are suitable constants, while x has been defined in equation 2.47.

$$\varepsilon_X^{PW91} = \varepsilon_X^{LDA} \left(\frac{1+xa_1 \sinh^{-1}(xa_2)+(a_3+a_4e^{-bx^2})x^2}{1+xa_1 \sinh^{-1}(xa_2)+a_5x^2} \right) \quad 2.49$$

- Lee, Yang and Parr (LYP)⁷⁸ proposed a functional for the correlation energy which is fairly popular. Parameters a, b, c and d are determined by fitting them to data for the helium atom.

$$\begin{aligned}E_c^{LYP} &= -a \frac{\gamma}{(1+d\rho^{-1/3})} - ab \frac{\gamma e^{-c\rho^{-1/3}}}{9(1+d\rho^{-1/3})\rho^{8/3}} \\ &\quad \times \left[18(2^{2/3})C_F(\rho_\alpha^{8/3} + \rho_\beta^{8/3}) - 18\rho t_w + \rho_\alpha(2t_w^\alpha + \nabla^2\rho_\alpha) \right. \\ &\quad \left. + \rho_\beta(2t_w^\beta + \nabla^2\rho_\beta) \right]\end{aligned}\quad 2.50$$

$$\gamma = 2 \left[1 - \frac{\rho_\alpha^2 + \rho_\beta^2}{\rho^2} \right] \text{ and } t_w^\sigma = \frac{1}{8} \left(\frac{|\nabla \rho_\sigma|^2}{\rho_\sigma} - \nabla^2 \rho_\sigma \right)$$

The t_w functional is called the local Weizsacker kinetic energy density. The LYP functional does not predict any parallel spin correlation when the γ factor becomes zero, which means that when all the spins are aligned the $\rho = \rho_\alpha, \rho_\beta = 0$.

5. Perdew (P86 functional)^{79,80} proposed a gradient correction to the LSDA result.

$$\varepsilon_c^{P86} = \varepsilon_c^{LDA} + \Delta\varepsilon_c^{P86} \quad 2.51$$

6. The P86 functional was later modified by Perdew and Wang in 1991, known as PW91 or P91.

$$\Delta\varepsilon_c^{PW91}[\rho] = \rho(H_0(t, r_s, \zeta) + H_1(t, r_s, \zeta)) \quad 2.52$$

GGA methods are considered to be the slaves of DFT and gives significant improvement over LSDA methods.

(iii) Hybrid Methods⁷¹

Hybrid methods are probably the most commonly used in DFT. A hybrid method is conceived as a Hartree-Fock approximation to the exchange energy and a DFT approximation to the exchange energy all combined with the functional that includes electron correlation. This is done by connecting the exchange-correlation energy and the corresponding potential, linking both the fictitious and the real system. The Adiabatic Connection Formula (ACF) is obtained from this relationship and involves integration over the parameter λ which “turns on” the electron-electron interaction.

$$E_{xc} = \int_0^1 \langle \Psi_\lambda | V_{xc}(\lambda) | \Psi_\lambda \rangle d\lambda \quad 2.54$$

Taking V_{xc} to be linear in λ the integral is given as the average value at both endpoints.

$$E_{xc} \simeq \frac{1}{2} \langle \Psi_0 | V_{xc}(0) | \Psi_0 \rangle + \frac{1}{2} \langle \Psi_1 | V_{xc}(1) | \Psi_1 \rangle \quad 2.55$$

Only the exchange energy exists when $\lambda = 0$, as the electrons are non-interacting, and consequently no correlation energy is produced. The exact wavefunction here is due to a single Slater determinant made up of KS orbitals, and the exchange energy is exactly that given by HF theory. On the other hand, if the KS orbitals are identical to the HF orbitals, then the “exact” exchange can be considered to be the exchange energy calculated by HF wave mechanics methods. As the last term in equation 2.55 is unknown, the LSDA result is used as an approximation,⁸¹ giving,

$$E_{xc} = \frac{1}{2} E_x^{exact} + \frac{1}{2} (E_x^{LSDA} + E_c^{LSDA}) \quad 2.56$$

Because GGA methods have shown improvement on some results obtained by LDA methods, a generalized version of the H+H method is defined by giving the exchange energy as an agreeable collection of LSDA, exact exchange and a gradient correction term. Similarly, the correlation energy can be taken as a sum of the LSDA formula and a gradient correction term.

$$E_{xc}^{B3} = (1 - a) E_x^{LSDA} + a E_x^{exact} + b \Delta E_x^{B88} + E_c^{LSDA} + c \Delta E_c^{GGA} \quad 2.57$$

The a , b and c parameters are determined by fitting to experimental data, and depend on the form chosen for E_c^{GGA} . Models that include exact exchange are called hybrid methods. The Becke 3 term with Lee, Yang, Parr exchange (B3LYP)⁸² is one such example and is described by the following equation⁷¹:

$$E_{xc}^{B3LYP} = (1 - a)E_x^{LSDA} + aE_x^{exact} + b\Delta E_x^{B88} + (1 - c)E_c^{LSDA} + cE_c^{LYP} \quad 2.58$$

2.1.4 TD-DFT

The TD-DFT approach is an extension of Hohenberg-Kohn-Sham DFT found on the Runge-Gross (RG) theorem.⁸³ It allows one to calculate the properties of a system in its ground state, subject to a time-dependent perturbation, or in the process changing its external potential.⁸⁴⁻⁸⁶ The excitation energy of a system corresponds to the poles of the function describing the linear electron density change when the external potential changes. Within this approach, the excitation energies and oscillator strengths are acquired from the eigenvalue equation 2.59,⁸⁷⁻⁸⁹

$$\Omega \vec{F}_i = \omega_i^2 \vec{F}_i \quad 2.59$$

where, ω_i are the excitation energies, and the oscillator strengths may be obtained from the eigenvectors \vec{F}_i .⁸⁷ TD-DFT linear response theory^{85,87,89,90} is reported as the most dominant electronic structure method for the calculation of vertical electronic excitation energies.^{91,92} TD-DFT has shown its reliability by successfully calculating oscillator strengths and excitation energies^{83,88,89,93-97} of large organic molecules,^{89,97,98} transition metal complexes such as metalporphyrins⁹⁹ as well as higher fullerenes.⁹⁵

2.1.5 CURRENT STUDY

The DFT and TD-DFT method is used in this investigation to examine the organometallic bond of B₁₂ analogues, since it has already proven its superiority in describing the electronic structure of atoms, molecules, clusters, surfaces and solids. In addition, the DFT method is proven successful as a universal language for electronic structure theory across the disciplines of organic chemistry, inorganic

chemistry, surface chemistry, materials science and physics.⁵³ The four functionals chosen and used in this study are BP86 (GGA),^{77,79,80} M06L (meta-GGA),¹⁰⁰ B3LYP¹⁰¹ and PBE1PBE (hybrid).^{102,103}

CHAPTER 3

LITERATURE REVIEW

This chapter aims to review the computational efforts made towards discovering factors that lead to the homolytic cleavage of the Co–C bond in AdoCbl. Although there has been a substantial amount of theoretical research^{7,11,17,19,22,34,35,45,46,51,55,56,104-138} conducted in the area of vitamin B₁₂ chemistry, in this chapter the main emphasis is placed on those studies highlighting and using DFT methods; other methods are briefly mentioned. The chapter concludes with a brief rationale on the types of functionals chosen and used in the current investigation.

3.1 STERIC AND ELECTRONIC EFFECTS

Kozłowski *et al.*^{58,59} shed some light on the nature of the Co–C bond through DFT studies. They investigated the steric and electronic factors by using the B3LYP hybrid functional with the 6-31G(d) (for H, C, N) and Ahlrichs' VTZ (for Co) basis sets. The models used included a truncated corrin macrocycle plus cobalt atom and studies were conducted by altering the nature of both the α and β ligands, see **Figure 3.1**.

Imidazole (Im), dimethylbenzimidazole (DBI) and water, presumably, were used as the α *trans* ligand while the β axial ligand was modelled by various groups with different steric sizes including cyano, ethynyl, methyl, ethyl, *isopropyl*, *tert*-butyl and 5'-deoxy-5'-adenosyl. The variation of the *trans* ligand had no major effect on the Co–R bond length (varied by 0.002Å when DBI was replaced by Im) which was consistent with spectroscopic evidence from Spiro *et al.*¹³⁹ However, they found that as the nature of the ligand became more basic (Im > DBI > H₂O) so did the strength

of the bond to the Co atom. Irrespective of the ligand basicity, a simultaneous stretching or compression of the Co–R (upper ligand) and Co–Y (lower ligand) bond was found by the authors. This effect was also noticed by De Ridder *et al.*¹⁴⁰ in crystallographic data and was initially described by Bürgi *et al.*¹⁴⁰ as the “inverse” *trans* effect.

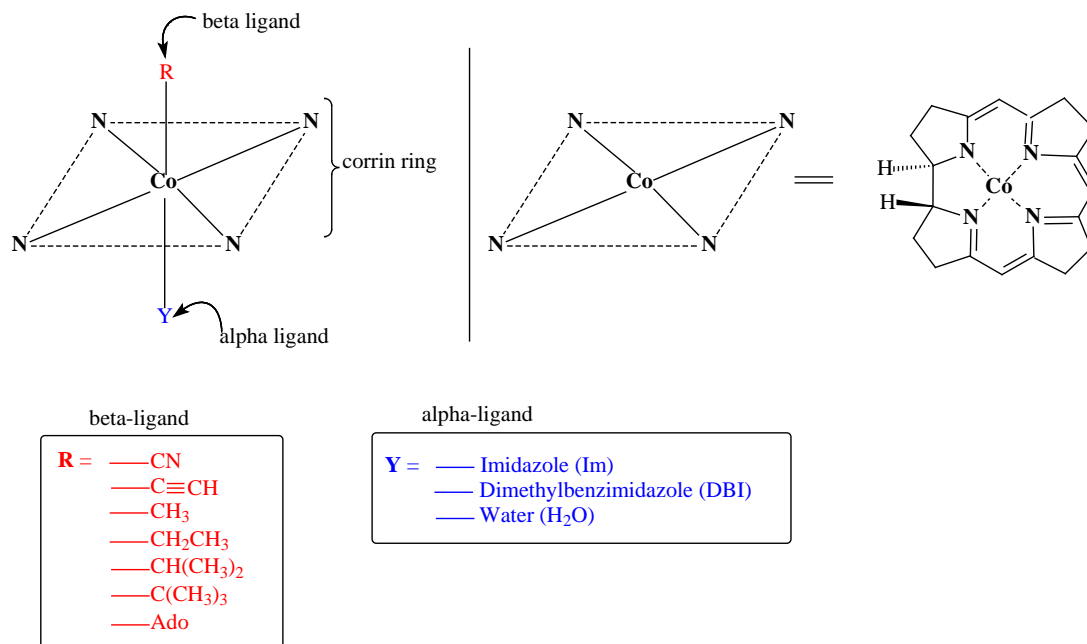


Figure 3.1: Molecular structure of model cobalamins with a change in R and Y, as used in the study by Kozłowski *et al.*^{58,59}

This effect was attributed to the conformational change of the corrin macrocycle ring. As the Co–R bond increased in length, the distortion of the corrin ring was described to flatten itself with respect to the corrin average plane (torsion angles used are further defined in Chapter 5). Also, manipulation of the Co–Y bond length and the angle of the β ligand relative to the macrocycle had no significant effect on the organometallic bond length. However, a change in the β ligand affected a change in both the Co–R and Co–Y bonds lengths. If an electron-withdrawing β ligand was used, the Co–Y bond decreased in length while the Co–R bond experienced virtually no change. When the β ligand was replaced by an electron-donating group the

“inverse” *trans* effect occurred, and a systematic effect on the conformation of the corrin macrocycle took place.

Finally, based on the DFT calculations made, Kozłowski *et al.* concluded that the initial activation of the organometallic bond can be comprehended only on the basis of electronic factors. They suggested that when the coenzyme is surrounded, or embedded, in a rich polar amino acid protein matrix, this electrostatic atmosphere would allow the electron density to be reorganised in the X–Co–R moiety. This rearrangement would consequently lead to a homolytic breaking of the organometallic bond, since changes in electron density as a form of redistribution may arise in the forming or breaking of chemical bonds. In support of this statement they conducted calculations on a model of MeCbl, Im–[Co(III)corrin]–Me, in the presence and absence of an external negative charge. This charge was placed 3Å above the Co atom and in line with the Co–R bond.

Figure 3.2 graphically represents the trend observed in their investigation. It was found that energy curves for the model showed minima (A' and B') when in the presence of an electric field while those models (A and B) in the absence of the electric field steadily increased together with a systematic increase of the Co–R bond. Energy curves A and A' correspond to the model where only the Co–R bond was elongated, while B and B' represent the elongation of both the Co–R and Co–Y bonds according to the inverse *trans* effect. Kozłowski and co-workers observed significant energy costs when stretching both the Co–R and Co–Y bonds in the absence of an electric field (see B in **Figure 3.2**) and therefore concluded that two important factors encouraging labilisation would be the presence of an external electric field and cooperative motion between the Co–R and Co–Y inter-ligand bonds.

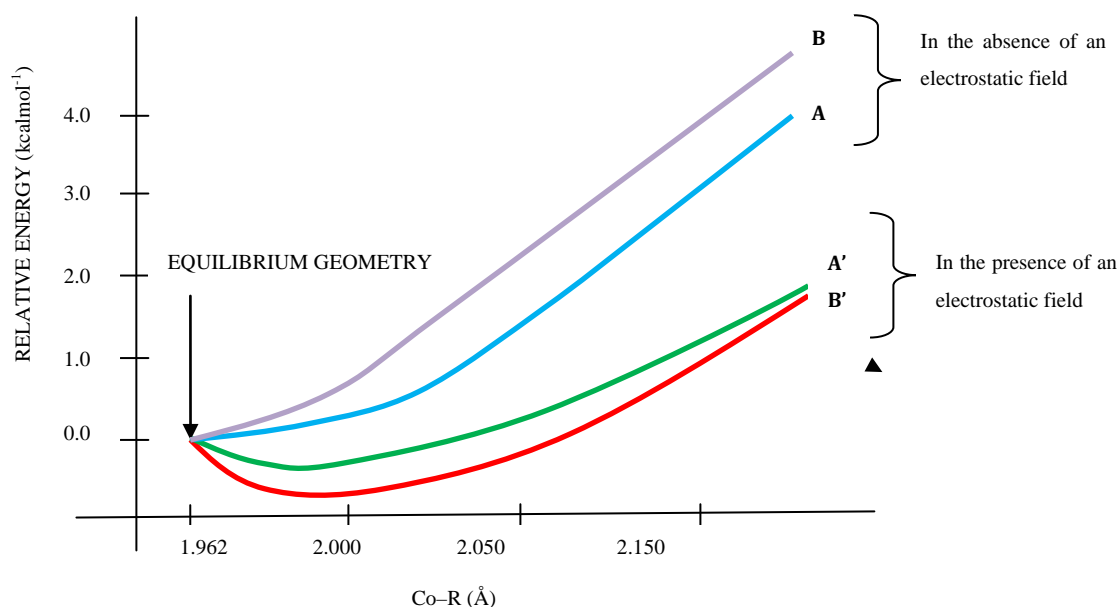


Figure 3.2: Illustrative trends of relative energies of Im-[Co(III)corrin]-Me in the presence and absence of an electrostatic environment.⁵⁹ A and B represents the Co-R and Co-Y bonds, respectively. A (blue line) and A' (green line) correspond to the elongation of the Co-R bond while B (purple line) and B' (red line) correspond to simultaneous elongation of both the Co-R and Co-Y bonds.

To study the energetics and structures of the bioactive cobalamins, Norrby and co-workers employed two DFT methods; B3LYP/lacvp^{**}, for geometry optimizations, and B3LYP/lacv3p^{**}, for a single point energy calculation on the optimized geometry. The lacvp^{**} basis set (lacvp is a valence + outermost core-basis) included effective core (Neon core) potentials and the m-shell for Co alone, while the rest of the atoms were treated with the 6-31G(d,p) basis set.

The intention of the authors was to explore the steric control of the Co-C bond strength by substituting β ligands of different sizes onto the Co atom while also probing electronic effects using a cyano (-CN) group as the β ligand. The model used was a naked corrin ring (as the presence of the amide side chains and nucleotide

loop had a minor influence on axial bond lengths)¹⁶, with the Co atom, an alkyl ligand, and a detached axial base, and included [Bzm-(Co(III)corrin)-R]ⁿ⁺, where R = methyl, ethyl, cyano, Ado, *isopropyl* and *tert*-butyl and [L-(Co(III)corrin)-CH₃]⁺, and where L=NH₃ or Im. The steric effect of the R group was found to increase the Co-C bond length in the [Bzm-(Co(III)corrin)-R]⁺ series in the order methyl < ethyl < *isopropyl* < *tert*-butyl from 1.97 Å to 2.11 Å. Similarly, under the same steric influence, the Co-N_{axial} bond length obtained was a poorly overestimated 2.33 Å for R=methyl to an incredible 2.77 Å for R=*tert*-butyl. When the axial base was changed for the [L-(Co(III)corrin)-CH₃]⁺ series, a minimal change to the Co-N_{axial} bond length was reported with no effect on the Co-C bond length or corrin ring folding, again in contrast to previous experiments. Finally, B3LYP calculations indicated that the LUMO and HOMO energy difference is higher (5.4 kcal mol⁻¹) in AdoCbl than in MeCbl, favouring homolytic breaking of the Co-C bond in AdoCbl. The electronic nature of the Co-C bond in both these equilibrium structures is different, and it was suggested that the 5'-deoxyadenosyl group of the AdoCbl interacts with the corrin ring inducing more electron density on the cobalt atom thus favouring homolytic over heterolytic cleavage.

In addition to the plethora of research covering cobalamin complexes, Witko *et al.*⁷ chose to investigate the applicability of the DFT method for cobalamin-ligand interactions. Their selection of functionals included B3LYP, UB3LYP, LDA-VWN and RPBE. Truncated model complexes were used with imidazole as the α ligand, while diverse moieties such as NO, O₂, CH₃, NO₂⁻ and H₂O were employed for the β ligand. Not surprisingly, the UB3LYP/B3LYP functional underestimated the binding energy values while calculations using the RPBE functional gave good reproducibility of the exact energy values (see data in **Table 1** extracted from original article, reference 7-experimental results were compared to calculated results).

Table 1: Binding energies (in kcal) and bond lengths (in Å) for the derivatives of cobalamins						
System	Cob(II)	Cob(II)-NO	Cob(II)-O ₂	Cob(II)-CH ₃	Cob(III)-NO ₂	Cob(III)-H ₂ O
Binding energies						
B3LYP	22.4	1.9	2.8	21.6	193.0, ^a 49.3 ^b	16.8
UB3LYP	–	5.4	–	–	–	–
RPBE	7.9	17.8	6.2	32.0	180.2 ^a	3.8
Exp	–	18.2 ^c	8.2, ^d 7.4, ^e 6 ^f	31.0 – 37.0 ^g	–	–
Co–L (Bond lengths/Å)						
B3LYP	–	1.873	2.836	1.960	1.948	2.069
UB3LYP	–	2.062	–	–	–	–
RPBE	–	1.840	1.910	1.940	1.910	2.000
Exp	–	–	1.930 ^h	1.990 ⁱ	1.941 ^j	1.962 ^k
Co–Imi (Bond lengths/Å)						
B3LYP	2.263	2.338	2.274	2.263	2.089	1.928
UB3LYP	–	2.355	–	–	–	–
RPBE	2.020	2.180	1.990	2.050	1.990	1.870
Exp	2.130 ^l	–	2.060 ^h	2.190 ⁱ	2.008 ^j	1.925 ^k
^a For NO ₂ [–] ^b For NO ₂ ^c pH = 7.4 ^d – 1 (references in original article)						

Both these functionals gave satisfactory geometric parameters for the Co–ligand bonds. The use of B3LYP and UB3LYP, by contrast, often resulted in an overestimated Co–C bond length. Finally, the LDA-VWN methodology produced shorter bonds when compared to experimental values and calculations that used hybrid functionals.

Jensen and Ryde⁴⁸ concluded from their study that irrespective of the nature of the N–base, constraints in the axial Co–N bond lengths cannot be the main reason for the catalytic power of cobalamin enzymes. Their investigation made use of the B3LYP functional and the basis sets used for geometry optimisation and potential energy curves were 6-31G(d) for all atoms except cobalt. The double- ζ basis set used by Schäfer *et al.*⁴⁹, consisting of one f, one d and two p functions with the contraction scheme (DZpdf), was used for the cobalt atom. Further noteworthy conclusions obtained from their study included the change in β ligand substituents as being responsible for inverse *trans* effects, as well as the fact that α to β *trans* induction effects with changed ligands were minimal, while β to α *trans* effects were found to

be quite large (electronic induction). In addition, the compression of the Co–N_{axial} bond had a modest effect on the corrin ring, (verified when measuring the corrin fold angle).

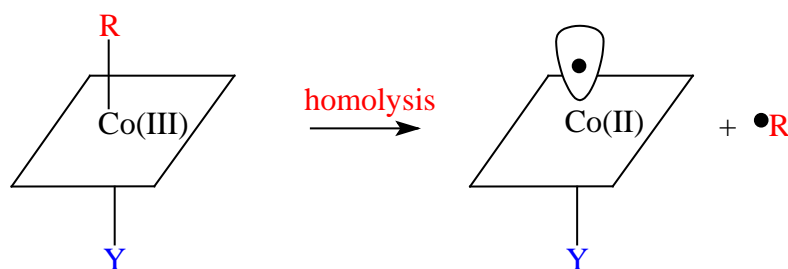
3.2 BOND DISSOCIATION ENERGIES

Maseras *et al.*^{9,141} focused on exploring the effect of the Co(III)–N_{axial} bond length on the homolytic cleavage of the organometallic bond. Their findings correlated with experimental observations^{41,130}, showing a negligible effect on the thermodynamics and kinetics of the homolytic cleavage. In addition, they looked at the effect of the protein environment on the axial ligand, as a significant enhancement to the homolysis of Co–C bond occurs in a biological environment. By using a nonlocal DFT method they investigated the dependence of both thermodynamics and kinetics of the Co–C bond homolysis. B3LYP was used in all calculations with the LANL2DZ¹⁴² basis set describing the valence electrons of Co (the 10 innermost electrons of Co were replaced by a quasi-relativistic core potential), while atoms directly connected to the Co were described by the 6-31G(d) basis set.^{143,144} All of the calculations used a large model for the cobalamin under full and restricted geometry optimizations. The models used were: Benz–(Co(III)corrin)–CH₃(1); the demethylated form Benz–(Co(III)corrin)(2); and the respective base-off forms (Co(III)corrin)–CH₃(3) and (Co(III)corrin)(4). The computed energy for the scission of the Co–C bond for (1) was 22.9 kcal mol⁻¹; this was an underestimate when compared with the experimentally recorded value of 36–37 kcal mol⁻¹.^{145,146}

The authors went on to explore the lengthening and shortening of the Co–benzimidazole distance induced by the protein by carrying out restricted geometry optimizations of structures (1) and (2) while restricting the Co–N_{axial} distance. A “normal” *trans* influence was observed between the axial ligands with the lowest BDE value of 22.9 kcal mol⁻¹, calculated at the equilibrium Co–N_{axial} distance of 2.3 Å. A small increase of 1 kcal mol⁻¹ was observed for the BDE on a

change of 0.5 Å in the Co–N_{axial} distance. As a result, Maseras *et al.*⁹ were the first to show in their work the weakness of the Co–N_{axial} bond. In addition, changes to the BDE obtained due to the manipulation of the Co–N_{axial} were very small and therefore no explanations could be provided for the large enzymatic effect. In terms of kinetics, the profile of the Co–C dissociation curve was minimally affected when the position of the axial base was altered. When increasing or decreasing the Co–benzimidazole distance by 0.3 Å the energy curve was observed to change by only 2 kcal mol⁻¹. Finally, the authors concluded that the acceleration of the Co–C cleavage could not be due to the applied strain of the protein on the benzimidazole ligand but rather attributed to other factors not yet accounted for.¹⁴⁷

Kozłowski and co workers⁶⁰ were acknowledged as the first to quantum mechanically determine Co–C BDEs (**Figure 3.3**), performed on a few models used in their earlier studies^{58,59} (see **Figure 3.1**) by using gradient-corrected DFT with the B3LYP functional in a gas phase environment.



$$\text{BDE} = \text{Y}-(\text{Co(III)corrin})-\text{R}_{\text{opt}} - \text{Y}-(\text{Co(II)corrin})_{\text{opt}}^{\bullet} - \text{R}_{\text{opt}}^{\bullet} + \Delta_{\text{ZPE}} \quad \ddagger\ddagger$$

Figure 3.3: Homolytic activation of the Y–(Co(III)corrin)–R cobalamin model.⁶⁰

^{‡‡} opt= optimized structures; Δ_{ZPE} = vibrational zero-point energy correction

Although the calculated BDE values (see **Table 2**, renumbered and reproduced directly from the original article)⁶⁰ underestimated the experimental values (17–34 kcal mol⁻¹ for model compounds and 26–37 kcal mol⁻¹ for cobalamins),⁶⁰ the DFT computations were reported to reproduce the trend of BDE values that were obtained experimentally (see **Table 2** in reference 60).

Table 2: Co–C BDEs (in kcal mol⁻¹) and bond distances (in Å) of B–(Co(III)corrin)–R			
	R	Co–C Bond length Å	Co–C BDE kcal mol ⁻¹
Im	Me	1.962	28
	Et	1.989	22
	Ado	1.994	19
	<i>isopropyl</i>	2.033	14
	<i>tert-butyl</i>	2.103	3
DBI	Me	1.962	25
	Et	1.990	19
	Ado	1.992	18
	<i>isopropyl</i>	2.027	13
	<i>tert-butyl</i>	2.091	3
H ₂ O	Me	1.948	29
	Et	1.975	24
	Ado	1.975	21
	<i>isopropyl</i>	2.015	17
	<i>tert-butyl</i>	2.083	7

Two interesting points were highlighted from this study. Firstly, where these calculations are concerned, the *trans* axial ligand plays no role in determining the BDE of the Co–C bond, and secondly, there exists an inverse relationship between the BDE and length of the Co–C bond. This means that as the bond weakens (increases in length) the BDE value decreases. The Co–C BDEs were found to decrease in the following order: Me > Et > Ado > *isopropyl* > *tert-butyl*, (see **Table 2**). From the results obtained, the authors concluded that a change in the α -*trans* axial base has no influence on the β axial ligand.

The BDE is important for the reactions of cobalamin enzymes; thus far, calculated homolytic BDEs ($22\text{--}28 \text{ kcal mol}^{-1}$)^{9,48,60} for MeCbl show a large discrepancy when compared to experimental values ($37 \pm 3 \text{ kcal mol}^{-1}$).^{9,148} Because of this, Jensen and Ryde⁵⁷ investigated the possible errors in the calculations by including variations in the basis set and the theoretical method. Criteria such as relativistic effects, basis set superposition error, zero-point energies, thermal effects and solvation effects were considered. Their aim was to show that the Co–C BDE depends heavily on the basis set and method used and that possibly the B3LYP functional could be held accountable for the discrepancies in the BDE values. The B3LYP functional with six different basis sets (see **Table 3** below, data reproduced from reference 57) was used for models consisting of a naked Co–Corrin, a detached axial ligand, and an alkyl ligand, including Im–(Co(III)-corrin)–Me, Bzm–(Co(III)-corrin)–Me and Im–(Co(III)-corrin)–Ribosyl.

No.	Co	Other atoms	Basis functions in Im–(Co(III)-corrin)–Me
1	DZspd2f	6-311+G(2d,2p)	1099
2	TZVPP	6-311+G(2d,2p)	1076
3	TZV	TZV	520
4	DZpdf	6-31G(d)	518
5	TZV	6-31G(d)	492
6	LANL2DZ	Dunning95	339

In the first part of the study the authors used the same functional, B3LYP, and changed the basis sets while monitoring the BDE values. All the structures were geometry optimised using basis set 4 (see **Table 3** above). The results obtained are presented in **Table 4** (results extracted from reference 57).

Table 4: Co–C BDEs (kcalmol⁻¹) obtained with the various basis sets, with or without relativistic corrections			
Basis set no.	BDE	Relativistic correction	BDE with correction
1	21.7	1.6	23.3
2	21.3	1.4	22.7
3	20.6	1.5	22.1
4	24.4	1.5	25.9
5	26.1	1.5	27.6
6	21.4	–	–

It was found that BDE decreases (discrepancy increases) as the basis set is improved. With the introduction of a relativistic correction the BDE increased by 1.4 kcal mol⁻¹ for five of the basis sets while the basis set superposition error using the largest basis set decreased the calculated BDE by < 1 kcal mol⁻¹.

The solvation effects, simulated by the conductor polarizable continuum model (CPCM), were found to be quite small (see **Table 5**, data extracted from reference 57), showing an increase of the BDE by 1.4 kcal mol⁻¹. Similar results are shown for the first two species which inadvertently describes them as having similar charge distributions and solvent-accessible surfaces.

Table 5: Solvation energies and the solvation correction to the BDE		
Species	Solvation energy (kcalmol ⁻¹)	
	$\epsilon = 4^{\text{§§}}$	$\epsilon = 78.4$
Im–[Co(III)-corrin]–Me	-21.7	-33.6
Im–[Co(II)corrin]	-21.7	-33.6
Me	1.2	1.7
BDE	1.2	1.7

^{§§} ϵ is the relative permittivity of the solvent.

This small value was an expected result as there is no charge separation involved in the reaction; any effects experienced could have been attributed to cavitation, dispersion and repulsion energies. However, performing the same calculation with Turbomole's COSMO model resulted in a decrease of the BDE by 0.2 kcal mol⁻¹.

Zero-point energy corrections lowered the calculated BDE by 5 kcal mol⁻¹, while calculations for thermal corrections (experiments were conducted at 120–140°C) increased the BDE by 1.4 kcal mol⁻¹. Finally, the summation of all these corrections gave a value of 20.6 kcal mol⁻¹, 1.2 kcal mol⁻¹ lower than the calculated value (without corrections) and still offered no solution to the initial dilemma.

Subsequently, Jensen and Ryde used ten different DFT methods (see **Table 6** data reproduced from reference 57) to calculate the Co–C BDE (without the corrections) and found them to differ widely, while only two methods produced very comparable results to that of experimental values; BP86 showed BDE values in the range 37.2–38.2 kcal mol⁻¹ and MP2 gave a BDE=37.3 kcal mol⁻¹. This led the authors to believe that the B3LYP functional itself was responsible for the poor BDE values obtained until then. They suggested that due to open and closed shell transition metal complexes having different numbers of unpaired electrons, a difference occurs in the correlation energies and therefore poor results are obtained when compared to experiment.

Table 6: Uncorrected Co–C BDEs calculated with various methods using basis set 4 and optimized geometries^a

Method	BDE (kcalmol ⁻¹)	Method	BDE (kcalmol ⁻¹)
HF	-42.4	B-LYP	33.7
B1LYP	20.3	BPW91	35.3
B3LYP	24.4 (24.7)	BP86	37.2 (38.2)
B3PW91	26.0	MP2	37.3
B3P86	29.5	S-VWN	62.5

^avalues in brackets were obtained from Gaussian-98 software, rather than by Turbomole

Dolker *et al.*¹³ reported that the best experimental estimate of AdoCbl's Co–C BDE was kinetically²⁷ determined as 31.4 ± 1.5 kcal mol⁻¹, while photoacoustic calorimetry gave BDE values for MeCbl in the range of 36 ± 3 kcal mol⁻¹.¹⁴⁵ Furthermore, from crystallographic data, we know these two cofactors have very similar Co–C bond lengths.¹⁴⁹⁻¹⁵³ Based on results obtained by Jensen and Ryde⁵⁷ as well as Rutkowska-Zbik *et al.*,⁷ Dolker and co-workers chose to work with the BP86^{77,79,80} functional for their investigation into cobalamin chemistry. Although they found that the absolute Co–C BDE for MeCbl was improved by using BP86, a lower Co–C BDE for AdoCbl as well as the experimental difference of 5 kcal mol⁻¹ between these two cofactors, could not be reproduced.

In light of this, the authors continued to explore the BDEs for both MeCbl and AdoCbl by using the integrated quantum mechanics and molecular mechanics approach (IMOMM, or hybrid QM/MM). This approach allowed them to use models containing all of the substituents and any peripheral side chains that were deemed relevant in recent studies on CNCbl,¹⁵⁴ MeCbl¹⁵⁵ and AdoCbl.¹⁵³ For the calculations, the BP86 functional was used together with the following assigned basis sets: the standard double- ζ LANL2DZ plus polarization with the corresponding pseudopotentials^{142,156-158} was used for the Co atom, and all of the atoms directly attached to Co as well as all of the atoms for the alkyl groups were described by 6-31G(d),^{143,144,159-161} and 6-31G was used for the rest of the model. The Miertus-Scrocco-Tomasi (MST) ab initio continuum method was used for the exploration of solvent effects; however since BP86 was not implemented in this method all of the calculations were carried out using B3LYP/6-31G(d).

The Co–C homolytic cleavage of the free cofactor was analysed by investigating AdoCbl models sporting a change in the β -ligand in the presence and absence of a solvent. By using different fragments as the β -ligand (see **Figure 3.4**) they could easily evaluate the effects of the different regions of the cofactor, *via* the QM/MM methodology, on Co–C bond homolysis and were able to distinguish between their

steric and electronic effects. Their calculations revealed MeCbl (**Figure 3.4**, Model **1**) to have a BDE of 36 kcal mol^{-1} , a result that compares favourably with documented experimental data. On the other hand, when using model **2** (**Figure 3.4**) a BDE of $33.5 \text{ kcal mol}^{-1}$ was obtained. Dolker *et al.* considered this decrease in BDE was solely due to steric effects between the bulk of the tetrahydrofuran (THF) ring and cobalamin. This observation was further motivated by an increase in the Co–C bond length from 1.973 \AA (model **1**) to 1.998 \AA (model **2**).¹³

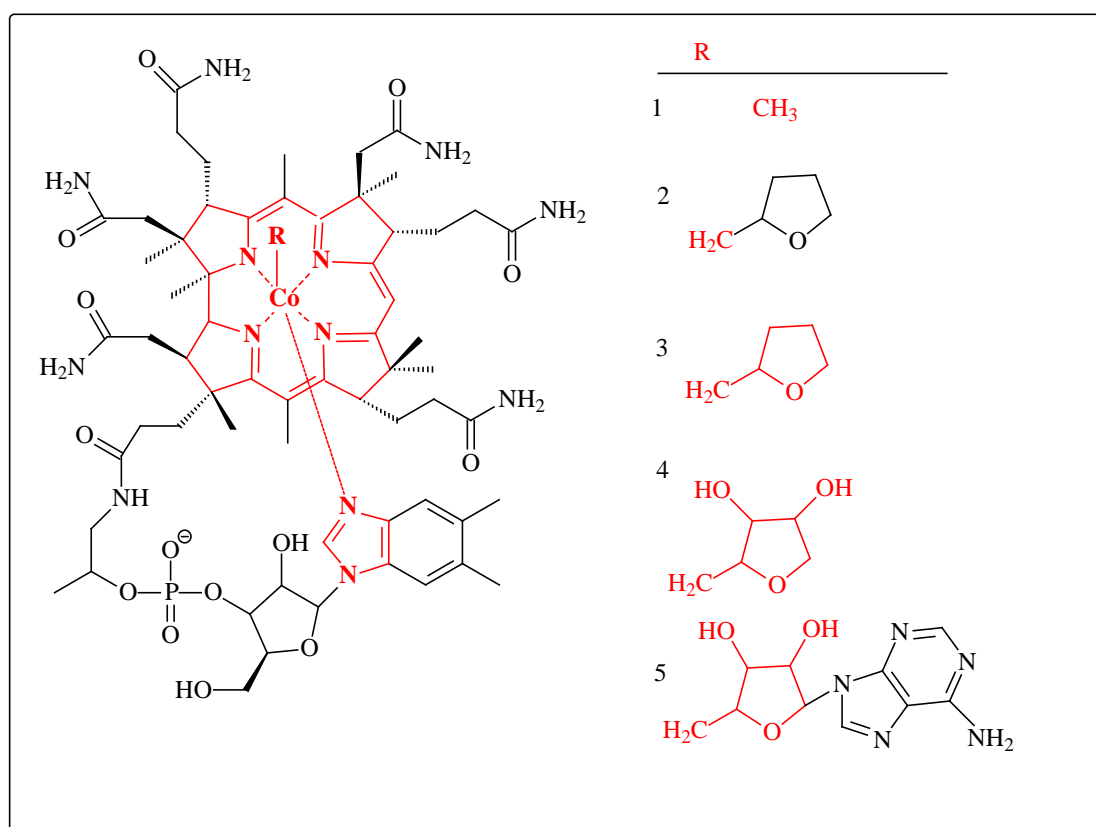


Figure 3.4: Models used by Dolker *et al.* to calculate Co–C BDE. QM in red, MM in black (redrawn from reference 13).

Both the steric and electronic effects were awarded the same level of importance, as, on using model **3** (treated at QM level) in the calculations the BDE decreased further by 2.3 kcal mol⁻¹. At this stage the BDE was calculated as 31.2 kcal mol⁻¹ and was considered a fair reproduction of the experimental value for AdoCbl.¹³ Steric interactions between the THF ring of the ribose part of the Ado group and the amide side chains of the corrin, together with the electronic effects of the THF ring were considered to additively destabilize the Co–C bond by 4.8 kcal mol⁻¹. In contrast, hydrogen bonding between the oxygen from the Ado group (model **4**) and the amide side chains of the cobalamin stabilized AdoCbl, thus making the cleavage of the Co–C bond unfavourable. An increase of 1.4 kcal mol⁻¹ for the Co–C BDE in AdoCbl over MeCbl was recorded. This form of stabilization was not observed for calculations with model **3**.

In the case of model **5**, the BDE was calculated to be 37.4 kcal mol⁻¹. The authors found this high BDE was mainly due to the interactions between adenine and the corrin side chains, as in a previous study of theirs⁵² the side chains of the corrin were not included and both MeCbl and AdoCbl were recorded as having very similar Co–C BDEs. It is also worth mentioning that all of the Co–C BDEs discussed thus far were based on the potential energy, in other words zero-point and thermal corrections were not taken into consideration. Later on frequency calculations were carried out on model structures (model **6** in **Figure 3.5**) minus the corrin side chains in order to obtain an estimate for the zero-point energy and thermal corrections to the Co–C BDEs.

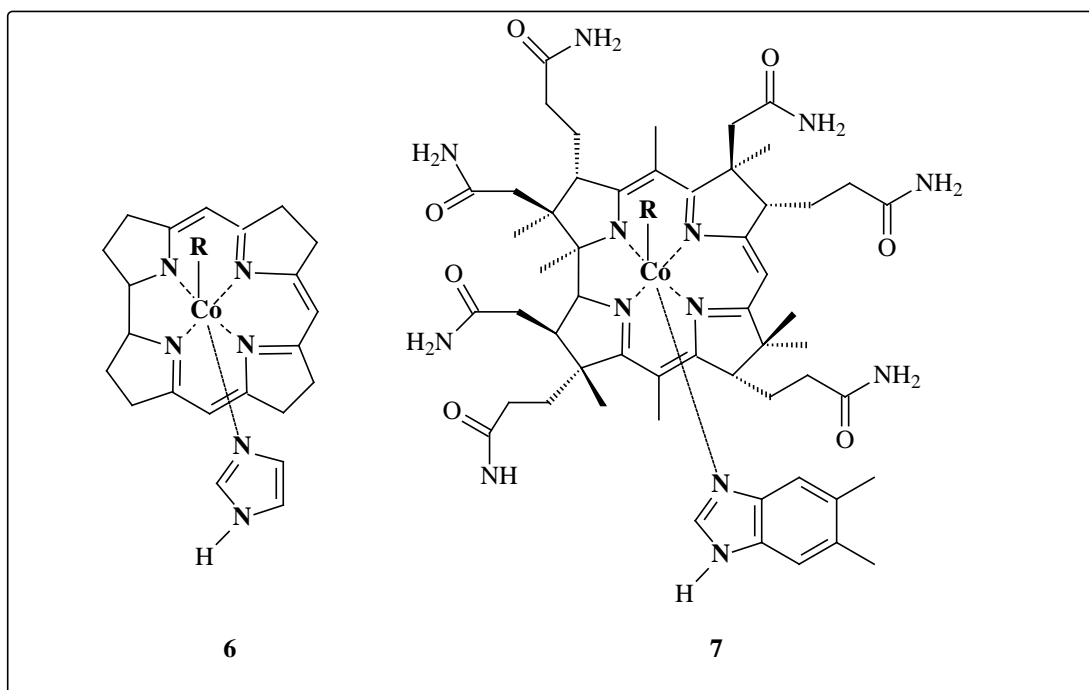


Figure 3.5: Models for frequency (6) and solvent effects (7). R is a Me or an Ado group, dependent on the cobalamin modelled (reproduced from reference 13).

The results are summarised and presented in **Table 7** below. These results indicate a difference of only $0.3 \text{ kcal mol}^{-1}$ in the corrections between the two cofactors. The authors have used this argument to validate their comparisons of potential energies of both systems, however, these calculations were still considered a failure since AdoCbl continued to have a higher BDE than MeCbl.

Table 7: Co–C BDEs and corrections to them arising from zero-point energies and thermal corrections (kcal mol^{-1})		
	MeCbl	AdoCbl
BDE (models 1 and 5 in Figure 3.4)	36.0	37.4
BDE (model 7 in Figure 3.5)	35.3	35.2
Zero-point correction	-4.9	-3.8
Thermal correction to energy	0.8	0.0
Thermal correction to enthalpy	0.6	0.6
Total corrections	-3.5	-3.2

On investigating solvent effects (model **7** in **Figure 3.5**) it was discovered that van der Waals interactions between the Ado group and the amide side chains were important for the gas phase only, as the Ado Co(II) species was well stabilized through solvolysis. The Co–C BDEs were underestimated with MeCbl at 32.3 kcal mol⁻¹ and AdoCbl with 24.7 kcal mol⁻¹. In this instance, the experimental observation for AdoCbl having the lower BDE was reproduced. Dolker *et al.* concluded that calculated BDEs in solution were important in order to reproduce experimental data. Furthermore, there are no hidden intrinsic factors in the two structures, contributing to the differences in the Co–C bond cleavage. Finally, they also felt that the key to solving this cleavage may lie in the interacting relationship between the cofactor and its enzymatic environment. This warranted further interrogation.

3.3 STRUCTURAL AND ELECTRONIC PROPERTIES OF THE Co-CORRIN MACROCYCLE

Parrinello *et al.*⁶¹ used DFT within the LSD (spin unrestricted) approximation to study the structural and electronic properties of the Co-corrin. Three different spin states were considered with the lowest value for the singlet ($S=0$, closed shell), followed by the triplet ($S=1$) at 10 kcal mol⁻¹ higher in energy and the quintet ($S=2$) at the highest energy of 46 kcal mol⁻¹. In all three cases the optimization of the free corrin converged to a nonplanar structure of C_2 symmetry showing a similar distortion to the Co-corrin conformation in B₁₂. This result showed the corrin core to be the cause for the distortion of the macrocycle, supporting Banerjee *et al.*'s⁴¹ conclusion from their spectroscopic study that conformational changes to the corrin macrocycle do not play a decisive role in the functionality of coenzyme B₁₂, reiterating the low sensitivity of the Co-corrin to steric interactions. In addition, these changes in the spin states are accompanied by electron excitation from Co d orbitals into empty corrin orbitals (triplet Co-corrin) or from filled corrin orbitals into empty corrin orbitals (quintet Co-corrin). Notably, these electronic excitations could lead to changes in the carbon-ring structure with minor changes to the Co-N_{ring} distances.

This led to suggestions as to why nature has chosen the corrin and not porphyrin (which is commonly part of other biomolecules) in the makeup of the B₁₂ coenzyme. In porphyrin-containing biomolecules like myoglobin and haemoglobin, the release of oxygen causes a change in the spin state of the Fe-porphyrin, moving from a singlet to a quintet (excitation energy of 14.7–16.9 kcal mol⁻¹), occupying the $d_{x^2-y^2}$ orbital. Consequently, as this occurs, the Fe atom moves out-of-plane and the Fe-N bond distance is found to increase. In the case of Co-corrin none of this occurs. Co-corrin exercises a non planar geometry, which means less overlap between the σ orbital of nitrogen and $d_{x^2-y^2}$ of Co can take place. This results in less repulsion between the orbitals, and no effect on the Co-N_{ring} bond lengths is identified. In

addition, an excitation energy of 46 kcal mol⁻¹ is related to the occupation of the $d_{x^2-y^2}$ orbital (quintet Co–corrin) in the corrinoids. This is mainly attributed to the high energy of the antibonding orbital as a consequence of the Co–corrin’s rigid core and stronger ligand field.⁶¹ On the rare occasion when the orbital becomes occupied, an extremely large energy is associated with the excitation.

3.4 A FREE COENZYME COMPLEX VERSUS A COENZYME COMPLEX EMBEDDED IN PROTEIN

DFT and MM calculations have been used extensively in order to explore the labilisation of the organometallic bond in vitamin B₁₂ coenzymes. Kozłowski *et al.*³¹ decided to combine both these methods to try and elucidate the relationship between the structure of a free coenzyme and that bound to a protein. DFT (B3LYP functional, 6-31G(d) basis set for [H,C,N,O] and Ahlrich’s VTZ basis set for Co) was used to describe the N_{His}–Co–C_{Ado} bond lengths, corrin, Ado group and the histidine bound to the protein chain, while the rest of the system not in a close vicinity to the Co atom was treated at the MM level. Both the Co–C_{Ado} bond length and corrin were unaffected by the presence of the apoenzyme whereas the Co–N_{His} bond length revealed a change from 2.23 Å (free complex) to 2.30 Å, leading to bond labilisation, and described to be energetically supported by an electrostatic field exerted by the surrounding protein matrix. Although other computational studies^{9,25,48,60,141} have shown the axial base as having no effect on the breaking of the Co–C bond, the breaking of the Co–N_{His} bond can significantly contribute to controlling the heterolytic breaking of the Co–C bond in this biological relevant complex. The heterolytic cleavage of the Co–C bond during enzymatic catalysis involves the internal fragmentation of the Ado group and this cleavage is considered a nonproductive side reaction. Therefore, by actively controlling the Co–N_{His} bond length, any abiological side reactions involving the heterolysis of the Co–C bond can be inhibited.

3.5 IS DFT THE ANSWER?

DFT is a more than appropriate investigative tool; unfortunately, its biggest shortfall lies in the type of functional being used. Literature has revealed that DFT with the hybrid B3LYP functional is the most commonly used variant and it has in turn provided valuable insights into the structural and electronic properties of B₁₂ cofactors. However, this particular functional has also shown a poor performance by either overestimating or underestimating BDE values when compared to experimental data. Further, it is considered to be better for main-group chemistry than for the transition metals¹⁶²⁻¹⁶⁴ and tends to be inaccurate when describing van der Waals' attraction,^{165,166} aromatic–aromatic stacking and alkane isomerisation energies.¹⁶³

These are serious shortcomings for this popular density functional (B3LYP) and so Truhlar *et al.*¹⁶³ saw a need to develop a variety of databases for testing and designing new density functionals that would have a broader applicability. One such class of new functional developed by Truhlar *et al.* is called M06. The M06-class of functionals depend on spin densities (spin up and spin down), spin density gradients, spin kinetic energy densities and, for nonlocal (hybrid) functionals, HF exchange.

3.6 THE TRUHLAR GROUP FUNCTIONALS^{100,167-172}

These new M06-class functionals can be regarded as another avenue to probe the nature of the homolytic cleavage of the organometallic bond of AdoCbl.

Over the years, improvements have been made to exchange correlation functionals to increase the applicability of Kohn-Sham DFT. The six strategies used for designing density functionals were summarised by Scuseria and Staroverov^{100,173} and are:

- (1) density-gradient expansion,
- (2) LSDA,
- (3) modelling the exchange-correlation hole,

- (4) constraint satisfaction,
- (5) empirical fits, and
- (6) mixing HF and approximate DFT exchange.

Truhlar and his co-workers based the design of their local functional, M06-L, on strategy (3), (4) and (5) while M06-HF was designed using (3), (4), (5) and (6). The M06-L functional is claimed to be the most accurate functional for transition metals.¹⁶³ This local functional with no HF exchange was rated to have a better performance than B3LYP, making it an affordable functional for large systems.¹⁶³

The M06 and M06-2X functionals depend on three local variables: spin density (ρ_σ) reduced spin density gradient x_σ , and kinetic energy density τ_σ given by the following equations:

$$x_\sigma = \frac{|\nabla\rho_\sigma|}{\rho_\sigma^{4/3}} \quad \sigma^{***} = \alpha, \beta \quad 3.1$$

$$\tau_\sigma = \frac{1}{2} \sum_i^{occup} |\varphi_{i\sigma}|^2 \quad 3.2$$

The M06 functional includes terms based on the VSXC functional, which in turn uses a working variable z_σ and two working functions γ and h :

$$z_\sigma = \frac{2\tau_\sigma}{\rho_\sigma^{5/3}} - C_F, \quad \text{where } C_F = \frac{3}{5}(6\pi^2)(6\pi^2)^{2/3} \quad 3.3$$

$$\gamma(x_\sigma, z_\sigma) = 1 + \alpha(x_\sigma^2 + z_\sigma) \quad 3.4$$

$$h(x_\sigma, z_\sigma) = \left(\frac{d_0}{\gamma(x_\sigma, z_\sigma)} + \frac{d_1 x_\sigma^2 + d_2 z_\sigma}{\gamma_\sigma^2(x_\sigma, z_\sigma)} + \frac{d_3 x_\sigma^4 + d_4 x_\sigma^2 z_\sigma + d_5 z_\sigma^2}{\gamma_\sigma^3(x_\sigma, z_\sigma)} \right) \quad 3.5$$

***The component along an arbitrary space-fixed axis of electron spin angular momentum

3.6.1 META-GGA EXCHANGE FUNCTIONAL¹⁰⁰

Both the M06 and M06-L functionals are similar and comprise a linear combination of the functional forms of the M05 and VSXC exchange functionals. The M06 exchange functional is given by

$$E_X^{M06} = \sum_{\sigma} \int dr [F_{X\sigma}^{PBE}(\rho_{\sigma}, \nabla\rho_{\sigma})f(\omega_{\sigma}) + \varepsilon_{X\sigma}^{LSDA}h_X(x_{\sigma}, z_{\sigma})] \quad 3.6$$

where $h_X(x_{\sigma}, z_{\sigma})$ is defined in equation 3.5, $F_{X\sigma}^{PBE}(\rho_{\sigma}, \nabla\rho_{\sigma})$ is the exchange energy density of the PBE exchange model (actually a modified version of the B86 exchange functional¹⁷⁴), and $\varepsilon_{X\sigma}^{LSDA}$ is the local spin density approximation for exchange⁷³

$$\varepsilon_{X\sigma}^{LSDA} = -3/2 \left(\frac{3}{4\pi}\right)^{1/3} \rho_{\sigma}^{4/3} \quad 3.7$$

and $f(\omega_{\sigma})$ is the spin kinetic-energy density enhancement factor

$$f(\omega_{\sigma}) = \sum_{i=0}^m a_i \omega_{\sigma}^i \quad 3.8$$

where the variable ω_{σ} is a function of t_{σ} , and t_{σ} is a function of the spin kinetic energy density τ_{σ} and spin density ρ_{σ} .

$$\omega_{\sigma} = (t_{\sigma} - 1)/(t_{\sigma} + 1) \quad 3.9$$

$$t_{\sigma} = \tau_{\sigma}^{LSDA}/\tau_{\sigma} \quad 3.10$$

where

$$\tau_{\sigma}^{LSDA} \equiv \frac{3}{10} (6\pi^2)^{2/3} \rho_{\sigma}^{5/3} \quad 3.11$$

3.6.2 META-GGA CORRELATION FUNCTIONAL¹⁰⁰

The functional form of the M06 and M06-2X correlation functionals is described as similar to the M06-L and M06-HF functionals, which were based on the M05 and VSXC correlation functionals. In these correlation functionals, the opposite-spin and parallel-spin correlation are treated differently. .

The opposite-spin M06 correlation energy is expressed as:

$$E_C^{\alpha\beta} = \int e_{\alpha\beta}^{\text{UEG}} [\mathbf{g}_{\alpha\beta}(x_\alpha, x_\beta) + h_{\alpha\beta}(x_{\alpha\beta}, z_{\alpha\beta})] dr \quad 3.12$$

where $\mathbf{g}_{\alpha\beta}(x_\alpha, x_\beta)$ is defined as:

$$\mathbf{g}_{\alpha\beta}(x_\alpha, x_\beta) = \sum_{i=0}^n c_{C\alpha\beta,i} \left(\frac{\gamma_{C\alpha\beta}(x_\alpha^2 + x_\beta^2)}{1 + \gamma_{C\alpha\beta}(x_\alpha^2 + x_\beta^2)} \right)^i \quad 3.13$$

and $h_{\alpha\beta}(x_{\alpha\beta}, z_{\alpha\beta})$ is defined in equation 3.5, with $x_{\alpha\beta}^2 \equiv x_\alpha^2 + x_\beta^2$ and $z_{\alpha\beta} \equiv z_\alpha + z_\beta$.

The parallel spins are defined as:

$$E_C^{\sigma\sigma} = \int e_{\sigma\sigma}^{\text{UEG}} [\mathbf{g}_{\sigma\sigma}(x_\sigma) + h_{\sigma\sigma}(x_\sigma, z_\sigma)] D_\sigma dr \quad 3.14$$

where $\mathbf{g}_{\sigma\sigma}(x_\sigma)$ is defined as:

$$\mathbf{g}_{\sigma\sigma}(x_\sigma) = \sum_{i=0}^n c_{C\sigma\sigma,i} \left(\frac{\gamma_{C\sigma\sigma} x_\sigma^2}{1 + \gamma_{C\sigma\sigma} x_\sigma^2} \right)^i \quad 3.15$$

and $h_{\sigma\sigma}(x_\sigma, z_\sigma)$ is defined in equation 3.5. D_σ is the self-interaction correction factor

$$D_\sigma = 1 - \frac{x_\sigma^2}{4(z_\sigma + C_F)} \quad 3.16$$

For a one electron system,¹⁷³ D_σ becomes irrelevant, and the UEG correlation energy density for the anti-parallel spin and parallel spin cases¹⁷⁵ are dependent on $e_{\alpha\beta}^{\text{UEG}}$ (equation 3.14) and $e_{\sigma\sigma}^{\text{UEG}}$ (equation 3.16). The total M06 correlation energy of the new correlation functional is given by

$$E_C = E_C^{\alpha\beta} + E_C^{\alpha\alpha} + E_C^{\beta\beta} \quad 3.17$$

Truhlar *et al.* used values from their previous work for the two non-linear parameters: $\gamma_{C\alpha\beta}$ and $\gamma_{C\sigma\sigma}$ ^{176,177} as well as the three non-linear parameters, α_x , $\alpha_{C\alpha\beta}$ and $\alpha_{C\sigma\sigma}$.¹⁷³

3.6.3 HYBRID META FUNCTIONAL¹⁰⁰

The M06-HF hybrid meta functional is expressed as follows:

$$E_{XC}^{\text{hyb}} = \frac{X}{100} E_X^{\text{HF}} + \left(1 - \frac{X}{100}\right) E_X^{\text{DFT}} + E_C^{\text{DFT}} \quad 3.18$$

where E_X^{HF} is the non-local HF exchange energy, X is the percentage of HF exchange in the hybrid functional, E_X^{DFT} is the local DFT exchange energy and E_C^{DFT} is the local DFT correlation energy.

Using diverse databases, Truhlar *et al.*¹⁰⁰ compared the performance of the suite of M06 functionals with sixteen other DFT functionals amongst which were some popular functionals such as BLYP,^{77,78} PBE,¹⁰² B3LYP^{77,78,101,178} and B98.¹⁷⁹ Table 8 (duplicated from reference 163) describes the databases developed by Truhlar *et al.*

Table 8: Database for Ground-state properties	
Databases	references
A. Thermochemistry (TC177)	
1. Atomization energies (109)	3
2. Ionization potentials (13)	3, 40, 44, 56
3. Electron affinities (13)	3, 40, 44, 56
4. Proton affinities of small molecules (8)	46
5. Alkyl bond dissociation energies (4)	2, 27, 57
6. π system isomerisation energies (3)	28, 46
7. Proton affinities of conjugated polyenes (5)	46
8. Proton affinities of conjugated Schiff bases (5)	46
9. Hydrocarbon thermochemistry (7)	4, 26
10. Difficult cases (10)	4
B. Diverse barrier heights (DBH76)	
1. Heavy-atom transfer (12)	21
2. Nucleophilic substitution (16)	21
3. Unimolecular and association (10)	21
4. Hydrogen transfer (38)	3, 21, 58
C. Noncovalent interaction energies (NCIE53)	
1. Hydrogen bonding (6)	39
2. Charge-transfer complexes (7)	39
3. Dipole-interaction complexes (6)	39
4. Weak interaction complexes (7)	40
5. π - π stacking (5)	40
6. Biological hydrogen bonding (7)	50, 59
7. Biological predominantly dispersion-like (8)	50, 59
8. Biological mixed (7)	50, 59
D. Electronic spectroscopy	
Electronic spectra (49)	4, 51
E. Transition Metal Reaction Energies (TMRE48)	
1. Transition metal atomization energies (9)	33
2. Metal-ligand bond energies (21)	34
3. 3d transition metal reaction energies (18)	45, 60
F. Structure Data	
1. Bond lengths (40)	4, 57
2. Vibrational frequencies (38)	4
3. Zero point energies (15)	4, 75

Testing the functionals for 496 data in 32 databases (Table 8) the following recommendations were made by the group for use on other molecular systems:

- (1) M06-2X (hybrid meta GGA functional). This is unsatisfactory for transition metals but excels in performance for main group chemistry, predicts accurate valence and Rydberg electronic excitation energies, and is more than satisfactory for aromatic-aromatic stacking interactions.
- (2) The M06 (hybrid meta GGA functional). This is a functional with good accuracy for all transition metals, main group thermochemistry, medium-range correlation energy and barrier heights.
- (3) M06-HF (hybrid meta GGA functional). This has a good performance for valence, Rydberg and charge transfer excited states with minimal sacrifice of ground state accuracy.
- (4) M06-L (meta-GGA local functional with no HF exchange). This functional, in comparison to M06, does not give very accurate barrier heights; however this is the most accurate functional for transition metals and is the only one that provides better across the board average performance over B3LYP.

3.7 SUMMARY

In their recent review, Jensen and Ryde¹⁸⁰ have described how, since the turn of the new century, computational methods have played a major role in cobalamin chemistry. Of particular interest for this study, is the contribution from DFT methods. The first DFT study made use of the B3LYP functional¹⁰¹ based on its reputation of performing well for main group elements⁷¹ and radical enzymes.¹⁸¹ This hybrid functional was successful in describing structures, frequencies and certain energy types (isomerisation and reaction energies and sometimes activation energies),⁵⁰ even for transition metal complexes.^{46,182} Another widely used functional highlighting the same success was BP86 (GGA).^{77,79,183-185}

One major disadvantage of the B3LYP functional is its inability to correctly predict energy differences in compounds when the electronic configurations are found to differ, that is, in open shell versus closed shell configurations.^{186,187} This is particularly important in cobalamin chemistry, as the cleavage of the Co–C bond produces two fragments that have open shell electronic configurations.⁵⁷ The B3LYP functional contains a certain amount of HF exchange, and it is this that biases it towards high spin states and open shell configurations, a characteristic not shared by BP86.⁵⁰ Due to this shortfall, B3LYP was found to underestimate BDEs of bonds between transition metals (TMs) and ligands, and to further underestimate those for organometallic systems.

On the other hand, the BP86 functional was not without its faults and was found to overestimate BDEs of TM systems even while it gave good performance for organometallic complexes.⁵⁰ In addition, BP86 was consistent in its performance for many related octahedral organometallic systems with errors of ~ 2 kcal mol⁻¹ while B3LYP exhibited errors between 8–19 kcal mol⁻¹. In the wake of these findings BP86 has been used extensively.¹⁸⁰

It also becomes apparent through literature review that there is no universally ideal functional,⁵⁰ however, one can attempt to choose a best-fit functional based on the model system and the property of interest requiring investigation. In a very recent study, Kozłowski *et al.*¹⁸⁸ examined 19 DFT approaches for an accurate assessment of key geometric parameters such as the axial bond lengths to the Co metal centre for the system Im–[Co(III)corrin]–CH₃. Although the authors found most of the pure and hybrid functionals provided satisfactory results when compared to available X-ray data, the best overall performing functional was B97-D^{189,190} followed closely by BP86-D3.^{189,191} These “D” type functionals differ from the standard formulation DFT functionals in that they make corrections for dispersion interactions that arise as a function of intermolecular correlation effects.¹⁸⁹ It is worth noting that these two functionals belong to the group of pure GGA-type functionals and were the only two

from the 19 DFT approaches that produced results for the Co–C BDEs in the experimental range for the MeCbl complex of 32–40 kcal mol⁻¹.¹⁸⁸

For this project, the B3LYP and BP86 functional were chosen based on their performance as reviewed in the literature. The M06L functional was chosen based on the recommendation from Truhlar *et al.* in that it gives better performances for TM systems over B3LYP. Finally, the PBE1PBE functional^{102,103,192}, which forms part of the hybrid functional family and is made up of 25% HF exchange and 75% correlation weighting, was also selected. This functional, together with B3LYP, was reported to yield the most accurate hydrogen binding energies (BDE) and equilibrium structures.¹⁹³ All of these functionals are used in this project and the results obtained will be compared and discussed in the chapters that follow.

CHAPTER 4

COMPUTATIONAL DETAILS

This chapter briefly describes the quantum mechanical software and hardware employed in this investigation.

4.1 SOFTWARE

4.1.1 GAUSSIAN 09 COMPUTER PROGRAM¹⁹⁴

GAUSSIAN programs are general purpose programs capable of performing DFT calculations based on the LDA, GGA and hybrid functional methods. As the name implies the program deals mainly with Gaussian-type orbitals, as described in Chapter 2. Computations can be carried out on systems in the gas phase or in solution, and in their ground states or in an excited state. This investigation involved both gas phase and solution phase calculations. The GAUSSIAN programs can serve as a powerful tool for exploring areas of chemical interest such as substituent effects, reaction mechanisms, potential energy surfaces, and excitation energies.⁶³

The required input data for the GAUSSIAN program must consist of the molecular charge and multiplicity together with the definition of the molecular structure, either in the form of the Z-matrix notation or in the form of Cartesian coordinates or mixed coordinates. These criteria define the molecular geometry in terms of bond lengths, bond angles and torsion angles. In addition, the task to be performed must be specified in other words, single-point calculation, geometry optimisation or frequency calculation specified at the appropriate level of theory by introducing a basis set, and for the purposes of DFT calculations, a functional must also be chosen. For this study a full geometry optimisation was performed for each model with a subsequent

frequency calculation using the 6-31+G(d,p) basis set for the GGA functional BP86,⁶⁵ meta-GGA functional M06L¹⁰⁰ and the hybrid functionals B3LYP⁷¹ and PBE1PBE⁷¹ in both a gas phase and solution phase. Time dependent-DFT (TD-DFT) was also used for exploring the *cis* effects of substituents on carbon 10 of the corrin, together with a change in the β ligand of the corrin macrocycle. The results are reported in Chapter 9.

4.1.2 GAUSSVIEW 5.0.8¹⁹⁵

GaussView 5.0.8 is a graphical user interface (GUI), or visualisation tool that was used for the preparation and analysis of all the models in this study.

4.1.3 AIMALL(version 10.05.04 and 12.06.03 professional)¹⁹⁶

AIMALL is a quantum chemistry software package used to perform comprehensive, quantitative and visual Quantum Theory of Atoms in Molecules (QTAIM) analyses of chemical systems. Data from wavefunction files are required as the input for this type of calculation.

4.1.4 CHEMCRAFT¹⁹⁷

Chemcraft was the software used to generate all uv-vis absorption spectra as well as molecular orbitals for the TD-DFT calculations.

4.2 HARDWARE¹⁹⁸

Four clusters from the Sun Hybrid system, Nehalem, Harpertown Westmere and DELL were used. These are available for researchers from all domains and are based at the Centre for High Performance Computing (CHPC) in Cape Town. All of the

calculations were carried out on these clusters. The hardware make-up of the four UNIX workstations is given in **Table 4.1**.

Table 4.1: Hardware parameters¹⁹⁸

	SUN Harpertown	SUN Nehalem	SUN Westmere	DELL Westmere
CPU	Intel Xeon processor	Intel Nehalem processor	Intel Westmere processor	Intel Westmere processor
CPU Clock(GHz)	3.0	2.93	2.93	2.93
CPU Cores	384	2304	1152	2880
Memory(GB)	768	3456	2304	8640
Peak performance(TFlops)	3	24	13.5	37.1

CHAPTER 5

INFLUENCE OF THE ALPHA LIGAND: PART 1^{†††}

5.1 INTRODUCTION

In 1987 Mealli *et al.*²¹ found support in their studies that the homolysis of the Co(III)–C_β bond was influenced by the Co(III)–N_α bond. Despite this, two years earlier a semi-empirical study conducted by Christianson and Lipscomb¹⁹⁹ revealed that the α ligand had no important electronic effect on the strength of the Co(III)–C_β bond, a view shared by others as a result of studies conducted at similar levels of theory.^{10,123} Due to these conflicting conclusions^{123,200,201}, derived from previous simple model calculations,^{10,21,123,199,201,202} this chapter focuses on examining and reporting DFT calculations on the steric and electronic effects of the α ligand on the BDE and ΔG for the homolysis of the Co(III)–C_β bond.

Although recent DFT studies^{6,58,59} have explored the steric and electronic properties of the cobalamins with a focus on the complexities of α and β ligands, as well as its environmental effects, the homolytic cleavage of the Co(III)–C_β bond still remains a mystery. This chapter includes and compares the trends of cobaloxime, corrole, corrin and porphyrin (**Figures 5.1** and **5.2**) model structures exposed to the same theoretical calculations. The rationale for choosing the cobaloxime model is based on its prior extensive use as a model system for the cobalamins in experiments^{34,36,203,204}

^{†††} The work reported in this Chapter forms part of a manuscript submitted to J. Phys. Chem. B titled DFT Studies of Trans and Cis Influences in the Homolysis of the Co-C Bond in Models of the Alkylcobalamins.

and theory^{10,204,205} while corrole and porphyrin were chosen because they are closely related macrocycles to the corrin.⁶¹ Of considerable interest is how these models behave when exposed to the same theoretical calculations, given the fact that the corrole model, although containing a similar sized metal cavity as the corrin, is also different from corrin because it is fully aromatic. Porphyrin, on the other hand, is different on two counts; it contains a larger metal cavity because of the additional methine group to its macrocycle and comprises a fully aromatic equatorial ligand. Acquiring knowledge of the structural and electronic properties of these tetrapyrrolic macrocycles, which act as tri-(corrole), mono-(corrin) and di-anionic (porphyrin) ligands towards the Co atom, would be highly desirable for a better understanding of B₁₂ analogues.

The purpose of this chapter was three-fold. First, to report on the effect of electronic interactions by using simple ligands such as NH₃, NH₂⁻, NH²⁻, NH₂F, NHF⁻, NF²⁻, NH₂CH₃ and NHCH₃⁻, second, to analyse steric interactions of the α ligand under relaxed conditions by initially changing the α ligand to ammonia and then to primary, secondary and tertiary substituted amines. In addition, the electronic interactions of this second set of ligands was also calculated by constraining the Co(III)-N _{α} and Co(II)-N _{α} bond at different bond length intervals. Third, the *cis* influence of the various equatorial ligands on the axial bond lengths and ΔG and BDEs of the homolysis of the Co(III)-C _{β} bond were analysed. In conclusion, the results obtained are compared and discussed with those presented in earlier literature.

The electronic effects in this study are evaluated by assessing the molecular charge distributions of the atomic populations as defined by Mulliken,²⁰⁶⁻²⁰⁸ Natural population analysis (NPA),^{206,209} Atomic Polar Tensor (APT)²⁰⁷ and Baders Quantum Theory of Atoms In Molecules (QTAIM)²¹⁰ analysis on Co(III), N _{α} and C _{β} from the axial ligands as well as the equatorial nitrogen donors (N_{eq}).²⁰⁸ A brief synopsis is provided on each of the methods.

(1) Mulliken

The electron population projected from this method depends on the reference basis set used in the calculation and relates directly to the atomic orbitals basis set.²⁰⁷ Simply stated, the atomic charge generated from the electron distribution is heavily dependent on the properties of the basis set and not on the distribution of the electrons in the molecule. Because of this, the Mulliken population analysis is unreliable in providing a proper charge distribution in many chemical systems.²⁰⁶ In addition to the basis set dependence, the Mulliken analysis produces values which have no physical meaning, and that tend to be of significant magnitude. Finally, Collins and Streitwieser²¹¹ found that the Mulliken analysis gave a very poor charge distribution for compounds having significant ionic character. Working with organic and inorganic lithium compounds they found significant charge differences of 0.7 e for lithium and a change of sign in some cases for Li that did not correlate with the electronegativity differences.

(2) NPA^{†††}

Weinhold *et al.*²⁰⁹ proposed the NPA method as an alternative to the Mulliken method, because this method reduced the basis set dependence of the electronic charges by using the natural atomic orbitals (NAOs) for a given molecule as its main focus. For the system of interest, the NPA represents the occupancies of the NAOs. This method presents many advantages in that the NAOs are intrinsic to the wavefunction and not to specific basis orbitals, and the natural populations provides a correct sum of the total number of electrons.

^{†††}Also referred to as Natural Bond Orbitals (NBO)

(3) APT

Cioslowski's²⁰⁷ APT approach was considered to show a modest sensitivity to the change in basis sets²⁰⁸ and is a method that can be related to observable quantities. APT is a method that is based on dipole moment derivatives. Geerlings *et al.*²⁰⁸ found in their studies that the APT and NPA methods assign the same polarities with a few exceptions. The APT method showed superiority over the NPA approach by being the most sensitive towards electron correlation while still preserving the polarity.

(4) Bader – (QTAIM) analysis

In the AIM approach, an atom is first defined as an open system. This means that the system will be able to share energy and electron density with other atoms because it is localised in 3-dimensional space. Each atom, representing one nucleus, and occupying an atomic volume in space, behaves in a manner able to attract electron density. A QTAIM analysis thus produces topological properties of the electron density and partial charges of atoms in a molecule. Moreover, the value of the electron density (ρ) at the bond critical point (bcp) can be used to predict the strength of the bond while the Laplacian ($\nabla^2\rho$) of the ρ at the bcp is used to characterize the nature of the bond, that is whether it is covalent, ionic or of intermediate character.

5.2 MODEL STRUCTURES

The four structures used were based on the model, $[\text{NX}_3-(\text{Co(III)}(\text{L})_4)-\text{CH}_3]^{n+}$ (**Figure 5.1**) where (L)₄ represents equatorial ligand(s) with a total of four N-donor atoms (**Figure 5.2**). All of these models were modified from starting crystal structures retrieved from the Cambridge Crystal Structure Database (CCSD).²¹² The α ligands were chosen for their simplicity and differences in proton affinities so that electronic interactions, if any, could also be explored.

The basicity of the ligand, starting from the weakest to the strongest according to their calculated proton affinities (E_{pa}),²¹³ measured in kcal mol⁻¹, are arranged as follows:

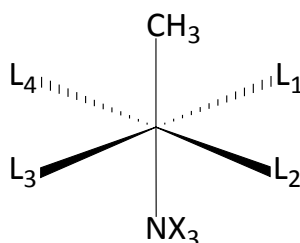
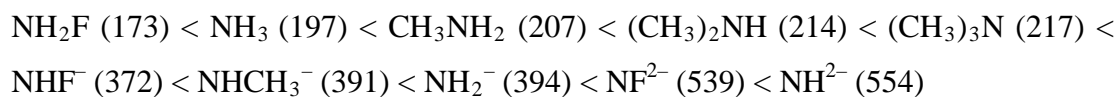


Figure 5.1: Model structure of the type $[\text{NX}_3-(\text{Co}(\text{III})(\text{L})_4)-\text{CH}_3]^{m+}$.

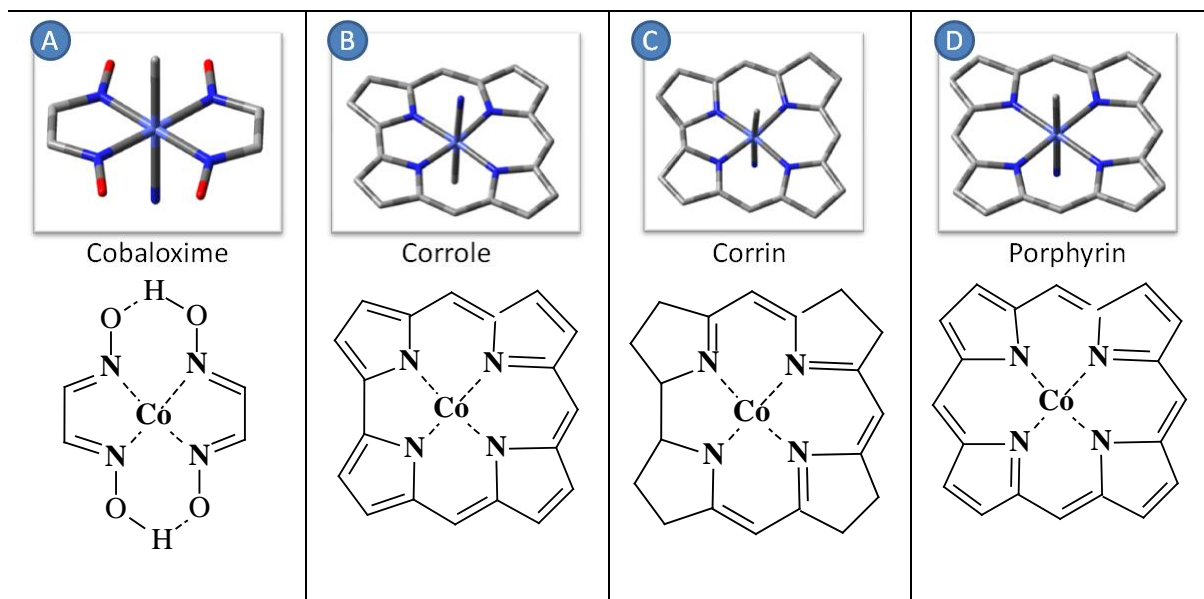


Figure 5.2: Models A–D showing the equatorial ligands, $(\text{L})_4$.

The gas-phase proton affinity (E_{pa}) of a neutral atom (molecule) or anion is a measure of its gas-phase basicity and is the energy released in general reactions of the type,^{214,215}



The standard ΔG for these reaction types is a measure of their relative acidities (E_{pa}) and in this chapter was theoretically calculated using the general equation 5.3.

$$\Delta G_{reaction} = G_{(products)} - G_{(reactants)} \quad 5.3$$

Model structures A–D (**Figure 5.2**) was used in all calculations. A methyl group was used as the β axial ligand for all of the calculations while the α axial ligand was varied from NH^{2-} ; NH_2^- ; NH_3 ; NH_2F ; NHF^- ; NF^{2-} ; $NHCH_3^-$; NH_2CH_3 ; $NH(CH_3)_2$; and $N(CH_3)_3$. In order to minimise computational time the peripheral side chains of the corrin were excluded and replaced by hydrogen atoms. The calculations were carried out with and without restrictions to the $Co(III)-N_\alpha$ and $Co(II)-N_\alpha$ bond lengths in order to explore the ligand effects on the bond lengths and angles, as well as the change in ΔG and the BDE of the $Co(III)-C_\beta$ bond. All structures were geometrically optimised using the GGA BP86 functional at the 6-31+G(d,p) level of theory in all relevant spin states and characterised as true minima by calculating their normal vibrations within the harmonic approximation or frequency. All energies reported included the correction to the zero-point energy. The same conditions were applied for the theoretical calculation of all E_{pa} values.

The calculations were carried out for both the low spin and high spin states of each species involved before and after the homolytic reaction. In all cases, the low spin state was energetically favoured, indicating greater stability. A brief explanation is presented below on how the multiplicity for a low spin state, and high spin state were calculated.

Cobalamin(III) exists as a tetragonally distorted d^6 complex (see **Figure 5.3**) and once homolysis takes place a d^7 complex is produced; in other words, Co(III) is reduced to

Co(II). In the low spin state, the electrons fill and pair up at the same time in the lowest degenerate orbital while in the high spin state the lowest degenerate orbital is completely filled whilst the remaining electrons occupy the remaining orbitals individually.

As part of the input for calculations using Gaussian a multiplicity value has to be assigned. Multiplicity is equal to $2S+1$, where S describes the sum of parallel or anti-parallel spin of electrons, that is, $+\frac{1}{2}$ or $-\frac{1}{2}$. For the given case study in **Figure 5.3** the low spin d^6 state has a multiplicity value of 1 while for the high spin d^6 state it equals 5.

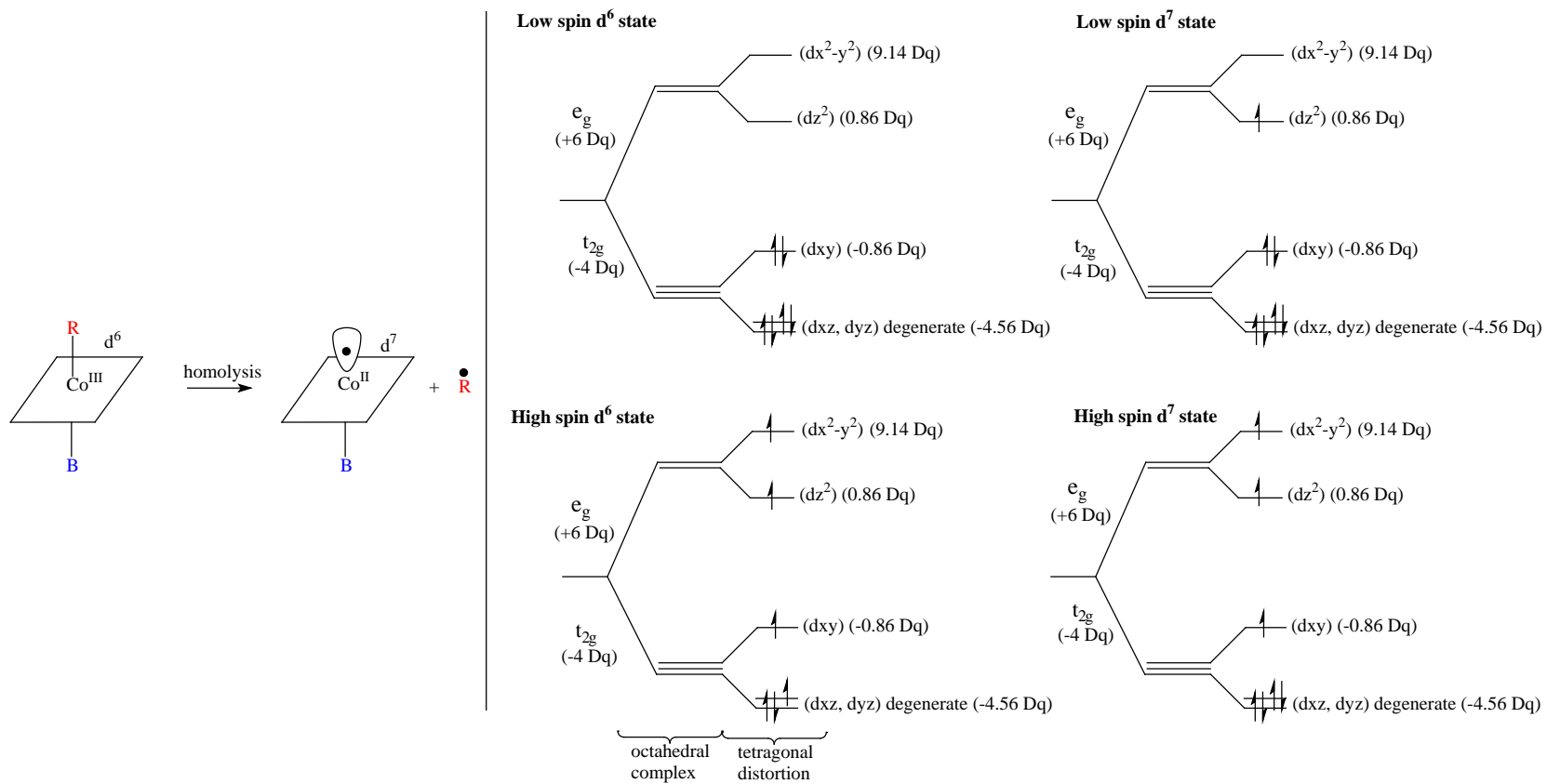


Figure 5.3: Crystal field description of the low spin and high spin states for Co(III) and Co(II) complexes.

5.3 RESULTS AND DISCUSSION

5.3.1 RELAXED CONDITIONS

Tables 5.1A and **5.1B** provide a summary of the geometric parameters and the ΔG and BDEs of the Co(III)–C $_{\beta}$ bond obtained for models A–D. Models A, B and D contain α ligands N(CH $_3$) $_3$, NH(CH $_3$) $_2$, NH $_2$ CH $_3$, NH $_3$, and NH $_2^-$ only, while in **Table 5.1B**, model C in addition to the above mentioned α ligands contains the α ligands NH $^{2-}$, NH $_2$ F, NHF $^-$, NF $^{2-}$, and NHCH $_3^-$. No convergence could be found for model D with α ligand = NF $^{3-}$, and for model C with α ligand = NCH $_3^{2-}$. This indicates that the structure(s) were unable to completely optimise as per the four convergence criteria used by Gaussian 09²¹⁶, which is that the maximum component of the force, the root-mean-square of the forces, the calculated and root-mean-square displacement must all equal zero.^{§§§} The chosen α ligands were of varying character. Some have minimal steric demands in order to factor out steric effects while the electronic properties of the α ligand was explored, while others were of different bulkiness (as assessed by the molar volume²¹⁶ and Tolman cone's angle²¹⁷) so that steric effects could be investigated.

The results obtained are presented and discussed in two separate sections. Section A reports on the electronic effects for model C only (**Tables 5.1B** and **5.1C**) where a large variety of α ligands were used. Section B discusses the steric effects of the α ligands as well as the *cis* influence of the equatorial ligands of models A–D.

^{§§§} One possible explanation could be the self-interaction error from the charge on the anionic α ligand with the corrin macrocycle, since the overall complex will not be neutral as in the case when a mono-ionic ligand is attached. This observation will be explored further in future studies.

Table 5.1A: Geometric parameters, ΔG and BDE for homolysis of the Co(III)–C $_{\beta}$ bond in models A, B and D

α -ligand	^a E _{pa} kcal mol ⁻¹	Bond lengths in cobalamin complexes Å				^b Tolman cone angle /°	Molar volume cm ³ mol ⁻¹	^c Co(III) shift from the mean plane /Å	^d Co(II) shift towards α ligand from mean plane /Å	Bond angle /°		Energies kcal mol ⁻¹	
		Co(III)		Co(II)						N $_{\alpha}$ -Co(III)–C $_{\beta}$	ΔG	BDE	
		^e Co–C $_{\beta}$	^f Co–N $_{\alpha}$	^g Co–N $_{\alpha}$	^h $\Delta_{(5c-6c)}$								
Cobaloxime													
NH ₃	197	2.002	2.076	2.091	0.015	34.81	21.5	0.023	0.159	179.28	28.92	41.06	
NH ₂ CH ₃	207	2.007	2.088	2.088	0.000	14.96	34.6	0.031	0.171	177.55	29.43	40.70	
NH(CH ₃) ₂	214	2.013	2.146	2.118	-0.028	11.22	46.9	0.069	0.213	177.87	26.60	40.79	
N(CH ₃) ₃	217	2.015	2.242	2.183	-0.059	15.43	69.2	0.089	0.241	178.91	25.37	37.55	
NH ₂ ⁻	394	2.039	2.029	1.885	-0.144	15.30	32.1	0.006	0.409	177.95	25.84	37.67	
Corrole													
NH ₃	197	1.970	2.197	2.192	-0.005	34.30	21.5	0.037	0.112	178.41	23.55	35.24	
NH ₂ CH ₃	207	1.972	2.222	2.208	-0.014	10.26	34.6	0.034	0.115	177.40	23.68	35.16	
NH(CH ₃) ₂	214	1.969	2.332	2.266	-0.066	10.15	46.9	0.032	0.123	177.90	22.89	34.56	
N(CH ₃) ₃	217	1.960	2.681	2.407	-0.274	15.94	69.2	0.053	0.134	178.51	23.65	34.69	
NH ₂ ⁻	394	2.046	2.077	2.013	-0.064	15.30	32.1	0.001	0.174	176.52	22.45	34.20	
Porphyrin													
NH ₃	197	1.973	2.167	2.173	0.006	34.05	21.5	0.025	0.101	178.97	22.75	33.28	
NH ₂ CH ₃	207	1.976	2.186	2.185	-0.001	10.38	34.6	0.020	0.105	178.45	21.74	33.07	
NH(CH ₃) ₂	214	1.977	2.253	2.231	-0.022	10.76	46.9	0.014	0.113	177.53	21.37	32.55	
N(CH ₃) ₃	217	1.973	2.482	2.365	-0.117	15.58	69.2	0.009	0.131	178.11	20.92	31.80	
NH ₂ ⁻	394	2.043	2.044	1.977	-0.067	15.30	32.1	0.003	0.145	176.85	19.40	30.90	

^aTheoretically calculated proton affinities. ^bThe Tolman cone angle is further defined in Appendix 2:2.1 ^cThe distance measured (in Å) of the Co ion, from the defined mean plane of the N_{eq} donors for the Co(III) complex. The Co metal centre is found below the mean plane in corrin and cobaloxime and above the mean plane for corrole and porphyrin. ^dThe distance measured (in Å) of the Co ion, from the defined mean plane of the N_{eq} donors for the Co(II) complex. ^eThe axial bond length between Co(III) and C $_{\beta}$ ligand in the 6 coordinate complex. ^fThe axial bond length between Co(III) and N $_{\alpha}$ ligand in the 6 coordinate complex. ^gThe axial bond length between Co(II) and N $_{\alpha}$ ligand in the 5 coordinate complex. ^hThe difference in Co–N $_{\alpha}$ bond length between the 5 coordinate and 6 coordinate complex.

Table 5.1B: Geometric parameters, ΔG and BDE for homolysis of the Co(III)–C $_{\beta}$ bond in model C

α -ligand	^a E _{pa} kcal mol ⁻¹	Bond lengths in cobalamin complexes Å				Tolman cone angle /°	Molar volume cm ³ mol ⁻¹	^b Co(III) shift from the mean plane /Å	^c Co(II) shift towards α ligand from mean plane / Å	Bond angle /°	Energies kcal mol ⁻¹	
		Co(III)		Co(II)							N _{α} –Co(III)–C _{β}	ΔG
		^d Co–C _{β}	^e Co–N _{α}	^f Co–N _{α}	^g $\Delta_{(5c-6c)}$	N _{α} X ₃ –Co–N _{α}	α -ligand					
NH ₃	197(204)	1.982	2.220	2.196	-0.024	33.14	21.5	0.007	0.135	176.24	20.63	32.85
NH ₂ ⁻	394	2.044	2.062	2.144	0.082	15.30	32.1	0.016	0.110	178.28	21.15	32.29
NH ²⁻	553	2.066	2.002	1.828	-0.174	8.20	48.3	0.056	0.246	173.56	8.81	20.47
NH ₂ F	173	1.982	2.162	2.098	-0.064	33.20	24.1	0.009	0.146	179.43	20.64	32.61
NHF ⁻	372	2.042	2.047	2.127	0.080	26.00	28.8	0.018	0.107	175.88	19.46	31.59
NF ²⁻	539	2.058	1.969	1.783	-0.186	12.70	45.8	0.087	0.293	168.48	8.63	20.59
NH ₂ CH ₃	207(214)	1.986	2.227	2.203	-0.024	10.23	34.6	0.003	0.137	175.34	20.25	32.48
NHCH ₃	391	2.046	2.076	2.174	0.098	30.10	38.7	0.007	0.112	176.64	19.26	31.10
NH(CH ₃) ₂	214(220)	1.987	2.302	2.247	-0.055	10.83	46.9	0.001*	0.146	173.45	20.03	31.88
N(CH ₃) ₃	217(225)	1.983	2.549	2.362	-0.187	15.56	69.2	0.001*	0.171	176.19	19.83	31.15

^aCalculated proton affinity values. The values given in parenthesis are literature values. ^bThe distance measured (in Å) of the Co ion, from the defined mean plane of the N_{eq} donors for the Co(III) complex. The Co metal centre is found below the mean plane in corrin and cobaloxime and above the mean plane for corrole and porphyrin. ^cThe distance measured (in Å) of the Co ion, from the defined mean plane of the N_{eq} donors for the Co(II) complex. ^dThe axial bond length between Co(III) and C _{β} ligand in the 6 coordinate complex. ^eThe axial bond length between Co(III) and N _{α} ligand in the 6 coordinate complex. ^fThe axial bond length between Co(II) and N _{α} ligand in the 5 coordinate complex. ^gThe difference in Co–N _{α} bond length between the 5 coordinate and 6 coordinate complex. *The Co metal centre was found below the corrin mean plane towards the α ligand.

Table 5.1C: α ligands used to explore electronic and steric effects in model C

Electronic effects			Steric effects	
NH ₃	NH ₂ F	NH ₂ CH ₃	NH ₃	N(CH ₃) ₃
NH ₂ ⁻	NHF ⁻	NHCH ₃ ⁻	NH ₂ CH ₃	
NH ²⁻	NF ²⁻		NH(CH ₃) ₂	

SECTION A: Electronic effects

(a) Bond lengths and BDEs

For those models containing the α ligands used to explore the electronic effects (Tables 5.1B and C), it is evident that as the basicities of the α ligand increases a normal *trans* influence is experienced between the two axial ligands (Figure 5.4). As the basicity of the α ligand increases, the Co(III)–N $_{\alpha}$ bond length decreases and there is a simultaneous increase in length for the Co(III)–C $_{\beta}$ bond. Consequent to the lengthening of the Co(III)–C $_{\beta}$ bond, a decrease in ΔG for the homolysis of the Co(III)–C $_{\beta}$ and the BDE for this bond is also observed.

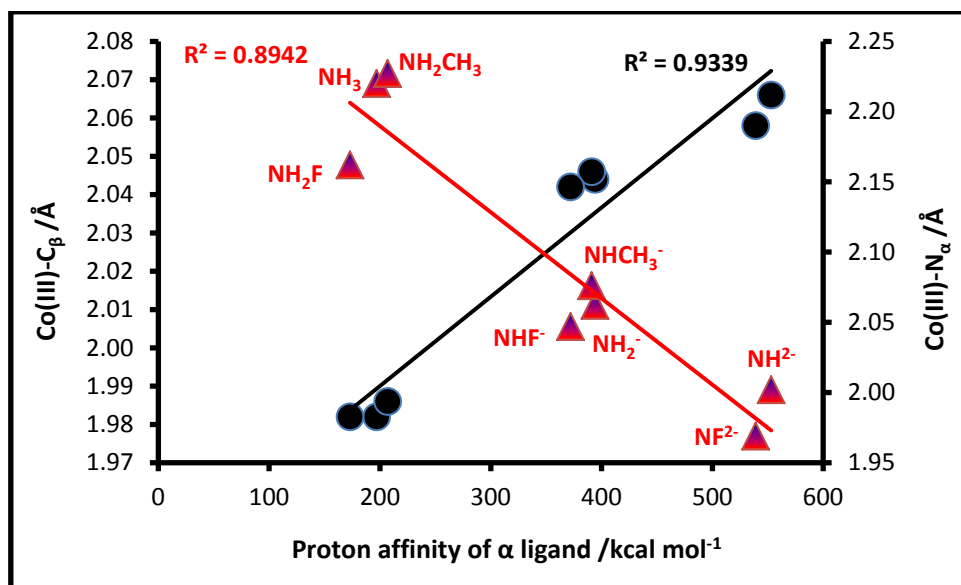


Figure 5.4: The change in length of the Co(III)–C $_{\beta}$ and Co(III)–N $_{\alpha}$ bond versus the calculated proton affinity values (kcal mol⁻¹) in the corrin model.

b) Electron densities and partial charges

From the results presented in **Table 5.1B**, a significant decrease in BDE is noted when the α ligand increases in proton affinity. This large decrease in the Co(III)–C $_{\beta}$ BDE is verified by the weakening of the Co(III)–C $_{\beta}$ bond as is shown by an analysis of the topological properties of electron density of the Co(III)–C $_{\beta}$ bond, see **Table 5.2**, conducted using the Bader AIM approach.²¹⁸ The decrease in ρ -value at the bond critical point (bcp) is indicative of the weakening of the bond.

The Co(III)–N $_{\alpha}$ bond is considerably weaker than the Co(III)–C $_{\beta}$ bond, as indicated by the value of ρ at the bcp. This parameter also confirms the normal *trans* influence between the axial bonds. As the ρ -value at the bcp for the Co(III)–C $_{\beta}$ bond decreases (**Table 5.2**) the ρ -value at the bcp for the Co(III)–N $_{\alpha}$ bond increases, consistent with the lengthening and shortening of these two bonds, respectively, and with an increase in the basicity of the α ligand.

The Laplacian of the electron density, $\nabla^2\rho$, at the bcp of a covalent bond (a shared interaction) is negative whilst a positive value is usually found for an ionic bond.²¹⁹ The same usually applies to the transition metals; however, it has been noted that a positive value will not clearly define the ionic character of the bond because the bcp is always in a region of charge depletion.²²⁰ Therefore, the results presented in **Table 5.2** for the $\nabla^2\rho$ of the electron density for the Co(III)–C $_{\beta}$ bond, although greater than zero, may not be a sufficient condition to describe the bond as ionic.

This challenge was overcome by providing descriptors that would probe into the nature of the axial and equatorial bonds of the cobalamins. Two properties of the electron density, the kinetic energy density $G(r)$ and potential energy density $V(r)$ at the bcp show different behaviour in different bond types.^{220,221}

Table 5.2: BP86/Corrin:- Topological properties of the electron density (ρ) at the bcp (au) of Co(III)-CH₃, Co(III)-N _{α} and Co(II)-N _{α} ^a

α -ligands	Corrin						
	Co(III)-CH ₃						
	E _{pa}	ρ	$\nabla^2\rho$	V(r)	G(r)	H(r)	V(r) /G(r)
NH ₃	197	0.1162	0.0483	-0.1296	0.0708	-0.0588	1.8295
NH ₂ ⁻	394	0.1025	0.0948	-0.1174	0.0705	-0.0468	1.6639
NH ²⁻	553	0.0964	0.1239	-0.1137	0.0723	-0.0414	1.5718
NH ₂ F	173	0.1163	0.0446	-0.1293	0.0702	-0.0591	1.8412
NHF ⁻	372	0.1030	0.0895	-0.1174	0.0699	-0.0475	1.6797
NF ²⁻	539	0.0979	0.1239	-0.1156	0.0733	-0.0423	1.5775
NH ₂ CH ₃	207	0.1153	0.0493	-0.1286	0.0705	-0.0582	1.8252
NHCH ₃	391	0.1021	0.0913	-0.1165	0.0697	-0.0468	1.6724
NH(CH ₃) ₂	214	0.1150	0.0461	-0.1281	0.0698	-0.0583	1.8348
N(CH ₃) ₃	217	0.1153	0.0390	-0.1282	0.0690	-0.0592	1.8587
Co(III)-N _{α}							
NH ₃	197	0.0534	0.1980	-0.0716	0.0606	-0.0111	1.1827
NH ₂ ⁻	394	0.0857	0.2365	-0.1069	0.0830	-0.0239	1.2878
NH ²⁻	553	0.0985	0.2703	-0.1269	0.0973	-0.0297	1.3051
NH ₂ F	173	0.0593	0.2518	-0.0854	0.0742	-0.0112	1.1513
NHF ⁻	372	0.0889	0.2732	-0.1162	0.0922	-0.0239	1.2596
NF ²⁻	539	0.1050	0.3351	-0.1459	0.1148	-0.0310	1.2704
NH ₂ CH ₃	207	0.0541	0.1881	-0.0709	0.0590	-0.0119	1.2025
NHCH ₃	391	0.0833	0.2267	-0.1033	0.0800	-0.0233	1.2915
NH(CH ₃) ₂	214	0.0473	0.1437	-0.0579	0.0469	-0.0110	1.2345
N(CH ₃) ₃	217	0.0297	0.0751	-0.0294	0.0241	-0.0053	1.2204
Co(II)-N _{α}							
NH ₃	197	0.0582	0.2013	-0.0775	0.0639	-0.0136	1.2127
NH ₂ ⁻	394	0.0736	0.1609	-0.0867	0.0634	-0.0232	1.3660
NH ²⁻	553	0.1449	0.4036	-0.2121	0.1565	-0.0556	1.3553
NH ₂ F	173	0.0710	0.2907	-0.1040	0.0883	-0.0156	1.1771
NHF ⁻	372	0.0763	0.1855	-0.0938	0.0701	-0.0237	1.3384
NF ²⁻	539	0.1608	0.5341	-0.2602	0.1968	-0.0633	1.3217
NH ₂ CH ₃	207	0.0590	0.1904	-0.0768	0.0622	-0.0146	1.2347
NHCH ₃	391	0.0696	0.1454	-0.0801	0.0582	-0.0219	1.3757
NH(CH ₃) ₂	214	0.0551	0.1600	-0.0682	0.0541	-0.0141	1.2609
N(CH ₃) ₃	217	0.0445	0.1123	-0.0497	0.0389	-0.0108	1.2778

^aE_{pa} is given in kcal mol⁻¹. The values of charge density (ρ) and its Laplacian ($\nabla^2\rho$) at the bcps are in au (1 au of $\rho = 6.7483 \text{ e}\text{\AA}^{-3}$, and 1 au of $\nabla^2\rho = 24.099 \text{ e}\text{\AA}^{-5}$). The values of the total potential energy density V(r), the kinetic energy density G(r) and the total energy density H(r) at the bcps are in au (1 au = 627.5095 kcal mol⁻¹).

The total energy density, $H(r)$, is then given as: $H(r)=G(r) +V(r)$. If the total density at the bcp is negative, this means that $V(r)$ dominates and the bond is of a covalent or dative nature. Mebs *et al.*²¹⁹ reported negative $H(r)$ values for Co(III)-C_β , Co(III)-N_α and $\text{Co(III)-N}_{\text{eq}}$ and found the values to be much higher than $H(r)$ values at the bcp of a C–C bond (ethane was used as an example). This confirmed the dative character and closed shell interactions of the former bonds. The ratio of $|V(r)|/G(r)$ (that is, the potential and kinetic energies, respectively, at the bcp) is used to characterise a bond.²²¹ Typically, $|V(r)|/G(r)$ values greater than 2 describe covalent interactions; values less than 1 are characteristic of ionic interactions, while values between 1 and 2 are characteristic of bonds of intermediate character.

From the results provided in **Table 5.2**, the Co(III)-C_β bond is shown to decrease its covalent character as the α ligand is varied from the neutral NH_3 to the charged NH_2^- ligand; from NH_2F to charged ligand NF_2^- , and from NH_2CH_3 to NHCH_3^- , a trend that parallels the decrease in the BDE of this bond. At the same time, the Co(III)-N_α bond becomes less ionic and acquires a distinctively intermediate character, a change that complements the noticeable decrease in the Co(III)-N_α bond length.

Further to this, the partial charges were calculated for these model systems using all four methodologies discussed in the introduction to this chapter. These methods generate numerically different values (shown in **Table 5.3**) and in all of these methods, a similar trend is exhibited for the partial charges of the C_β atom only, while the results for the Co metal centre, N_α and N_{eq} donors of the macrocyclic ring are seen to fluctuate considerably. In light of this, the partial charges are found to be unreliable for these particular model systems, and therefore are not used further to provide possible explanations for observed changes to the geometric and thermodynamic parameters.

Table 5.3: Mulliken and APT partial charges (e) for the corrin model C

α ligands	MULLIKEN							APT						
	Co(III)	C $_{\beta}$	N $_{\alpha}$	N $_1$	N $_2$	N $_3$	N $_4$	Co(III)	C $_{\beta}$	N $_{\alpha}$	N $_1$	N $_2$	N $_3$	N $_4$
Corrin														
NH $_3$	-3.088	-0.272	-0.871	0.365	0.468	0.513	0.405	0.218	0.176	-0.288	-0.233	-0.531	-0.530	-0.227
NH $_2^-$	-3.504	-0.450	-0.869	0.711	0.499	0.503	0.550	0.212	0.039	-0.388	-0.163	-0.521	-0.530	-0.169
NH $^{2-}$	-3.047	-0.625	-0.674	0.645	0.535	0.481	0.569	0.295	-0.027	-0.558	-0.203	-0.358	-0.180	-0.076
NH $_2$ F	-2.885	-0.219	-0.441	0.316	0.409	0.473	0.364	0.126	0.184	0.234	-0.249	-0.538	-0.531	-0.241
NHF $^-$	-2.934	-0.417	-0.469	0.607	0.504	0.469	0.439	0.176	0.037	0.038	-0.175	-0.527	-0.509	-0.179
NF $^{2-}$	-3.379	-0.532	-0.206	0.511	0.694	0.576	0.468	0.219	-0.013	-0.011	-0.021	-0.073	-0.415	-0.172
NH $_2$ CH $_3$	-3.023	-0.202	-0.547	0.407	0.403	0.379	0.389	0.221	0.163	-0.305	-0.228	-0.522	-0.525	-0.224
NHCH $_3$	-3.134	-0.385	-0.389	0.556	0.457	0.454	0.496	0.221	0.025	-0.383	-0.166	-0.503	-0.527	-0.161
NH(CH $_3$) ₂	-2.736	-0.203	-0.344	0.386	0.285	0.307	0.422	0.232	0.159	-0.362	-0.220	-0.518	-0.510	-0.218
N(CH $_3$) $_3$	-2.610	-0.196	-0.490	0.327	0.373	0.430	0.351	0.233	0.166	-0.448	-0.229	-0.497	-0.493	-0.221
NBO														
NH $_3$	0.189	-0.711	-1.048	-0.339	-0.377	-0.375	-0.336	1.079	-0.140	-1.052	-1.088	-1.103	-1.105	-1.088
NH $_2^-$	0.140	-0.834	-1.113	-0.269	-0.340	-0.338	-0.282	1.126	-0.201	-1.054	-1.055	-1.087	-1.094	-1.060
NH $^{2-}$	0.131	-0.902	-0.860	-0.293	-0.326	-0.326	-0.311	1.123	-0.227	-0.906	-1.049	-1.085	-1.095	-1.028
NH $_2$ F	0.154	-0.705	-0.377	-0.357	-0.376	-0.370	-0.350	1.073	-0.139	-0.440	-1.097	-1.102	-1.100	-1.096
NHF $^-$	0.118	-0.829	-0.414	-0.285	-0.355	-0.338	-0.290	1.121	-0.199	-0.452	-1.061	-1.092	-1.087	-1.059
NF $^{2-}$	0.109	-0.898	-0.152	-0.322	-0.321	-0.350	-0.314	1.110	-0.226	-0.262	-0.988	-1.096	-1.096	-1.048
NH $_2$ CH $_3$	0.215	-0.720	-0.821	-0.339	-0.380	-0.383	-0.340	1.076	-0.142	-0.993	-1.085	-1.102	-1.106	-1.088
NHCH $_3$	0.177	-0.839	-0.838	-0.279	-0.345	-0.349	-0.289	1.122	-0.199	-0.985	-1.059	-1.084	-1.095	-1.060
NH(CH $_3$) ₂	0.258	-0.721	-0.631	-0.345	-0.395	-0.392	-0.344	1.070	-0.138	-0.948	-1.083	-1.103	-1.104	-1.082
N(CH $_3$) $_3$	0.326	-0.709	-0.483	-0.368	-0.405	-0.404	-0.364	1.057	-0.126	-0.916	-1.083	-1.096	-1.096	-1.082

N $_1$, N $_2$, N $_3$ and N $_4$ are the partial charge on the N $_{eq}$ of the cobalamin macrocycle. The numbering system used is per Figure 5.8.

Andruniow *et al.*⁵⁹ reported on the basicity of ligands and found that the stronger the basicity of the *trans* ligand, the stronger would be its bond to cobalt. This is the same trend observed in **Table 5.1B**, as the α ligand changes from a neutral species to a charged one. Contrary to other literature reports,^{9,48,219} these results firmly imply that the α ligand does indeed have an electronic influence on the strength of the Co(III)–C $_{\beta}$ bond and therefore contributes somewhat to the lowering of the BDE of the Co(III)–C $_{\beta}$ bond for the model systems investigated in this section.

SECTION B: Steric effects

a) Bond lengths, BDEs, steric and stereo-electronic effects

Tables 5.1A and **B** provide data for models A–D that are attached to the α ligands NH₃; NH₂CH₃; NH(CH₃)₂ and N(CH₃)₃. These ligands are of varying proton affinities, are progressively more bulky (quantified per cone angle²²² and molar volume²¹⁶) and neutral in character as compared to the α ligands carrying charges. As a result, they are expected to generate data different to that observed in Section A.

What is immediately clear from the results presented in **Table 5.1B** is the simultaneous elongation in bond length that occurs for both the Co(III)–C $_{\beta}$ and Co(III)–N $_{\alpha}$ bond as the stereo-electronic properties (quantified by both the molar volume²¹⁶ plus Tollman cone angle^{217,222} and E_{pa} values,²¹⁴ respectively) of the α ligand changes. This is notably a very different result to that of the charge-bearing ligands of Section A. While the Co(III)–C $_{\beta}$ bond length is observed to marginally increase, the Co(III)–N $_{\alpha}$ bond length steadily increases as the molar volume of the α ligand increases. This effect, where both the axial bond lengths are seen to simultaneously increase or decrease, is referred to as an inverse *trans* influence.¹²²

An assessment of all the corrin models with the variation in α ligands show that the Co(III)–C $_{\beta}$ bond lengths compare well with experimentally determined distances in MeCbl: 1.98–1.99 Å with X-ray crystallography^{149,152} and 2.00 ± 0.03 Å with

extended X-ray absorption fine structure (EXAFS).²²³ Calculations for the models with the neutral ligands were also found to compare well for the Co(III)–N_α bond length. The experimental findings (where the base is 5,6-dimethylbenzimidazole) were reported as follows: MeCbl was 2.16–2.19 Å (X-ray) and 2.20 ± 0.03 Å (EXAFS),^{149,150,152,223} while AdoCbl gave 2.19–2.24 Å.¹⁵⁰

The report by Bürgi *et al.*,¹⁴⁰ and several other reports,^{6,9,58,60} have shown that a change in the β-ligand will promote an inverse *trans* influence on the Co(III)–N_α bond. In addition, these reports have also shown that a linear relationship exists between the Co(III)–C_β bond length and its BDE. Moreover, they revealed that no significant changes were noted when the Co(III)–N_α bond length or the type of N_α ligand was varied.

The results in **Table 5.1B** are in disagreement with these reports. Although there is some indication of a linear relationship between the Co(III)–C_β bond length and the Co(III)–C_β BDE in all of the model systems used, there are a few exceptions as well.

The corrin and porphyrin models display a similar trend, showing an increase of the Co(III)–C_β bond length as the proton affinity and steric bulk of the α ligand increases. **Figure 5.5** shows the increase in proton affinity to parallel the ΔG and BDEs for the Co(III)–C_β bond.

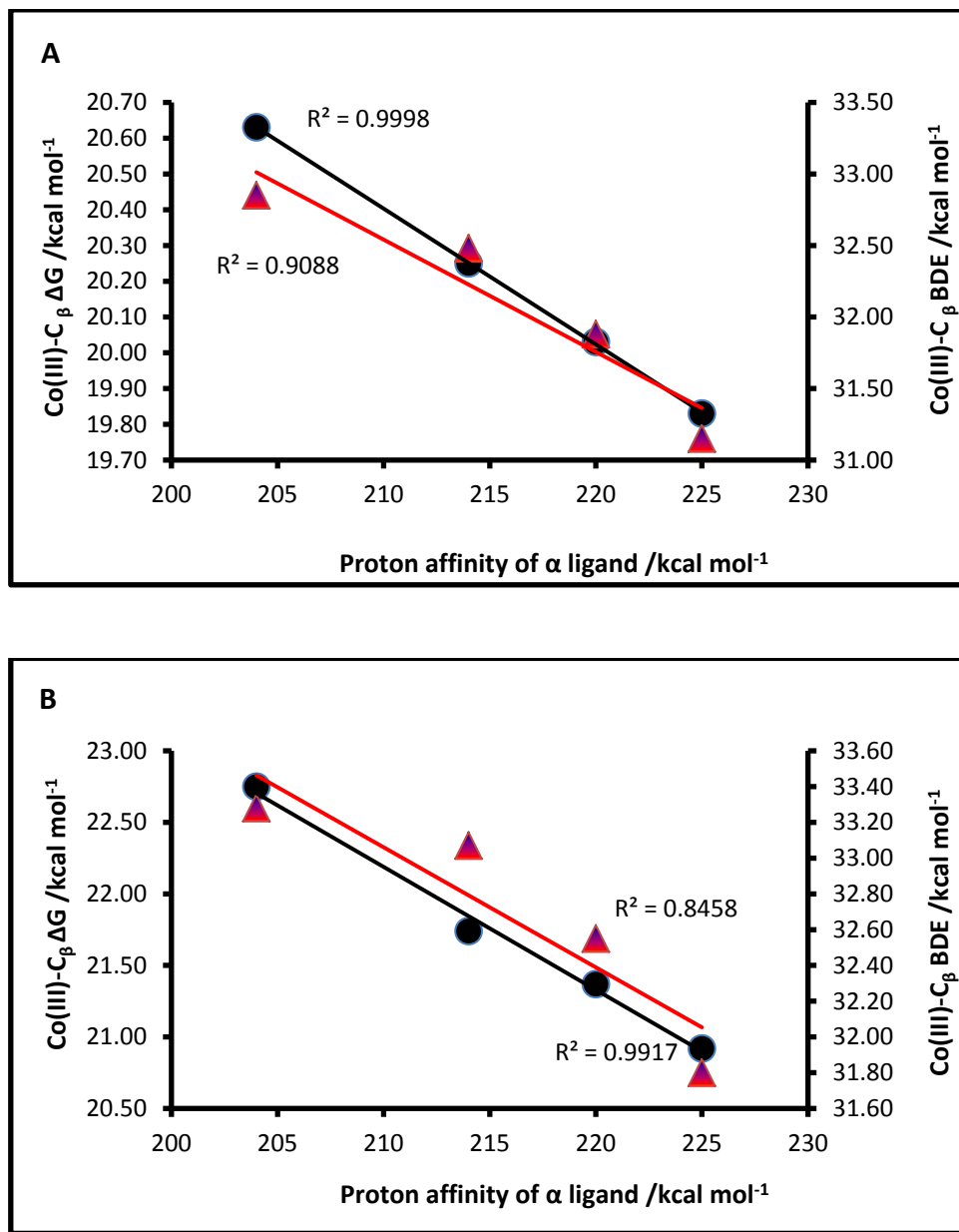


Figure 5.5: Proton affinity values (kcal mol⁻¹) of the α axial ligand versus ΔG (●) and BDE (▲) (kcal mol⁻¹) of the Co-C _{β} bond for A) corrin and B) porphyrin model systems.

Interestingly, and independent of the E_{pa} , a direct relationship is observed between the Co(III)-N _{α} and Co(II)-N _{α} bond length with the ΔG and BDE of the Co(III)-C _{β} bond for the corrin and porphyrin models (see **Figure 5.6** where only the corrin

model is graphically presented). These two trends are not observed for the cobaloxime and corrole models.

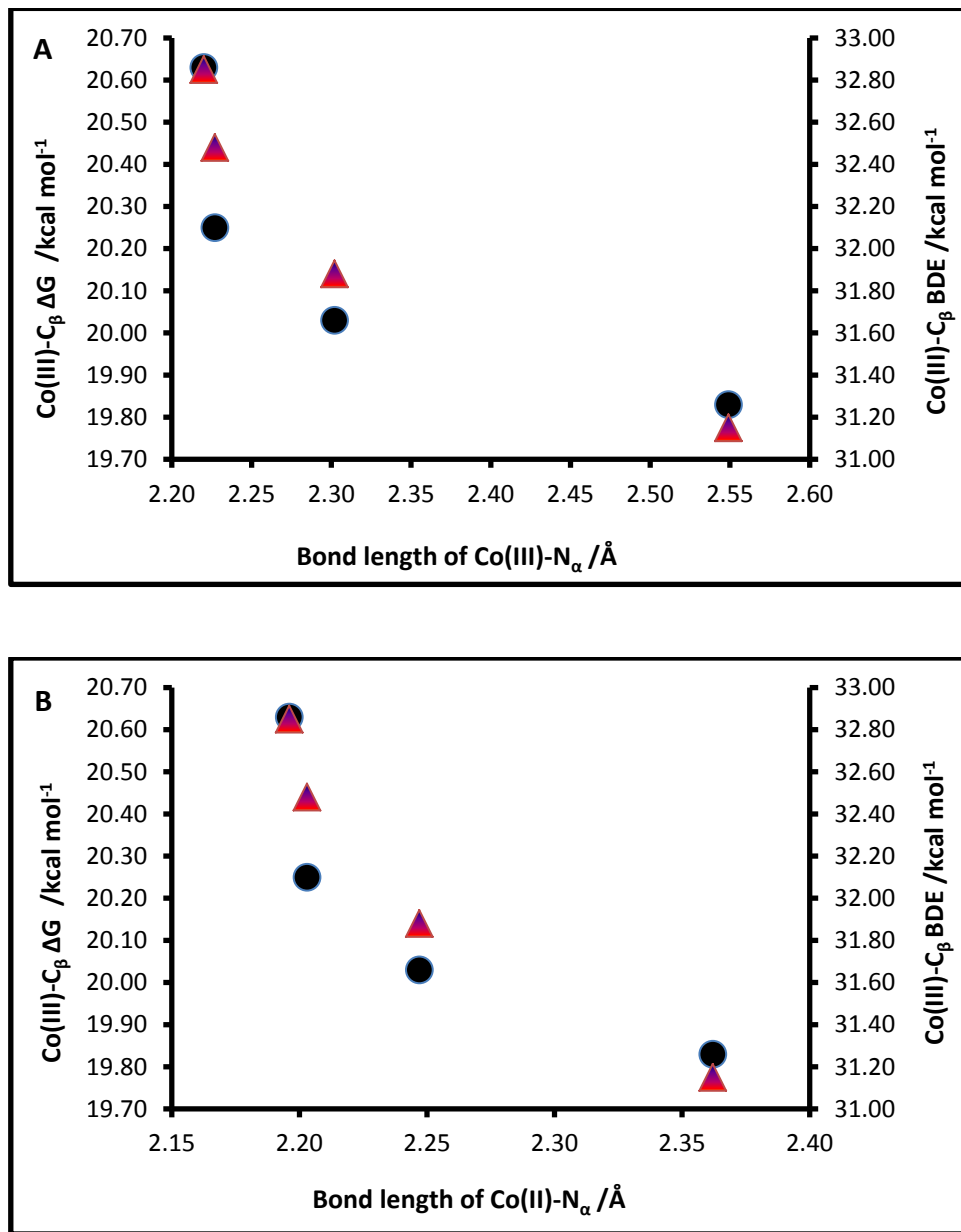


Figure 5.6: A) Co(III)-N_α and B) Co(II)-N_α bond lengths (Å) are plotted against ΔG (●) and BDE (▲) (kcal mol⁻¹) of the Co-C_β bond for the corrin model.

Even more interesting is the difference of the Co–N_α bond length between the Co(II)-5 coordinate and Co(III)-6 coordinate complex (see $\Delta_{(5c-6c)}$ in **Tables 5.1A** and **B**) where in most instances the Co(II)–N_α bond length is found to be shorter than the Co(III)–N_α bond. This decrease in bond length arises from the change in coordination number of the complexes. Thus the cobalt ion in the 5-coordinate complex is found ~0.1 Å below the corrin plane towards the α ligand, and the orbital overlap between the atoms is found to increase^{48,224}, leading to a shorter bond. This contraction of the bond was reported in experimental work on the thermolysis of AdoCbl, conducted by Finke *et al.*²²⁴. Jensen *et al.*⁴⁸ confirmed the shift of the cobalt ion by calculation, and the current data in **Tables 5.1A** and **B** support their calculations by showing a similar lowering of the Co ion below the mean plane, together with a shortening of the Co(II)–N_α bond length.

In fact, the data implies that the larger the difference in contraction of the Co–N_{α(5c-6c)}} bond length from the 5-coordinate to the 6-coordinate complex, the greater the thermodynamic drive towards the formation of the Co(II) complex. As a result, the $\Delta_{(5c-6c)}$ for the Co–N_α bond is shown to parallel the BDE and ΔG for the Co(III)–C_β bond, shown in **Figure 5.7**.

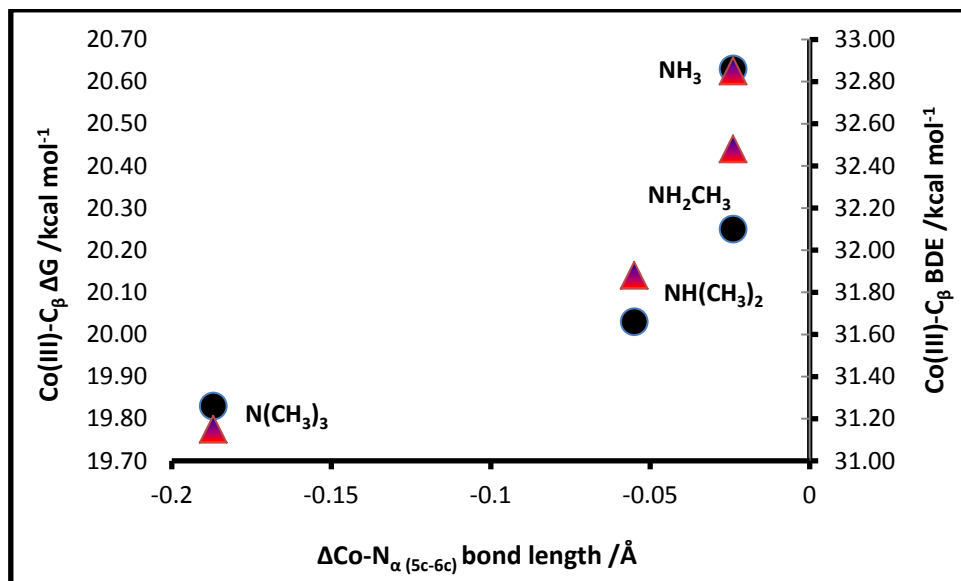


Figure 5.7: The Co(III)-C $_{\beta}$ ΔG (●) and BDE (▲) (kcal mol $^{-1}$) as a function of $\Delta\text{Co-N}_{\alpha(5c-6c)}$ bond length (Å) for the corrin model.

The lengthening of the Co(III)-C $_{\beta}$ bond does not imply a lowering of the ΔG and BDEs of the Co(III)-C $_{\beta}$ bond, in agreement with Coe *et al.*'s²²⁵ view that bond weakening is not necessarily synonymous with bond lengthening. The results presented for the charges and neutral ligands are completely different. The cobalamin models carrying charged α ligands produce a normal *trans* influence between the axial bonds, while the models with the neutral α ligands show the same axial bonds experiencing an inverse *trans* influence. Further to this, the data for the neutral ligands show the $\Delta_{(5c-6c)}$ of the Co-N $_{\alpha}$ bond length as parallel to the BDE for the homolysis of the Co(III)-C $_{\beta}$ bond, however, models with the charged ligands show no such correlation between the same parameter with the associated BDE, although, the given Co(III)-C $_{\beta}$ BDE continues to decrease as the E_{pa} of the ligand increases. It is therefore clear that for these model complexes there is more than one factor contributing towards the changes observed in both the geometric and thermodynamic parameters.

For all of the complexes containing the tri-substituted ligand $\text{N}(\text{CH}_3)_3$, the large increase in the $\text{Co(III)}-\text{N}_\alpha$ bond length is indeed expected and is attributed to the larger steric demand (as assessed by its molar volume) of the α ligand. From the data given in **Tables 5.1A** and **B**, each model is found to behave differently for this particular ligand. While the additional electron-releasing methyl group may be partly responsible for the continued lowering of the BDE (*trans* electronic effect and a better stabilization for the Co(II) complex) irrespective of the strengthening in the $\text{Co(III)}-\text{C}_\beta$ bond, this is not a common trend for all of the models. Thus, the partial charge (although shown to be unreliable for the cobalamin models with the charged α ligands) are calculated and reported, not in isolation but together with the topological properties from the QTAIM analysis, for all of these complexes (reported later in this chapter) as a means to find possible reasons for some of the deviations seen for the $\text{Co(III)}-\text{C}_\beta$ bond lengths and their associated BDEs. However, it must be stated that major emphasis is placed on discussing data from the QTAIM analysis rather than the generated partial charges.

Christianson and Lipscomb¹⁹⁹ did not consider this inverse *trans* influence of the α ligand to have an electronic effect on the labilisation of the $\text{Co(III)}-\text{C}_\beta$ bond. They suggested that the weakening of the $\text{Co(III)}-\text{C}_\beta$ bond arises from a steric interaction as opposed to an electronic one. They investigated the extent of the $\text{Co(III)}-\text{C}_\beta$ reduced overlap population (ROP) against the strength of the $\text{Co(III)}-\text{C}_\beta$ bond, and found the steric effects, without the electronic effects, to activate the homolysis of the $\text{Co(III)}-\text{C}_\beta$ bond. In another study, Andruniow *et al.*⁶⁰ also reported the lack of influence that the α ligand has on the homolysis of the $\text{Co(III)}-\text{C}_\beta$ bond. They used cobalamin models with a range of α ligands having different complexities, that is, steric and electronic, and found that a manipulation (made longer or shorter) of the lower axial bond ($\text{Co(III)}-\text{N}_\alpha$) had no influence on the upper axial bond ($\text{Co(III)}-\text{C}_\beta$) length and the associated BDE. In addition, calculations with a “base off” (without the α ligand) cobalamin model revealed an increase of the $\text{Co(III)}-\text{C}_\beta$ BDE; however they reported this increase as comparable to experimental error. Arguably, the results

presented in **Tables 5.1A** and **B** may accommodate the same conclusions about the role of the α ligand, however modern DFT calculations^{6,58,59} provide evidence that indeed the *trans* ligand does make a contribution, however small, to the Co(III)–C $_{\beta}$ bond breaking, an observation also noted from the results for the charged ligands. This discrepancy is further examined and discussed in Chapter 6.

(b) *Conformational change of the macrocycle*

The inverse *trans* influence has been associated with the conformational change of the corrin macrocycle ring.⁵⁹ This variation in the stereochemistry of the macrocycle has been described as a swivel of the pyrrolinyl groups in the plane of the N_{eq} donors instead of the upward folding normally used when describing this type of movement in the corrins conformation.⁵⁹ In their studies, Andruniow *et al.*⁵⁹ observed the corrin ring to **flatten** as the Co(III)–C $_{\beta}$ bond elongated.

For this study, each model (**Figures 5.9(A)–(D)**) hints at a slight upward tilting of the ring as the Co(III)–C $_{\beta}$ bond length increases. As confirmation, eight torsion angles (ω) were measured. The eight torsion angles used are defined by Jensen *et al.*⁶ as follows:

ω_1	=	N3-Co-N2-C7
ω_2	=	N3-Co-N4-C10
ω_3	=	N4-Co-N3-C9
ω_4	=	N4-Co-N1-C12
ω_5	=	N1-Co-N4-C11
ω_6	=	N1-Co-N2-C6
ω_7	=	N2-Co-N1-C5
ω_8	=	N2-Co-N3-C8

The larger the value of the average ω (ω_{avg}) obtained, the greater is the degree of distortion of the macrocyclic ring, while on the other hand a zero value will imply a

completely planar ring.²²⁶ For the corrin moiety the experimental crystallographic results were found to be about 8.2° .^{149,150,227,228}

The numbering format as defined by Jensen *et al.* was implemented and is illustrated in **Figure 5.8**. The respective torsion angles were measured and the ω_{avg} is presented in **Table 5.4**, while $\omega_1 - \omega_8$ can be found in Appendix 2: Tables A2.1–A2.4.

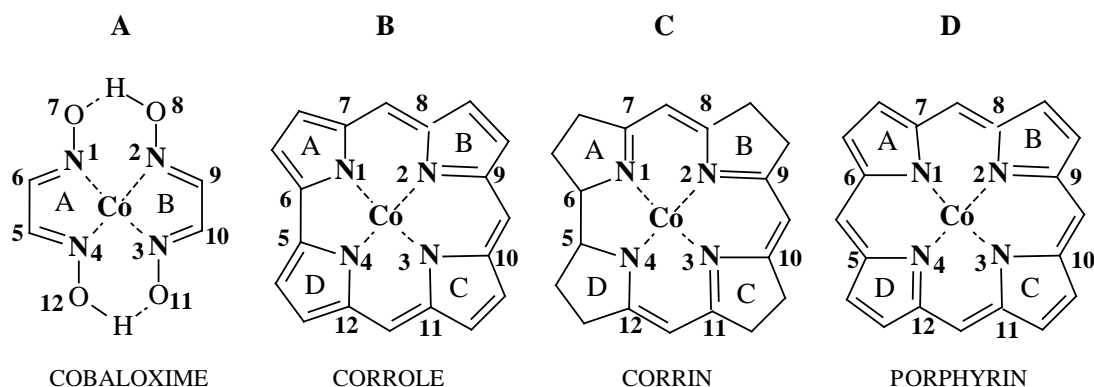


Figure 5.8: Numbering format used for measurement of torsion angles ($\omega_1 - \omega_8$) for models A–D.

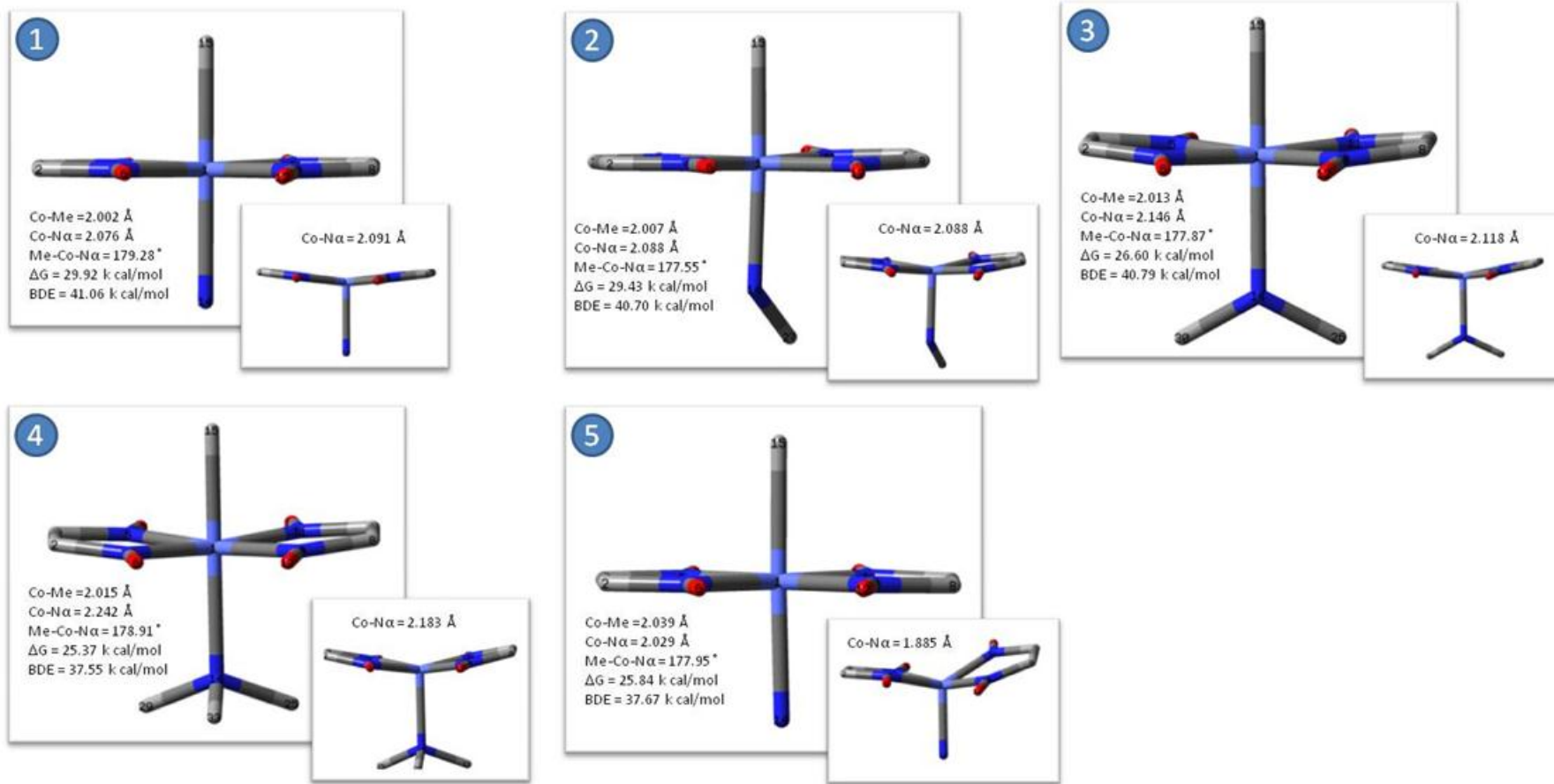


Figure 5.9A: Cobaloxime: Co(III) and Co(II) species with α ligands, 1=NH₃; 2=NH₂CH₃; 3=NH(CH₃)₂; 4=N(CH₃)₃ and 5=NH₂⁻.

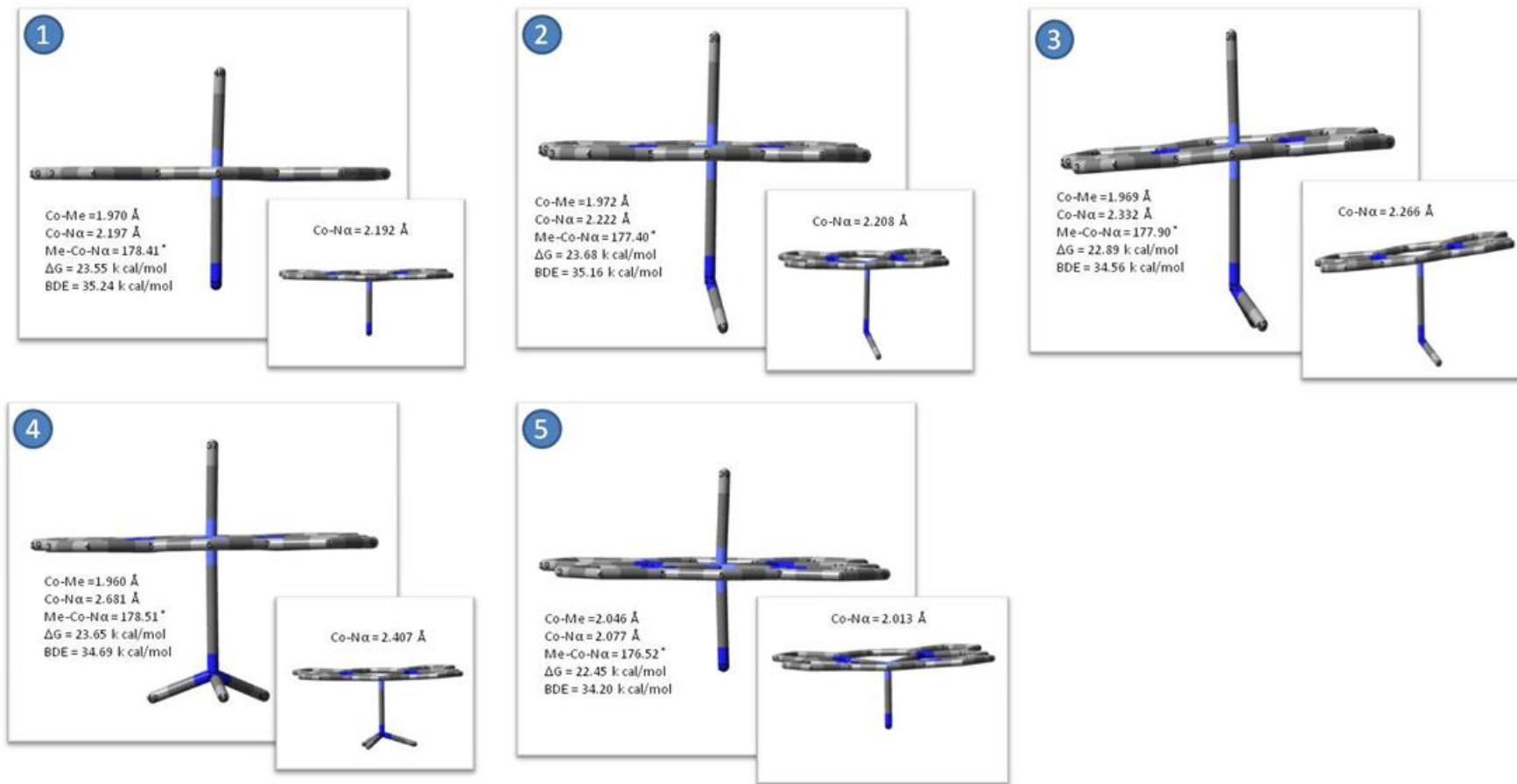


Figure 5.9B: Corrole: Co(III) and Co(II) species with α ligands, 1= NH_3 ; 2= NH_2CH_3 ; 3= $\text{NH}(\text{CH}_3)_2$; 4= $\text{N}(\text{CH}_3)_3$ and 5= NH_2^- .

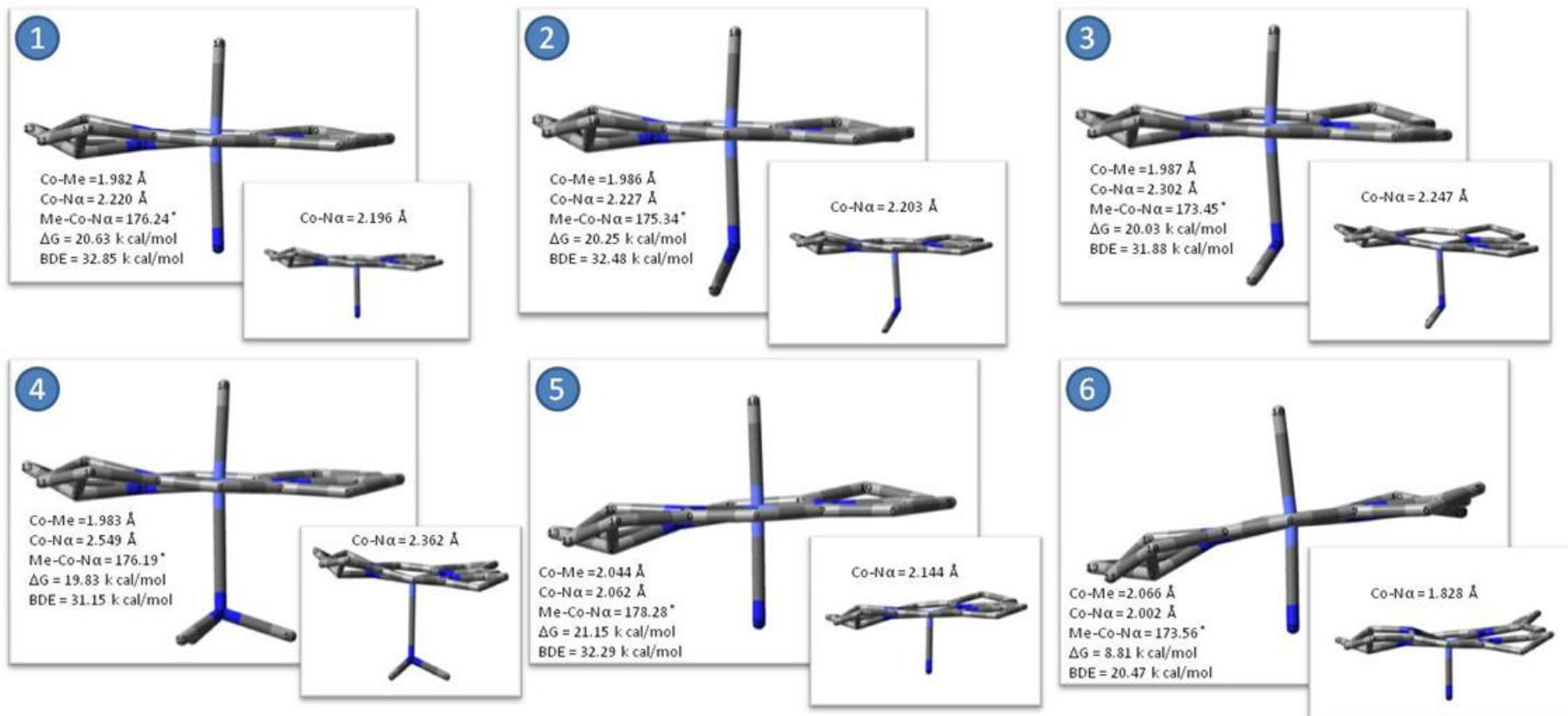


Figure 5.9C: Corrin: Co(III) and Co(II) species with α ligands, 1= NH_3 ; 2= NH_2CH_3 ; 3= $\text{NH}(\text{CH}_3)_2$; 4= $\text{N}(\text{CH}_3)_3$; 5= NH_2^- and 6= NH^{2-} .

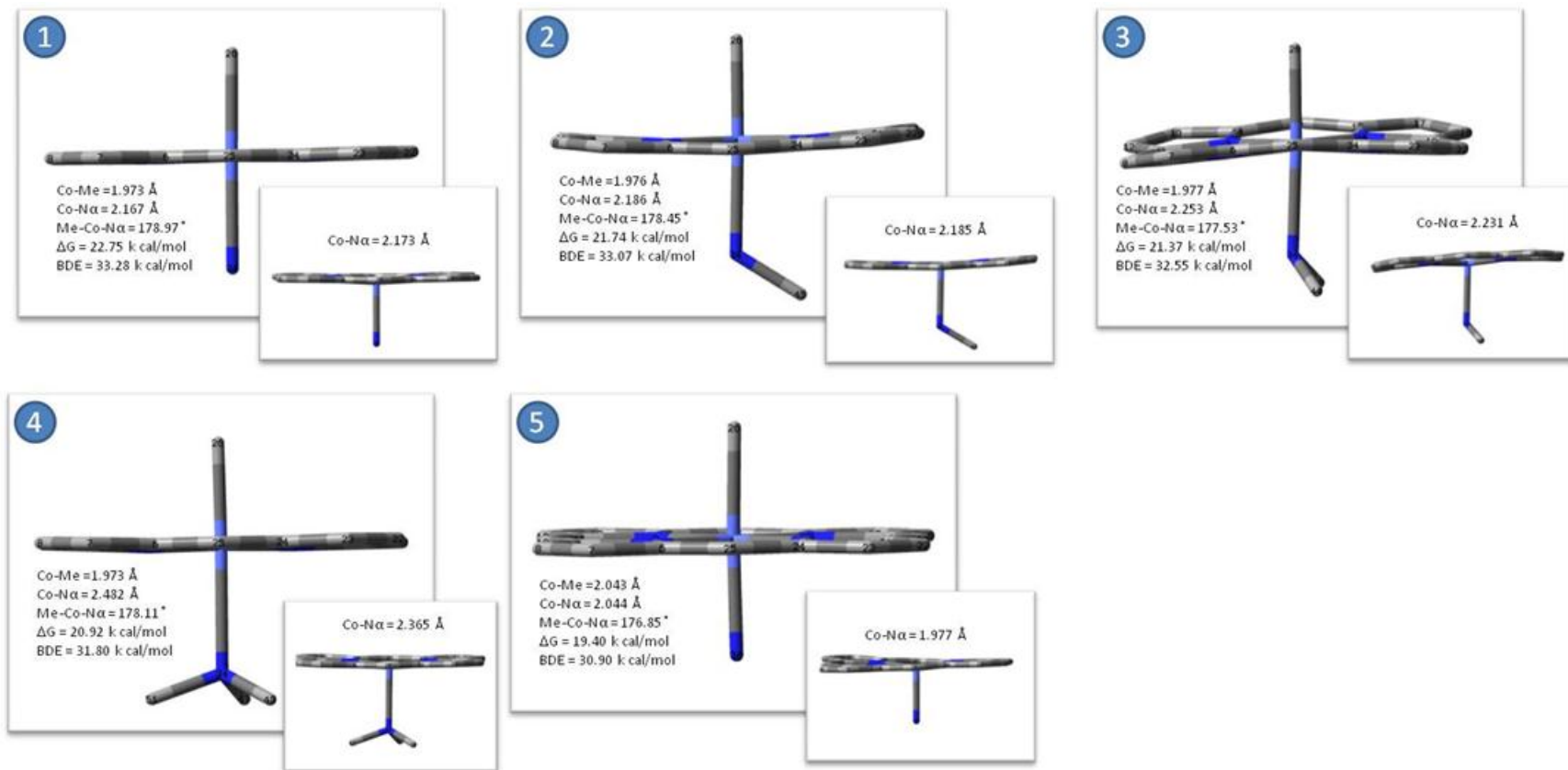


Figure 5.9D: Porphyrin: Co(III) and Co(II) species with α ligands, 1= NH_3 ; 2= NH_2CH_3 ; 3= $\text{NH}(\text{CH}_3)_2$; 4= $\text{N}(\text{CH}_3)_3$ and 5= NH_2^- .

An assessment of the results obtained (**Table 5.4**) shows no distortion in the corrin moiety that contain ligands 1 to 5, and changes for those models with ligands 6 to 10 for the Co(III) complex. There are greater changes observed for those models with the charge-bearing α ligands, a state which possibility arises from van der Waals interactions between the ring and the lone pair of electrons on the α ligand. Small changes for the Co(II) species with ligands 1 to 10 are also observed and this is expected, as the methyl group has left (Co(II)-N $_{\alpha}$ gets shorter) and the Co(II) complex has a greater conformational freedom and is therefore more flexible.

Table 5.4: Torsion angles of cobaloxime, corrole, corrin and porphyrin

$[\text{NX}_3-(\text{Co(III)}(\text{L})_4)-\text{CH}_3]^{n+}$										
Average torsion angles (ω_{avg}) / $^{\circ}$										
Models	1	2	3	4	5	6	7	8	9	10
A	0.5	0.8	0.6	0.4	0.1					
B	0.0	0.0	0.0	0.0	0.0					
C	3.3	3.3	3.3	3.3	3.3	2.8	3.3	3.1	3.7	3.3
D	0.0	0.0	0.0	0.0	0.0					
$[\text{NX}_3-(\text{Co(II)}(\text{L})_4)]^{n+}$										
A	0.4	0.9	0.7	0.3	2.2					
B	0.0	0.0	0.0	0.0	0.0					
C	3.4	3.3	3.2	3.5	3.0	4.3	3.5	2.9	4.2	3.0
D	0.0	0.0	0.0	0.0	0.0					

In the table, Models A=Cobaloxime; B=Corrole; C=Corrin and D=Porphyrin while 1–6 indicates the type of α ligand present in the complex where 1=NH $_3$; 2=NH $_2$ CH $_3$; 3=NH(CH $_3$) $_2$, 4=N(CH $_3$) $_3$, 5=NH $_2^-$, 6=NH $^{2-}$, 7=NH $_2$ F, 8=NH F^- , 9=NF $^{2-}$ and 10=NHCH $_3^-$. Blank spaces indicate no calculations were performed for those models.

The corrin model with ligand 6, does confirm an observation made by Andruniow *et al.*⁵⁹, that is, the ring flattens as the Co(III)-C $_{\beta}$ bond is seen to increase in length, effectively distorting the macrocycle by 0.5 $^{\circ}$. The ω_{avg} of distortion for model C with ligands 1–10 compares favourably with the experimental value of 8.2 $^{\circ}$, because in the actual full structure of AdoCbl and MeCbl the α ligand is the much bigger DMB ligand, and therefore a larger angle of distortion is expected.

On the other hand, the ω_{avg} for the cobaloxime fluctuates considerably as the α ligand grows in bulkiness. The highest angle of distortion is found for the Co(III) complex with the unsymmetrical ligand, $-\text{NH}_2\text{CH}_3$. These distortions observed for the cobaloxime complexes are attributed to the flexibility of the cobaloxime's smaller equatorial ligand as compared to the corrin's larger macrocyclic ring. The porphyrin and corrole models are different from the corrin and cobaloxime because of their planar framework. For both models the planarity of the macrocycle is retained in all cases, irrespective of the various ligands. The measured ω_{avg} presented in **Table 5.4** confirms this by returning a zero value for both of the models for the Co(III) and Co(II) species.

(c) *Partial charges and electron densities*

Of note, is Grinberg's²²⁹ 'polarisation theory', which provides a theoretical description of *trans* influences. The simplicity of this theory describes the amassing of negative charge on the metal, which then repels negative charge on the *trans* ligand, thereby weakening the *trans* bond. Many attempts²³⁰⁻²³⁹ have been made to either modify or add to this theory; however quantum chemical calculations have served to restate Grinberg's original polarisation theory.²²⁵

The Mulliken, APT, NBO and Bader charges for Co, C_β , N_α atoms and N_{eq} are presented in **Tables 5.5A** and **B** for the cobaloxime, corrole, corrin and porphyrin model systems. As poor results were obtained for the partial charges in Section A, and no correlations could be made, in this section, Grinberg's polarisation theory was used as a point of reference while analysing the generated partial charges for the models.

Table 5.5A: Mulliken and APT charges (e) for model complexes A–D

α ligands	MULLIKEN							APT						
	Co(III)	C $_{\beta}$	N $_{\alpha}$	N $_1$	N $_2$	N $_3$	N $_4$	Co(III)	C $_{\beta}$	N $_{\alpha}$	N $_1$	N $_2$	N $_3$	N $_4$
Cobaloxime														
NH $_3$	-1.165	-0.315	-0.916	-0.221	-0.261	-0.275	-0.265	-0.085	0.215	-0.202	0.536	0.408	0.538	0.412
NH $_2$ CH $_3$	-1.430	-0.184	-0.648	-0.203	-0.164	-0.276	-0.239	-0.105	0.205	-0.207	0.536	0.396	0.534	0.407
NH(CH $_3$) $_2$	-1.596	-0.156	-0.437	-0.413	-0.138	-0.334	-0.331	-0.093	0.193	-0.262	0.518	0.398	0.517	0.394
N(CH $_3$) $_3$	-1.250	-0.122	-0.578	-0.197	-0.196	-0.280	-0.237	-0.070	0.193	-0.335	0.501	0.383	0.507	0.390
Corrole														
NH $_3$	-2.748	-0.483	-0.771	0.373	0.412	0.412	0.379	0.301	0.139	-0.293	-0.277	-0.280	-0.287	-0.277
NH $_2$ CH $_3$	-2.515	-0.368	-0.468	0.251	0.465	0.465	0.331	0.304	0.126	-0.331	-0.278	-0.287	-0.281	-0.273
NH(CH $_3$) $_2$	-2.185	-0.415	-0.210	0.205	0.397	0.398	0.205	0.317	0.131	-0.416	-0.274	-0.274	-0.278	-0.278
N(CH $_3$) $_3$	-1.931	-0.330	-0.445	0.321	0.374	0.374	0.239	0.296	0.158	-0.553	-0.272	-0.262	-0.263	-0.272
Corrin														
NH $_3$	-3.088	-0.272	-0.871	0.365	0.468	0.513	0.405	0.218	0.176	-0.288	-0.233	-0.531	-0.530	-0.227
NH $_2$ CH $_3$	-3.023	-0.202	-0.547	0.407	0.403	0.379	0.389	0.221	0.163	-0.305	-0.228	-0.522	-0.525	-0.224
NH(CH $_3$) $_2$	-2.736	-0.203	-0.344	0.386	0.285	0.307	0.422	0.232	0.159	-0.362	-0.220	-0.518	-0.510	-0.218
N(CH $_3$) $_3$	-2.610	-0.196	-0.490	0.327	0.373	0.430	0.351	0.233	0.166	-0.448	-0.229	-0.497	-0.493	-0.221
Porphyrin														
NH $_3$	-1.756	-0.490	-0.835	0.282	0.330	0.344	0.279	0.362	0.152	-0.285	-0.248	-0.247	-0.247	-0.240
NH $_2$ CH $_3$	-1.743	-0.335	-0.531	0.250	0.199	0.327	0.411	0.368	0.139	-0.311	-0.250	-0.251	-0.246	-0.245
NH(CH $_3$) $_2$	-1.514	-0.389	-0.269	0.192	0.193	0.342	0.341	0.380	0.137	-0.370	-0.252	-0.252	-0.241	-0.241
N(CH $_3$) $_3$	-0.755	-0.370	-0.584	0.205	0.178	0.236	0.174	0.384	0.151	-0.466	-0.242	-0.240	-0.241	-0.241

N $_1$, N $_2$, N $_3$ and N $_4$ are the partial charge on the N $_{eq}$ of the cobalamin macrocycle. The numbering system used for the N $_{eq}$ is per Figure 5.8. A, B, C and D represent the α ligands used, that is A=NH $_3$; B=NH $_2$ CH $_3$; C=NH(CH $_3$) $_2$ and D=N(CH $_3$) $_3$, respectively.

Table 5.5B: NBO and BADER charges (e) for model complexes A–D

Model	NBO							BADER						
	Co(III)	C $_{\beta}$	N $_{\alpha}$	N $_1$	N $_2$	N $_3$	N $_4$	Co(III)	C $_{\beta}$	N $_{\alpha}$	N $_1$	N $_2$	N $_3$	N $_4$
Cobaloxime														
A	0.032	-0.744	-1.01	0.037	-0.011	0.035	-0.012	1.046	-0.160	-1.051	-0.500	-0.503	-0.579	-0.581
B	0.051	-0.750	-0.788	0.036	-0.009	0.031	-0.019	1.042	-0.160	-0.990	-0.496	-0.505	-0.574	-0.582
C	0.081	-0.750	-0.604	0.031	-0.016	0.021	-0.026	1.033	-0.156	-0.947	-0.496	-0.505	-0.572	-0.583
D	0.134	-0.747	-0.452	0.016	-0.033	0.013	-0.035	1.025	-0.148	-0.908	-0.499	-0.503	-0.577	-0.582
Corrole														
A	0.189	-0.730	-1.039	-0.372	-0.395	-0.395	-0.376	1.099	-0.140	-1.050	-1.101	-1.067	-1.067	-1.101
B	0.220	-0.736	-0.816	-0.382	-0.403	-0.397	-0.375	1.092	-0.140	-0.991	-1.100	-1.063	-1.068	-1.103
C	0.269	-0.732	-0.630	-0.394	-0.406	-0.406	-0.393	1.081	-0.133	-0.946	-1.102	-1.061	-1.061	-1.102
D	0.344	-0.719	-0.488	-0.407	-0.424	-0.425	-0.407	1.067	-0.121	-0.919	-1.098	-1.058	-1.057	-1.098
Corrin														
A	0.189	-0.711	-1.048	-0.339	-0.377	-0.375	-0.336	1.079	-0.140	-1.052	-1.088	-1.103	-1.105	-1.088
B	0.215	-0.720	-0.821	-0.339	-0.380	-0.383	-0.340	1.076	-0.142	-0.993	-1.085	-1.102	-1.106	-1.088
C	0.258	-0.721	-0.631	-0.345	-0.395	-0.392	-0.344	1.070	-0.138	-0.948	-1.083	-1.103	-1.104	-1.082
D	0.326	-0.709	-0.483	-0.368	-0.405	-0.404	-0.364	1.057	-0.126	-0.916	-1.083	-1.096	-1.096	-1.082
Porphyrin														
A	0.263	-0.727	-1.048	-0.380	-0.388	-0.386	-0.381	1.065	-0.142	-1.056	-1.056	-1.056	-1.056	-1.056
B	0.288	-0.734	-0.825	-0.393	-0.394	-0.387	-0.386	1.063	-0.144	-0.994	-1.058	-1.058	-1.054	-1.053
C	0.322	-0.731	-0.636	-0.401	-0.401	-0.391	-0.391	1.057	-0.139	-0.945	-1.057	-1.057	-1.051	-1.052
D	0.379	-0.715	-0.486	-0.410	-0.410	-0.409	-0.409	1.043	-0.125	-0.911	-1.050	-1.050	-1.050	-1.050

N $_1$, N $_2$, N $_3$ and N $_4$ are the partial charge on the N $_{eq}$ of the cobalamin macrocycle. The numbering system used for the N $_{eq}$ is per Figure 5.8. A, B, C and D represent the α ligands used, that is, NH $_3$; B=NH $_2$ CH $_3$; C=NH(CH $_3$) $_2$ and D=N(CH $_3$) $_3$, respectively.

Although the partial charge obtained from the Mulliken, APT and NBO methods are numerically very different, they exhibit a systematic increase in positive charge on the Co atom for the corrin and porphyrin models as ligands A–D increase in bulk by the substitution of methyl groups. A linear relationship arises between the partial charge on Co(III) and the BDE of the Co(III)–C β bond as seen in **Figure 5.10 (A–C)**.

For both the cobaloxime and corrole models there is also an increase of positive charge on Co(III) in response to the different α ligands as is observed for the corrin and porphyrin models; however, there are also a few exceptions. The exceptions are seen only for the Mulliken and APT method (NBO for corrole and cobaloxime model shows the same trend as the corrin and porphyrin models described above) and it is not clear why this is so.

On the other hand, and completely different to the other three methods, the partial charge generated from the Bader methodology shows a decrease of positive charge (increase in negative) on the metal centre as the Co(III)–C β BDE decreases, see **Figure 5.10 (D)**.

Overall, the partial charges assigned to the N $_{eq}$ (**Tables 5.5A and B**) and generated from all of the methods are numerically different; however, within each specific method the reported values are fairly consistent with no significant changes observed as the bulkiness of the α ligand was varied.

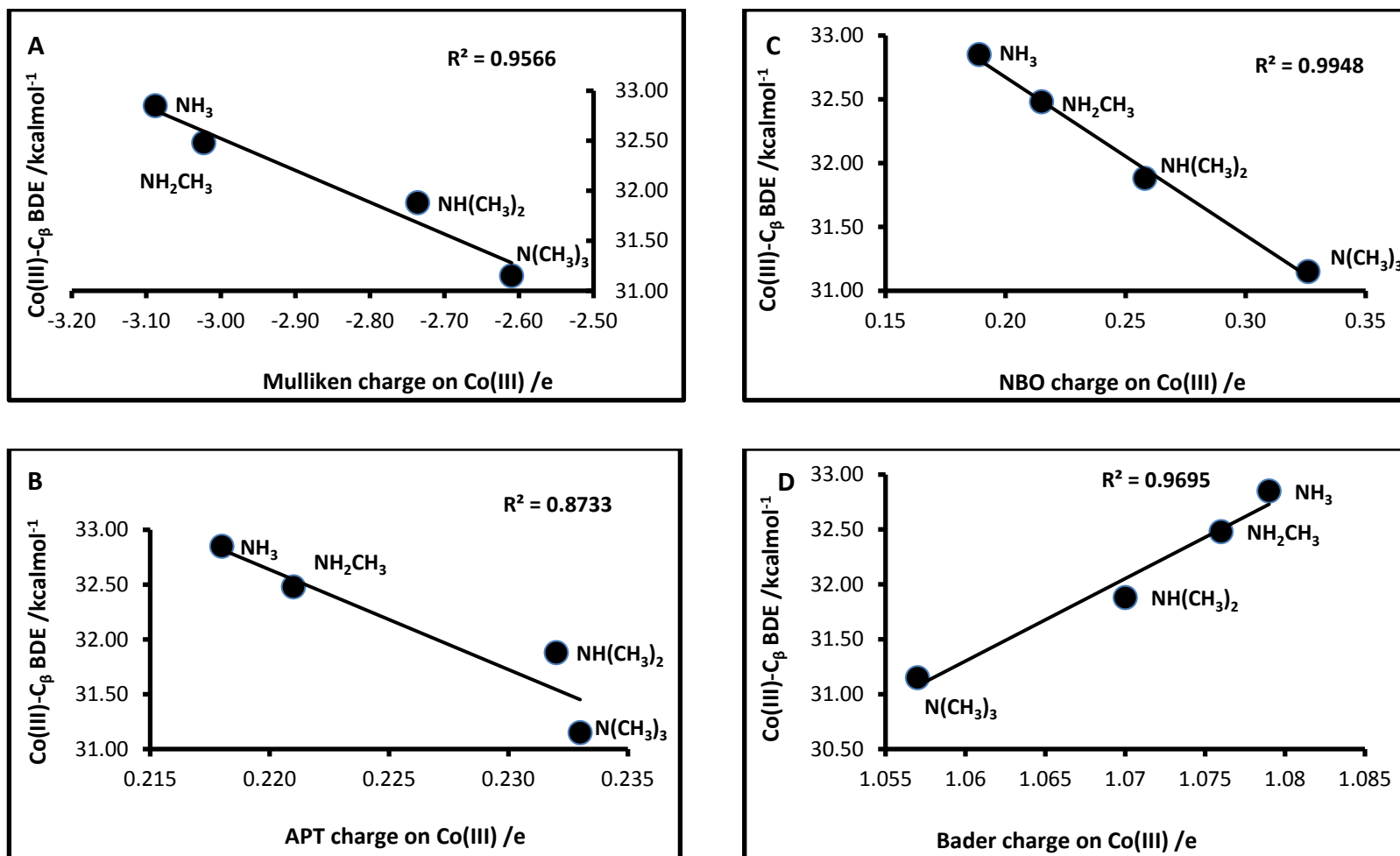


Figure 5.10: Partial charges (e) for: A) Mulliken; B) APT; C) NBO and D) Bader on the Co atom versus BDE (kcal mol⁻¹) of the Co(III)-C β bond for the corrin model.

In contrast, and applying to all of the models, the partial charge on the C_β and N_α atoms decrease in negative charge as assessed by the methods of Mulliken, NBO and Bader, while the APT charges show a decrease in positive charge and an increase in negative charge for these same atoms, respectively. The change of the partial charges as evidenced by the APT methodology is indicative of a normal *trans* influence experienced between the two axial ligands.

Irrespective of the numerical differences, these results complement the trend observed earlier with the $\text{Co(III)}\text{-}N_\alpha$ bond length and the associated $\text{Co(III)}\text{-}C_\beta$ BDE. The graphical presentation of the corrin model provided in **Figure 5.11** shows that the partial charge on the N_α atom (except for Mulliken) parallels the BDE of the homolysis of the $\text{Co(III)}\text{-}C_\beta$ bond.

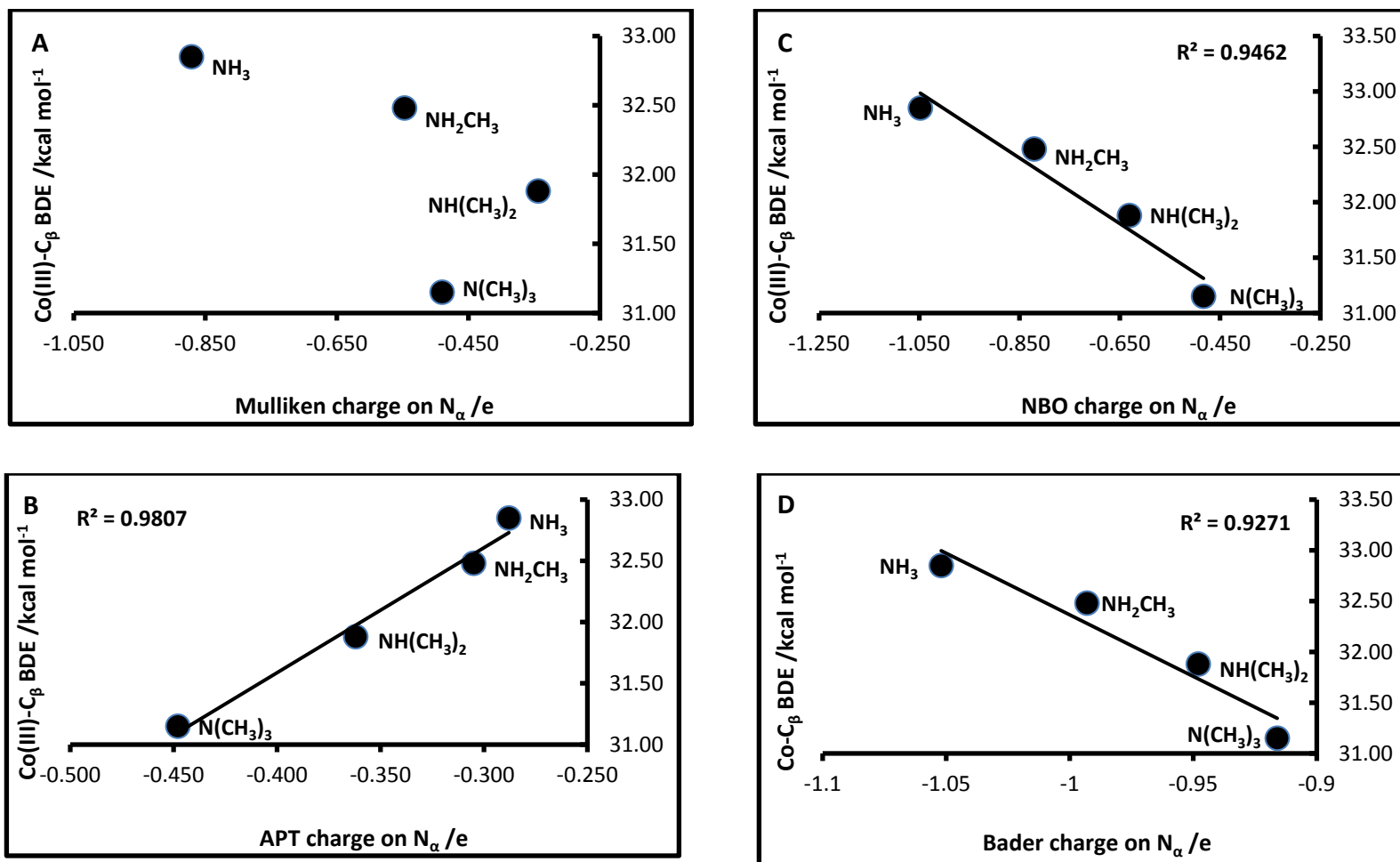


Figure 5.11: Partial charges (e) for: A) Mulliken; B) APT; C) NBO and D) Bader on the N_α atom versus BDE (kcal mol⁻¹) of the Co(III)- C_β bond for the corrin model.

The topological properties of the electron density of the corrin model with the neutral ligands, provided in **Table 5.2**, confirm the covalent and ionic character of the Co(III)–CH₃ and Co(III)–NH₃ bonds respectively, as assessed by their $|V(r)|/G(r)$ values. In addition, the data provided for the ρ at the bcp of both these bonds correlates well with the bond lengths observed in **Table 5.1B**, that is, an increase in bond length is described by a lower ρ -value at the bcp, implying a weaker bond and therefore a lower Co(III)–C _{β} BDE.

(d) The N_{eq} donors

The Co–N_{eq} bond distances for cobaloxime and corrin, see **Table 5.6** and **Figure 5.8** (for the numbering system used), ranges from 1.887–1.910 Å and 1.871–1.999 Å respectively. In comparison to the recorded crystallographic values^{149,152,224} of 1.810 to 1.980 Å for MeCbl, AdoCbl, and Co(II)Cbl, it can be concluded that there is no significant change in bond lengths, as the data obtained falls within the experimental values.

Overall, the corrole model displays a smaller bond length between its Co atom and the N_{eq} donor atoms when compared to the cobaloxime, corrin and porphyrin models. This is attributed to firstly, a relatively small metal binding cavity (as compared to porphyrin) because of the absence of one of the methine groups and secondly, to the macrocycle being relatively rigid (as compared to corrin) because of the full conjugation of π electrons in the macrocyclic ligand.

As was expected, the porphyrin's Co(III)–N_{eq} bond length was the longest amongst the models studied, and ranged from 1.984 Å to 2.001 Å. This is primarily due to the porphyrin's larger macrocyclic ring because of the extra methine group. From this analysis, the results indicate that the α ligand does not make an impact on the bond lengths of the N_{eq} connected to the Co atom.

Table 5.6: Bond lengths (Å) for N_{eq} donors in the Co(III) models

	Bond Lengths/Å			
	Cobaloxime			
	Co-N ₁	Co-N ₂	Co-N ₃	Co-N ₄
NH ₃	1.892	1.908	1.910	1.889
NH ₂ ⁻	1.892	1.878	1.893	1.876
NH ₂ CH ₃	1.892	1.908	1.907	1.887
NH(CH ₃) ₂	1.891	1.905	1.908	1.887
N(CH ₃) ₃	1.889	1.907	1.909	1.888
Corrole				
NH ₃	1.884	1.911	1.911	1.884
NH ₂ ⁻	1.883	1.918	1.918	1.881
NH ₂ CH ₃	1.882	1.908	1.912	1.885
NH(CH ₃) ₂	1.883	1.905	1.905	1.883
N(CH ₃) ₃	1.878	1.901	1.900	1.877
Corrin				
NH ₃	1.883	1.938	1.936	1.877
NH ₂ ⁻	1.869	1.938	1.940	1.873
NH ²⁻	1.877	1.954	1.940	1.887
NH ₂ F	1.891	1.936	1.931	1.880
NHF ⁻	1.874	1.940	1.933	1.873
NF ²⁻	1.889	1.931	1.960	1.868
NH ₂ CH ₃	1.881	1.937	1.938	1.876
NHCH ₃ ⁻	1.867	1.934	1.943	1.878
NH(CH ₃) ₂	1.879	1.936	1.937	1.873
N(CH ₃) ₃	1.878	1.934	1.928	1.871
Porphyrin				
NH ₂ ⁻	1.997	1.999	1.997	2.001
NH ₃	1.999	1.997	1.994	1.997
NH ₂ CH ₃	1.996	1.999	1.992	1.988
NH(CH ₃) ₂	1.995	1.995	1.984	1.984
N(CH ₃) ₃	1.991	1.989	1.990	1.992

The atom labels of the Neq ligands correspond to Figure 5.8.

(e) Cis effect of the equatorial ligands

What is evident from the results presented in **Tables 5.1A and B**, and **Figure 5.12** below is the different behaviour of the cobaloxime model when compared to the corrole, corrin and porphyrin models. The results reaffirm, as mentioned in

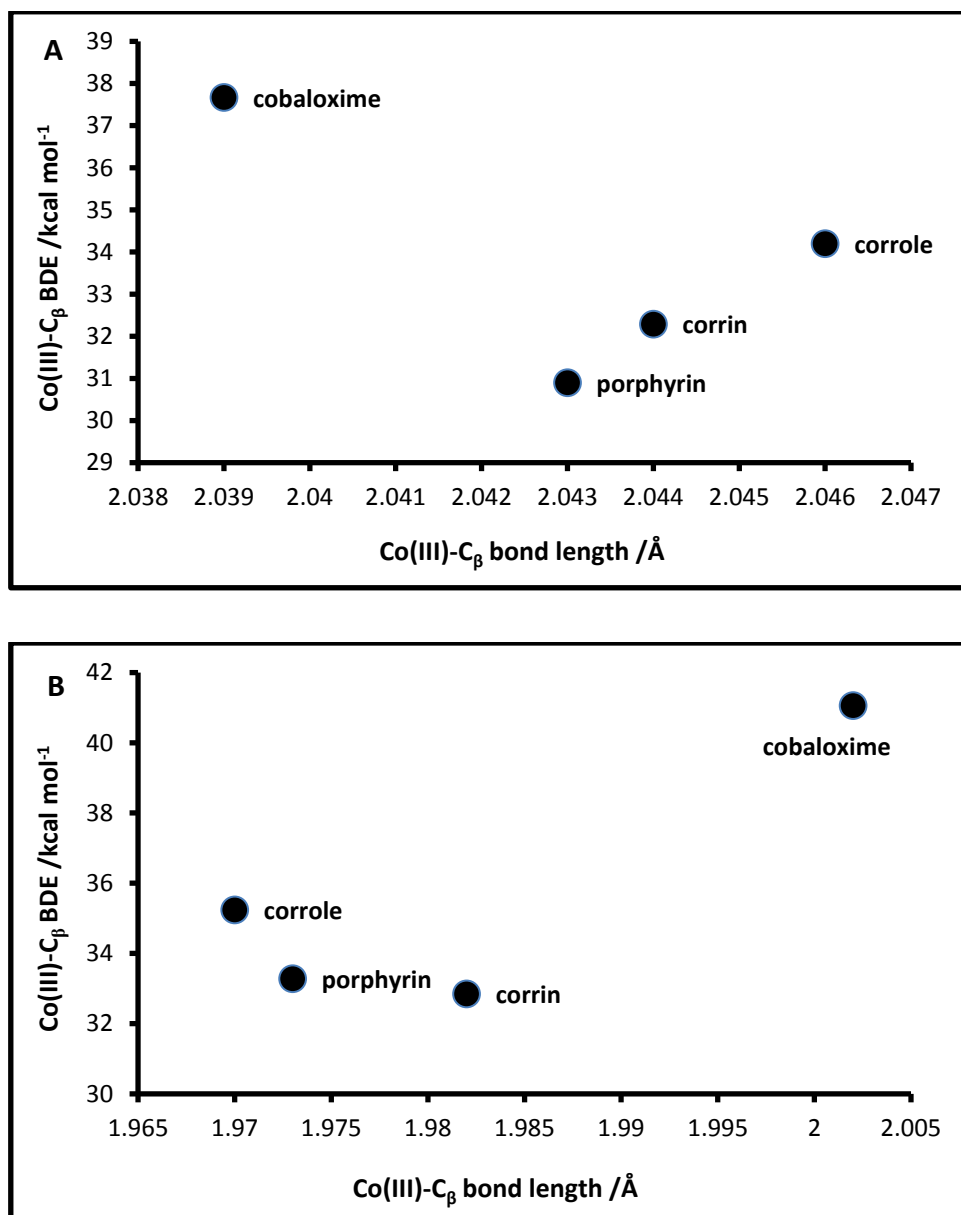


Figure 5.12: A plot of the Co(III)-C_β bond length (Å) with its associated BDE (kcal mol⁻¹) for models with a change in (L)₄ and α ligands A) NH₂⁻ (charged ligand) and B) NH₃ (neutral ligand).

earlier reports,^{10,16} that cobaloxime is an unsuitable cobalamin model because it lacks the aromaticity of the corrin ligand and as a result is more flexible. Therefore, from this point, only the corrole, corrin and porphyrin models, are compared and discussed.

The model compounds corrole, corrin, and porphyrin contain α ligands that are neutral (only NH_3 is discussed as the trends for the other ligands are the same) and charge bearing (NH_2^- which is common in all of the models) in character. The corrole model, irrespective of the type of α ligand attached, retains the most stable Co(III)-C_β bond (high BDE), see **Figure 5.12**. On the other hand, the BDE for the homolysis of the Co(III)-C_β bond in the corrin and porphyrin models are observed to be dependent on the type of α ligand attached, that is, porphyrin with α ligand NH_2^- , exhibits the lowest BDE, while the corrin model with neutral α ligand NH_3 , provides the lowest Co(III)-C_β BDE. Although for all the models with the neutral α ligand NH_3 shows the Co(III)-C_β bond length as parallel to the associated BDEs, the same is not observed for the models with the α ligand NH_2^- .

Cobalamin models, in the given order, corrole, corrin, porphyrin, with α ligand NH_2^- , shows an inverse *trans* influence between the Co(III)-C_β and Co(III)-N_α axial bond lengths while the same models with the NH_3 ligand, show an inverse *trans* influence in the order of corrole, porphyrin and then corrin. The trends however, are different; the former shows a decrease in the axial bond lengths while the latter shows an increase in the axial bond lengths. In addition, by keeping the equatorial ligand constant and altering the α ligands from NH_2^- to NH_3 , the axial bond lengths are shown to experience a *normal* trans influence where the Co(III)-C_β bond length decreases, from a charged to neutral α ligand, while the Co(III)-N_α bond length increases. These observations suggests that a *cis* influence occurs from the macrocyclic equatorial ligand to the Co(III)-C_β bond. The results presented in **Table 5.4** confirm the absence of a *cis*-steric influence from the macrocyclic ring on the

Co(III)–C_β bond; therefore it can only be assumed that a *cis*-electronic influence is taking place.

The distance measured for the movement of the Co metal centre (see **Figure 5.13**) from the mean plane of the equatorial macrocyclic ring are given in **Tables 5.1A** and **B**. These results parallel the observations made previously about the Co(III)–C_β bond lengths and the associated BDEs for all three models.

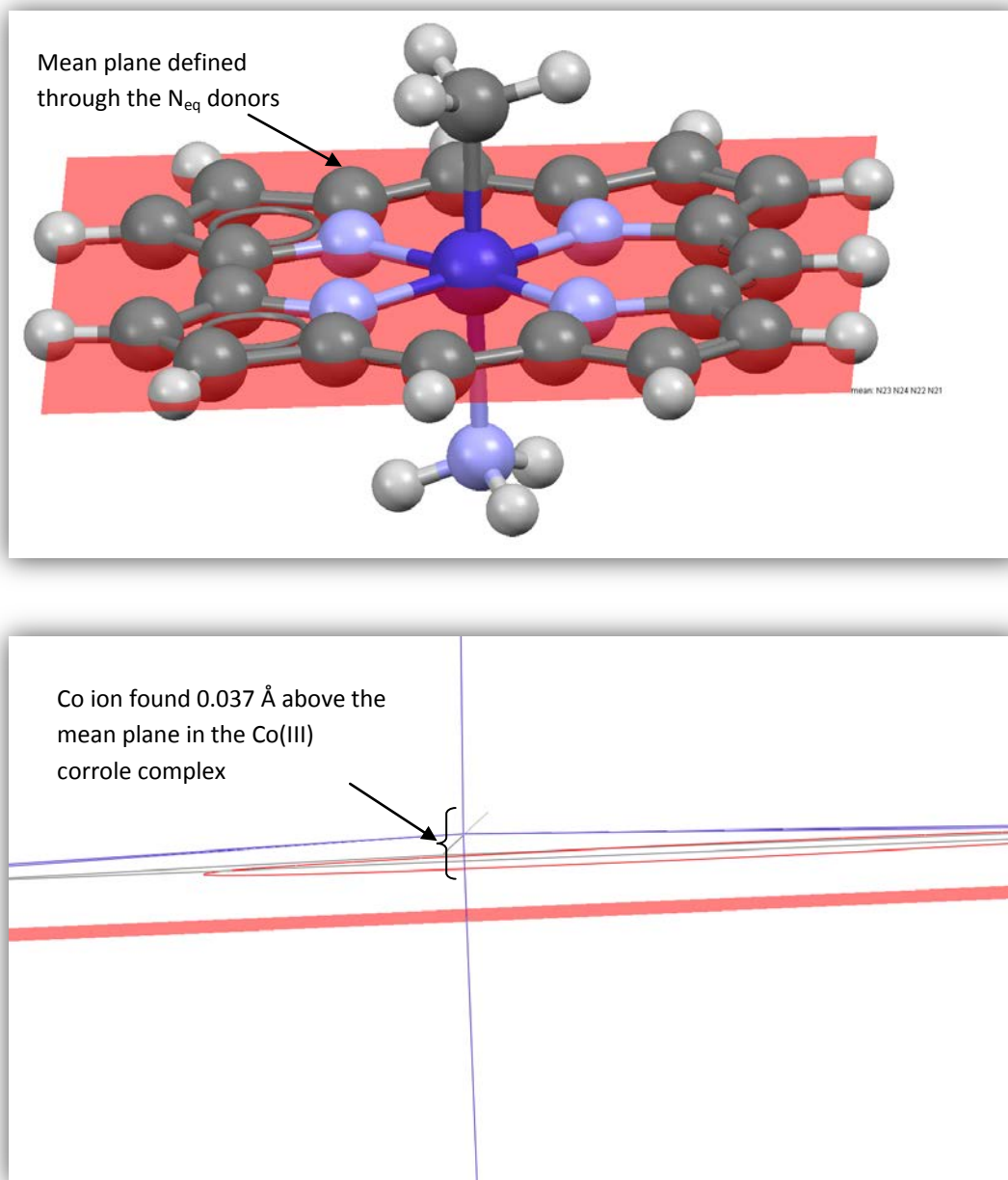


Figure 5.13: Corrole model where the Co(III) ion is identified 0.037 Å above the mean plane defined through the N_{eq} donors.

For the corrole and porphyrin models the Co ion in the Co(III) complex is found high above the mean plane and closer towards the β axial ligand. In the corrole and porphyrin models, this would then imply that there is a greater overlap, and therefore

a stronger bond, between the orbitals of the metal centre and C_β of the β ligand. As a result of this, a larger BDE would be expected for the homolysis of the $\text{Co(III)}-C_\beta$ bond, a trend that is clearly shown in **Figure 5.14(B)**.

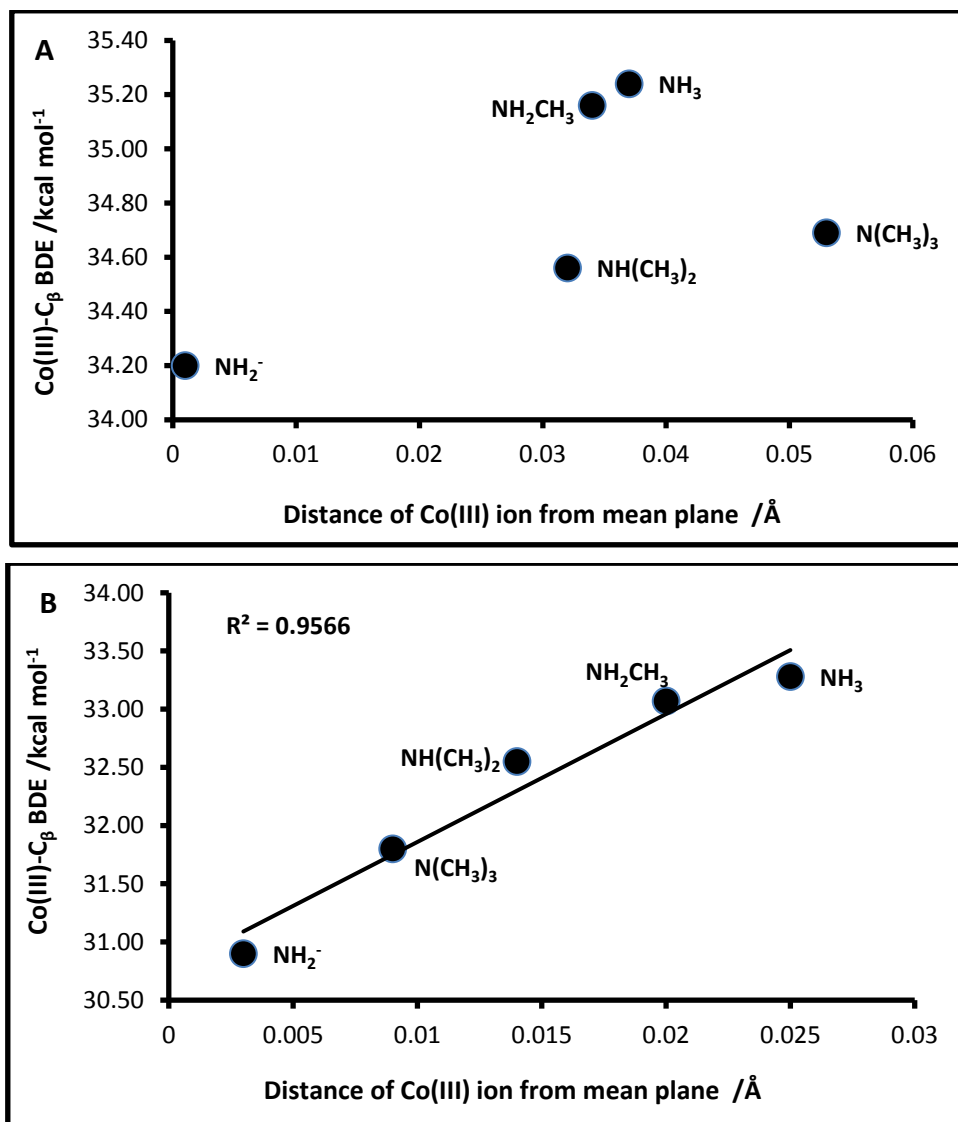


Figure 5.14: The distance of the Co(III) ion from the macrocyclic mean plane (Å) is plotted against the Co(III)-C_β BDE (kcal mol⁻¹) for A) corrole and B) porphyrin.

On the other hand, in the corrin model, the Co ion is also found above, yet close towards the mean plane, while Co in the models with the α ligands; $\text{NH}(\text{CH}_3)_2$ and

$\text{N}(\text{CH}_3)_3$ is identified 0.001 Å below the mean plane. In addition, the ρ -values (**Tables 5.7A** and **B**) at the bcp of the $\text{Co}(\text{III})\text{-C}_\beta$ bond (from the topological properties of the electron density of these systems), confirms that the corrole and porphyrin models have stronger $\text{Co}(\text{III})\text{-C}_\beta$ bonds as compared to the corrin models.

Table 5.7A: Topological properties of the electron density (ρ) at the bcp (au) of Co(III)–CH₃ and Co(III)–NH₃ in the [NX₃–(Co(III)(L)₄)–CH₃]ⁿ⁺ model with (L)₄ = cobaloxime and corrole^a

Co(III)–CH ₃												
α -ligands	Cobaloxime						Corrole					
	ρ	$\nabla^2\rho$	V(r)	G(r)	H(r)	V(r) /G(r)	ρ	$\nabla^2\rho$	V(r)	G(r)	H(r)	V(r) /G(r)
NH ₃	0.1099	0.0695	-0.1236	0.0705	-0.0531	1.7535	0.1178	0.0831	-0.1352	0.0780	-0.0572	1.7335
NH ₂ CH ₃	0.1088	0.0697	-0.1224	0.0699	-0.0525	1.7509	0.1174	0.0823	-0.1348	0.0777	-0.0571	1.7351
NH(CH ₃) ₂	0.1076	0.0646	-0.1204	0.0683	-0.0521	1.7635	0.1178	0.0771	-0.1350	0.0771	-0.0579	1.7502
N(CH ₃) ₃	0.1073	0.0579	-0.1193	0.0669	-0.0524	1.7835	0.1193	0.0692	-0.1367	0.0770	-0.0597	1.7754
NH ₂ ⁻	0.0995	0.1148	-0.1169	0.0728	-0.0441	1.6057	0.1002	0.1152	-0.1167	0.0728	-0.0440	1.6041
Co(III)–NH ₃												
NH ₃	0.0731	0.3242	-0.1084	0.0947	-0.0137	1.1443	0.0544	0.2227	-0.0761	0.0659	-0.0102	1.1552
NH ₂ CH ₃	0.0728	0.3029	-0.1052	0.0905	-0.0147	1.1627	0.0528	0.2009	-0.0717	0.0610	-0.0107	1.1760
NH(CH ₃) ₂	0.0650	0.2457	-0.0892	0.0753	-0.0139	1.1846	0.0425	0.1399	-0.0532	0.0441	-0.0091	1.2071
N(CH ₃) ₃	0.0538	0.1778	-0.0689	0.0567	-0.0122	1.2158	0.0216	0.0612	-0.0203	0.0178	-0.0025	1.1394
NH ₂ ⁻	0.0897	0.2664	-0.1155	0.0910	-0.0244	1.2684	0.0815	0.2323	-0.1012	0.0797	-0.0216	1.2709

^aThe values of charge density (ρ) and its Laplacian ($\nabla^2\rho$) at the bcps are in au (1 au of $\rho = 6.7483 \text{ e}\text{\AA}^{-3}$, and 1 au of $\nabla^2\rho = 24.099 \text{ e}\text{\AA}^{-5}$). The values of the total potential energy density $V(r)$, the kinetic energy density $G(r)$ and the total energy density $H(r)$ at the bcps are in au (1 au = 627.5095 kcal mol⁻¹).

Table 5.7B: Topological properties of the electron density (ρ) at the bcp (au) of Co(III)–CH₃ and Co(III)–NH₃ in the [NX₃–(Co(III)(L)₄)–CH₃]ⁿ⁺ model with (L)₄ = corrin and porphyrin^a

Co(III)–CH ₃												
α -ligands	Corrin						Porphyrin					
	ρ	$\nabla^2\rho$	V(r)	G(r)	H(r)	V(r) /G(r)	ρ	$\nabla^2\rho$	V(r)	G(r)	H(r)	V(r) /G(r)
NH ₃	0.1162	0.0483	-0.1296	0.0708	-0.0588	1.8295	0.1181	0.0586	-0.1331	0.0739	-0.0592	1.8016
NH ₂ CH ₃	0.1153	0.0493	-0.1286	0.0705	-0.0582	1.8252	0.1174	0.0585	-0.1322	0.0734	-0.0588	1.8008
NH(CH ₃) ₂	0.1150	0.0461	-0.1281	0.0698	-0.0583	1.8348	0.1171	0.0548	-0.1316	0.0726	-0.0589	1.8115
N(CH ₃) ₃	0.1153	0.0390	-0.1282	0.0690	-0.0592	1.8587	0.1175	0.0452	-0.1315	0.0714	-0.0601	1.8417
NH ₂ ⁻	0.1025	0.0948	-0.1174	0.0705	-0.0468	1.6639	0.1022	0.1004	-0.1176	0.0714	-0.0462	1.6481
Co(III)–NH ₃												
NH ₃	0.0534	0.1980	-0.0716	0.0606	-0.0111	1.1827	0.0592	0.2396	-0.0830	0.0714	-0.0115	1.1614
NH ₂ CH ₃	0.0541	0.1881	-0.0709	0.0590	-0.0119	1.2025	0.0584	0.2204	-0.0796	0.0673	-0.0122	1.1817
NH(CH ₃) ₂	0.0473	0.1437	-0.0579	0.0469	-0.0110	1.2345	0.0514	0.1733	-0.0664	0.0548	-0.0115	1.2100
N(CH ₃) ₃	0.0297	0.0751	-0.0294	0.0241	-0.0053	1.2204	0.0328	0.0895	-0.0355	0.0290	-0.0066	1.2271
NH ₂ ⁻	0.0857	0.2365	-0.1069	0.0830	-0.0239	1.2878	0.0592	0.2396	-0.1120	0.0872	-0.0248	1.2839

^aThe values of charge density (ρ) and its Laplacian ($\nabla^2\rho$) at the bcps are in au (1 au of $\rho = 6.7483 \text{ e}\text{\AA}^{-3}$, and 1 au of $\nabla^2\rho = 24.099 \text{ e}\text{\AA}^{-5}$). The values of the total potential energy density $V(r)$, the kinetic energy density $G(r)$ and the total energy density $H(r)$ at the bcps are in au (1 au = 627.5095 kcal mol⁻¹).

In the corrin model (with the NH_3 ligand), the Co metal centre is observed to be closer to the corrin mean plane. This implies that there is a weak overlap between the orbitals of the Co ion and C_β from the β ligand. As a result, and compared to porphyrin and corrole, the corrin model has the lowest BDEs for the homolysis of the $\text{Co(III)}-\text{C}_\beta$ bond. This observation was further confirmed by the ρ value (**Table 5.7B**) at the bcp of the $\text{Co(III)}-\text{C}_\beta$ bond. As the Co metal centre is further displaced from the mean plane, the $\text{Co(III)}-\text{C}_\beta$ bond length decreases, and the BDE for the homolysis of the same bond increases, **Figure 5.15**.

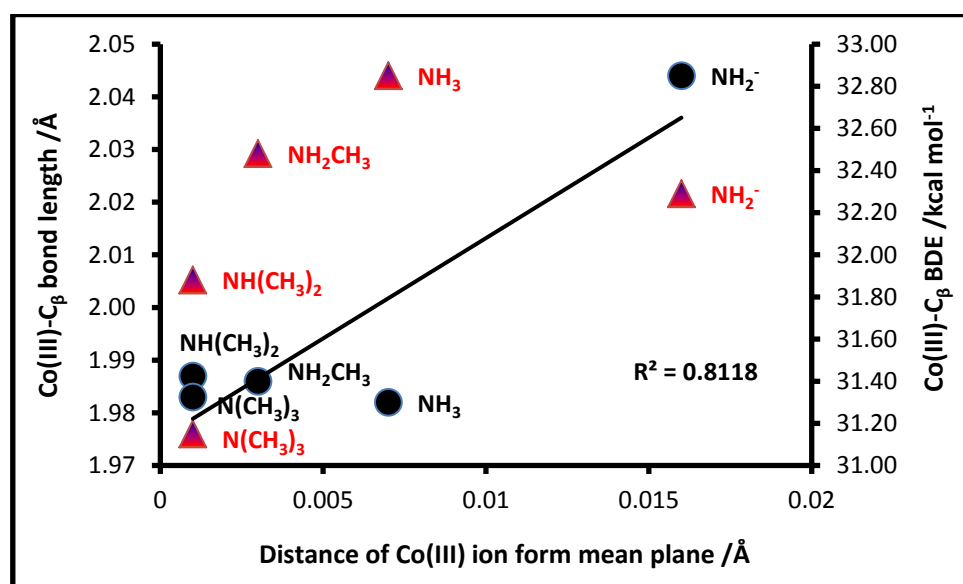


Figure 5.15: The distance of the Co(III) ion from the macrocyclic mean plane is plotted against the $\text{Co(III)}-\text{C}_\beta$ (●) bond length (Å) and its associated BDE (▲) (kcal mol^{-1}) for the corrin model.

For the corrole and porphyrin models, the *cis* effect of the macrocyclic equatorial ligand is evident when the porphyrin model shows lower BDEs for the homolysis of the $\text{Co(III)}-\text{C}_\beta$ bond. The difference between these two models lies in their equatorial ligands and it can only be suggested that because the porphyrin model has a larger aromatic framework, it also has the greater ability to stabilise the Co(II)

complex once homolysis occurs, and thus the Co(III)–C $_{\beta}$ bond in the porphyrin models are cleaved at lower BDEs.

SECTION C: Steric effects

5.3.2 RESTRICTED CONDITIONS

In order to examine whether the change in α ligand or the strain of bond lengths plays an electronic role in lowering the values of ΔG and BDE of the Co(III)–C $_{\beta}$ bond, the Co(III)–N $_{\alpha}$ bond length was restricted within a range of values starting from 1.9 Å to 2.5 Å at 0.1 Å increments (**Figure 5.16**) for both the Co(III) complex and Co(II) species. Calculations were performed and compared for the cobaloxime, corrin, corrole and porphyrin models as a function of the four different α ligands. All of the models were optimised with the BP86 functional and the 6-31+G(d,p) basis set.

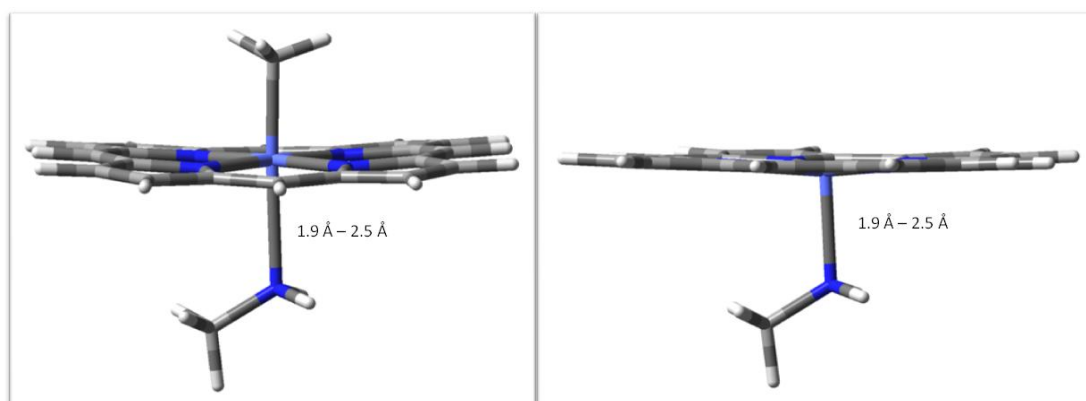


Figure 5.16: Co(III)–N $_{\alpha}$ restricted bond lengths (Å) for Co(III) complex and Co(II)–N $_{\alpha}$ for Co(II) species.

(a) *Bond lengths and BDEs*

In this section, two trends are reported and discussed. These are 1) the effect on the Co(III)–C_β bond length and associated BDE as the nature of the α ligand is varied together with the Co(III)–N_α bond length restricted from 1.9–2.5 Å (*trans* steric effect), and 2) the effect on the Co(III)–C_β bond length and BDE as the Co(III)–N_α bond length is restricted from 1.9–2.5 Å (*trans* induction) with the α ligand kept constant.

In all of the models, the Co(III)–C_β bond length (see **Tables 5.8–5.11**) is found to increase as the α ligand changes from the –NH₃ ligand to the more sterically hindered –N(CH₃)₃ ligand.

Table 5.8: Geometric parameters, ΔG and BDE for the homolysis of the Co(III)–C $_{\beta}$ bond in cobaloxime

Cobaloxime							
Co(III)–N $_{\alpha}$ /Å	1.9	2.0	2.1	2.2	2.3	2.4	2.5
Bond Lengths: Co(III)–C $_{\beta}$ /Å							
NH $_3$	2.021	2.009	2.000	1.993	1.987	1.982	–
NH $_2$ CH $_3$	2.029	2.016	2.005	1.997	1.990	1.985	1.981
NH(CH $_3$) $_2$	2.045	2.030	2.018	2.008	1.999	1.992	1.987
N(CH $_3$) $_3$	2.065	2.047	2.032	2.019	2.008	2.000	1.993
Co(III) displacement below the mean plane /Å							
NH $_3$	0.046	0.032	0.020	0.009	0.000	0.009*	–
NH $_2$ CH $_3$	0.064	0.047	0.029	0.015	0.002	0.009*	0.019*
NH(CH $_3$) $_2$	0.126	0.102	0.079	0.058	0.038	0.021	0.004
N(CH $_3$) $_3$	0.186	0.156	0.127	0.100	0.075	0.050	0.029
Bond Angle: N $_{\alpha}$ –Co(III)–C $_{\beta}$ /°							
NH $_3$	179.35	179.31	179.27	179.24	179.22	179.22	–
NH $_2$ CH $_3$	177.40	177.82	177.54	177.64	177.83	178.07	178.34
NH(CH $_3$) $_2$	177.70	177.77	177.84	177.90	178.00	178.10	178.18
N(CH $_3$) $_3$	178.89	178.89	178.88	178.91	178.95	178.96	178.99
ΔG : Energies /kcal mol $^{-1}$							
NH $_3$	28.92	28.67	28.79	28.84	28.59	28.25	–
NH $_2$ CH $_3$	27.96	28.65	29.14	28.86	28.50	28.31	28.01
NH(CH $_3$) $_2$	24.54	25.56	26.26	26.74	27.01	27.02	26.96
N(CH $_3$) $_3$	21.63	23.01	24.12	24.93	25.50	25.93	26.19
$\Delta(\Delta G)^a$	7.29	5.66	4.67	3.91	3.09	2.32	–
BDE: Energies /kcal mol $^{-1}$							
NH $_3$	40.93	41.13	41.06	40.86	40.58	40.27	–
NH $_2$ CH $_3$	40.12	40.53	40.71	40.68	40.57	40.36	40.11
NH(CH $_3$) $_2$	37.14	38.04	38.65	39.05	39.28	39.36	39.36
N(CH $_3$) $_3$	34.21	35.51	36.54	37.31	37.86	38.26	38.51
ΔBDE	6.72	5.62	4.52	3.55	2.72	2.01	–

$\Delta(\Delta G)$ (and ΔBDE) is the difference in the ΔG (BDE) of the cobalamin model with the NH $_3$ ligand from the ΔG (BDE) of the cobalamin model with the N(CH $_3$) $_3$ ligand. Blank spaces indicate that no low energy conformers were identified as the structures failed to optimise as per the convergence criteria used in Gaussian.*The Co metal centre was found above the mean plane.

Table 5.9: Geometric parameters, ΔG and BDE for the homolysis of the Co(III)–C $_{\beta}$ bond in corrole

Corrole							
Co(III)-N $_{\alpha}$ /Å	1.9	2.0	2.1	2.2	2.3	2.4	2.5
Bond Lengths Co(III)–C $_{\beta}$ /Å							
NH $_3$	1.996	1.985	1.976	1.970	1.964	1.960	–
NH $_2$ CH $_3$	–	1.990	1.980	1.973	1.967	1.963	1.959
NH(CH $_3$) $_2$	2.008	1.995	1.985	1.977	1.971	1.966	1.962
N(CH $_3$) $_3$	2.022	2.007	1.996	1.986	1.978	1.972	1.967
Co(III) displacement below the mean plane /Å							
NH $_3$	0.006*	0.016*	0.027*	0.037*	0.047*	0.056*	–
NH $_2$ CH $_3$	0.012	0.003*	0.017*	0.031*	0.043*	0.055*	0.065*
NH(CH $_3$) $_2$	0.050	0.029	0.009	0.009*	0.026*	0.042*	0.056*
N(CH $_3$) $_3$	0.116	0.090	0.065	0.041	0.017	0.005*	0.025
Bond Angle N $_{\alpha}$ –Co(III)–C $_{\beta}$ /°							
NH $_3$	178.29	178.31	178.35	178.41	178.56	178.71	–
NH $_2$ CH $_3$	–	177.52	177.42	177.40	177.44	177.56	177.74
NH(CH $_3$) $_2$	177.90	177.94	177.94	177.94	177.92	177.87	177.80
N(CH $_3$) $_3$	177.15	177.26	177.39	177.56	177.76	177.97	178.20
ΔG : Energies /kcal mol $^{-1}$							
NH $_3$	–	23.14	22.96	23.48	23.93	24.38	–
NH $_2$ CH $_3$	–	21.82	23.12	23.60	23.81	23.96	24.81
NH(CH $_3$) $_2$	20.58	21.11	21.55	22.01	22.49	23.01	23.54
N(CH $_3$) $_3$	16.66	17.49	18.50	19.56	20.24	21.36	21.64
$\Delta(\Delta G)$	–	5.65	4.46	3.92	3.69	3.02	–
BDE: Energies/kcal mol $^{-1}$							
NH $_3$	–	35.20	35.16	35.23	35.41	35.68	–
NH $_2$ CH $_3$	–	34.86	34.96	35.11	35.30	35.38	35.92
NH(CH $_3$) $_2$	32.89	33.23	33.59	33.98	34.42	34.88	35.35
N(CH $_3$) $_3$	29.05	29.97	30.85	31.69	32.50	33.31	34.21
ΔBDE	–	5.23	4.31	3.54	2.91	2.37	–

$\Delta(\Delta G)$ (and ΔBDE) is the difference in the ΔG (BDE) of the cobalamin model with the NH $_3$ ligand from the ΔG (BDE) of the cobalamin model with the N(CH $_3$) $_3$ ligand. Blank spaces indicate that no low energy conformers were identified as the structures failed to optimise as per the convergence criteria used in Gaussian. *The Co metal centre was found above the mean plane.

Table 5.10: Geometric parameters, ΔG and BDE for the homolysis of the Co(III)–C $_{\beta}$ bond in corrin

		Corrin						
Co(III)–N $_{\alpha}$ /Å	1.9	2.0	2.1	2.2	2.3	2.4	2.5	
Bond Lengths Co(III)–C $_{\beta}$ /Å								
NH $_3$	2.004	1.995	1.988	1.983	1.979	1.976	1.973	
NH $_2$ CH $_3$	2.010	2.001	1.993	1.988	1.983	1.979	1.976	
NH(CH $_3$) $_2$	2.021	2.008	2.000	1.993	1.988	1.985	1.981	
N(CH $_3$) $_3$	2.034	2.021	2.011	2.002	1.996	1.990	1.985	
Co(III) displacement below the mean plane /Å								
NH $_3$	0.026	0.016	0.005	0.007*	0.015*	0.025*	0.034*	
NH $_2$ CH $_3$	0.041	0.027	0.013	0.001	0.011*	0.023*	0.033*	
NH(CH $_3$) $_2$	0.085	0.060	0.042	0.024	0.009	0.001	0.013*	
N(CH $_3$) $_3$	0.140	0.116	0.092	0.069	0.048	0.028	0.010	
Bond Angle N $_{\alpha}$ –Co(III)–C $_{\beta}$ /°								
NH $_3$	176.46	176.41	176.34	176.25	176.19	176.08	176.98	
NH $_2$ CH $_3$	175.31	175.39	175.39	175.36	175.30	175.23	175.13	
NH(CH $_3$) $_2$	174.36	179.44	179.49	179.43	179.27	174.25	174.19	
N(CH $_3$) $_3$	176.17	176.16	176.15	176.15	176.15	176.18	176.19	
ΔG : Energies /kcal mol $^{-1}$								
NH $_3$	–	19.91	20.22	20.52	20.94	21.44	22.06	
NH $_2$ CH $_3$	19.67	19.98	20.06	20.25	20.65	21.28	21.86	
NH(CH $_3$) $_2$	16.07	18.27	18.78	19.32	19.89	19.53	20.13	
N(CH $_3$) $_3$	13.81	14.86	15.86	16.82	17.56	18.49	19.06	
$\Delta(\Delta G)$	–	5.05	4.36	3.70	3.38	2.95	3.00	
BDE: Energies /kcal mol $^{-1}$								
NH $_3$	–	32.48	32.58	32.78	33.07	33.44	33.86	
NH $_2$ CH $_3$	32.13	32.22	32.32	32.51	32.79	33.17	33.55	
NH(CH $_3$) $_2$	29.12	30.55	30.97	31.39	31.83	31.46	32.07	
N(CH $_3$) $_3$	26.42	27.30	28.16	28.99	29.61	30.56	31.28	
ΔBDE	–	5.18	4.42	3.79	3.46	2.88	2.58	

$\Delta(\Delta G)$ (and ΔBDE) is the difference in the ΔG (BDE) of the cobalamin model with the NH $_3$ ligand from the ΔG (BDE) of the cobalamin model with the N(CH $_3$) $_3$ ligand. Blank spaces indicate that no low energy conformers were identified since the structures failed to optimise as per the convergence criteria used in Gaussian. *The Co metal centre was found above the mean plane.

Table 5.11: Geometric parameters, ΔG and BDE for the homolysis of the Co(III)–C $_{\beta}$ bond in porphyrin

Porphyrin							
Co(III)–N $_{\alpha}$ /Å	1.9	2.0	2.1	2.2	2.3	2.4	2.5
Bond Lengths Co(III)–C $_{\beta}$ /Å							
NH $_3$	–	1.983	1.976	1.971	1.967	1.964	–
NH $_2$ CH $_3$	1.997	1.987	1.981	1.975	1.963	1.967	1.964
NH(CH $_3$) $_2$	2.004	1.994	1.986	1.980	1.975	1.970	1.967
N(CH $_3$) $_3$	2.018	2.006	1.997	1.988	1.982	1.976	1.972
Co(III) displacement below the mean plane /Å							
NH $_3$	0.003*	0.012*	0.019*	0.027*	0.034*	0.041*	–
NH $_2$ CH $_3$	0.012	0.000	0.011*	0.022*	0.032*	0.041*	0.048*
NH(CH $_3$) $_2$	0.043	0.026	0.009	0.006*	0.020*	0.032*	0.043*
N(CH $_3$) $_3$	0.120	0.095	0.070	0.047	0.026	0.006	0.012*
Bond Angle N $_{\alpha}$ –Co(III)–C $_{\beta}$ /°							
NH $_3$	–	179.21	179.11	179.02	178.90	178.86	–
NH $_2$ CH $_3$	177.77	178.30	177.10	177.08	177.32	177.18	177.27
NH(CH $_3$) $_2$	177.03	177.15	177.29	177.44	177.55	177.78	177.83
N(CH $_3$) $_3$	178.46	178.25	178.71	177.88	177.95	178.07	178.52
ΔG : Energies /kcal mol $^{-1}$							
NH $_3$	–	20.80	21.22	21.12	22.37	22.44	–
NH $_2$ CH $_3$	–	–	–	21.56	21.77	21.92	21.96
NH(CH $_3$) $_2$	19.95	20.35	20.78	21.15	21.55	22.39	21.99
N(CH $_3$) $_3$	16.09	17.27	17.57	17.59	18.89	21.29	21.28
$\Delta(\Delta G)$	–	3.53	3.65	3.53	3.48	1.15	–
BDE: Energies /kcal mol $^{-1}$							
NH $_3$	–	33.28	33.19	33.15	33.37	33.52	–
NH $_2$ CH $_3$	–	–	–	33.05	33.17	33.31	33.52
NH(CH $_3$) $_2$	31.73	31.92	32.16	32.40	32.67	32.94	33.18
N(CH $_3$) $_3$	28.04	28.80	29.45	30.10	30.79	31.47	21.98
ΔBDE	–	4.48	3.74	3.05	2.58	2.05	–

$\Delta(\Delta G)$ (and ΔBDE) is the difference in the ΔG (BDE) of the cobalamin model with the NH $_3$ ligand from the ΔG (BDE) of the cobalamin model with the N(CH $_3$) $_3$ ligand. Blank spaces indicate that no low energy conformers were identified as the structures failed to optimise as per the convergence criteria used in Gaussian. *The Co metal centre was found above the mean plane.

This trend implies that with the increase in the number of methyl groups on the α ligand the β ligand is pushed further away from the Co atom, thus increasing the Co(III)–C $_{\beta}$ bond length. This observation is consistent with the increase in orbital overlap between the Co metal centre and the α ligand (**Tables 5.8–5.11**). As the Co(III)–C $_{\beta}$ bond length increases, a weakening of the bond occurs and a decrease in the ΔG and BDEs for the Co(III)–C $_{\beta}$ bond is observed. For the corrin models (**Table 5.10**) a decrease of 5.18 kcal mol $^{-1}$ for the BDE ($\Delta(\Delta G) = 5.05$ kcal mol $^{-1}$) was noted as the α ligand was changed from NH $_3$ to N(CH $_3$) $_3$ at a constant Co–N $_{\alpha}$ bond length of 2.0 Å. When comparing the variation of 2.0–2.5 Å for the Co–N $_{\alpha}$ bond, the change in Co(III)–C $_{\beta}$ BDEs, ranged from 5.18–2.58 kcal mol $^{-1}$ ($\Delta(\Delta G) = 5.05$ –3.00 kcal mol $^{-1}$). This seems to suggest the preferred bond length for the Co(III)–N $_{\alpha}$ bond to fall in the 1.9–2.0 Å range. It is also noted that with the exception of cobaloxime, all of the Co(III)–C $_{\beta}$ BDEs of the other three models compare well with experimentally determined values that range from 17–34 kcal mol $^{-1}$ for model compounds while recorded values for the actual cobalamins range from 26–37 kcal mol $^{-1}$.⁶⁰

Although the Co(III)–C $_{\beta}$ bond is shown to be quite stiff, a change of 0.03–0.012 Å was recorded as the Co(III)–N $_{\alpha}$ bond length increased from 1.9–2.5 Å. There is a significant change in the dissociation energy of the Co(III)–C $_{\beta}$ bond as the Co(III)–N $_{\alpha}$ bond length and α ligand are varied. The subsequent increase in the Co(III)–C $_{\beta}$ bond length as a function of the various ligands parallels the greater orbital overlap taking place between the Co metal centre and the lower axial ligand as the Co(III)–N $_{\alpha}$ bond is kept constant. This observation suggests that the large electron density from the increased number of methyl groups on the α ligand pushes the β ligand (CH $_3$ group) away from the macrocyclic ring, thus causing the Co(III)–C $_{\beta}$ bond to elongate. Consequently, the partial charges were assessed and are later reported in this chapter to ascertain whether an electronic influence (induction) or *trans* steric influence may be responsible for the lowering of the BDEs of the Co(III)–C $_{\beta}$ bond.

At the same time a normal *trans* influence is observed for the axial bond lengths of each model carrying the same ligand, that is, as the Co(III)–N_α bond length is increased from 1.9 Å to 2.5 Å, the Co(III)–C_β bond length decreases. This trend linearly relates to both the ΔG and BDE values (see **Figure 5.17**), which means that as the Co(III)–C_β bond decreases in length the ΔG and BDE of the Co(III)–C_β bond increases. This observation is clearly supported by the recorded data for the movement of the Co ion in the Co(III) complex. As the Co(III)–C_β bond grows stronger because of a greater orbital overlap between the Co ion and the C_β atom from the β ligand the Co(III)–C_β BDE increases as well. This trend was also observed for the charged α ligands reported in **Tables 5.1A** and **B**.

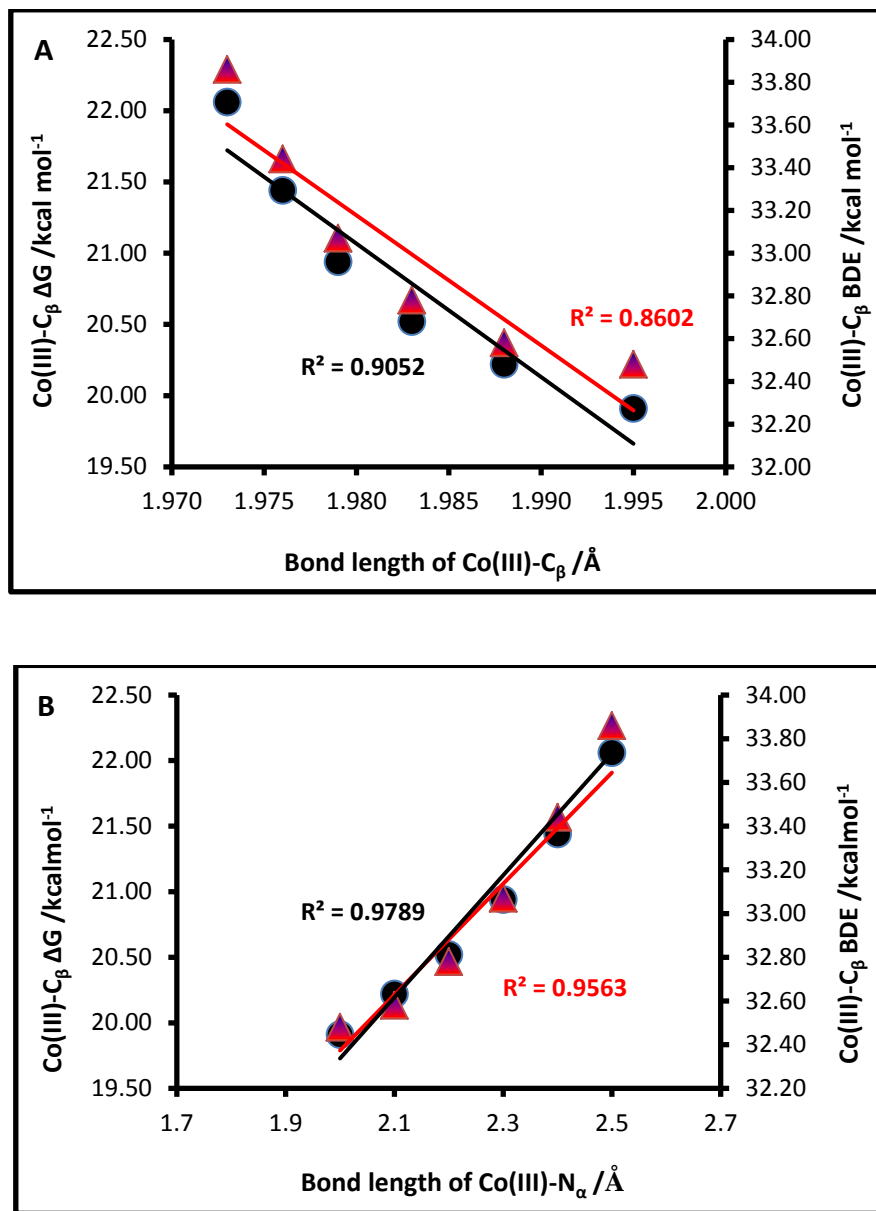


Figure 5.17: $\text{Co(III)-C}_\beta \Delta G$ (●) and BDE (▲) (kcal mol^{-1}) of the corrin model as a function of the A) Co(III)-C_β and B) Co(III)-N_α bond length (Å).

(b) *Partial charges and electron densities*

The partial charges for the corrin model are captured in **Tables 5.12A** and **B** while the data for the other three models are recorded in Appendix 2: A2.5–A2.7. From the data presented, it is observed for all of the methodologies used that the negative charge on N_α increases for the complexes where the α ligand is kept constant, and the Co(III)– N_α bond length is increased from 1.9–2.5 Å. This is again found to be consistent with the shifting of the Co metal centre; as the Co ion moves further away from the α ligand so the negative charge of N_α increases. At the same time the collective negative charge for the N_{eq} ligands, as generated by the APT and Bader methods, begins to decrease whilst the Mulliken and NBO methods show the N_{eq} as increasing in positive charge and increasing in negative charge, respectively.

The Mulliken, NBO and Bader charges for C_β of the β ligand are similar, in that they describe the C_β as having a negative charge which decreases in value as the Co(III)– N_α bond length increases from 1.9–2.5 Å. At the same time, the distance of the Co ion increases from the mean plane, shifting closer to the β ligand. On the other hand, the APT charge, which is different and describes C_β as carrying a positive charge, increases in value as the Co(III)– N_α bond length increases from 1.9–2.5 Å. These trends further suggest that a *trans* electronic influence exists between the α and β ligands.

Table 5.12A: Mulliken and APT partial charges (in e) for the corrin model

α ligands	MULLIKEN							APT						
	1.9	2.0	2.1	2.2	2.3	2.4	2.5	1.9	2.0	2.1	2.2	2.3	2.4	2.5
Co(III)								Co(III)						
NH ₃	-3.127	-3.123	-3.104	-3.087	-3.090	-3.102	-3.125	0.190	0.203	0.212	0.218	0.220	0.218	0.213
NH ₂ CH ₃	-3.382	-3.271	-3.149	-3.048	-2.972	-2.947	-2.970	0.195	0.205	0.213	0.219	0.223	0.224	0.221
NH(CH ₃) ₂	-3.753	-3.490	-3.219	-2.968	-2.798	-2.844	-2.748	0.208	0.216	0.223	0.228	0.231	0.232	0.230
N(CH ₃) ₃	-3.002	-2.541	-2.206	-1.995	-3.115	-1.917	-1.995	0.208	0.218	0.226	0.231	0.235	0.235	0.234
C _{β}								C _{β}						
NH ₃	-0.310	-0.304	-0.293	-0.277	-0.254	-0.227	-0.198	0.144	0.155	0.165	0.174	0.182	0.188	0.194
NH ₂ CH ₃	-0.162	-0.173	-0.187	-0.199	-0.208	-0.210	-0.205	0.129	0.140	0.151	0.160	0.168	0.175	0.182
NH(CH ₃) ₂	-0.112	-0.170	-0.200	-0.230	-0.249	-0.216	-0.217	0.116	0.130	0.140	0.149	0.157	0.163	0.170
N(CH ₃) ₃	-0.023	-0.029	-0.085	-0.132	-0.099	-0.178	-0.181	0.114	0.124	0.133	0.142	0.158	0.157	0.163
N _{α}								N _{α}						
NH ₃	-0.843	-0.850	-0.857	-0.866	-0.886	-0.910	-0.940	-0.170	-0.221	-0.257	-0.284	-0.302	-0.314	-0.322
NH ₂ CH ₃	-0.441	-0.464	-0.495	-0.534	-0.583	-0.633	-0.682	-0.202	-0.245	-0.276	-0.299	-0.316	-0.328	-0.336
NH(CH ₃) ₂	-0.054	-0.129	-0.174	-0.229	-0.280	-0.344	-0.412	-0.257	-0.280	-0.309	-0.330	-0.344	-0.372	-0.380
N(CH ₃) ₃	-0.672	-0.739	-0.775	-0.786	-0.480	-0.759	-0.731	-0.298	-0.344	-0.377	-0.401	-0.418	-0.432	-0.443
N _{eq}								N _{eq}						
NH ₃	0.443	0.437	0.434	0.437	0.445	0.459	0.476	-0.395	-0.390	-0.385	-0.381	-0.377	-0.373	-0.369
NH ₂ CH ₃	0.424	0.408	0.397	0.394	0.400	0.416	0.440	-0.392	-0.386	-0.381	-0.376	-0.372	-0.368	-0.364
NH(CH ₃) ₂	0.408	0.379	0.358	0.345	0.346	0.388	0.403	-0.387	-0.392	-0.386	-0.380	-0.374	-0.363	-0.360
N(CH ₃) ₃	0.287	0.246	0.224	0.220	0.383	0.260	0.296	-0.394	-0.387	-0.380	-0.375	-0.370	-0.366	-0.362

Table 5.12B: NBO and Bader partial charges (e) for the corrin model

α ligands	NBO							BADER							
	1.9	2.0	2.1	2.2	2.3	2.4	2.5	1.9	2.0	2.1	2.2	2.3	2.4	2.5	
Co(III)								Co(III)							
NH ₃	0.112	0.135	0.160	0.184	0.209	0.232	0.253	1.111	1.100	1.087	1.080	1.074	1.069	1.067	
NH ₂ CH ₃	0.145	0.166	0.188	0.210	0.230	0.250	0.268	1.110	1.100	1.088	1.079	1.071	1.068	1.065	
NH(CH ₃) ₂	0.185	0.205	0.223	0.242	0.259	0.275	0.289	1.108	1.097	1.087	1.076	1.070	1.061	1.060	
N(CH ₃) ₃	0.238	0.252	0.266	0.281	0.295	0.308	0.320	1.104	1.092	1.080	1.071	1.065	1.061	1.058	
C _{β}								C _{β}							
NH ₃	-0.749	-0.734	-0.722	-0.713	-0.705	-0.700	-0.695	-0.170	-0.159	-0.149	-0.141	-0.135	-0.130	-0.126	
NH ₂ CH ₃	-0.760	-0.745	-0.733	-0.723	-0.715	-0.708	-0.703	-0.172	-0.160	-0.152	-0.144	-0.138	-0.132	-0.128	
NH(CH ₃) ₂	-0.767	-0.753	-0.740	-0.730	-0.722	-0.714	-0.708	-0.171	-0.160	-0.152	-0.144	-0.138	-0.133	-0.129	
N(CH ₃) ₃	-0.768	-0.753	-0.741	-0.731	-0.723	-0.716	-0.711	-0.166	-0.156	-0.148	-0.141	-0.136	-0.131	-0.127	
N _{α}								N _{α}							
NH ₃	-0.994	-1.014	-1.031	-1.046	-1.058	-1.070	-1.081	-1.027	-1.038	-1.045	-1.051	-1.056	-1.061	-1.065	
NH ₂ CH ₃	-0.782	-0.797	-0.808	-0.818	-0.826	-0.834	-0.841	-0.968	-0.978	-0.985	-0.991	-0.996	-1.000	-1.005	
NH(CH ₃) ₂	-0.605	-0.615	-0.621	-0.626	-0.630	-0.633	-0.637	-0.971	-0.920	-0.928	-0.936	-0.942	-0.951	-0.956	
N(CH ₃) ₃	-0.477	-0.483	-0.485	-0.484	-0.484	-0.483	-0.483	-0.857	-0.871	-0.882	-0.890	-0.897	-0.905	-0.913	
N _{eq}								N _{eq}							
NH ₃	-0.343	-0.347	-0.352	-0.356	-0.361	-0.364	-0.368	-1.100	-1.099	-1.098	-1.096	-1.095	-1.094	-1.092	
NH ₂ CH ₃	-0.347	-0.351	-0.355	-0.359	-0.364	-0.367	-0.370	-1.098	-1.098	-1.097	-1.096	-1.094	-1.093	-1.092	
NH(CH ₃) ₂	-0.353	-0.360	-0.364	-0.368	-0.371	-0.373	-0.375	-1.093	-1.095	-1.094	-1.094	-1.093	-1.092	-1.091	
N(CH ₃) ₃	-0.365	-0.369	-0.373	-0.376	-0.379	-0.382	-0.384	-1.089	-1.089	-1.089	-1.089	-1.089	-1.089	-1.089	

The topological properties of the electron density at the bcp of both the axial bond lengths were analysed and the data are provided in **Tables 5.13A** and **B**. The recorded data show that the ρ -value of the Co(III)–CH₃ bond increases as the Co(III)–NH₃ bond length increases from 1.9–2.5 Å for any of the models with any of the α ligands. This suggests that the Co(III)–CH₃ bond becomes stronger as the Co(III)–NH₃ weakens, an observation verified by the ρ -value given in **Table 5.13B**. Clearly, this is also an indicator of the *trans* influence of one axial ligand on the other.

Moreover, the carbon from the methyl group (β ligand) is less electronegative than nitrogen (α ligand) and is therefore more electron releasing. This presents a greater attraction of the β ligand to the positive metal centre which results in the decrease of the Co(III)–CH₃ bond (*trans* induction mentioned earlier on) while the *trans* bond is seen to simultaneously weaken (see **Figure 5.18** below).

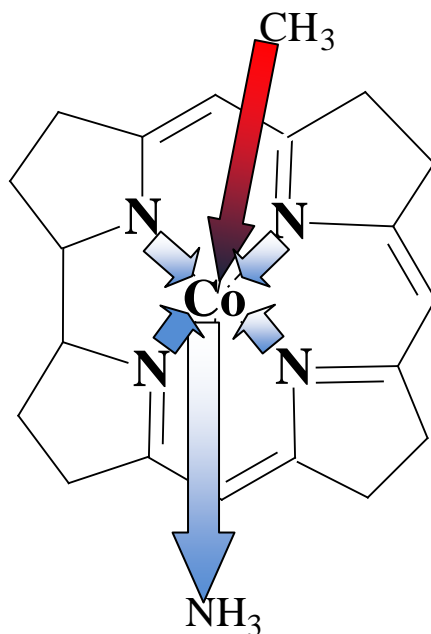


Figure 5.18: Corrin model depicting the decrease of the Co(III)–C _{β} bond length (Å) as a function of the attractive charge (e) between the Co metal centre and β ligand.

Table 5.13A: Topological properties of the electron density (ρ) at the bcp of Co(III)–CH₃ for the corrin complex

Co(III)–CH ₃						
Bond length	ρ	$\nabla^2\rho$	V(r)	G(r)	H(r)	V(r) /G(r)
NH ₃						
1.9	0.1118	0.0669	-0.1250	0.0709	-0.0542	-1.7641
2.0	0.1137	0.0598	-0.1269	0.0709	-0.0560	-1.7893
2.1	0.1150	0.0539	-0.1284	0.0709	-0.0574	-1.8099
2.2	0.1161	0.0492	-0.1295	0.0709	-0.0586	-1.8263
2.3	0.1167	0.0453	-0.1302	0.0708	-0.0594	-1.8398
2.4	0.1172	0.0423	-0.1308	0.0707	-0.0601	-1.8505
2.5	0.1176	0.0397	-0.1312	0.0706	-0.0606	-1.8593
NH ₂ CH ₃						
1.9	0.1105	0.0675	-0.1235	0.0702	-0.0533	-1.7596
2.0	0.1125	0.0607	-0.1256	0.0704	-0.0552	-1.7843
2.1	0.1140	0.0551	-0.1272	0.0705	-0.0567	-1.8046
2.2	0.1151	0.0504	-0.1284	0.0705	-0.0579	-1.8213
2.3	0.1159	0.0467	-0.1293	0.0705	-0.0588	-1.8343
2.4	0.1165	0.0436	-0.1300	0.0704	-0.0595	-1.8451
2.5	0.1169	0.0412	-0.1306	0.0704	-0.0601	-1.8538
NH(CH ₃) ₂						
1.9	0.1084	0.0655	-0.1204	0.0684	-0.0520	-1.7605
2.0	0.1111	0.0596	-0.1236	0.0692	-0.0544	-1.7849
2.1	0.1127	0.0541	-0.1254	0.0695	-0.0559	-1.8043
2.2	0.1140	0.0502	-0.1269	0.0697	-0.0572	-1.8202
2.3	0.1149	0.0466	-0.1280	0.0698	-0.0582	-1.8331
2.4	0.1153	0.0433	-0.1283	0.0696	-0.0587	-1.8443
2.5	0.1159	0.0410	-0.1291	0.0697	-0.0594	-1.8528
N(CH ₃) ₃						
1.9	0.1059	0.0596	-0.1164	0.0657	-0.0508	-1.7731
2.0	0.1084	0.0544	-0.1194	0.0665	-0.0529	-1.7955
2.1	0.1104	0.0500	-0.1218	0.0672	-0.0546	-1.8136
2.2	0.1120	0.0466	-0.1238	0.0677	-0.0561	-1.8280
2.3	0.1132	0.0438	-0.1254	0.0682	-0.0572	-1.8395
2.4	0.1142	0.0416	-0.1267	0.0685	-0.0582	-1.8484
2.5	0.1150	0.0397	-0.1277	0.0688	-0.0589	-1.8558

Table 5.13B: Topological properties of the electron density (ρ) at the bcp of Co(III)–NH₃ for the corrin complex

Co(III)–NH ₃						
Bond length	ρ	$\nabla^2\rho$	V(r)	G(r)	H(r)	V(r) /G(r)
NH ₃						
1.9	0.1104	0.5686	-0.1903	0.1662	-0.0241	-1.1449
2.0	0.0872	0.4147	-0.1374	0.1205	-0.0168	-1.1398
2.1	0.0694	0.2971	-0.1011	0.0877	-0.0134	-1.1532
2.2	0.0557	0.2118	-0.0758	0.0644	-0.0114	-1.1776
2.3	0.0452	0.1534	-0.0574	0.0479	-0.0095	-1.1992
2.4	0.0369	0.1149	-0.0436	0.0362	-0.0074	-1.2053
2.5	0.0303	0.0898	-0.0330	0.0277	-0.0053	-1.1901
NH ₂ CH ₃						
1.9	0.1123	0.5588	-0.1914	0.1655	-0.0258	-1.1561
2.0	0.0889	0.4067	-0.1383	0.1200	-0.0183	-1.1528
2.1	0.0710	0.2904	-0.1020	0.0873	-0.0147	-1.1685
2.2	0.0573	0.2063	-0.0766	0.0641	-0.0125	-1.1951
2.3	0.0466	0.1487	-0.0580	0.0476	-0.0104	-1.2186
2.4	0.0382	0.1111	-0.0440	0.0359	-0.0081	-1.2263
2.5	0.0314	0.0866	-0.0333	0.0275	-0.0058	-1.2120
NH(CH ₃) ₂						
1.9	0.1132	0.5537	-0.1919	0.1651	-0.0267	-1.1618
2.0	0.0897	0.4049	-0.1390	0.1201	-0.0189	-1.1572
2.1	0.0718	0.2885	-0.1025	0.0873	-0.0152	-1.1741
2.2	0.0580	0.2044	-0.0770	0.0641	-0.0130	-1.2025
2.3	0.0473	0.1468	-0.0584	0.0476	-0.0109	-1.2285
2.4	0.0389	0.1084	-0.0442	0.0356	-0.0085	-1.2399
2.5	0.0321	0.0844	-0.0334	0.0272	-0.0061	-1.2256
N(CH ₃) ₃						
1.9	0.1137	0.5602	-0.1932	0.1666	-0.0266	-1.1596
2.0	0.0904	0.4061	-0.1399	0.1207	-0.0192	-1.1588
2.1	0.0725	0.2886	-0.1033	0.0877	-0.0156	-1.1775
2.2	0.0587	0.2038	-0.0776	0.0643	-0.0133	-1.2076
2.3	0.0479	0.1459	-0.0589	0.0477	-0.0112	-1.2352
2.4	0.0394	0.1082	-0.0447	0.0359	-0.0088	-1.2464
2.5	0.0326	0.0839	-0.0339	0.0274	-0.0064	-1.2350

In addition, the Co(III)–C $_{\beta}$ bond length was found to increase as the α ligand was changed from NH $_3$ to N(CH $_3$) $_3$ (see **Tables 5.8–5.11**). This weakening of the Co(III)–C $_{\beta}$ bond is proportional to the decrease of the ρ -value at the bcp (**Table 5.13A**) while at the same time the Co(III)–N $_{\alpha}$ bond becomes stronger as quantified by its ρ -value at the bcp.

Because the Co(III)–N $_{\alpha}$ bond was kept constant, the increase in length of the Co(III)–C $_{\beta}$ bond could not be attributed to a *trans* steric influence of the various α ligands as they grew in bulkiness by the substitution of methyl groups. This was further confirmed by measuring the torsion angles of the corrin macrocycle as well as assessing the distortion of the N $_{\alpha}$ –Co(III)–C $_{\beta}$ angle, (see **Table 5.14**).

Table 5.14: Torsion and N $_{\alpha}$ –Co(III)–C $_{\beta}$ ($^{\circ}$) angles for the corrin model at the restricted Co(III)–N $_{\alpha}$ bond length of 1.9 Å

	[NX $_3$ –(Co(III)corrin)–CH $_3$]				[NX $_3$ –(Co(II)corrin)]			
	Torsion angles (ω) / $^{\circ}$							
	1	2	3	4	1	2	3	4
ω_1	-9.2	-10.2	-7.3	-8.0	-1.7	-1.5	1.7	0.8
ω_2	0.1	-0.7	4.0	2.2	-5.0	-7.2	-3.8	-4.7
ω_3	-0.5	0.3	-5.2	-3.2	3.1	5.7	0.4	2.8
ω_4	-7.0	-7.2	-11.0	-6.9	-14.5	-11.8	-14.5	-15.2
ω_5	6.9	7.0	12.2	9.4	16.1	14.2	18.2	18.8
ω_6	-10.3	-10.3	-4.0	-10.2	-13.8	-14.2	-12.8	-14.6
ω_7	-15.0	-14.7	-18.8	-14.7	-11.4	-11.1	-12.3	-10.7
ω_8	8.1	8.7	1.4	3.8	-0.8	-0.2	-5.1	-5.7
ω_{avg}	3.4	3.4	3.6	3.4	3.5	3.3	3.5	3.6
N $_{\alpha}$ –Co(III)–								
C $_{\beta}$	176.46	175.31	174.36	176.17				

In the table, 1–4 indicates the type of α ligand present in the complex where 1=NH $_3$; 2=NH $_2$ CH $_3$; 3=NH(CH $_3$) $_2$, 4=N(CH $_3$) $_3$.

From these results, it is evident that the negligible changes observed to the conformation of the corrin macrocycle as well as the N_{α} -Co(III)- C_{β} angle of distortion does not play a major role in the lengthening of the Co(III)- C_{β} bond. Even Grinberg's polarisation theory, whereby an electrostatic repulsion between the metal centre and β ligand would result in an increase of the Co(III)- C_{β} bond length could only be proved true for the partial charges generated by the APT method, while the Mulliken, NBO and Bader charges described the partial charges for the Co and C_{β} to be oppositely charged.

Finally, these results are compared to a study conducted by Jensen *et al.*⁴⁸ where a change in the β ligand promoted the lengthening of the Co(III)- N_{α} bond. In their studies they eventually eliminated the Co(III)- C_{β} bond as responsible for this behaviour because a change of 0.2 Å in the Co(III)- C_{β} bond length resulted in only a 0.05 Å change in the Co(III)- N_{α} bond length. In addition, the relationship between the two axial ligands changed from an inverse *trans* influence to a normal *trans* influence. They eventually deduced that the lengthening of the Co(III)- N_{α} bond and the inverse *trans* influence (an effect that was also observed in other studies)^{6,58} was due to the ligand, more specifically the substituents of the ligand, and not the elongation of the Co(III)- C_{β} bond length. In light of this and the recorded data in this chapter, the same conclusion is drawn for these complexes comprising the different α ligands.

5.4 CONCLUSION

The BP86 functional is widely recognised as a density functional for transition metal chemistry, and in this analysis has performed well in describing the structures and energies of the various complexes under investigation. A comparison of energies between cobaloxime, corrin, corrole and porphyrin shows the corrin as having the lowest BDE and ΔG , sufficient reason for nature to choose the Co–corrin to perform specific essential biological functions catalysed by B₁₂-dependent enzymes.^{41,240}

The corrin macrocycle is not fully conjugated and therefore is more flexible than corrole and porphyrin but not as flexible as cobaloxime. This in itself poses an advantage which may enhance the breaking of the Co(III)–C_β bond.^{241,242} However, from the assessment carried out on the distortion of the corrin macrocycle it was evident that it does not play a role in promoting a lower Co(III)–C_β BDE. The same can be said for the porphyrin and corrole models but cobaloxime, because of its extreme flexibility, once again was proved to be a poor model for cobalamin chemistry.

The nature of the α ligand does play an important role in cobalamin chemistry. From the results presented for the charged and neutral α ligands, different trends were observed in terms of the *trans* influence on the Co(III)–C_β bond as well as the electronic effects in the system. Jensen *et al.*¹⁸⁰ reported that the Co(III)–N_α bond was very flexible, and could never have a significant *trans* influence on the Co(III)–C_β bond, because the latter is ~5 times stronger than the Co(III)–N_α bond. The results reported in this chapter corroborate this statement, as there was a minimal change of the Co(III)–C_β bond length when changes were made to the α ligands as well as to the Co(III)–N_α bond length. However, electronically the α ligand is shown to contribute to a lower Co(III)–C_β BDE. The greater the difference in the decrease of the Co–N_α bond length from the 5 coordinate to the 6 coordinate ($\Delta_{(5c-6c)}$) complex, the lower the recorded Co(III)–C_β BDE would become. In addition, the

nature of the α ligand, together with the size of the Co(III)–N $_{\alpha}$ bond length, plays a role in the displacement of the Co metal centre from the mean plane. This was an important contributing factor towards the observed changes of the Co(III)–C $_{\beta}$ bond lengths and BDEs for this bond.

Moreover, the *cis* influence of the equatorial ligands was also analysed. The problem of how the equatorial ligands electronically influence the homolysis of the Co(III)–C $_{\beta}$ bond could not be isolated. The partial charges were unable to show a trend for the models as a result of a change in the equatorial ligands. However, the results obtained from the differences in the displacement of the metal centre from the mean plane for the different models were very informative. Porphyrin and corrole, with their tight planar framework, induced the Co metal centre to displace largely towards the β ligand, ensuring a strong orbital overlap between them, and as a consequence high BDEs were required for the homolysis of the Co(III)–C $_{\beta}$ bond. Of these two models porphyrin gave slightly lower BDEs and it was suggested that its larger aromatic macrocyclic ring was responsible for providing a more stable environment for the Co(II) complex. On the other hand, the corrin models are more flexible because they have a partially aromatic macrocyclic ring. It then becomes apparent that the small distortion of the corrin macrocycle (**Tables 5.4** and **5.14**) actually occurs so that the Co metal is accommodated closer to the corrin mean plane, resulting in the lowest BDEs for the Co(III)–C $_{\beta}$ bond from both the corrole and porphyrin models. These observations are confirmed by the data presented in **Table 5.10**.

Finally, the results presented in this chapter show that there is no specific perturbation that currently can be held uniquely accountable for promoting an easy homolytic scission of the Co(III)–C $_{\beta}$ bond. As seen in this chapter the activation of the homolytic cleavage arises from a cluster of effects, *namely*, steric crowding (increasing the number of substituents on the α ligand), electronic upsets, induced *trans* influences, manipulation of geometric parameters or simply a combination of all these factors together with many others not yet discovered.

CHAPTER 6

TRANS INFLUENCE OF THE ALPHA LIGAND: PART 2****

6.1 INTRODUCTION

It has been reported,^{141,243-246} that in an enzymatic environment the axial DMB ligand in cobalamin enzymes is sometimes replaced by a histidine^{54,247} from a protein side chain or by the imidazole²⁴⁸ from the histidine residue. Due to this exchange the potential role of the amino acid is of considerable interest. Several other reports have shown various amino acid side chains providing the α ligand to the metal centre, such as Asp (to Co(II) in human methionine aminopeptidase²⁴⁹ and Fe(III) in human serum transferrin²⁵⁰), Tyr (to Co(II) in human methionine aminopeptidase²⁵¹ and Fe(III) in lactoferrin²⁵²) and Cys (to Co(III) in Co-containing nitrile hydratase²⁵³ and Fe(III) in human cytochrome P450²⁵⁴). From this a question arises. Why, with the large number of existing amino acid side chains, are only histidine and imidazole found as the replacement α ligand for some B₁₂ analogues?

This chapter focuses on investigating whether indeed the nature of the α ligand would affect the homolytic cleavage of the Co(III)–C β bond. A range of models with actual amino acids, realistic models or side chains of amino acids as α ligands to the Co(III) metal centre were used that included: cysteine, methanethiol and methanethiolate as

**** The work reported in this chapter forms part of a manuscript submitted to J. Phys. Chem. B titled DFT Studies of Trans and Cis Influences in the Homolysis of the Co-C Bond in Models of the Alkylcobalamins.

models for cysteine; acetate and tyrosine as a model for glutamine and aspartate; serine, methanol and 2-propanol as a model for serine and threonine; and histidine, imidazole, glycine and *p*-aminopyridine as a model for histidine, see **Figure 6.1**. Although, *p*-aminopyridine does not form part of the amino acids or side chains thereof, it was included in the calculations as Halpern *et al.*²⁵⁵ reported the homolysis of the Co(III)–C β bond to be dependent on the basicity of *trans*-4-substituted pyridines. In addition, *p*-aminopyridine has a close structural resemblance and character to histidine and imidazole, and it was important to include it as an α ligand for the cobalamin models under investigation.

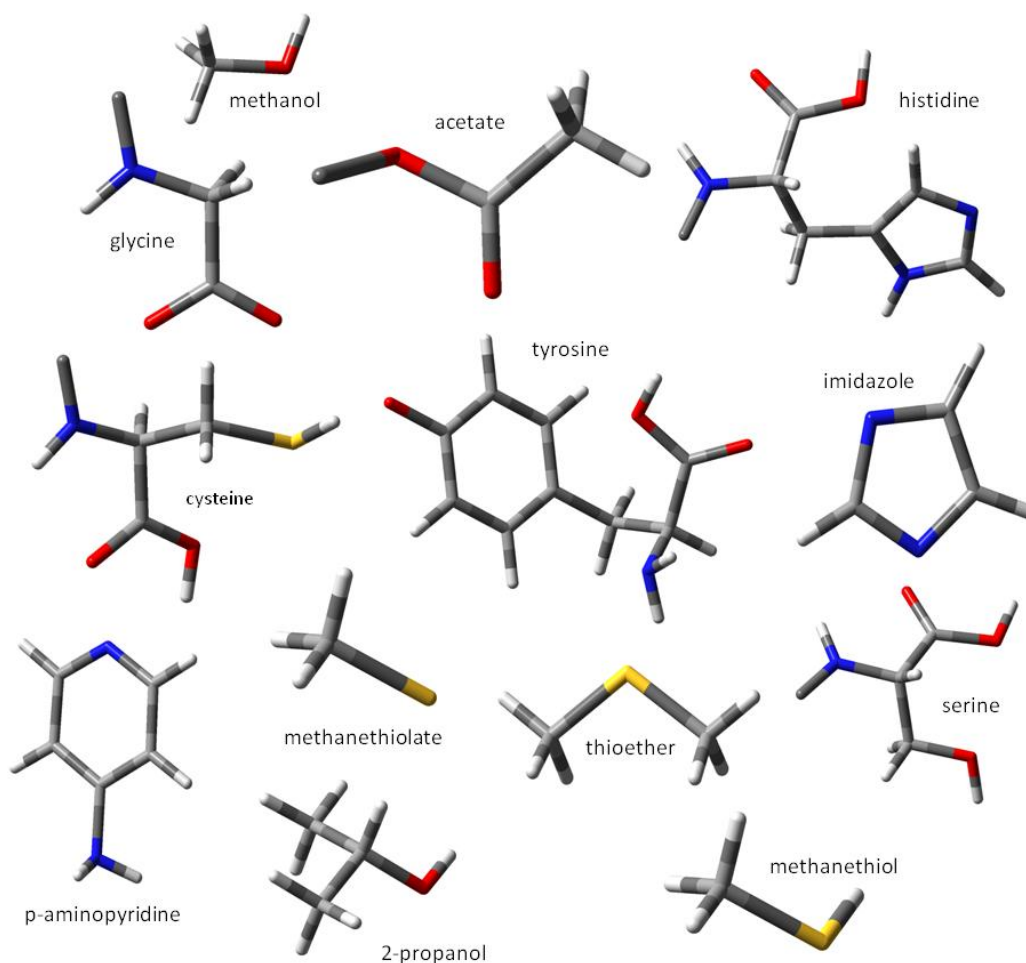


Figure 6.1: Structures of the α -ligands used to investigate *trans* influences.

These ligands also represent a range of compounds with different basicities as seen by their proton affinity values provided later in the chapter. The effects of these α ligands on the homolysis of the Co(III)–C $_{\beta}$ bond (ΔG and BDE) and the geometric parameters such as key bond lengths and angles were monitored. In addition, the absolute chemical hardness of the α ligands, together with the contraction of the lower axial, Co–B $_{\alpha}$, bond length and the shift of the Co metal centre from the corrin plane in the Co(III) and Co(II) complex were assessed.

The absolute hardness (η) of a(n) atom, ion, molecule or radical is defined as,

$$\eta = \left(\frac{IP - EA}{2} \right) \quad 6.1$$

where, IP is the ionisation potential and EA the electron affinity.^{256,257} The chemical hardness of a system parallels its stability, that is, as the hardness increases so does the stability of the chemical system.^{256,258} The ionisation potential values (experimental and calculated) with the electron affinities are provided in Appendix 3: 3.1.

6.2 MODEL STRUCTURES

Figure 6.2A represents the cobalamin models used in this chapter while **Figure 6.2B** provides a sketch of the same models. The modified cobalamin model from Chapter 5 was used with changes made to the α ligand only.

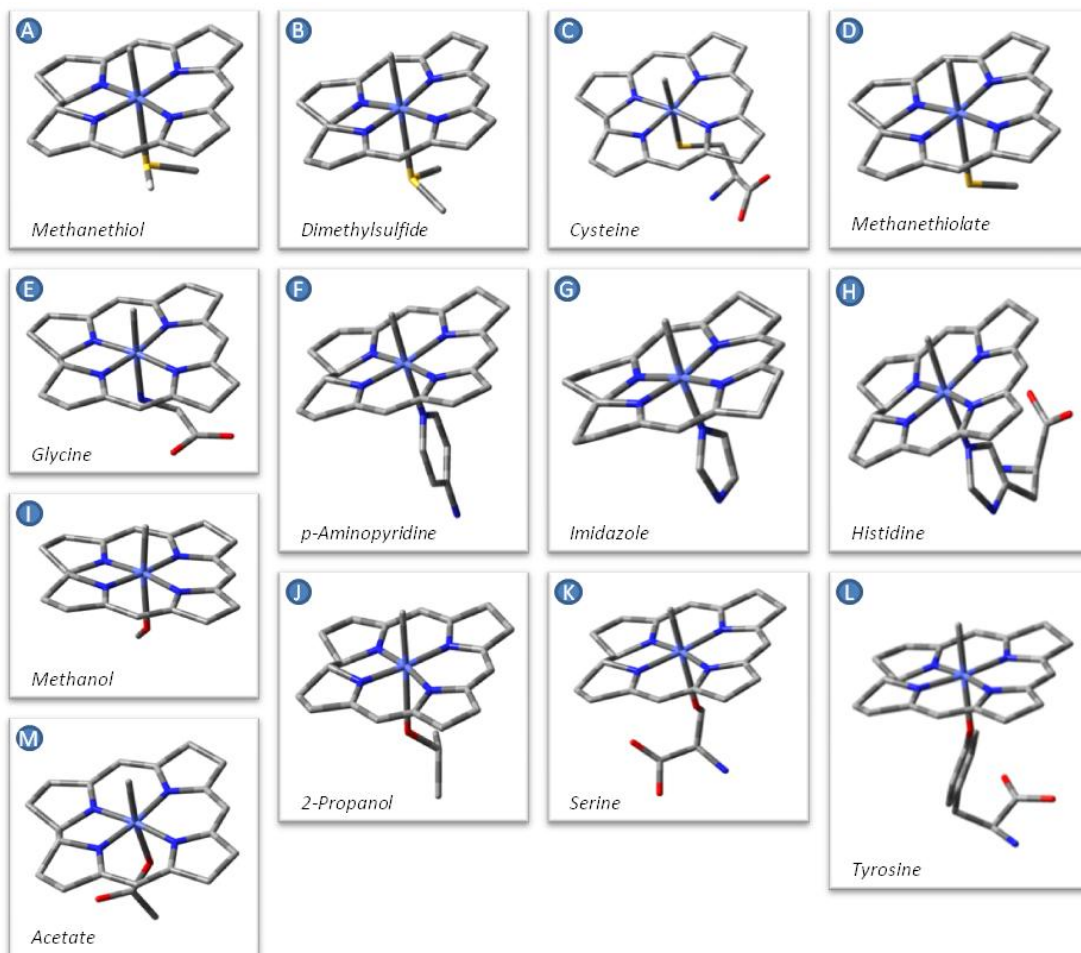
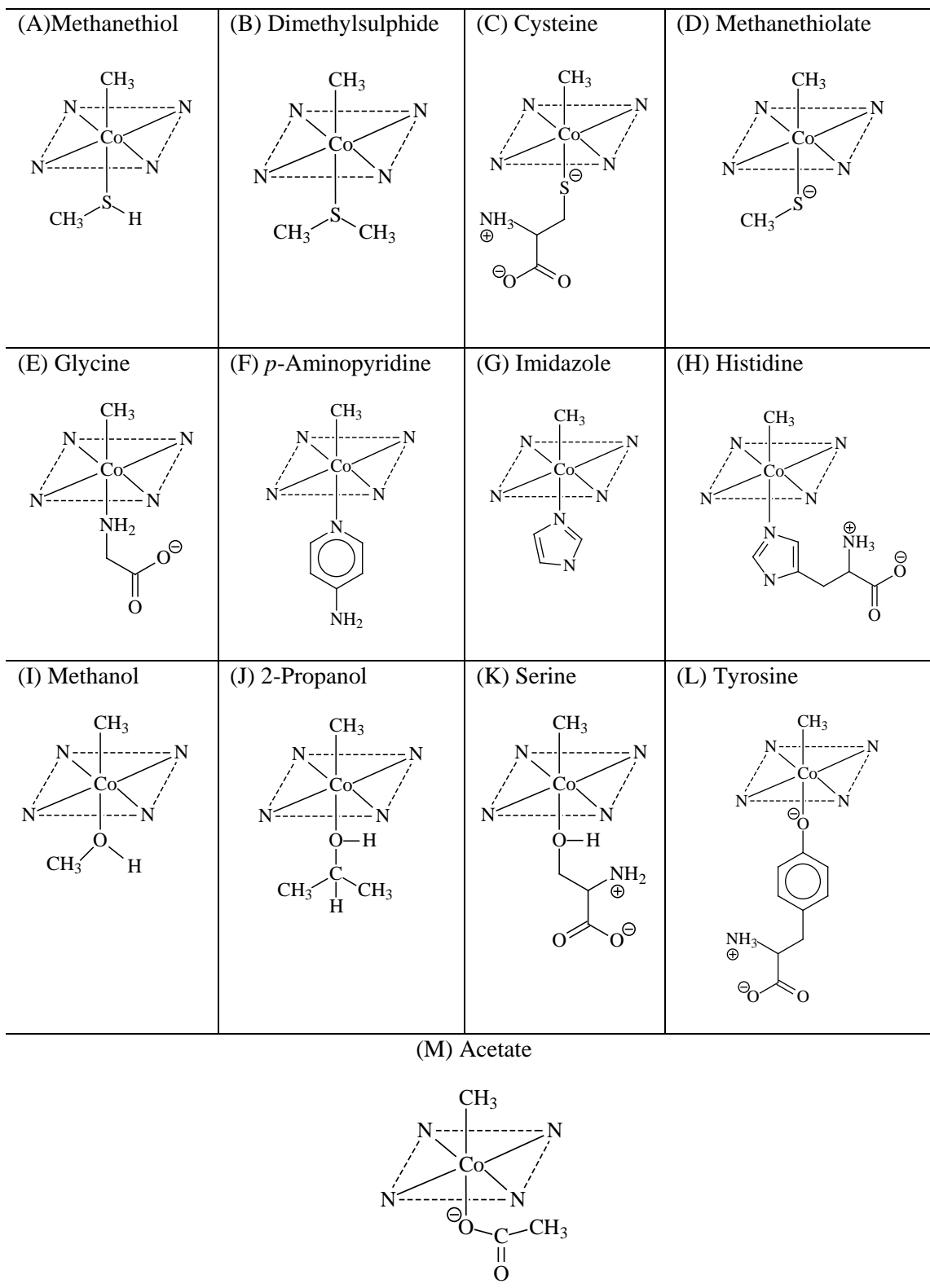


Figure 6.2A: Corrin models A–M with a change in the α -ligands.

Figure 6.2B: Sketch of the corrin models A–M with a change in the α -ligands.

6.3 METHOD

All the model structures shown in **Figure 6.2** retained a methyl group as the β axial ligand while the α ligand was varied. The corrin macrocycle contained only hydrogen atoms on its periphery. All calculations were carried out under relaxed conditions with the BP86 functional and 6-31+G(d,p) basis set. Both the geometry optimisation and frequency calculations were conducted at the same level of theory for all spin states. All reported energies were zero-point corrected.

6.4 RESULTS AND DISCUSSION

A co-ordinated ligand can have an effect on the metal-to-ligand bonding and lability of other ligands within a molecular system, more especially those in a *trans* position.²²⁵ A *trans*-effect is defined as “the effect of a co-ordinated group on the rate of substitution reactions of ligands *trans* to itself”²⁵⁹ while a ‘*trans* influence’ is used to describe the ability of a ligand to selectively weaken the bond *trans* to itself.²⁶⁰

In this chapter the *trans* influence is explored as a function of the change in α ligands made to the corrin models A–M. **Table 6.1** contains the geometric parameters, **Table 6.2** provides the topological properties for the electron densities at the bcp of the axial ligands in the Co(III) and Co(II) complex, and **Table 6.3 A** and **B** give the partial charges generated for models A to M. The α ligands are divided into three classes, namely, soft, intermediate and hard ligands. The softer the ligand the smaller the effective nuclear charge between the nucleus and valence electrons of that particular element (or donor atom, B_α).

Table 6.1: Geometric parameters for corrin BP86/6-31+G(d,p) with a change in the types of α -ligands

Model	^a E _{pa} ^{213,261}	α -ligand	Bond lengths / Å				Tolman cone angle /°	^f Shift of Co from the mean plane / Å		^g η /eV	Energies kcal mol ⁻¹	
			^b Co(III)-C _{β}	^c Co(III)-B _{α}	^d Co(II)-B _{α}	^e $\Delta_{(5c-6c)}$		Co(III)	Co(II)		α -ligand	ΔG
Soft ligands												
A	185	Methanethiol	1.979	2.721	2.511	-0.210	33.64	0.024*	0.145	4.91	20.46	32.27
B	199	Dimethylsulfide	1.983	2.676	2.512	-0.164	39.27	0.013*	0.147	4.77	19.90	31.52
C	216	Cysteine	2.010	2.509	2.509	0.000	35.85	0.003*	0.128	4.16	18.05	30.02
D	359	Methanethiolate	2.025	2.457	2.496	0.039	19.81	0.011*	0.120	3.38	17.22	29.39
Intermediate ligands												
E	212	Glycine	1.995	2.176	2.180	0.004	43.15	0.004	0.146	4.94	20.72	32.03
F	234	<i>p</i> -aminopyridine	1.988	2.202	2.157	-0.046	39.62	0.007	0.154	4.39	19.97	32.08
G	235	Imidazole	1.984	2.176	2.140	-0.036	35.79	0.003	0.149	4.80	20.42	32.45
H	236	Histidine	1.982	2.196	2.140	-0.056	35.87	0.000	0.147	4.58	19.98	31.89
Hard ligands												
I	180	Methanol	1.969	2.369	2.268	-0.101	29.86	0.046*	0.100	5.86	23.17	34.66
J	190	2-Propanol	1.970	2.408	2.297	-0.111	32.88	0.045*	0.108	5.29	23.15	34.96
K	219	Serine	1.968	2.497	2.309	-0.188	47.86	0.056*	0.096	4.64	23.42	34.89
L	221	Tyrosine	1.994	2.094	2.119	0.025	31.57	0.017*	0.116	3.97	20.83	32.54
M	348	Acetate	1.991	2.097	2.107	0.010	18.59	0.013*	0.123	5.58	21.05	32.95

^aReported theoretical proton affinity values. ^bThe axial bond length between the Co(III) and C _{β} ligand in the 6 coordinate complex. ^cThe axial bond length between Co(III) and B _{α} ligand in the 6 coordinate complex. ^dThe axial bond length between Co(II) and B _{α} ligand in the 5 coordinate complex. ^eThe difference in Co-B _{α} bond length between the 5 coordinate and 6 coordinate complex. ^fDistance (in Å) of the Co(III) and Co(II) metal centre from the mean plane defined through the N_{eq} donors of the macrocyclic ring. ^{*}The Co ion is found above the mean plane towards the β ligand. ^gChemical hardness calculated as ((Ionisation potential(IP)-Electron affinity(EA))/2).^{258,262}

Table 6.2: Topological properties of the electron density (ρ) (in au) at the bcp of Co(III)–CH₃, Co(III)–B _{α} ^a and Co(II)–B _{α} ^a for model complexes A–M with soft, hard and intermediate (interm.) ligands

		Models	ρ	$\nabla^2\rho$	V(r)	G(r)	H(r)	V(r) /G(r)	
Soft ligands	Co(III)–CH ₃	A	0.1159	0.0387	-0.1288	0.0693	-0.0596	1.8604	
		B	0.1151	0.0412	-0.1280	0.0691	-0.0588	1.8510	
		C	0.1094	0.0747	-0.1238	0.0712	-0.0525	1.7379	
		D	0.1061	0.0843	-0.1207	0.0709	-0.0498	1.7028	
Interm. ligands		E	0.1131	0.0702	-0.1278	0.0727	-0.0552	1.7587	
		F	0.1151	0.0487	-0.1283	0.0702	-0.0581	1.8265	
		G	0.1160	0.0483	-0.1292	0.0707	-0.0586	1.8292	
		H	0.1163	0.0474	-0.1297	0.0708	-0.0589	1.8326	
Hard ligands		I	0.1183	0.0371	-0.1321	0.0707	-0.0614	1.8687	
		J	0.1181	0.0358	-0.1316	0.0703	-0.0613	1.8727	
		K	0.1182	0.0350	-0.1319	0.0702	-0.0617	1.8781	
		L	0.1134	0.0728	-0.1288	0.0735	-0.0553	1.7523	
	M	0.1140	0.0719	-0.1293	0.0737	-0.0557	1.7559		
Soft ligands	Co(III)–B _{α}	A	0.0318	0.0744	-0.0324	0.0255	-0.0069	1.2709	
		B	0.0353	0.0783	-0.0369	0.0283	-0.0087	1.3072	
		C	0.0510	0.0784	-0.0539	0.0367	-0.0171	1.4662	
		D	0.0589	0.0759	-0.0619	0.0405	-0.0215	1.5307	
Interm. ligands		E	0.0620	0.2115	-0.0808	0.0669	-0.0140	1.2092	
		F	0.0559	0.2046	-0.0747	0.0629	-0.0118	1.1875	
		G	0.0574	0.2268	-0.0794	0.0680	-0.0113	1.1666	
		H	0.0547	0.2108	-0.0747	0.0637	-0.0110	1.1729	
Hard ligands		I	0.0321	0.1183	-0.0414	0.0355	-0.0059	1.1660	
		J	0.0305	0.1045	-0.0377	0.0319	-0.0058	1.1810	
		K	0.0255	0.0848	-0.0296	0.0254	-0.0042	1.1656	
		L	0.0615	0.2660	-0.0851	0.0758	-0.0093	1.1226	
		M	0.0613	0.2677	-0.0849	0.0759	-0.0090	1.1185	
Soft ligands		Co(II)–B _{α}	A	0.0500	0.0985	-0.0573	0.0410	-0.0163	1.3990
			B	0.0506	0.0957	-0.0573	0.0406	-0.0167	1.4109
	C		0.0527	0.0710	-0.0529	0.0353	-0.0176	1.4976	
	D		0.0558	0.0655	-0.0548	0.0356	-0.0192	1.5395	
Interm. ligands	E		0.0640	0.1906	-0.0812	0.0644	-0.0168	1.2601	
	F		0.0639	0.2212	-0.0859	0.0706	-0.0153	1.2165	
	G		0.0644	0.2395	-0.0890	0.0745	-0.0146	1.1957	
	H		0.0642	0.2401	-0.0890	0.0745	-0.0145	1.1945	
Hard ligands	I		0.0413	0.1559	-0.0554	0.0472	-0.0082	1.1739	
	J		0.0393	0.1400	-0.0510	0.0430	-0.0080	1.1864	
	K		0.0387	0.1356	-0.0500	0.0420	-0.0081	1.1923	
	L		0.0614	0.2223	-0.0805	0.0680	-0.0125	1.1831	
	M		0.0601	0.2185	-0.0789	0.0668	-0.0121	1.1816	

^aB _{α} represents the element from the α (lower) ligand that is directly attached to the Co metal centre. A–M represents the cobalamin models with the different α ligands, see Figure 6.1 A and B.

Table 6.3A: Mulliken and APT partial charges (e) for model complexes A–M

E _{pa}	Model	Mulliken							APT						
		Co(III)	C _β	B _α ^a	N ₁	N ₂	N ₃	N ₄	Co(III)	C _β	B _α	N ₁	N ₂	N ₃	N ₄
Soft ligands															
185	A	-2.976	-0.252	0.151	0.455	0.628	0.558	0.447	0.208	0.189	-0.075	-0.233	-0.504	-0.513	-0.237
199	B	-3.162	-0.231	0.325	0.451	0.653	0.631	0.468	0.202	0.176	-0.033	-0.234	-0.508	-0.502	-0.227
216	C	-2.929	-0.332	-0.362	0.511	0.665	0.668	0.454	0.223	0.084	-0.536	-0.161	-0.528	-0.494	-0.197
359	D	-2.667	-0.353	-0.189	0.534	0.535	0.549	0.481	0.112	0.067	-0.387	-0.124	-0.503	-0.499	-0.166
Intermediate ligands															
212	E	-3.061	-0.266	-0.467	0.284	0.441	0.431	0.412	0.244	0.122	-0.309	-0.230	-0.569	-0.501	-0.248
234	F	-2.137	-0.146	0.553	0.308	0.283	0.321	0.313	0.271	0.163	-0.427	-0.225	-0.533	-0.524	-0.225
235	G	-3.001	-0.128	0.287	0.358	0.341	0.369	0.359	0.250	0.171	-0.288	-0.227	-0.533	-0.533	-0.223
236	H	-2.496	-0.047	0.308	0.273	0.362	0.411	0.262	0.255	0.175	-0.297	-0.226	-0.523	-0.535	-0.229
Hard ligands															
180	I	-3.360	-0.260	-0.239	0.477	0.463	0.540	0.376	0.196	0.202	-0.495	-0.232	-0.502	-0.502	-0.235
190	J	-3.660	-0.267	-0.117	0.625	0.573	0.526	0.394	0.217	0.201	-0.587	-0.220	-0.484	-0.496	-0.225
219	K	-3.757	-0.244	-0.110	0.466	0.650	0.678	0.475	0.196	0.207	-0.584	-0.228	-0.483	-0.479	-0.250
221	L	-3.742	-0.203	-0.106	0.471	0.553	0.676	0.673	0.389	0.089	-1.031	-0.198	-0.506	-0.504	-0.191
348	M	-3.430	-0.285	-0.067	0.451	0.542	0.619	0.492	0.316	0.112	-0.808	-0.155	-0.515	-0.500	-0.166

^aB_α represents the element from the α (lower) ligand that is directly attached to the Co metal centre. A–M represents the cobalamin models with the different α ligands, see Figure 6.1 A and B. N₁, N₂, N₃ and N₄ are the partial charge on the equatorial nitrogen of the cobalamin macrocycle.

Table 6.3B: NBO and Bader partial charges (e) for model complexes A–M

E _{pa}	Model	NBO							BADER						
		Co(III)	C _β	B _α ^a	N ₁	N ₂	N ₃	N ₄	Co(III)	C _β	B _α	N ₁	N ₂	N ₃	N ₄
Soft ligands															
185	A	0.155	-0.691	0.116	-0.349	-0.390	-0.391	-0.354	1.031	-0.125	0.041	-1.089	-1.101	-1.106	-1.091
199	B	0.144	-0.698	0.376	-0.352	-0.392	-0.389	-0.347	1.029	-0.129	0.007	-1.090	-1.102	-1.105	-1.087
216	C	0.072	-0.766	-0.253	-0.310	-0.361	-0.360	-0.320	1.053	-0.161	-0.461	-1.072	-1.093	-1.095	-1.075
359	D	0.035	-0.798	-0.172	-0.299	-0.351	-0.351	-0.306	1.053	-0.177	-1.068	-1.068	-1.091	-1.091	-1.069
Intermediate ligands															
212	E	0.215	-0.754	-0.828	-0.342	-0.373	-0.366	-0.341	1.097	-0.155	-1.025	-1.083	-1.097	-1.100	-1.082
234	F	0.209	-0.719	-0.427	-0.332	-0.381	-0.373	-0.333	1.089	-0.142	-1.142	-1.081	-1.099	-1.099	-1.084
235	G	0.193	-0.714	-0.426	-0.329	-0.375	-0.372	-0.330	1.092	-0.141	-1.105	-1.084	-1.100	-1.102	-1.083
236	H	0.201	-0.711	-0.422	-0.333	-0.385	-0.373	-0.336	1.088	-0.139	-1.105	-1.083	-1.012	-1.101	-1.084
Hard ligands															
180	I	0.292	-0.690	-0.703	-0.358	-0.391	-0.385	-0.360	1.077	-0.122	-1.056	-1.084	-1.094	-1.093	-1.089
190	J	0.304	-0.690	-0.714	-0.345	-0.395	-0.400	-0.354	1.071	-0.121	-1.048	-1.079	-1.096	-1.102	-1.084
219	K	0.307	-0.685	-0.712	-0.362	-0.395	-0.386	-0.371	1.063	-0.119	-1.069	-1.089	-1.094	-1.090	-1.092
221	L	0.251	-0.756	-0.641	-0.314	-0.361	-0.346	-0.309	1.138	-0.157	-1.128	-1.073	-1.086	-1.080	-1.061
348	M	0.233	-0.750	-0.632	-0.299	-0.352	-0.349	-0.298	1.135	-0.155	-1.131	-1.069	-1.080	-1.083	-1.059

^aB_α represents the element from the α (lower) ligand directly attached to the Co metal centre. A–M represents the cobalamin models with the different α ligands, see Figure 6.1 A and B. N₁, N₂, N₃ and N₄ are the partial charge on the equatorial nitrogen of the cobalamin macrocycle.

(a) *Proton affinities of α -ligands, bond lengths, and BDEs*

As early as 1982, Halpern *et al.*²⁵⁵ investigated cobalamin models with *trans*-4-substituted pyridines as the α ligand, and were convinced that the dissociation energy of the Co(III)–C $_{\beta}$ bond systematically increases with an increasing basicity of the *trans* ligand.¹⁹⁹ This view of the *trans*-electronic influence would then imply that the longer the Co(III)–B $_{\alpha}$ bond *trans* to the β -ligand, the poorer the electron donation to the Co atom, and therefore the weaker the Co(III)–C $_{\beta}$ bond. These trends paralleled the decrease in the oxidation state of the metal from +3 to +2, and it was concluded that higher oxidation states are favoured in the presence of a strong basic ligand, and as a result the organometallic Co(III) complex is better stabilized.¹⁹⁹ In addition, the added steric interactions of the *trans* ligand with the equatorial ligand resulted in the α ligand also moving further away from the metal centre. These observations were confirmed in crystallographic studies^{263,264} when long Co–N $_{\alpha}$ bonds were found *trans* to the Co–C $_{\beta}$ bonds.

The results (**Table 6.1**) show that the cobalamin model with the soft ligands²⁶⁵ have low Co(III)–C $_{\beta}$ ΔG and BDEs while the highest BDEs are obtained for the serine, acetate, methanol, 2-propanol and tyrosine ligands (hard ligands). Those ligands connecting to Co *via* the N-atom the BDEs for the homolysis of the Co(III)–C $_{\beta}$ bond lie between the soft and hard ligands, in the intermediate category. Histidine and imidazole fall into the intermediate category, and are of particular interest since, as mentioned in the introduction, they are the only known protein side chains found in cobalamin enzymes.^{45,247,266}

An assessment of the proton affinities of all the α ligands against the homolysis of the Co(III)–C $_{\beta}$ BDEs, **Figure 6.3** ((Soft ligands (●), Intermediate ligands (▲), Hard ligands (■)), gives no correlation.

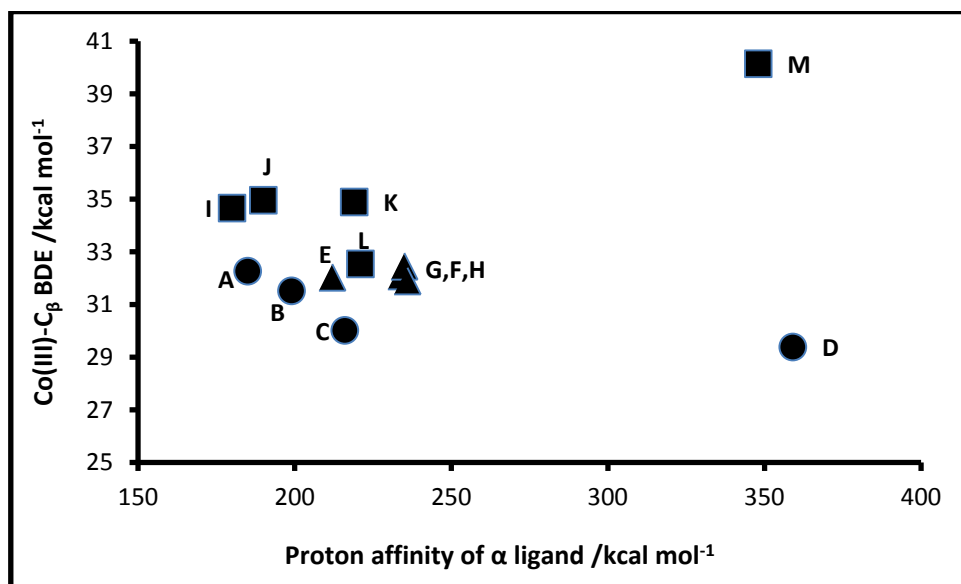


Figure 6.3: Proton affinities (kcal mol $^{-1}$) is plotted against the Co(III)–C $_{\beta}$ BDEs (kcal mol $^{-1}$) for models A–M.

In fact, a correlation can be identified if the α ligands from the same class are assessed against each other. Therefore, the *trans* influence of the α ligand to the Co(III)–C $_{\beta}$ bond and its associated BDEs are discussed for three separate classes of α ligands as follows:

Soft ligands

α ligands; methanethiol, dimethylsulphide, cysteine and methanethiolate fall into this category. These ligands connect to Co *via* the sulfur atom (**Figures 6.2 A and B**). Sulfur in the methanethiol and dimethylsulphide α ligand are neutral while the sulfur in the other models are negatively charged.

The data provided in **Table 6.1** show a decrease in Co(III)–B_α bond length as the E_{pa} of the α ligand increases, however, it must be noted that other contributing factors such as the nature (neutral and charged α ligand) and steric effect of the α ligand (quantified by the Tolman cone angle)²¹⁷ may affect the observed trend. Concurrently, the Co(III)–C_β bond length increases, thereby exhibiting a normal *trans* influence between the two axial ligands. This weakening of the Co(III)–C_β bond length is consistent with the decreased orbital overlap of the Co(III) metal centre with the orbitals of C_β from the β ligand (**Table 6.1**), and the concomitant decrease in the Co(III)–C_β BDE. The electron density at the bcp of the Co(III)–C_β bond (**Table 6.2**) is shown to decrease and therefore parallels the observation made above, **Figure 6.4**.

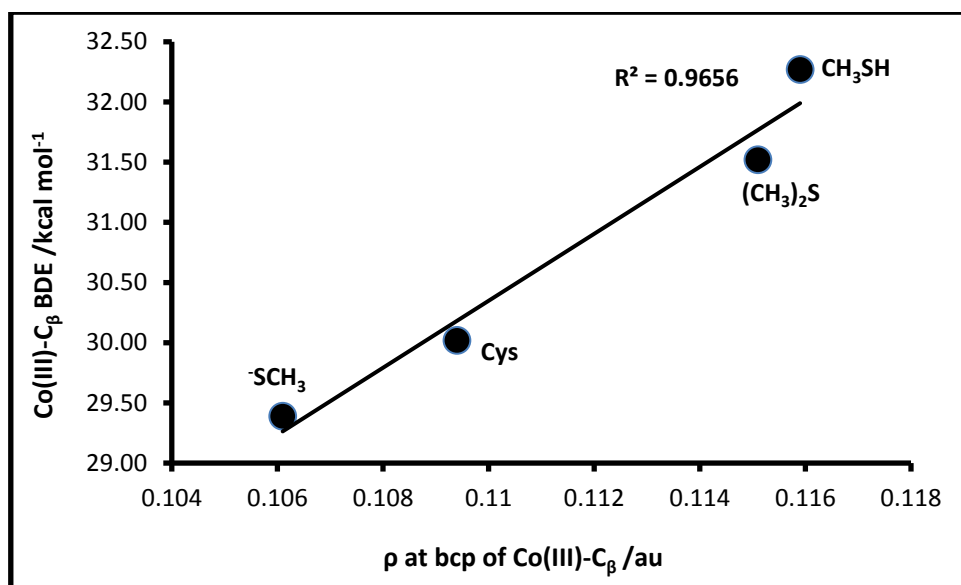


Figure 6.4: The dependence of the homolysis of the Co(III)–C_β BDE (kcal mol⁻¹) as a result of the electron density at the bcp of the Co(III)–C_β bond.

After homolysis, the formal Co oxidation state decreases from +3 to +2; however, the ionic radius²⁶⁷ increases from 0.63 Å to 0.74 Å, respectively. The subsequent steric effect is reduced because the Co(II) ion in the Co(II) complex is found ~ 0.1 Å below

the corrin mean plane and closer to the α ligand (see **Table 6.1**). This is an observation confirmed by crystallographic experiments by Finke and Hay,²²⁴ and which Jensen *et al.*⁴⁸ noticed in their theoretical calculations on cobalamin models. This change promotes a greater overlap between the orbitals of Co and the α ligand, thus producing a shorter lower axial bond length and better stabilisation for the Co(II) complex.

The results show that the Co(II)–B $_{\alpha}$ bond length decreases for those models with the neutral (methanethiol and dimethylsulfide) α ligand. This observation is consistent with the increased orbital overlap of the Co(II) metal centre with the lower α ligand. Charged ligands, cysteine and methanethiolate, show respectively no change, and an increase in the Co(II)–B $_{\alpha}$ bond length (lower ligand). This increase in bond length of the lower axial ligand from the Co(III) to the Co(II) complex is also consistent with a weaker orbital overlap of the metal centre with the α ligand. These observations reflect a normal *trans* influence between the axial ligands.

The absolute chemical hardness (η) of the α ligand parallels the BDE of the homolysis of the Co(III)–C $_{\beta}$ bond, that is, the BDE increases as η (chemical stability) increases (**Figure 6.5A**). These results are contrary to those observed for the change in the lower axial bond length from the 5-coordinate to the 6-coordinate complex, $\Delta\text{Co–B}_{\alpha(5c-6c)}$. A larger contraction of the Co–B $_{\alpha}$ bond from the 5- to the 6-coordinate complex is in agreement with a more stabilised Co(II) complex (a trend observed in Chapter 5), thus exhibiting a lower BDE for the cleavage of the Co(III)–C $_{\beta}$ bond. The opposite is true in this case, see **Figure 6.5B**. These observations suggest that the Co(III) complex was stable and the nature of the α ligand is important in controlling the axial bond lengths and the associated BDEs.

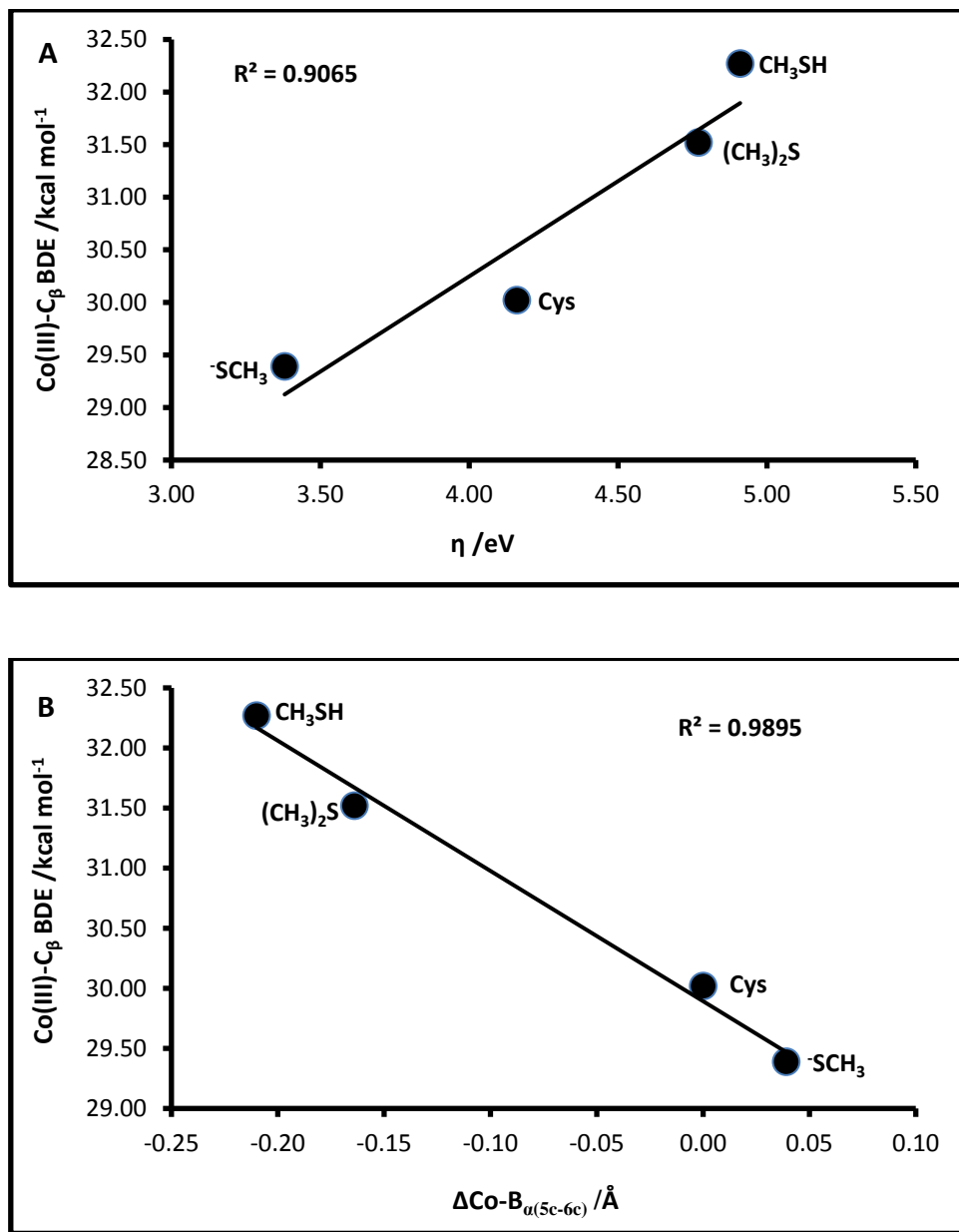


Figure 6.5: A) Absolute chemical hardness (eV) and B) the change in the lower axial bond length from the 5- to the 6-coordinate complex (\AA) is plotted against the Co(III)-C β BDE (kcal mol $^{-1}$).

Hard ligands

The methanol, 2-propanol, serine, acetate and tyrosine ligands connect to Co *via* the oxygen atom (**Figures 6.2 A and B**). Both, acetate and tyrosine are charge bearing α ligands whilst the oxygen in α ligands; methanol, 2-propanol, and serine, are neutral. The results obtained for these ligands are erratic and there is no trend observed between the E_{pa} of the α ligand and the Co(III)–C $_{\beta}$ BDE, as was the case for the soft ligands. In addition, there appears to be no associated relationship between the axial bond lengths, steric effects of the α ligand or even the contraction of the lower axial bond length from the Co(III) to the Co(II) complex with the BDE of the homolysis of the Co(III)–C $_{\beta}$ bond.

Notably, the Co(II)–B $_{\alpha}$ bond for the model with the acetate and tyrosine α ligands, which carries a negative charge, exhibits an increase rather than a decrease of the bond length, while the converse is observed for the other three ligands. This increase in bond length for the lower axial ligand when a charge bearing ligand is present has also been discussed in Chapter 5 and in the results for the soft ligands given above. Strangely, the changes observed for the Co(II)–B $_{\alpha}$ bond lengths does not seem to parallel the orbital overlap between the Co(II) metal centre and the α ligand, shown in **Figure 6.6A**, as is observed for the orbitals of the Co(III) metal centre with the orbitals of the β ligand. Depending on the orbital overlap between the metal centre and axial ligand, the respective axial bond lengths either increased or decreased, see **Figure 6.6B**.

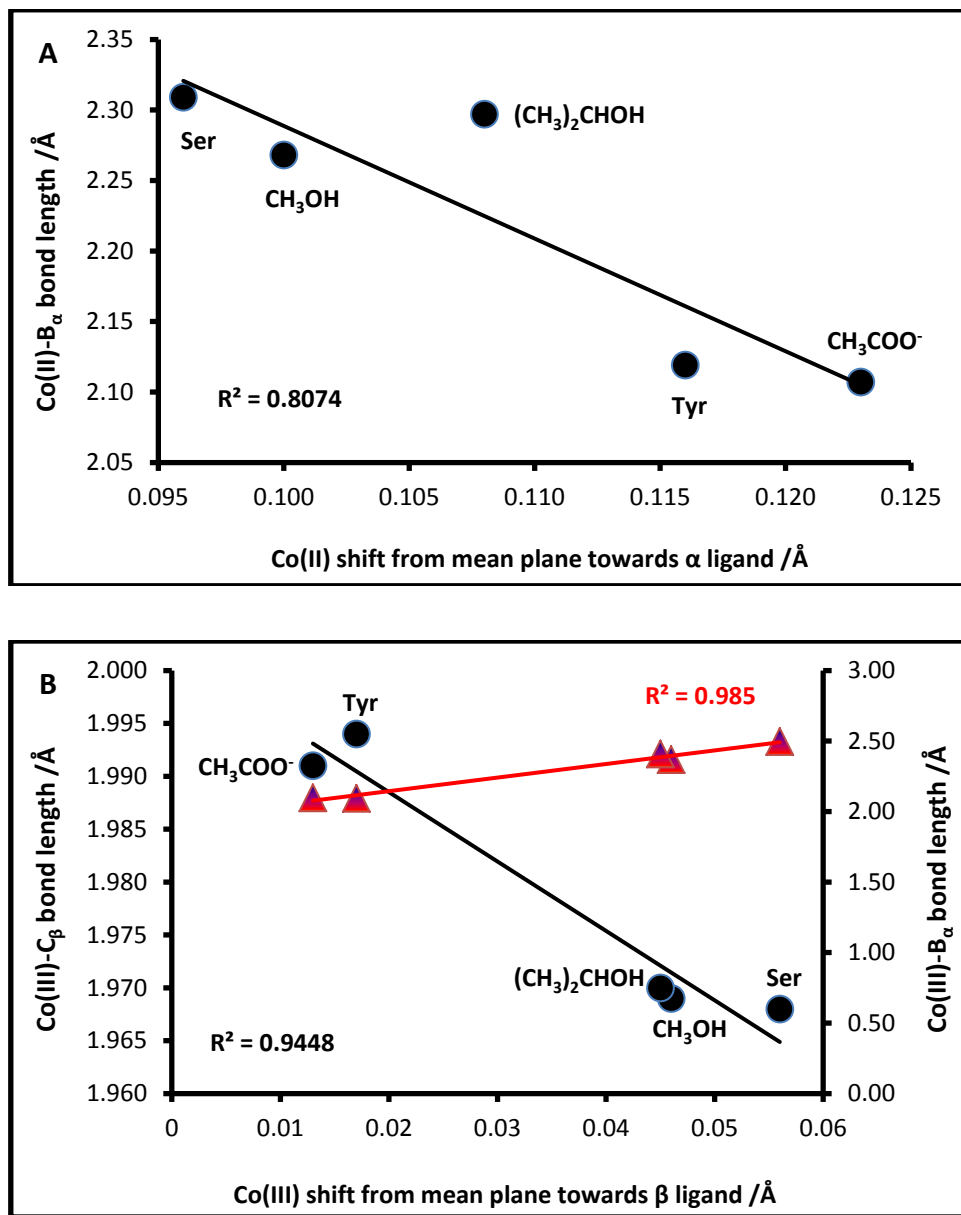


Figure 6.6: The shift of the Co metal centre (Å) in the Co(II) and Co(III) complexes respectively, versus the change in A) Co(II)-B_α bond length (Å) and B) Co(III)-C_β (●) and Co(III)-B_α (▲) bond lengths (Å).

The anomalous behaviour of the Co(II)–B_α bond can be attributed possibly to the high electronegative nature (*trans* electronic influence) of the oxygen atom directly attached to the Co metal centre for models L and M. The model with the acetate ligand shows a larger increase in the lower axial bond length (0.031 Å) than the model with the tyrosine ligand (0.025 Å). Naturally, the acetate ligand is simplistic and of smaller steric bulk (assessed by the Tolman cone angle)²¹⁷ when compared to tyrosine, therefore steric effects were eliminated as a possible cause for the lengthening of the Co(III)–B_α bond. Acetate differs from tyrosine because of the added electronegative effect of the carbonyl oxygen directly attached to this oxygen. Consequently, this makes it a poor electron donor to the metal centre, causing an electron withdrawing effect on the Co(III)–B_α bond and elongating the bond length in the process. On the other hand, tyrosine has a phenyl group directly attached to the oxygen, and although the oxygen inductively withdraws electrons from the metal centre, resulting in the elongation of the Co(III)–B_α bond, the effect is not as strong as the acetate ligand because of the phenyl group (less electron withdrawing) compared with a carbonyl group. A very basic ligand such as acetate ($E_{\text{pa}} = 348 \text{ kcal mol}^{-1}$) applies a strong inductive effect (*trans* electronic) on the upper axial bond, which correlates well with the BDE for the Co(III)–C_β bond (40.14 kcal mol⁻¹). However, this same bond is longer (1.991 Å) than the Co(III)–C_β bond in the methanol model (1.969 Å), and which in addition has a lower Co(III)–C_β BDE of 5.48 kcal mol⁻¹ than the former model, confirming the fact that bond lengthening is not synonymous with bond weakening.

For the models with α ligands, methanol, 2-propanol and serine ligand the oxygen connected to the Co(III) ion is protonated and it is this that makes it less electronegative compared to the oxygen in the acetate and tyrosine ligands. In addition, for the serine ligand, the oxygen is attached to the β carbon of the ligand structure, indicating that it is not directly attached to the carbonyl carbon and therefore a lower inductive effect is applied to the Co metal centre and axial β ligand, compared with the acetate ligand.

The Co(III)–C_β bond lengths do not systematically increase or decrease, but are consistent with the shift of the Co(III) metal centre towards the β ligand, while the Co(III)–B_α and Co(II)–B_α bond lengths increase as the E_{pa} and steric bulk (quantified by the Tolman cone angle)²¹⁷ of the α ligand increases and the absolute chemical hardness (stability) of the α ligands decrease. The correlation between the η and the Co(III)–C_β BDE is weak when all the “O” donor ligands are compared, **Figure 6.7**.

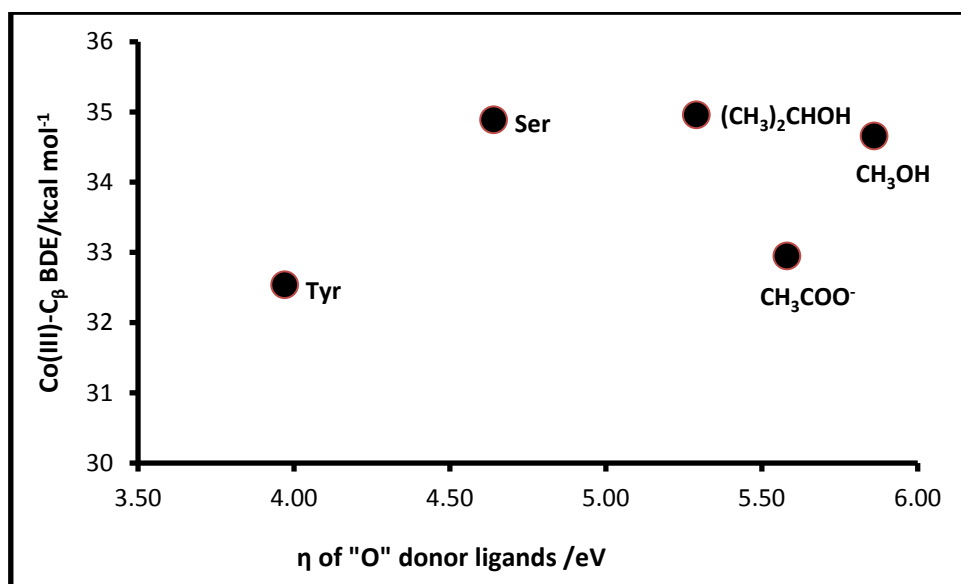


Figure 6.7: The Co(III)–C_β BDE (kcal mol⁻¹) is plotted against the absolute chemical hardness (η) (eV) of α ligands in cobalamin models where oxygen is both neutral and negatively charged.

Intermediate ligands:

For these particular ligands, the bond is between the metal centre and the nitrogen from the α ligand (**Figure 6.2A and B**). Both histidine and imidazole already form part of the make up of many B₁₂ analogues as α ligands. It is therefore important to explore other N-donor type models, together with histidine and imidazole, so that additional knowledge may be acquired as to why these two form such key α ligands.

The four N-donor ligands used included glycine, *p*-aminopyridine, histidine and imidazole. Both of the former ligands were purposefully chosen because of their similarities and slight differences to the histidine and imidazole ligands. The similarities included their steric bulk (assessed by Tolman cone angle²¹⁷), proton affinities and the aromatic nature in the case of *p*-aminopyridine. The differences included glycine being aliphatic (acyclic) in nature and *p*-aminopyridine being a non-natural amino acid, however, despite this, *p*-aminopyridine was found to be the best model for α ligands histidine, and imidazole.

The results shown in **Table 6.1** depict a fairly good correlation between the proton affinity of the α ligands with the Co(III)–C $_{\beta}$ bond length, that is, as the E $_{pa}$ value increases so the Co(III)–C $_{\beta}$ bond decreases ($r^2 = 0.86$), see **Figure 6.8A**. However, on omitting the data for the aliphatic glycine ligand from the aromatic ligands an improved linear regression was observed ($r^2 = 0.96$), see **Figure 6.8B**. These Co(III)–C $_{\beta}$ bond lengths are found to parallel those for the shift of Co(III) metal centre from the corrin mean plane. As the glycine ligand differs from the others because of its aliphatic nature, and no further trends are observed with the glycine ligand, the cobalamin model with glycine has been removed from any subsequent discussions.

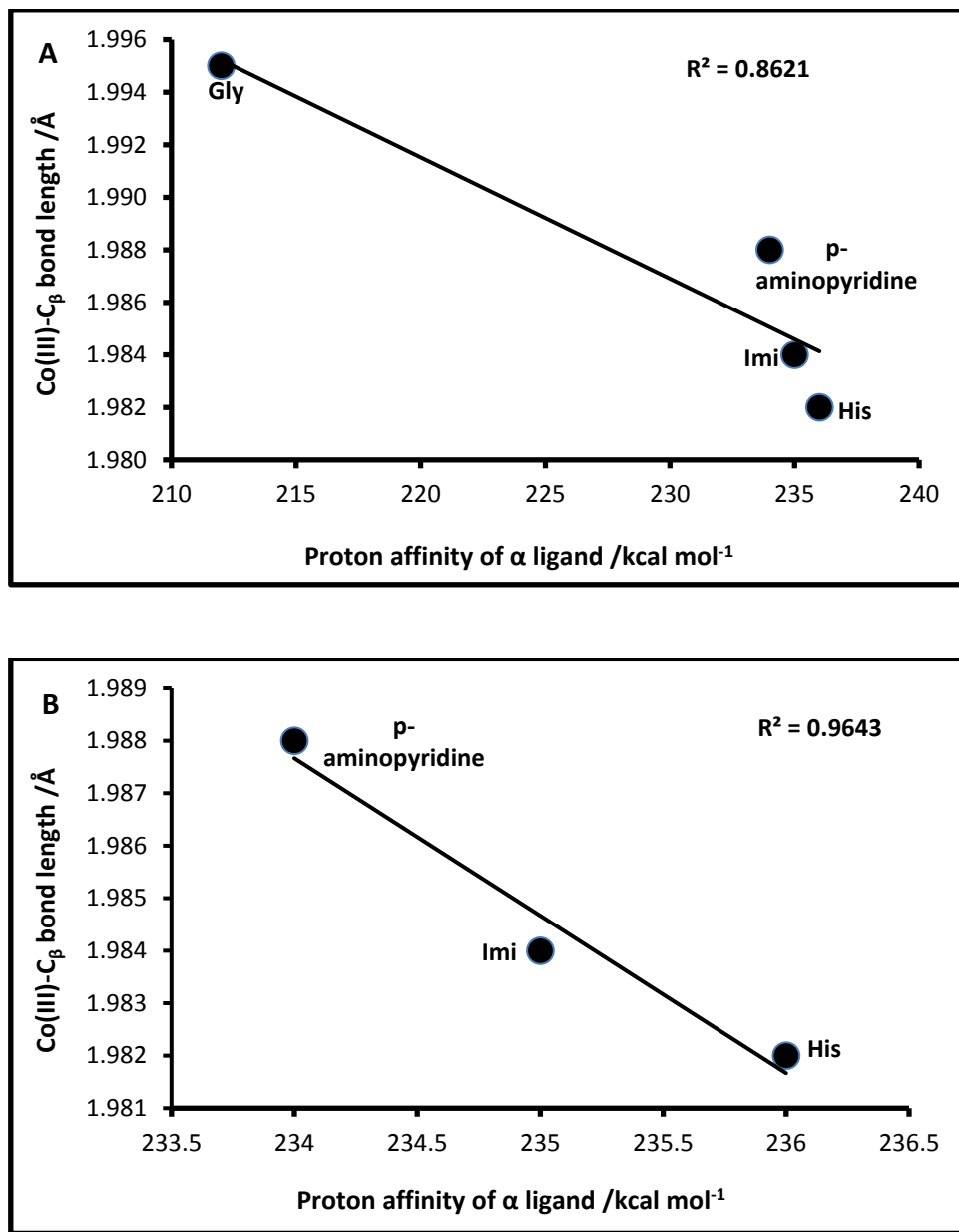


Figure 6.8: Proton affinity is plotted against the Co(III)–C β bond length for A) aliphatic and aromatic α ligands and B) aromatic α ligands only.

There is no trend observed for the Co(III)–B α axial bond lengths as the Co(III)–C β bond length decreases from *p*-aminopyridine to histidine. If *p*-aminopyridine were omitted there would be a normal *trans* influence between the two axial ligands from imidazole to histidine. The increase in the Co(III)–B α bond length of

p-aminopyridine is more likely due to its larger steric bulk (assessed by the Tolman cone angle)²¹⁷ over histidine and imidazole. A poor correlation is observed for the η of B_α , with the BDE of the $\text{Co(III)}\text{-C}_\beta$ bond, see **Figure 6.9A**, while the extent of contraction of the lower ligand, $\Delta\text{Co-B}_{\alpha(5c-6c)}$, from the Co(II) to the Co(III) complex correlates well with the homolysis of the $\text{Co(III)}\text{-C}_\beta$ BDE, shown in **Figure 6.9B**.

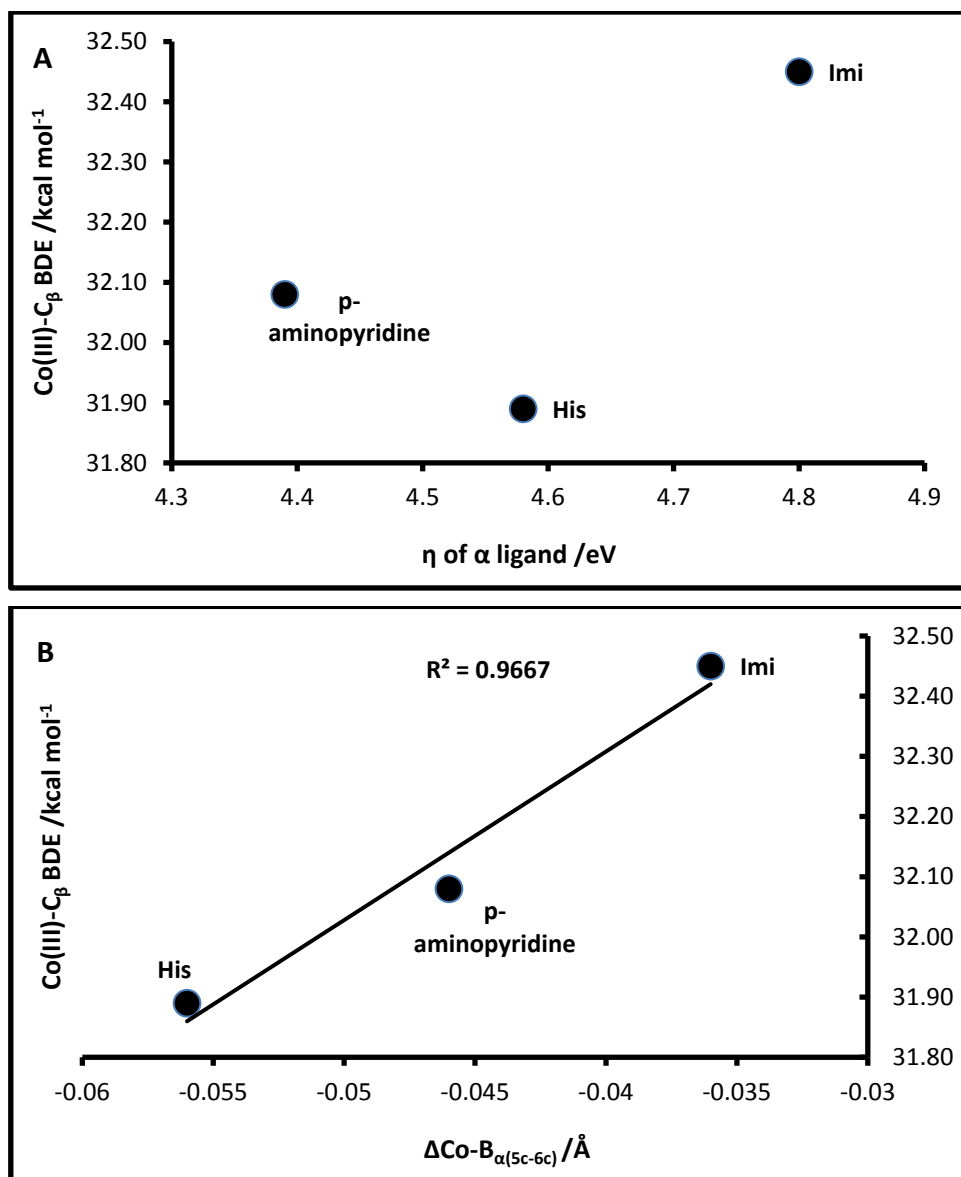


Figure 6.9: A correlation of the homolysis of the $\text{Co(III)}\text{-C}_\beta$ BDE (kcal mol⁻¹) against A) absolute chemical hardness (eV) and B) $\Delta\text{Co-B}_{\alpha(5c-6c)}$ (Å).

b) Electron densities and partial charges

The topological properties of the electron density and partial charges were generated and the data are recorded and presented in **Tables 6.2** and **6.3A-B**, respectively. The ρ -value at the bcp of the Co(III)–C $_{\beta}$ bond for models A–M were assessed and plotted as a function of the BDE of the Co(III)–C $_{\beta}$ bond, **Figure 6.10**. A fair correlation is obtained for the linear regression.

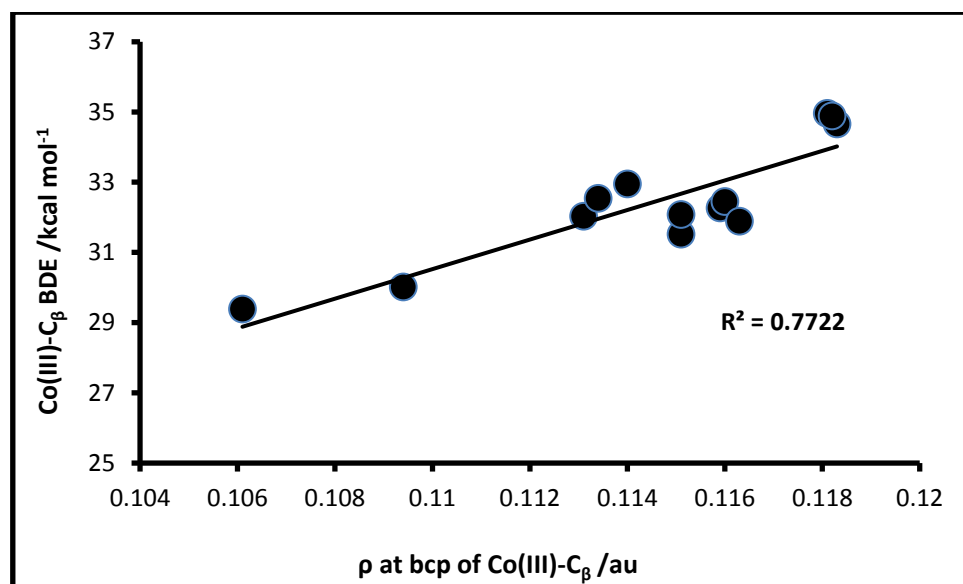


Figure 6.10: The dependence of the Co(III)–C $_{\beta}$ BDE (kcal mol $^{-1}$) as a function of the electron density (au) at the bcp of the Co(III)–C $_{\beta}$ bond.

Overall, the ρ at the bcp for both the upper and lower axial bonds, Co(III)–C $_{\beta}$ and Co(III)–B $_{\alpha}$, clearly shows an inverse relationship, confirming that a normal *trans* influence takes place. The ligands are of various character as they differ in charge and in the type (soft, intermediate or hard) of donor atom (B $_{\alpha}$ = S, O or N) of the base that is *trans* to the β ligand. A further evaluation of these ligands, from the results obtained thus far, shows them to amalgamate into two groups: those with aliphatic N (Gly), aromatic N (His, imidazole, *p*-aminopyridine) and anionic O (Tyr, acetate) donors, and those with neutral S (methanethiol, dimethylsulfide), anionic S (Cys,

methanethiolate) and neutral O (methanol, 2-propanol, Ser) donors, shown in **Figures 6.11 (A) and (B)**.

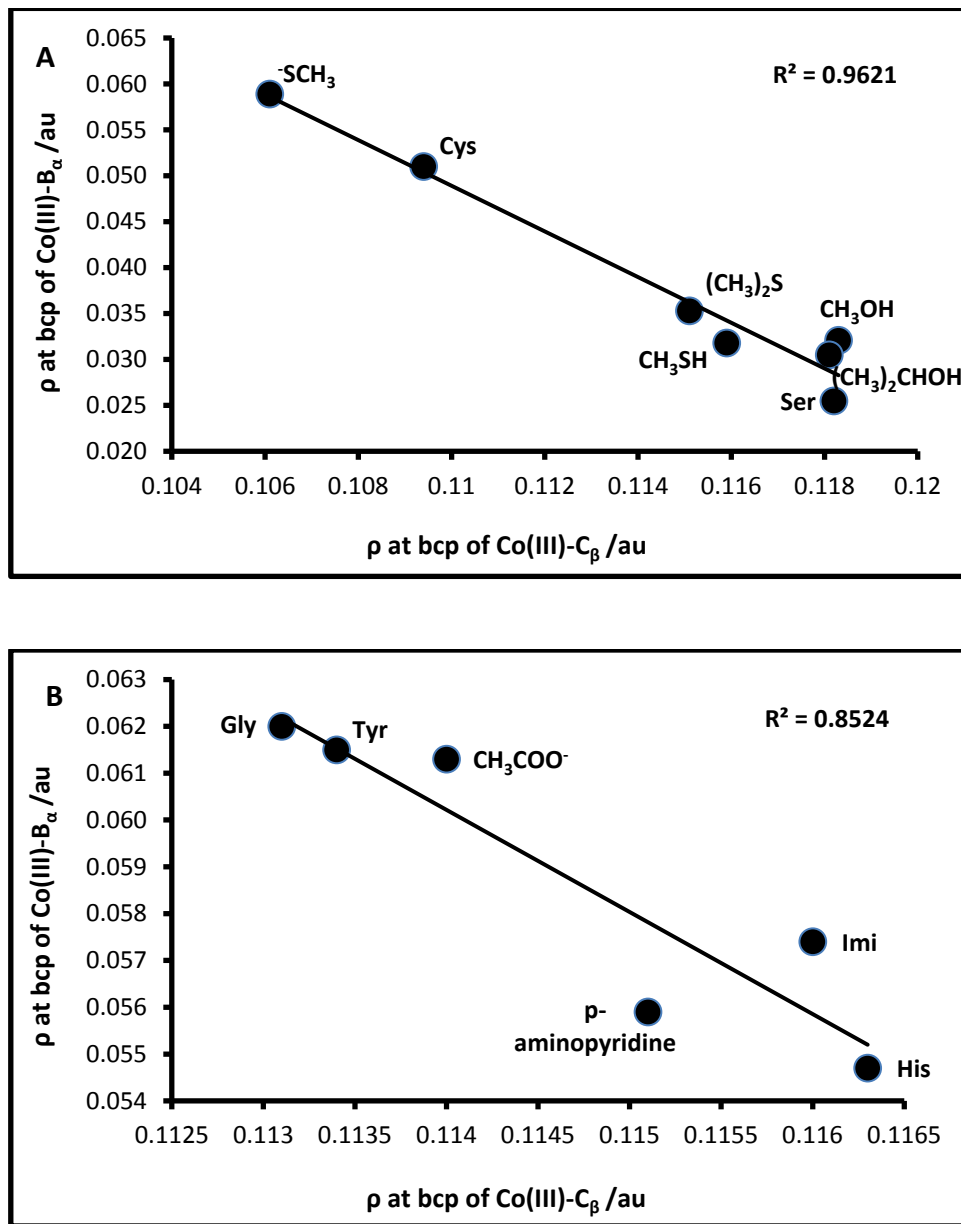


Figure 6.11: The inverse relationship of the electron densities at the bcps of the Co(III)-C $_{\beta}$ and Co(III)-B $_{\alpha}$ bonds for A) neutral O, S and anionic S donors and B) aliphatic and aromatic N and anionic O donors.

These trends suggest that the character of the B_α ligand plays a role in promoting the homolysis of the $\text{Co(III)}\text{-C}_\beta$ bond, that is, the softer the ligand the lower the BDE. It is evident for both the S- and O-donor ligands that the absolute chemical hardness and the change in the Co-B_α bond length from the Co(III) to Co(II) complex is important in controlling the BDE for the homolysis of the $\text{Co(III)}\text{-C}_\beta$ bond. Models for both these donor ligands showed the Co(III) metal centre to shift more towards the β ligand, resulting in stronger $\text{Co(III)}\text{-C}_\beta$ bonds (especially for the hard ligands) that paralleled the associated BDEs. Ultimately, the complexes with the hard ligands were found to be very stable while those with the soft ligands were unstable, obtaining very high and low $\text{Co(III)}\text{-C}_\beta$ BDEs, respectively.

In the N-donor ligand models, the Co(III) ion was observed to be below the corrin mean plane and therefore closer towards the α ligand. This implies that a stronger bond is formed between the Co and α ligand (shown as a decrease in bond length), when compared to the upper axial ligand, and is therefore a stable complex. After homolysis of the upper axial bond, a contraction of the lower axial $\text{Co(II)}\text{-B}_\alpha$ bond occurs. The greater this contraction, the lower the associated $\text{Co(III)}\text{-C}_\beta$ BDE. The implication is that a more stable Co(II) complex is formed. The stability of both the Co(III) and Co(II) complexes confirm why enzymes makes use of B_{12} coenzymes as radical catalysts.

Finally, although the generated partial charges were provided, as shown in **Tables 6.3A** and **B**, unfortunately they were found to be unreliable, as no trends were observed between the Co metal centre, axial ligands and N_{eq} donors.

6.5 CONCLUSION

As it was noted in the introduction to this chapter, in some cobalamin enzymes histidine or the imidazole ring from the histidine residue replaces the DMB group posing as the α ligand.⁴⁸ Why these two particular ligands serve as a replacement for

the DMB is of considerable interest, and this chapter investigated models of amino acids and actual amino acids as α ligands to investigate possible reasons explanations.

The α ligands were of a large variety with S-, O- and N-donor atoms. The ligands used in this study were categorized into three classes: soft (S donor atom), intermediate (N donor atom) and hard ligands (O donor atoms). The results showed that it is actually the character of the α ligand that controls the Co(III)–C $_{\beta}$ BDE and not the variation in the Co(III)–C $_{\beta}$ bond length itself. This was evidenced by the *trans* influence of the weakly bound (unstable) soft ligands on the Co(III)–C $_{\beta}$ bond which resulted in the homolytic breaking of the Co(III)–C $_{\beta}$ bond at low BDEs. The hard ligands were strongly bound (very stable) and these complexes produced high BDEs that were synonymous with short Co(III)–C $_{\beta}$ bond lengths. Finally, the intermediate ligands (with *p*-aminopyridine and histidine, softer than glycine and imidazole) proved to be the most stable as α ligands for the cobalamin model with the Co(III)–C $_{\beta}$ BDEs appearing in the 31.55–32.45 kcal mol⁻¹ range. The cobalamin models with the N-donor ligands show good catalytic character, in other words, stable in the pre- and post homolysis reactions, which suggests a reason why these aromatic side chains with an N-donor ligand of intermediate character as a good substitute for the DMB ligand.

To a very small extent, proton affinity values of the α ligand may be used to predict the BDE for the homolysis of the Co(III)–C $_{\beta}$ bond, however, only if the α ligands fall into the same area of classification. There is also a trend for the change of the Co–B $_{\alpha}$ bond length (Δ Co–B $_{\alpha(5c-6c)}$) with the Co(III)–C $_{\beta}$ BDE, however, this too is dependent on the character of the α ligand.

CHAPTER 7

CIS INFLUENCE: THE EFFECT OF THE EQUATORIAL MACROCYCLE

7.1 INTRODUCTION

While Chapters 1 and 3 have reflected on the importance of vitamin B₁₂ studies, it also becomes obvious through a literature review that the focus of historical research mainly covered the *trans* effects and influence of both the α and β axial ligands.

This Chapter focuses and reports on the *cis* effects of various equatorial ligands. Essentially this *cis* effect relates directly to the nature of each equatorial ligand and the influence it may have on the properties of Co, both the α and β axial ligand bond lengths to the metal centre and the N_{eq} bond length to the Co. As a consequence, the contribution to the thermodynamic properties of the homolytic reaction, namely ΔG and BDE for the homolysis of the Co(III)–C $_{\beta}$ bond, are also calculated. All calculations were carried out in the gas phase, or in a range of solvents using an implicit solvent model and are discussed accordingly. The BP86, M06L, B3LYP and PBE1PBE functionals were used, with all of the calculations performed at the 6-31+G(d,p) level of theory.

Since its discovery,²⁶⁸ vitamin B₁₂ has attracted considerable interest which has resulted in the synthesis of many analogous complexes.²⁶⁹⁻²⁷² An early failure to prepare Co(III)–alkyl complexes containing saturated equatorial ligands resulted in the belief that a stable Co(III)–alkyl complex would only form if it contained unsaturated equatorial ligands.²⁷³

Later on, Roche *et al.*²⁷³ successfully prepared and characterized the Co(III)–alkyl complex, [14-ane]N₄ (1,4,8,11-tetraazacyclotetradecane with H₂O and CH₃ as the α and β ligands, respectively), one of the first alkylcobalt(III) compounds containing only saturated ligands as its equatorial ligand.^{274,275} Since then a number of related compounds with a range of α and β ligands containing saturated macrocyclic equatorial ligands, such as [15-ane]N₄(1,5,9,12-tetraazacyclotetraundecane²¹² and [16-ane]N₄(1,5,9,13-tetraazacyclotetradodecane,²¹² have been synthesised.^{212,276-278} These compounds were relatively stable although a few were light sensitive (such as alkylcobalamins); nevertheless, this emphasises the fact that unsaturated ligands are not vital for a stable alkylcobalt(III) compound.²⁷⁹

Much later [NH₃–(Co(III)(NH₃)₄)–CH₃]²⁺ (methylcobalt(III)pentaamine)²⁷⁹ was successfully synthesized and was regarded as the archetype of model compounds for vitamin B₁₂ as it is the simplest alkyl Co(III) compound. As mentioned above, this chapter focuses on assessing the *cis* influence of the equatorial ligand; therefore Co(III)–alkyl, Co(III)–aromatic and the Co(III)–cobaloxime system(s) were selected for this study. These models represent a range of equatorial ligands (see **Figure 7.1**) and their effect on the Co(III)–C β ΔG and BDE was investigated.

The methylcobalt(III) pentaamine is largely different from the other models as it is the only acyclic model with a structure not as constrained as others of a cyclic nature. Because of this, the methylcobalt(III) pentaamine is also expected to be more flexible. On the other hand, the models of the cyclic hydrocarbons ([14-ane]N₄; [15-ane]N₄ and [16-ane]N₄) are fully saturated and differ from each other by the size of their macrocyclic cavity, which is a result of the increasing number of carbons to the macrocyclic ring. All of these models carry a formal charge of +3 at their metal centre.

Although cobaloxime is classed as a dianionic ligand,¹⁸⁰ the negative charges on both the oxygen atoms are far removed from the Co metal centre and therefore not

considered to interfere with the formal charge of Co. As a result, the net charge at the inner coordination sphere of the metal centre is also formally +3. It is not macrocyclic and because of this is expected to be very flexible when compared to the corrole, corrin and porphyrin models that contain larger macrocyclic rings. In addition, porphyrin has a larger macrocyclic cavity than the corrole and corrin models because it contains an extra methine group. These three models contain an extensive delocalised π electron system and they carry different charges at the metal centre; corrole has a net charge of 0, corrin +2 and porphyrin +1. Indeed, these defining characteristics are also expected to play a role when assessing the *cis* effects of these equatorial ligands.

7.2 MODEL STRUCTURES AND METHOD

Figure 7.1 shows the model structures used in this study starting from a saturated acyclic (model A) to saturated cyclic hydrocarbons (models B–D). These cyclic structures progressively increase by one carbon atom to the cyclic chain that forms part of the equatorial ligand. Model E has bis(dimethylglyoxime) as its equatorial ligand while F and H have fully conjugated macrocyclic ligand complexes, being corrole and porphyrin, respectively. Model G is also conjugated (with corrin as its equatorial ligand) up until the pentacyclic ring on the left hand side of the macrocycle where two sp^3 carbons, C-1 and C-19, are found, causing the upward tilting on that side of the corrin because of the tetrahedral geometry of these two carbons. The positions of both the α and β -ligands are kept constant, which are occupied by an ammonia molecule and methyl group, respectively.

All structures were geometry optimized using the 6-31+G(d,p) basis set, in all relevant spin states ($S = 0$ and 2 for Co(III) and $S = 1/2$ and $3/2$ for the Co(II) complex), followed by a frequency calculation to ensure that the structures used were completely minimized to a stable ground state. The calculations were performed with each of four functionals: BP86, M06L, B3LYP and PBE1PBE. All recorded values

for the Co(III)–C_β ΔG and BDEs included the zero-point energies and thermal corrections.

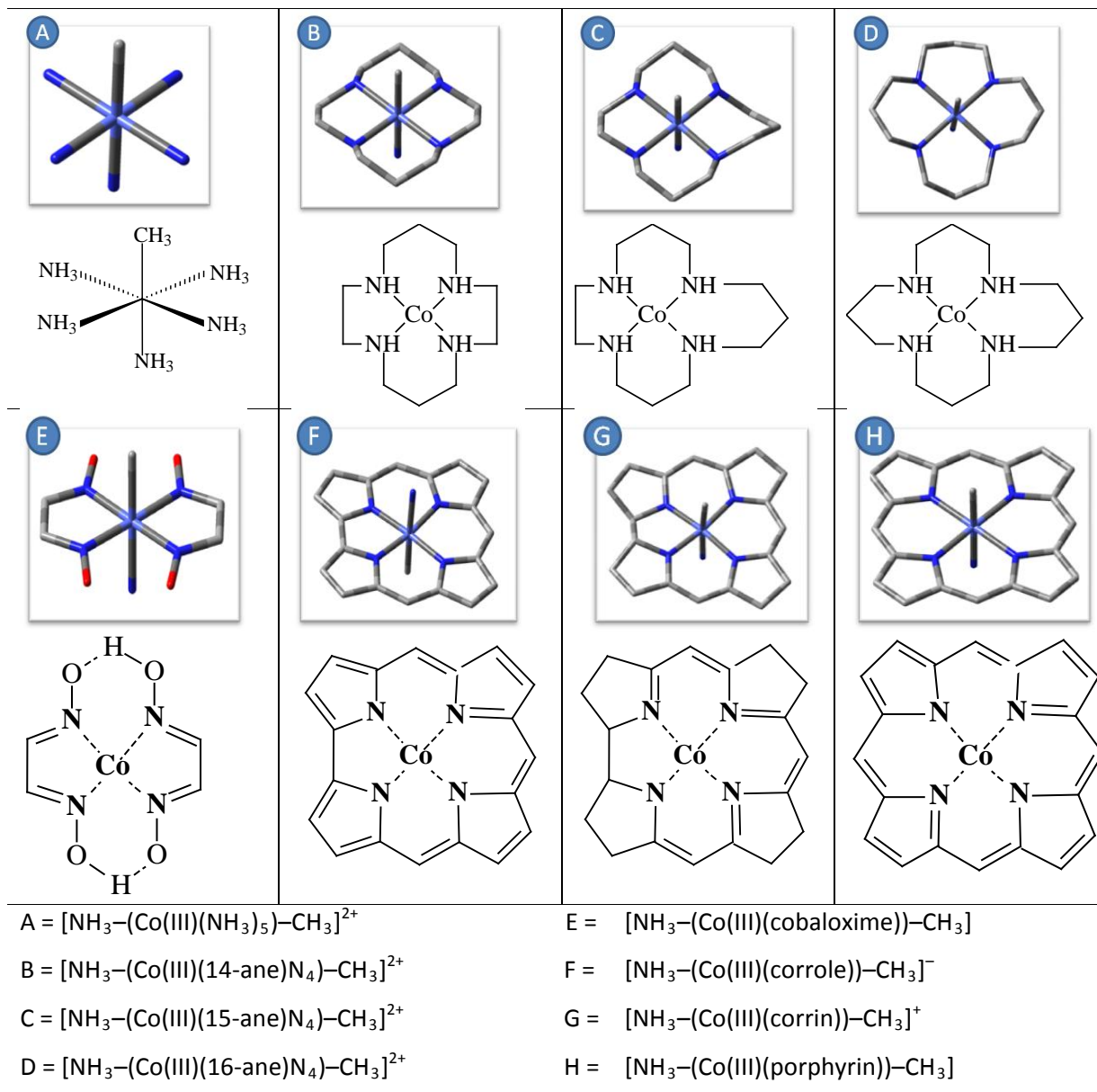


Figure 7.1: Model complexes A–H where the α and β axial ligands remain constant while the equatorial ligands are varied.

7.3 GAS PHASE: RESULTS AND DISCUSSION

(a) Bond lengths and energies for models A–H

Tables 7.1A and **B** provide a summary of the energies and geometric parameters obtained for the model systems explored. It is evident from these results that the BP86 and M06L functionals give similar values while the hybrid functionals differ quite significantly. Numerically there is a large difference for both the BP86 and M06L functionals from the hybrid functionals. For example, the Co(III)–C_β BDE for model A is 37.57 kcal mol⁻¹ and 33.48 kcal mol⁻¹ for BP86 and M06L, respectively, while B3LYP gives 18.22 kcal mol⁻¹ and PBE1PBE 16.32 kcal mol⁻¹. In addition, the Co(III) and Co(II) complexes were found to be the most stable in the low spin state for BP86 and M06L; however, this was not the same for the hybrid functionals. In light of this, a breakdown of the thermochemical data for each spin state is provided in Appendix 4: A4.1–4.4 for all of the functionals.

In **Table 7.1A**, the BP86 and M06L results obtained for the Co(III)–C_β and Co(III)–N_α bond lengths together with the Co(III)–C_β BDE compare favourably to recorded experimental data (see in **Tables 7.1A** and **B** for values).¹⁴⁹⁻¹⁵² On the other hand, results from the M06L calculations for the Co(III)–C_β bond lengths are underestimated (compared with the given experimental data) by ~ 0.04 – 0.01 Å. For the hybrid functionals (see **Table 7.1B**), B3LYP performed better than PBE1PBE in describing the Co(III)–C_β bond lengths. The PBE1PBE functional considerably underestimated the Co(III)–C_β bond lengths but was able to depict the Co(III)–N_α bond lengths within the range of the recorded experimental data. Even though these hybrid functionals successfully calculated the Co(III)–C_β BDEs within the experimental range, the values were always in the lower range and thus possibly underestimated the Co(III)–C_β BDEs when compared with experimental data.

A literature review¹⁸⁰ (Chapter 3) indicated this to be a downfall of B3LYP and discussed the 20% HF exchange component²⁸⁰ of this functional's composition as the

main source of error. In addition, the PBE1PBE^{102,103,192} functional, which has a slightly larger exchange contribution from HF (only 25%) has also provided low BDEs, sometimes even lower than B3LYP, for the Co(III)–C_β bond.

Table 7.1A: BP86 and M06L:-Energies (kcal mol⁻¹) and geometric parameters for models A–H

	Models	Bond Lengths /Å				Shift of Co from the mean plane /Å		^d ρ(bcp) /au		Bond Angle /°	Energies kcal mol ⁻¹	
		Co(III)–C _β	^a Co(III)–N _α	^b Co(II)–N _α	^c Δ _(5c-6c)	Co(III)	Co(II)	Co(III)–C _β	Co(III)–N _α	N _α –Co(III)–C _β	ΔG	BDE
BP86	A	1.985	2.181	2.212	0.031	0.042	0.197	0.1167	0.0578	177.49	24.52	37.57
	B	1.977	2.192	2.255	0.063	0.013	0.166	0.1175	0.0550	178.63	23.49	36.51
	C	1.973	2.180	2.245	0.065	0.012	0.172	0.1183	0.0566	177.29	22.84	35.32
	D	1.950	2.262	2.229	-0.033	*0.094	0.122	0.1232	0.0473	178.89	15.61	27.59
	E	2.001	2.076	2.091	0.015	0.023	0.159	0.1099	0.0731	179.28	28.92	41.06
	F	1.970	2.197	2.192	-0.005	0.037	0.112	0.1178	0.0544	178.41	23.55	35.24
	G	1.982	2.220	2.196	-0.024	0.007	0.135	0.1162	0.0534	176.24	20.63	32.85
	H	1.973	2.167	2.173	0.006	0.025	0.101	0.1181	0.0592	178.97	22.75	33.28
M06L	A	1.966	2.192	2.244	0.007	0.034	0.178	0.1211	0.0537	177.29	23.34	33.48
	B	1.963	2.207	2.298	-0.091	0.003	0.141	0.1206	0.0506	178.41	26.33	39.49
	C	1.960	2.197	2.288	-0.091	0.003	0.148	0.1214	0.0519	176.74	24.61	37.96
	D	1.935	2.278	2.268	0.001	*0.100	0.222	0.1272	0.0434	178.89	18.64	31.23
	E	1.980	2.099	2.141	-0.042	0.012	0.136	0.1146	0.0657	179.61	27.68	40.03
	F	1.957	2.225	2.284	-0.059	*0.056	0.081	0.1205	0.0479	177.90	23.62	35.48
	G	1.964	2.233	2.264	-0.031	*0.015	0.112	0.1205	0.0488	176.85	21.24	33.18
	H	1.956	2.187	2.233	-0.046	*0.038	0.084	0.1223	0.0535	178.97	21.69	32.85

Experimental data: MeCbl Co(III)–C_β = 1.98 – 1.99 Å (X-ray); 2.00 ± 0.03 Å (EXAFS); Co(III)–N_α = 2.16 – 2.19 Å (X-ray); 2.20 ± 0.03 Å (EXAFS) and BDE = 17 – 34 kcal mol⁻¹ (model systems); 26 – 37 kcal mol⁻¹ (actual compounds).^{149-152,223}

^aThe axial bond length between Co(III) and N_α ligand in the 6 coordinate complex. ^bThe axial bond length between Co(II) and N_α ligand in the 5 coordinate complex. ^cThe difference in Co–N_α bond length between the 5- and 6-coordinate complex. ^dThe ρ at the bcp of both the Co(III)–C_β and Co(III)–N_α bond lengths. *The Co metal centre was found above the mean plane towards the β ligand.

Table 7.1B: B3LYP and PBE1PBE:-Energies (kcal mol⁻¹) and geometric parameters for models A–H

	Models	Bond Lengths /Å				Bond Angle /°	Energies /kcal mol ⁻¹	
		Co(III)–C _β	Co(III)–N _α ^a	Co(II)–N _α ^b	Δ(5c-6c) ^c		N _α –Co(III)–C _β	ΔG
B3LYP	A	1.976	2.207	2.132	-0.075	177.23	4.37	18.22
	B	1.973	2.240	2.332	0.092	178.72	8.26	20.12
	C	1.970	2.222	2.191	-0.031	176.91	5.60	18.36
	D	1.944	2.349	2.178	-0.171	178.75	-1.44	10.78
	E	1.990	2.097	2.176	0.079	179.45	15.66	27.22
	F	1.963	2.240	2.312	0.072	178.86	10.25	21.43
	G	1.968	2.250	2.284	0.034	176.72	7.33	18.58
	H	1.960	2.194	2.255	0.061	178.97	8.86	18.79
PBE1PBE	A	1.953	2.151	2.116	-0.035	177.12	3.38	16.32
	B	1.951	2.166	2.275	0.109	178.53	10.99	23.12
	C	1.948	2.158	2.165	0.007	176.63	4.02	17.19
	D	1.923	2.245	2.154	-0.091	178.75	-4.69	7.57
	E	1.966	2.053	2.140	0.087	179.44	19.11	30.58
	F	1.940	2.161	2.249	0.088	178.88	12.97	23.68
	G	1.944	2.175	2.233	0.058	176.63	9.64	20.97
	H	1.936	2.136	2.206	0.007	178.79	9.83	20.37

Experimental data: MeCbl Co(III)–C_β = 1.98 – 1.99 Å (X-ray); 2.00 ± 0.03 Å (EXAFS); Co(III)–N_α = 2.16 – 2.19 Å (X-ray); 2.20 ± 0.03 Å (EXAFS) and BDE = 17 – 34 kcal mol⁻¹ (model systems); 26 – 37 kcal mol⁻¹ (actual compounds).^{149-152,223}

^aThe axial bond length between Co(III) and N_α ligand in the 6 coordinate complex. ^bThe axial bond length between Co(II) and N_α ligand in the 5 coordinate complex. ^cThe difference in Co–N_α bond length between the 5- and 6- coordinate complex.

Because of the poor performance by the hybrid functionals only the calculations conducted with BP86 and M06L are discussed from this point. **Figure 7.2** shows the Co(III)–C_β BDE to parallel the Co(III)–C_β ΔG trend for models A–H. The graphs indicate that a better linear regression ($r^2 = 0.96$) was obtained for the pure GGA functional, BP86, while M06L produces a slightly greater scatter of the results ($r^2 = 0.91$).

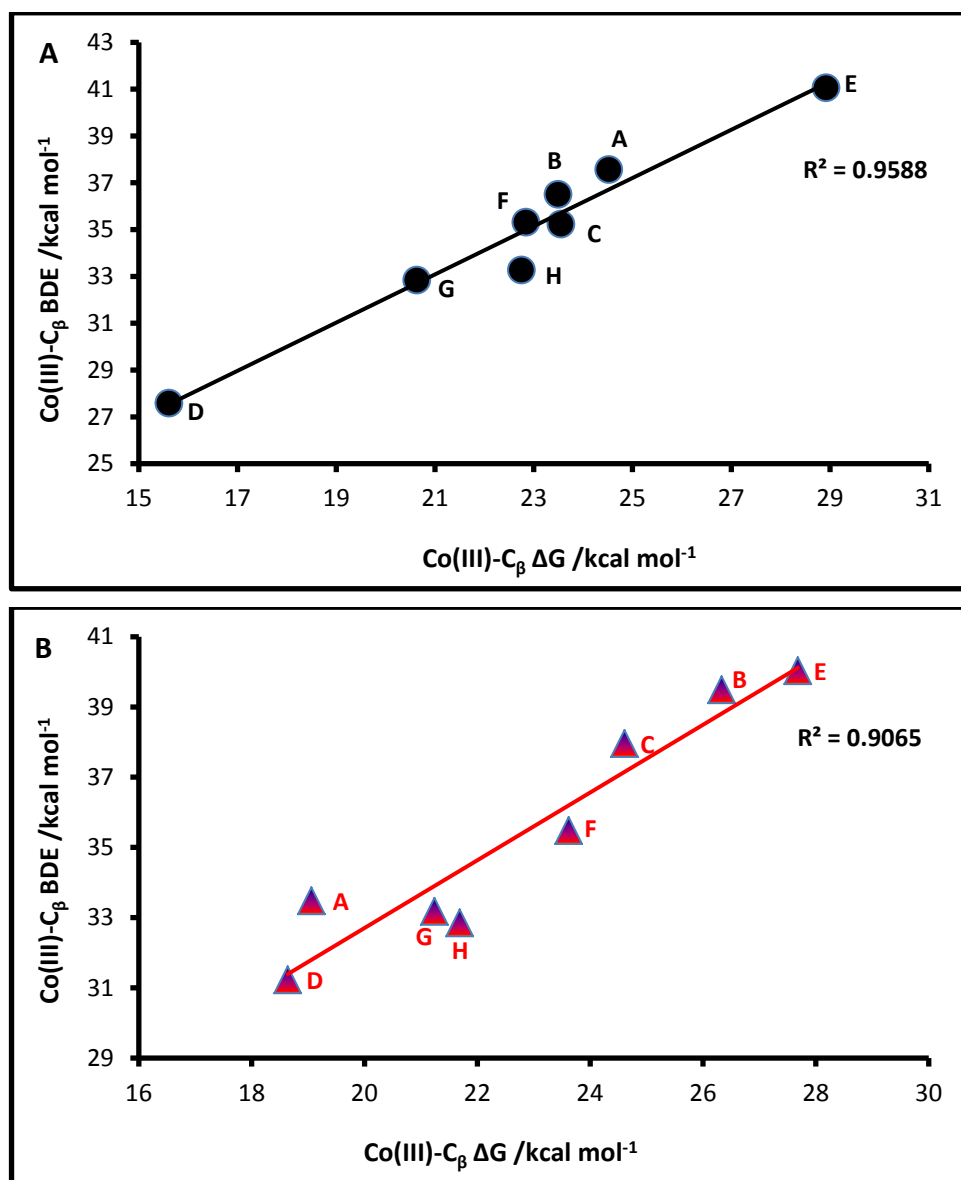


Figure 7.2: A) BP86 (●) and B) M06L (▲): ΔG and BDE (kcal mol⁻¹) trends for the Co(III)–C_β bond in models A–H.

For all these complexes, a normal *trans* influence between the axial ligands is shown in **Figure 7.3**, in other words, as the Co(III)–C $_{\beta}$ bond elongates the Co(III)–N $_{\alpha}$ bond shortens. While a straight line is obtained in **Figures 7.3A** and **B** because of the two extreme points (D and E), the results for the other models are concentrated in a cluster in the Co(III)–C $_{\beta}$ and Co(III)–N $_{\alpha}$ bond length regions of 1.97–1.99 Å and 2.15–2.25 Å, respectively.

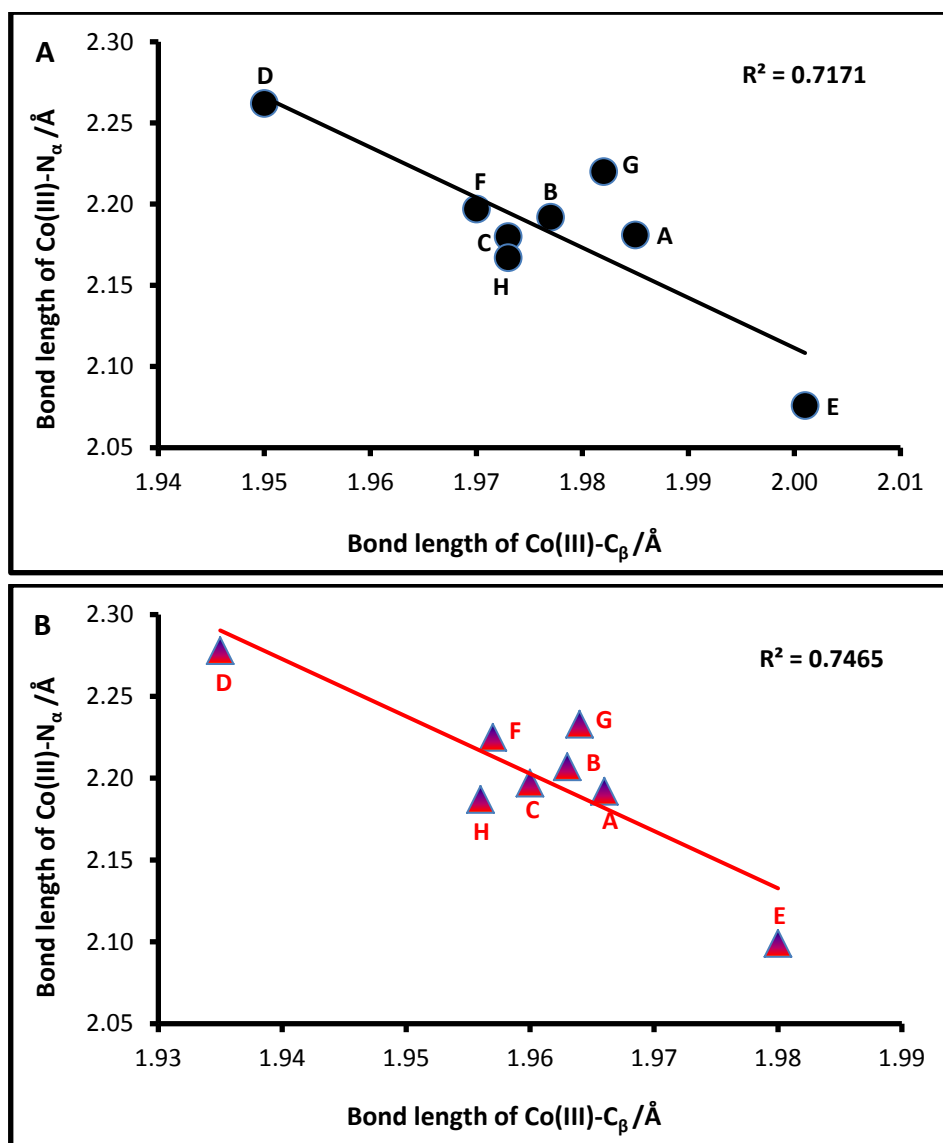


Figure 7.3: A) BP86 (●) and B) M06L (▲): Bond lengths (Å) for Co(III)–C $_{\beta}$ is plotted against Co(III)–N $_{\alpha}$ for models A–H.

For the different complexes A–H, the Co(III)–C $_{\beta}$ BDE (see **Figure 7.4**) was found to increase with an increase of the Co(III)–C $_{\beta}$ bond length; a similar trend is noticed for the M06L calculations. This counter-intuitive trend was discussed in both Chapters 5 and 6, and was explained by the fact that although bond lengthening is synonymous with bond weakening (assessed by the ρ -values at the bcp), the BDE for the homolysis of the Co(III)–C $_{\beta}$ bond is independent of this change, which is a direct correlation with the results presented in **Figure 7.4**. Another key factor such as the shift of the Co(III) metal centre in proximity to the β ligand was also observed to play a significant role towards the homolysis of the Co(III)–C $_{\beta}$ bond. This observation will be discussed later in the chapter.

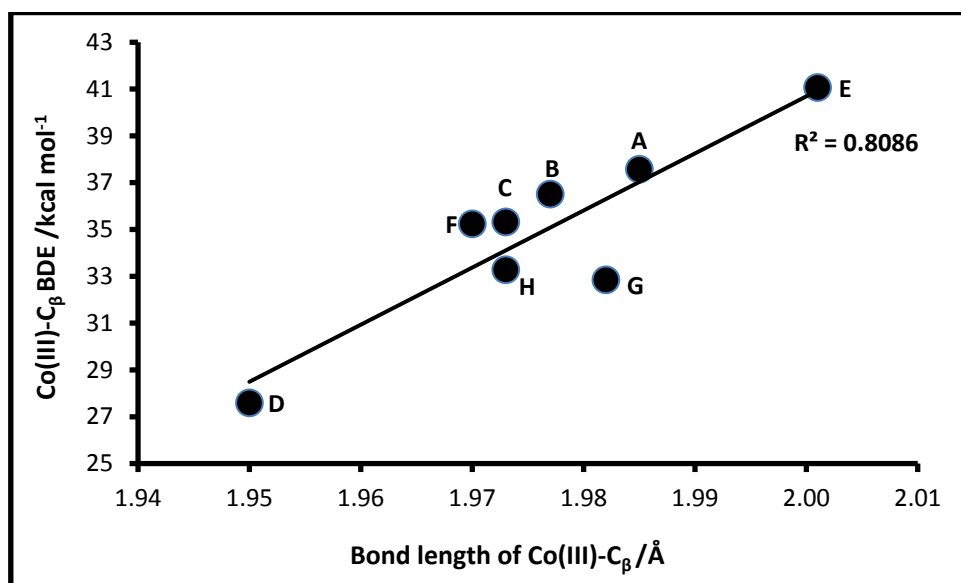


Figure 7.4: BP86: Co(III)–C $_{\beta}$ bond length (Å) is plotted against the Co(III)–C $_{\beta}$ BDE (kcal mol $^{-1}$) for models A–H.

After homolysis of the Co(III) complex to the Co(II) complex, the Co(II)–N $_{\alpha}$ bonds in some of the model compounds are observed to increase in length while others decrease, shown in **Table 7.1A**. A graphical plot, **Figure 7.5**, of the difference in the Co–N $_{\alpha}$ bond length from the 5-coordinate (Co(II)) to the 6-coordinate (Co(III)) complex indicates a weak correlation with the Co(III)–C $_{\beta}$ BDE. This drive to

increase the extent of bonding between the α ligand and Co promotes the thermodynamic drive for homolysis of the Co(III)–C $_{\beta}$ bond, an observation that was more pronounced in the studies reported in Chapters 5 and 6, and which is also observed later on in work reported in Chapter 8. The current results are fairly scattered and a poor correlation ($r^2 = 0.33$) is obtained for the independent variable, $\Delta\text{Co–N}_{\alpha(5c-6c)}$, against the BDE of the upper axial bond.

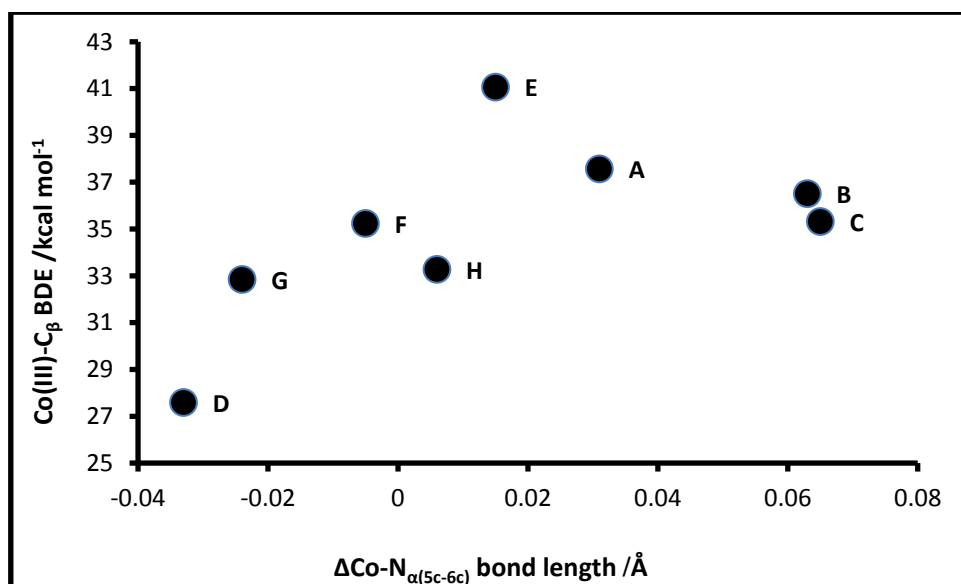


Figure 7.5: BP86: The change in the lower axial bond length, $\Delta\text{Co–N}_{\alpha(5c-6c)}$, (Å) is plotted against the Co(III)–C $_{\beta}$ BDE (kcal mol $^{-1}$) for models A–H.

As a result, a multiple linear regression was performed for the dependence of the Co(III)–C $_{\beta}$ BDE on two independent variables, Co(III)–C $_{\beta}$ and $\Delta\text{Co–N}_{\alpha(5c-6c)}$ bond lengths. A correlation of $r^2 = 0.84$ ($n = 8$) was obtained, of the form $\text{BDE} = (-4.41 \pm 1.0) \times 10^2 + ((2.4 \pm 0.5) \times 10^2 \text{ \AA} \text{ Co(III)–C}_{\beta}) + ((0.3 \pm 0.3) \times 10^2 \text{ \AA} \Delta\text{Co–N}_{\alpha(5c-6c)})$. Further analysis does show that the BDE can be predicted from a linear combination of the two independent variables; however, the p -values (probability that the correlation is fortuitous) is higher for $\Delta\text{Co–N}_{\alpha(5c-6c)}$ ($p = 36\%$) than Co(III)–C $_{\beta}$ ($p = 0.4\%$) bond. Therefore, these results suggest that not all the independent variables are necessary and that the Co(III)–C $_{\beta}$ BDE is mainly dependent on the

change in the Co(III)–C $_{\beta}$ bond length. Evidently, the multiple linear regression analysis does not provide much insight into the effect of the independent variables on the labilisation of the Co(III)–C $_{\beta}$ BDE and it is suggested that the diversity of the model systems studied (saturated alkylmacrocycles, bis(dimethylglyoxime and π electron rich macrocycles) may be held responsible.

An analysis of the topological properties of the electron density was conducted using Bader's AIM approach²¹⁸ and the data obtained are presented in **Table 7.1A**. The value of ρ at a bcp is related to the strength of the chemical bond, in other words, as the ρ -value at the bcp increases, so bond strength increases.²⁸¹⁻²⁸⁴ In **Table 7.1A** the ρ at the bcp of the Co(III)–C $_{\beta}$ bond shows a steady increase in value from models A to D, (see **Figure 7.6(A)**), complemented by a decrease in Co(III)–C $_{\beta}$ bond length. On the other hand, the Co(III)–N $_{\alpha}$ bond, which is considerably weaker than the Co(III)–C $_{\beta}$ bond (**Figure 7.6(B)**), (as evaluated by the ρ at the bcp), confirms the normal *trans* influence between the axial bond lengths. The same trends are observed for M06L (see **Table 7.1A**).

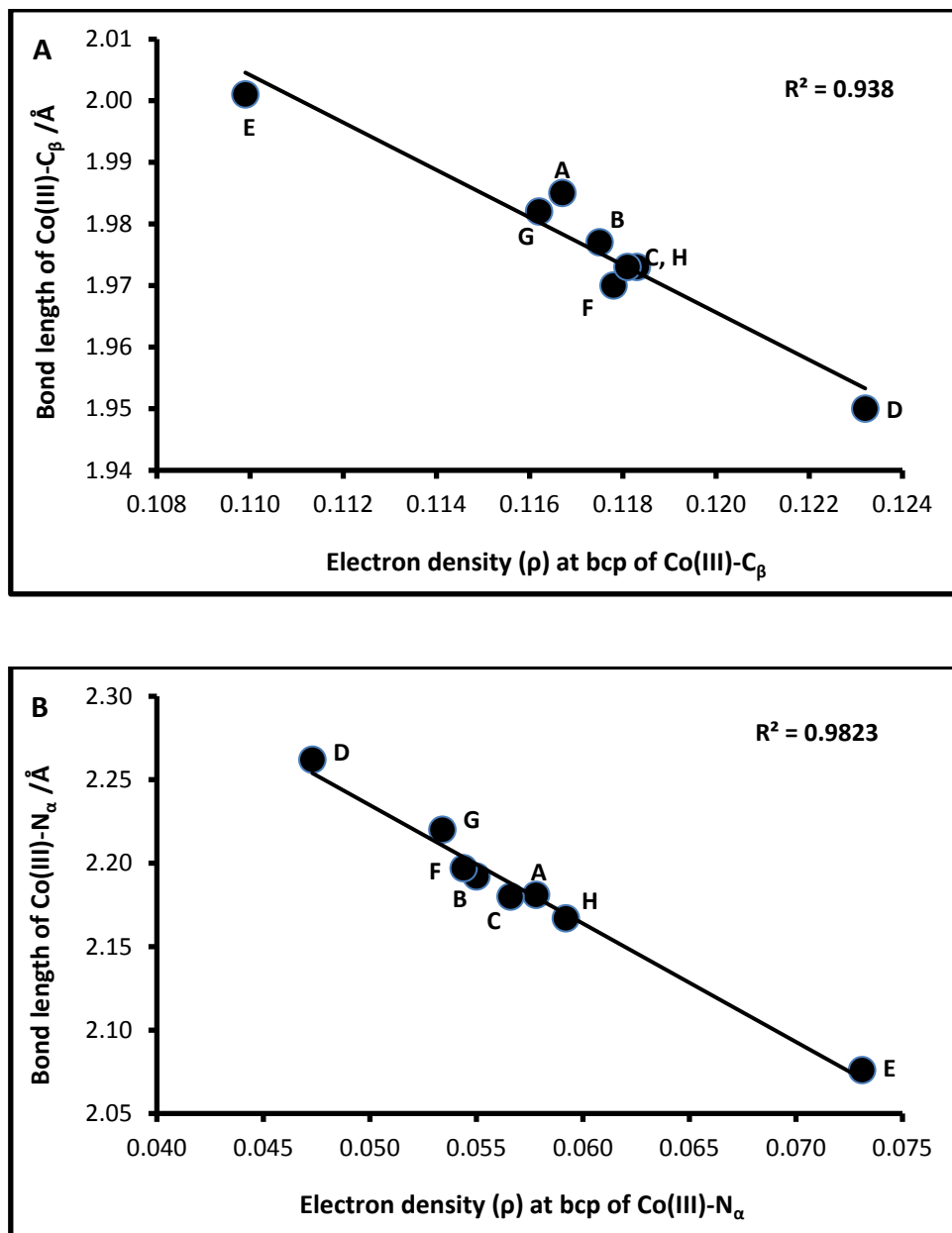


Figure 7.6: BP86: Electron density (au) at bcp of A) Co(III)-C_β and B) Co(III)-N_α bond lengths (Å) for models A-H.

Further data obtained from the topological analysis of the electron density for models A–H are collated and presented in **Tables 7.2A** and **B** for the BP86 and M06L functionals respectively. For these model systems the strength and weakness of the axial bonds are explained by the ratio of the $|V(r)|/G(r)$ values obtained for both the Co(III)–C $_{\beta}$ and Co(III)–N $_{\alpha}$ bonds. The $|V(r)|/G(r)$ value is used to characterise a bond; when $|V(r)|/G(r) > 2$, the bond is covalent, $|V(r)|/G(r) < 1$ implies an ionic bond, while $1 < |V(r)|/G(r) < 2$ indicates that the bond falls into the intermediate category. For both functionals, the $|V(r)|/G(r)$ value for the Co(III)–C $_{\beta}$ bond ranges from 1.7–1.8, which is close to 2, while the $|V(r)|/G(r)$ value for the Co(III)–N $_{\alpha}$ bond is ~1.1 and is close to 1. These values show that the Co(III)–C $_{\beta}$ bond has a significant covalent character while the Co(III)–N $_{\alpha}$ bond has a much more ionic nature.

Table 7.2A: BP86:- Topological properties of the electron density at the bcp of Co(III)–CH $_3$ and Co(III)–NH $_3$ for model complexes A–H

Co(III)–CH $_3$						
Models	ρ	$\nabla^2\rho$	V(r)	G(r)	H(r)	$ V(r) /G(r)$
A	0.1167	0.0704	-0.1329	0.0752	-0.0576	1.7660
B	0.1175	0.1059	-0.1372	0.0818	-0.0554	1.6764
C	0.1183	0.1051	-0.1382	0.0822	-0.0560	1.6806
D	0.1232	0.0875	-0.1432	0.0825	-0.0607	1.7350
E	0.1099	0.0695	-0.1236	0.0705	-0.0531	1.7534
F	0.1178	0.0831	-0.1352	0.0780	-0.0572	1.7335
G	0.1162	0.0483	-0.1296	0.0708	-0.0588	1.8295
H	0.1181	0.0586	-0.1331	0.0739	-0.0592	1.8016
Co(III)–NH $_3$						
A	0.0578	0.2390	-0.0819	0.0708	-0.0111	1.1565
B	0.0550	0.2410	-0.0798	0.0700	-0.0098	1.1394
C	0.0566	0.2474	-0.0821	0.0720	-0.0101	1.1404
D	0.0473	0.1924	-0.0664	0.0572	-0.0092	1.1599
E	0.0731	0.3242	-0.1084	0.0947	-0.0137	1.1442
F	0.0544	0.2227	-0.0761	0.0659	-0.0102	1.1552
G	0.0534	0.1980	-0.0716	0.0606	-0.0111	1.1827
H	0.0592	0.2396	-0.0830	0.0714	-0.0115	1.1614

Table 7.2B: M06L: Topological properties of the electron density at the bcp of Co(III)–CH₃ and Co(III)–NH₃ for model complexes A–H

Co(III)–CH ₃						
Models	ρ	$\nabla^2\rho$	V(r)	G(r)	H(r)	V(r) /G(r)
A	0.1211	0.0987	-0.1415	0.0831	-0.0584	1.7029
B	0.1206	0.1399	-0.1445	0.0898	-0.0548	1.6102
C	0.1214	0.1366	-0.1453	0.0897	-0.0556	1.6193
D	0.1272	0.1175	-0.1516	0.0905	-0.0611	1.6754
E	0.1146	0.1139	-0.1341	0.0813	-0.0528	1.6498
F	0.1205	0.1281	-0.1428	0.0874	-0.0554	1.6336
G	0.1205	0.0906	-0.1392	0.0809	-0.0583	1.7201
H	0.1223	0.0996	-0.1425	0.0837	-0.0588	1.7026
Co(III)–NH ₃						
A	0.0537	0.2470	-0.0789	0.0703	-0.0086	1.1218
B	0.0506	0.2472	-0.0762	0.0690	-0.0072	1.1046
C	0.0519	0.2500	-0.0778	0.0702	-0.0077	1.1091
D	0.0434	0.1945	-0.0633	0.0560	-0.0073	1.1307
E	0.0657	0.3328	-0.1013	0.0922	-0.0090	1.0979
F	0.0479	0.2227	-0.0700	0.0628	-0.0071	1.1138
G	0.0488	0.2098	-0.0691	0.0608	-0.0083	1.1371
H	0.0535	0.2469	-0.0783	0.0700	-0.0083	1.1182

In **Table 7.2C** below, a brief summary of the |V(r)|/G(r) value, BDE, ρ -value at the bcp and bond length for the Co(III)–C _{β} bond are provided.

Table 7.2C: Summary of factors that may influence the Co(III)–C _{β} BDEs

	A	B	C	D
V(r) /G(r)	1.7660	1.6764	1.6806	1.7350
ρ	0.1167	0.1175	0.1183	0.1232
Bond length (Å)	1.9850	1.9770	1.9730	1.9500
BDE (kcal mol ⁻¹)	37.57	36.51	35.32	27.59
	E	F	G	H
V(r) /G(r)	1.7534	1.7335	1.8295	1.8016
ρ	0.1099	0.1178	0.1162	0.1181
Bond length (Å)	2.0010	1.9700	1.9820	1.9730
BDE (kcal mol ⁻¹)	41.06	35.24	32.85	33.28

An assessment of these values indicates a good correlation between the covalency of the Co(III)–C $_{\beta}$ bond and the associated BDE and a weaker correlation with the bond length (shown in **Figure 7.7**), provided that the values for models A and E are omitted. It seems that the more covalent the Co(III)–C $_{\beta}$ bond (corrin-model G) the lower the associated BDE.

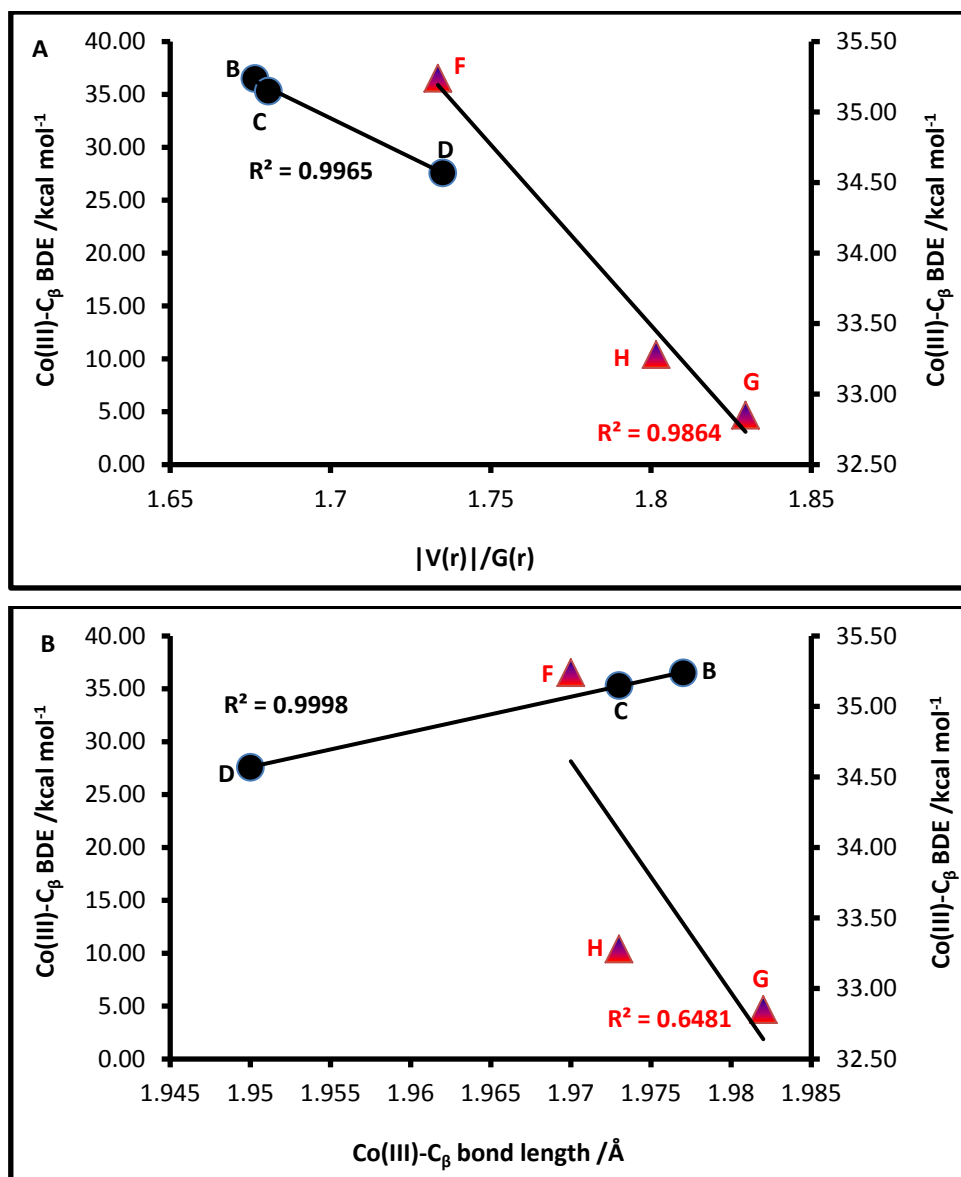


Figure 7.7: Correlation of the Co(III)–C $_{\beta}$ BDE (kcal mol $^{-1}$) with its associated bond length (Å) and $|V(r)|/G(r)$ value.

Once again the results shown in **Figure 7.7B** confirm that bond lengthening (weakening) of the Co(III)–C_β bond is not synonymous with obtaining a lower BDE for the bond of interest.

(b) Partial charges

In addition to the topological properties of the electron density, the partial charges were also calculated for these model systems. The data obtained using the APT, NBO and Bader methods for the generation of the partial charges are recorded in **Table 7.3**.

Table 7.3: APT, NBO and Bader partial charges for models A–H for BP86 and M06L

	Models	APT				NBO				BADER			
		Co(III)	C _β	N _α	N _{eq}	Co(III)	C _β	N _α	N _{eq}	Co(III)	C _β	N _α	N _{eq}
BP86	A	0.526	0.179	-0.328	-0.199	0.234	-0.773	-1.072	-0.983	1.002	-0.196	-1.079	-1.050
	B	0.417	0.125	-0.299	-0.230	0.354	-0.832	-1.091	-0.583	0.961	-0.198	-1.071	-0.940
	C	0.490	0.125	-0.296	-0.242	0.389	-0.834	-1.095	-0.585	0.950	-0.195	-1.072	-0.939
	D	0.588	0.142	-0.316	-0.237	0.427	-0.779	-1.118	-0.585	0.928	-0.163	-1.075	-0.924
	E	-0.085	0.215	-0.202	0.474	0.032	0.744	-1.010	0.012	1.046	-0.160	-1.051	-0.541
	F	0.301	0.139	-0.293	-0.282	0.189	-0.730	-1.039	-0.385	1.099	-0.140	-1.050	-1.084
	G	0.218	0.176	-0.288	-0.380	0.189	-0.711	-1.048	-0.357	1.079	-0.140	-1.052	-1.096
	H	0.362	0.152	-0.285	-0.248	0.263	-0.727	-1.048	-0.384	1.071	-0.142	-1.056	-1.056
M06L	A	0.799	0.130	-0.409	-0.287	0.277	1.040	0.669	0.756	1.170	-0.140	-1.111	-1.087
	B	0.665	0.073	-0.361	-0.316	0.528	-0.852	-1.109	-0.618	1.123	-0.143	-1.105	-1.025
	C	0.736	0.075	-0.363	-0.326	0.567	-0.854	-1.113	-0.622	1.116	-0.138	-1.103	-1.023
	D	0.813	0.094	-0.381	-0.320	0.610	-0.805	-1.130	-0.621	1.096	-0.110	-1.107	-1.006
	E	0.193	0.155	-0.284	0.447	0.218	-0.776	-1.037	-0.007	1.174	-0.109	-1.081	-0.580
	F	0.423	0.092	-0.333	-0.333	0.374	-0.752	-1.052	-0.441	1.249	-0.080	-1.070	-1.259
	G	0.399	0.136	-0.333	-0.493	0.321	-0.730	-1.058	-0.410	1.224	-0.085	-1.078	-1.246
	H	0.489	0.108	-0.334	-0.298	0.450	-0.753	-1.062	-0.443	1.219	-0.085	-1.075	-1.233

Unfortunately the three approaches are not comparable, as there is quite a large difference in their values as well as a change in sign for the partial charges of C_β generated by the APT method. The APT charges for the BP86 functional show good correlation between the partial charge on the Co atom and N_α ligand. As the positive atomic charge on Co increases, an increase in negative charge on the N_α ligand is observed, (see **Figure 7.8**). This correlation parallels the observation from the topological properties of the electron density that the Co(III)– N_α predominantly has an ionic character.

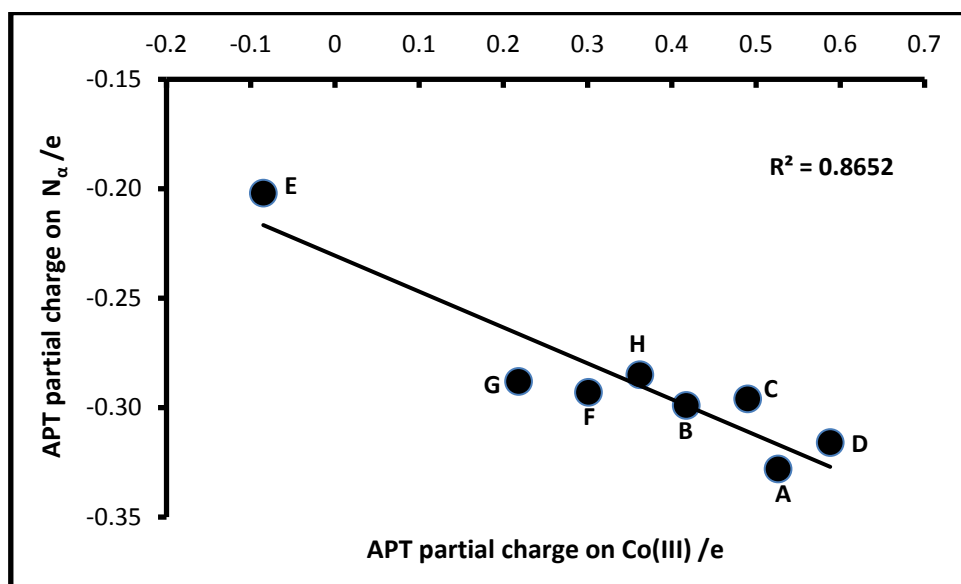


Figure 7.8: BP86: Correlation of the APT partial charges on Co(III) and N_α for models A–H.

On the other hand, results for the NBO charges for all of the models present a steady increase of the negative atomic charge on the α -ligand as the macrocyclic ring increases in size for both the Co-alkyl complexes (models A–D) and the cobalamin models with an extensive π electron system (models E–H). This increase in negative charge at the α -ligand is synonymous with a loss of charge on the Co as seen in **Figure 7.9**.

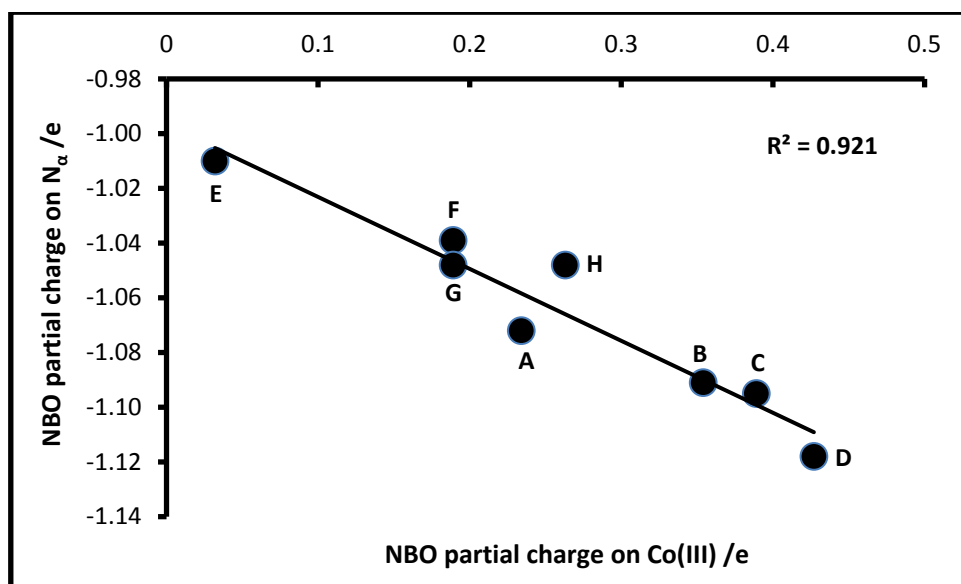


Figure 7.9: BP86: Correlation of the NBO partial charges on Co(III) and N_α for models A–H.

Based on previous results it is not surprising, that the partial charges generated from the Bader methodology show a different trend to that of the APT and NBO methods. As Co becomes less positive, the negative charge on N_α increases and the ionicity of the Co(III)– N_α bond decreases, as shown in **Figure 7.10**.

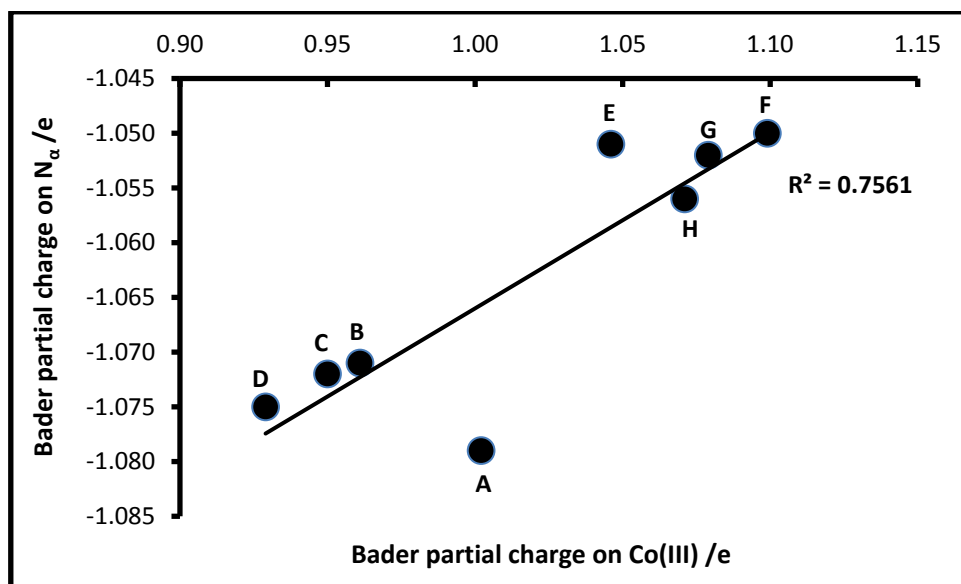


Figure 7.10: BP86: Correlation of the Bader partial charges on Co(III) and N_α for models A–H.

Again, the results from the partial charges are conflicting and show no common trends between the axial ligands and Co metal centre, or among the methodologies employed (with the exception of the APT and NBO charges discussed previously), and are thus found to be unreliable.

7.4 SOLUTION PHASE: UNIVERSAL SOLVATION MODEL

The environmental effect of the solvent on the homolysis of the Co(III)–C β bond was explored by using the universal solvation model based on solute electron density (SMD)²⁸⁵ with a range of solvents listed with their relative permittivities in **Table 7.4** below.²⁸⁶ Since solute-solvent interactions affect the overall behaviour of molecules, it is important to explore the effects in order to achieve quantitative accuracy. A relative permittivity of 37 was reported to reproduce more of a protein-like environment^{124,287} while other reports^{57,288,289} indicate that the protein has an effective relative permittivity of 2–16. The relative permittivity is important as it directly relates to an electrostatic environment in which a protein functions effectively. Therefore, in the calculations reported below, a range of solvents was used.

Table 7.4: Solvent relative permittivity (ϵ) values²¹⁶

Solvent	ϵ
Water (H ₂ O)	78.3553
Dimethylsulfoxide (DMSO)	46.8260
Methanol (MeOH)	32.6130
Dichloroethane (DCE)	10.1250
Octanol (Oct)	9.8629
Mebutanoate (MeBut)	5.5607
Hexane (Hex)	1.8819

The SMD model is considered to be universal, as its applicability includes charged or uncharged solutes in any solvent or liquid medium for which specific parameters such as the relative permittivity, ϵ , refractive index, bulk surface tension and acidity and basicity criterion are known.²⁹⁰ In this model, the full solute electron density is used without the need to define partial atomic charges, and the solvent is modelled as a continuum of uniform ϵ , that is, as a reaction field.^{63,285,291,292} Simply stated, this means that the solute is placed into an electrostatic cavity that takes on the shape of the molecule and after this is placed into a solvent (**Figure 7.11**).²¹⁶

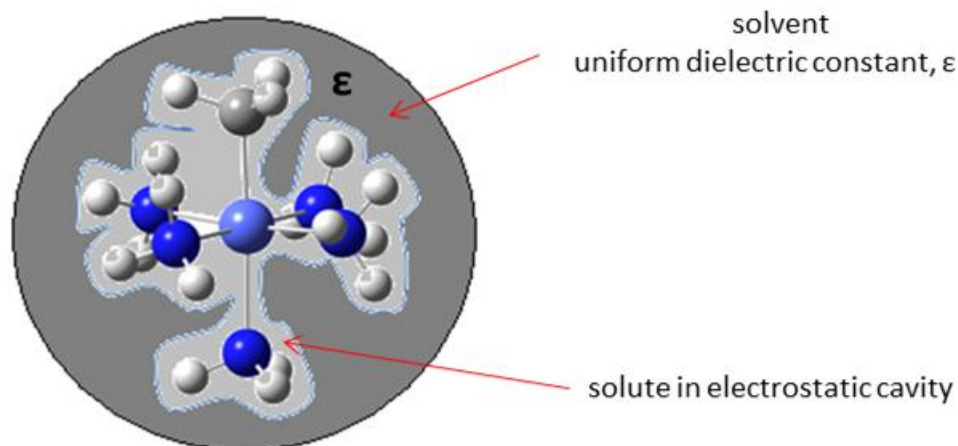


Figure 7.11: SMD method describing a solute-solvent interaction.

7.4.1 SOLVENT PHASE: RESULTS AND DISCUSSION

In this section, models A–H (**Figure 7.1**) were exposed to a range of solvents using different functionals so that the environmental effect on the energies of the system and change in any geometric parameters could be monitored. The BP86 results for the ΔG and BDE of the Co(III)–C $_{\beta}$ bond are summarised in **Table 7.5** while the geometric parameters are provided in **Table 7.6**. All of the data for M06L, B3LYP and PBE1PBE functionals are provided in Appendix4: A4.5–A4.7.

Table 7.5: BP86: Co(III)–C_β ΔG and BDE (kcal mol⁻¹) for models A–H in gas and solution phase

	Gas	H ₂ O	MeOH	Oct	DMSO	DCE	MeBut	Hex
Models	ΔG /kcal mol ⁻¹							
A	24.52	28.12	27.24	27.09	27.82	27.68	25.71	25.96
B	23.49	25.25	24.28	24.41	25.10	24.96	23.48	22.59
C	22.84	23.65	22.45	22.33	23.29	22.93	21.51	23.32
D	15.61	19.98	17.95	14.59	18.63	14.85	16.52	15.82
E	28.92	28.49	29.27	29.25	30.42	30.45	30.42	30.05
F	23.55	21.43	22.64	23.14	23.37	23.90	23.23	24.25
G	20.63	20.95	20.89	21.10	21.08	22.38	21.44	21.91
H	22.75	19.73	20.71	21.30	21.82	21.68	21.56	21.55
Models	BDE /kcal mol ⁻¹							
A	37.57	41.16	40.09	39.99	40.62	39.52	38.77	38.62
B	36.51	38.75	37.14	37.20	37.92	36.71	36.40	35.93
C	35.32	36.67	35.64	35.59	36.37	35.13	34.95	36.00
D	27.59	31.58	30.20	28.51	30.89	26.53	29.04	28.63
E	41.06	40.73	41.41	41.78	42.23	41.48	41.83	42.13
F	35.24	33.44	34.42	34.94	35.11	34.50	34.99	35.67
G	32.85	32.39	33.12	33.43	33.81	33.18	33.41	33.63
H	33.28	31.61	32.79	33.30	33.70	32.85	33.25	33.74

Table 7.6: BP86: Geometric parameters for models A–H in gas and solution phase

	Gas	H ₂ O	MeOH	Oct	DMSO	DCE	MeBut	Hex
Models	Co(III)–C _β /Å							
A	1.985	1.974	1.975	1.975	1.975	1.976	1.975	1.979
B	1.977	1.981	1.980	1.977	1.980	1.978	1.976	1.973
C	1.973	1.975	1.975	1.972	1.975	1.973	1.971	1.970
D	1.950	1.958	1.957	1.955	1.958	1.956	1.954	1.951
E	2.001	2.006	2.006	2.002	2.003	2.004	2.003	2.002
F	1.970	1.974	1.974	1.973	1.974	1.974	1.973	1.971
G	1.982	1.982	1.982	1.981	1.982	1.982	1.981	1.981
H	1.973	1.975	1.977	1.975	1.975	1.976	1.975	1.973
	Co(III)–N _α /Å							
A	2.181	2.088	2.093	2.102	2.090	2.102	2.109	2.143
B	2.192	2.110	2.114	2.124	2.111	2.123	2.135	2.160
C	2.180	2.106	2.109	2.114	2.108	2.114	2.120	2.150
D	2.262	2.134	2.140	2.164	2.137	2.164	2.170	2.203
E	2.076	2.051	2.052	2.076	2.054	2.058	2.061	2.070
F	2.197	2.173	2.175	2.181	2.173	2.182	2.184	2.196
G	2.220	2.220	2.161	2.168	2.158	2.169	2.176	2.198
H	2.167	2.132	2.133	2.140	2.133	2.139	2.146	2.158
	Co(II)–N _α /Å							
A	2.212	2.178	2.177	2.177	2.176	2.177	2.178	2.185
B	2.255	2.197	2.195	2.196	2.193	2.196	2.198	2.215
C	2.245	2.188	2.190	2.190	2.188	2.191	2.194	2.213
D	2.229	2.270	2.219	2.213	2.218	2.184	2.188	2.231
E	2.091	2.059	2.061	2.064	2.066	2.068	2.073	2.082
F	2.192	2.212	2.207	2.203	2.205	2.204	2.207	2.195
G	2.196	2.182	2.182	2.183	2.180	2.184	2.185	2.190
H	2.173	2.171	2.173	2.172	2.171	2.173	2.172	2.173
	N _α –Co(III)–C _β /°							
A	177.49	177.59	177.60	177.39	177.89	177.38	178.34	177.50
B	178.63	179.12	179.03	178.53	179.10	178.54	178.18	177.98
C	177.29	177.23	177.15	176.77	177.25	176.80	176.61	177.69
D	178.89	179.08	179.16	178.34	179.08	178.20	178.90	178.77
E	179.28	179.45	179.22	179.14	178.93	178.92	179.00	179.10
F	178.41	178.25	178.50	178.53	178.43	178.56	177.74	178.62
G	176.24	176.83	176.80	176.69	177.00	176.90	176.76	176.53
H	178.97	178.54	179.28	178.89	178.95	179.17	179.00	179.01

(a) *Energies and bond lengths*

It is immediately obvious on inspecting the tabulated results that the BP86 functionals give energies very similar to that obtained with M06L, while the values obtained using the hybrid functionals are similar to each other, but numerically different to those from BP86 and M06L. Although all of the functionals exhibit similar trends and ΔG is observed to parallel the BDEs of the Co(III)–C $_{\beta}$ bond, the hybrid functionals continue to give lower values for the Co(III)–C $_{\beta}$ BDEs in comparison to BP86 and M06L. In addition, the BP86 functional is observed to exhibit a better correlation for the change in equatorial ligands with both ΔG and BDE of the Co(III)–C $_{\beta}$ bond. In light of this, only the BP86 results are presented and discussed from here on.

As the saturated (models A–D) and unsaturated (models E–H) equatorial ligand increases in size, both the Co(III)–C $_{\beta}$ ΔG and BDE values decrease from H $_2$ O to hexane. The axial Co(III)–C $_{\beta}$ and Co(III)–N $_{\alpha}$ bond lengths, although slightly erratic, generally decrease and increase respectively, from models A–D and E–H, in all of the solvents. A normal *trans* influence occurs between the axial ligands in both model groups A–D and E–H.

When reviewing the change to the axial bond lengths from the gas to the solution phase, shown in **Table 7.6**, there are no significant changes observed in the Co(III)–C $_{\beta}$ bond length for all of the models. On the other hand, there is a notable change in the Co(III)–N $_{\alpha}$ and Co(II)–N $_{\alpha}$ bond lengths. Comparing the lower axial bond lengths in each solvent (H $_2$ O to hexane) from models A–H shows an increase in this bond from the Co(III) to the Co(II) complex. In addition, most of the lengths of the Co–N $_{\alpha}$ bonds are shorter for the models in the solvent as compared to the ones calculated in the gas environment. Earlier in this chapter, the value of the electron density at the bcp for the Co(III)–N $_{\alpha}$ bond confirmed this bond to be weaker and more ionic in character than the Co(III)–C $_{\beta}$ bond. These results then suggest that in a solvent medium the weaker lower axial bond is more susceptible to the permittivity

of its surroundings, that is, the nature of the solvent, and therefore it varies in length accordingly.

Evidently, many of the results indicated an increase in ΔG and BDE for the homolysis of the Co(III)–C $_{\beta}$ bond from the gas to the solution phase (see **Table 7.5**) for model systems A–H. While using the conductor-like polarisable continuum model (CPCM), Jensen and Ryde⁵⁷ also reported an increase of 1.2–1.7 kcal mol⁻¹ in BDEs because of solvent effects, and the results were dependent on the different ϵ values. This was not surprising to them as there is no charge separation involved in the homolytic reaction (which involves two radicals). The authors attributed the solvation effect to cavitation, dispersion and repulsion energies.

In another investigation into the role of solvent effects on cobalamin models, Dolker *et al.*¹³ suggested that perhaps the β -ligand radical is solvent-stabilised, which in turn may actually compensate for the additional stabilization of the starting model, AdoCbl. Electrostatic and hydrogen bonding interactions between the β -ligand and the side chains of the corrin were thought to be the main contributing stabilization factors in their investigation.

In this study, the models used were without the side chains (naked corrin); therefore, the conclusion from the study by Jensen *et al.*⁵⁷ may be taken as a possible explanation for what is observed here. For further insight, the free energies of solvation ($\Delta\Delta G_{\text{solv}}$)¹³, that is, the effect of solvation on the free energy of the Co(III)–C $_{\beta}$ bond cleavage, was investigated.

(b) *Gibbs free energy of solvation ($\Delta\Delta G_{\text{solv}}$) and BDE in solvent (BDE_{solv})*

In the process of solvation, energy changes that may be described as exo- or endothermic are associated with the solute-solvent interaction; this is called the Gibbs free energy of solvation, $\Delta\Delta G_{\text{solv}}$.²⁹³ $\Delta\Delta G_{\text{solv}}$ is defined as the change of the Gibbs free energy when a particle of the solute is transferred from a fixed position in the gas

phase into a fixed position in solution under constant temperature conditions.²⁹⁴ All the data for $\Delta\Delta G_{\text{solv}}$ for models A–H, in all of the solvents are presented in **Table 7.7**.

Table 7.7: BP86: $\Delta\Delta G_{\text{solv}}$ for models A–H in various solvents

Models (L ₄)	$\Delta\Delta G_{\text{solv}} / \text{kcal mol}^{-1}$						
	H ₂ O	MeOH	Oct	DMSO	DCE	MeBut	Hex
A	3.65	2.72	2.57	3.30	3.16	1.19	1.44
B	1.82	0.79	0.92	1.61	1.48	-0.01	-0.89
C	0.86	-0.39	-0.51	0.45	0.10	-1.33	0.48
D	4.42	2.34	-1.02	3.02	-0.76	0.91	0.20
E	-0.38	0.35	0.33	1.50	0.46	1.51	1.13
F	-2.06	-0.91	-0.40	-0.18	-0.71	-0.32	0.70
G	0.37	0.27	0.55	0.45	0.69	0.81	1.28
H	-2.97	-2.04	-1.44	-0.93	-2.13	-1.18	-1.20

The equation for $\Delta\Delta G_{\text{solv}}$ is given as:

$$\Delta\Delta G_{(\text{solv})} = \Delta G_{(\text{solv})} - \Delta G_{(\text{gas})} \quad (7.1)$$

where

$$\Delta G_{(\text{solv})} = (\Delta G_{\text{NH}_3 - [\text{Co(II)}(\text{L}_4)]^+} + \Delta G_{(\text{CH}_3)})_{\text{solvent}} - (\Delta G_{\text{NH}_3 - [\text{Co(III)}(\text{L}_4)] - \text{CH}_3^+})_{\text{solvent}}$$

and

$$\Delta G_{(\text{gas})} = (\Delta G_{\text{NH}_3 - [\text{Co(II)}(\text{L}_4)]^+} + \Delta G_{(\text{CH}_3)})_{\text{gas}} - (\Delta G_{\text{NH}_3 - [\text{Co(III)}(\text{L}_4)] - \text{CH}_3^+})_{\text{gas}}$$

On the other hand, there appears to be no such alternative that would allow the description of BDE changes (BDE_{solv}) during solvation processes. Literature has revealed that the Co(III)–C $_{\beta}$ BDE in solution can be attained by adding the enthalpic (potential energy) value to $\Delta\Delta G_{\text{solv}}$, shown in **Table 7.8**.¹³ Admittedly, Dolker *et al.*¹³ claimed it was not the best practice to add the $\Delta\Delta G_{\text{solv}}$ to enthalpies, however, it is a common practice (used by Jensen *et al.*⁵⁷) as no program provides enthalpies of solvation.¹³ The use of this methodology was also justified by the fact that as the degrees of freedom linked to translation and rotation is reduced from a gas to a solution phase, there is no significant difference in the enthalpies and free energies of solvation.

Table 7.8: BP86: BDE_{solv} for models A–H in gas phase and various solvents

Models	$BDE_{\text{solv}} / \text{kcal mol}^{-1}$							
	Gas	H ₂ O	MeOH	Oct	DMSO	DCE	MeBut	Hex
A	37.57	44.76	42.81	42.56	43.92	42.68	39.96	40.06
B	36.51	40.57	37.93	38.12	39.54	38.19	36.40	35.04
C	35.32	37.52	35.25	35.09	36.82	35.23	33.61	36.48
D	27.59	36.00	32.53	27.49	33.91	25.77	29.95	28.84
E	41.06	40.35	41.76	42.11	43.73	41.94	43.34	43.26
F	35.24	31.38	33.51	34.54	34.94	33.78	34.67	36.37
G	32.85	32.75	33.38	33.98	34.26	33.87	34.22	34.91
H	33.28	28.64	30.75	31.85	32.77	30.72	32.07	32.55

The results provided in **Tables 7.7** and **7.8** show that the increased stabilization interactions taking place between the solute and solvent on Co(III)–C $_{\beta}$ cleavage are noticeable for model H (-2.97 to -0.93 kcal mol⁻¹), followed closely by model F (-2.06 to -0.18 kcal mol⁻¹).¹³ The results of these calculations indicate that only the macrocyclic equatorial ligands (models F and H), with highly delocalised π electrons and having a planar framework, were better stabilised by the solvent. One possible explanation for this could be that their larger surface area is better exposed to the solvent, offering a better stabilization effect to the complex.

The assessment of the axial bond lengths, Co(III)–C_β and Co(III)–N_α, shows a poor correlation of the Co(III)–C_β bond length with the associated ΔBDE_{solv} (see **Figure 7.12**) for models A–D while less scatter is observed for models E–H. There appears to be a better linear relationship between the Co(III)–N_α bond length with the associated Co(III)–C_β ΔBDE_{solv}.

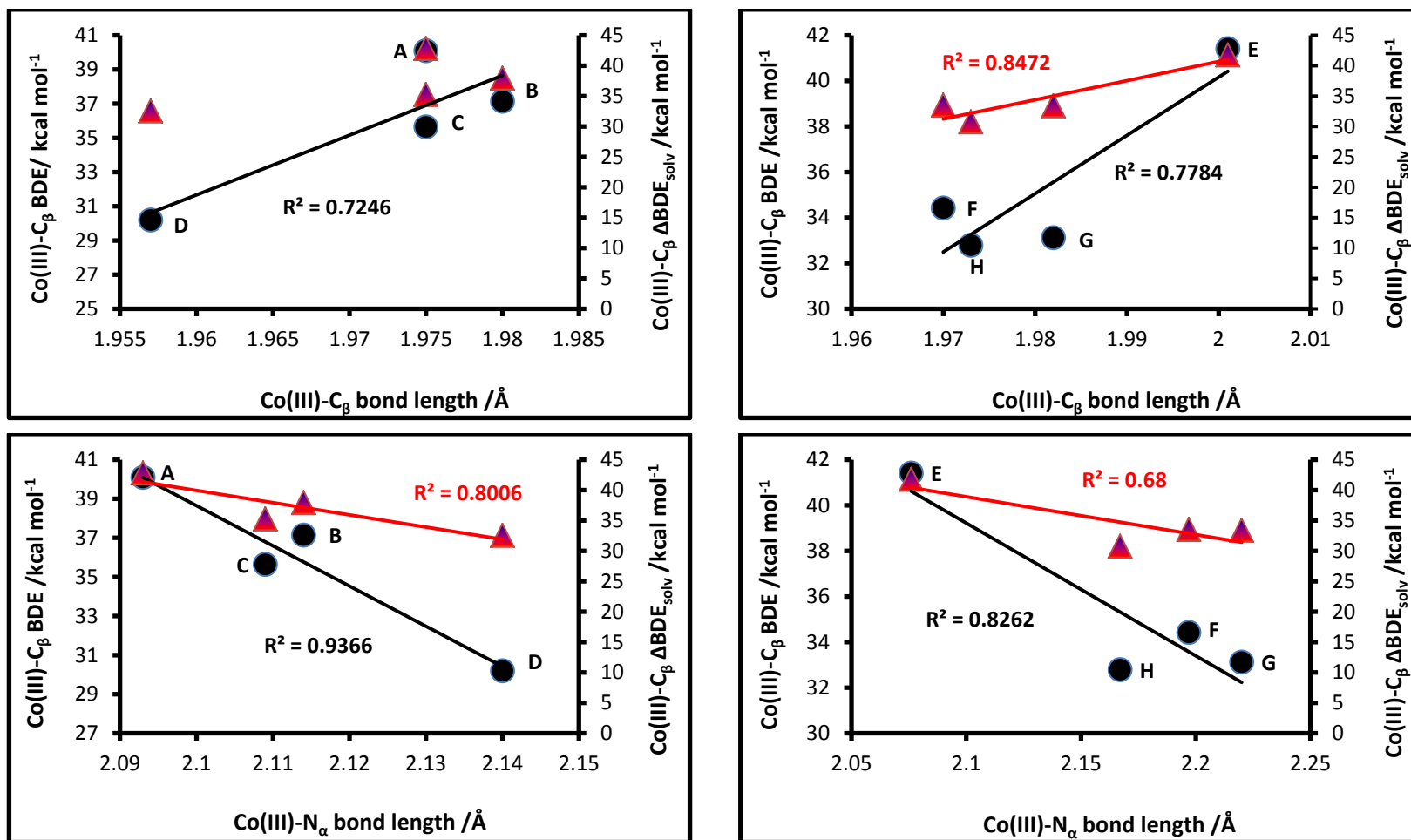


Figure 7.12 Co(III)-C_β BDEs (●) and Co(III)-C_β BDE_{solv} (▲) (kcal mol⁻¹) trends as a function of the Co(III)-C_β and Co(III)-N_α bond lengths (Å) for models A–D and E–H in MeOH.

c) Steric effects

The purpose of this analysis was to explore whether a steric *cis* effect of the equatorial ligand in models A–H plays a role in the homolytic cleavage of the Co(III)–C β bond. Models A–D are expected to have a greater flexibility because of their single bond framework (sp³ carbons) while models E–H, because of the high delocalisation of π electrons, should exhibit a lower flexibility. For models A–D, the level of distortion of the equatorial ligands was assessed by measuring the four N_{eq}–Co–C β bond angles, while eight torsion angles of the macrocyclic ring, as defined in Chapter 5, together with the N_{eq}–Co–C β bond angles, were measured for models E–H. The results obtained are provided in **Tables 7.9** and **7.10** respectively, while detailed data are given in Appendix 4: A4.10 and A4.11.

Experimental and theoretical values obtained from literature describing complexes that contain a rich π electron macrocyclic equatorial ligand and an α ligand of considerable bulkiness are listed in **Table 7.9** and **7.10**. Although both the equatorial and the α ligand used in the model complexes A–D were deficient of a rich π electron system and comprised an α ligand of little bulk respectively, a comparison was nevertheless made between the X-ray data obtained from the crystal structures of MeCbl¹⁴⁹ and AdoCbl,²⁹⁵ and the modified cobalamin model system used in a recent study by Dolker *et al.*¹⁴¹ Despite the large differences in the model systems used compared to that of the actual cobalamins, the BP86 and M06L functionals were found to reproduce similar Co(III)–C β bond lengths and BDEs for models A–H within range.

Table 7.9: Average $N_{eq}-Co-C_{\beta}$ bond angles ($^{\circ}$) and $Co(III)-C_{\beta}$ BDEs ($kcal\ mol^{-1}$) for models A–D in both gas and solution phase

	Gas	H ₂ O	MeOH	Oct	DMSO	DCE	MeBut	Hex
A = [NH ₃ –(Co(III)(NH ₃) ₅)–CH ₃]								
^a (N _{eq} –Co–C _β) _{avg} / $^{\circ}$	88.8	90.0	90.0	89.8	90.0	89.8	89.7	89.2
^b Co(III) shift / \AA	0.042	0.002*	0.002	0.008	0.001	0.007	0.009	0.029
BDE / $kcal\ mol^{-1}$	37.57	41.16	40.09	39.99	40.62	39.52	38.77	38.62
BDE _{solv} / $kcal\ mol^{-1}$		44.76	42.81	42.56	43.92	42.68	39.96	40.06
B = [NH ₃ –(Co(III)(14-ane)N ₄)–CH ₃]								
(N _{eq} –Co–C _β) _{avg} / $^{\circ}$	89.7	90.1	90.0	90.0	90.1	90.0	89.9	89.8
Co(III) shift / \AA	0.013	0.002*	0.001*	0.001	0.001*	0.001	0.004	0.009
BDE / $kcal\ mol^{-1}$	36.51	38.75	37.14	37.2	37.92	36.71	36.4	35.93
BDE _{solv} / $kcal\ mol^{-1}$		40.57	37.93	38.12	39.54	38.19	36.4	35.04
C = [NH ₃ –(Co(III)(15-ane)N ₄)–CH ₃]								
(N _{eq} –Co–C _β) _{avg} / $^{\circ}$	89.6	90.0	90.0	89.9	90.0	89.9	89.9	89.6
Co(III) shift / \AA	0.012	0.000	0.001	0.003	0.000	0.002	0.005	0.015
BDE / $kcal\ mol^{-1}$	35.32	36.67	35.64	35.59	36.37	35.13	34.95	36.00
BDE _{solv} / $kcal\ mol^{-1}$		37.52	35.25	35.09	36.82	35.23	33.61	36.48
D = [NH ₃ –(Co(III)(16-ane)N ₄)–CH ₃]								
(N _{eq} –Co–C _β) _{avg} / $^{\circ}$	92.6	92.9	92.9	92.8	92.9	92.8	92.8	92.7
Co(III) shift / \AA	0.094*	0.107*	0.106*	0.103*	0.106*	0.103*	0.101*	0.098*
BDE / $kcal\ mol^{-1}$	27.59	31.58	30.20	28.51	30.89	26.53	29.04	28.63
BDE _{solv} / $kcal\ mol^{-1}$		36.00	32.53	27.49	33.91	25.77	29.95	28.84
^c (N _{eq} –Co–C _β) _{avg} value for MeCbl and AdoCbl ¹⁴¹ = 90.3 $^{\circ}$.								
^{d,e} (N _{eq} –Co–C _β) _{avg} data for MeCbl ¹⁴⁹ = 89.5 $^{\circ}$ and AdoCbl ²⁹⁵ = 90.8 $^{\circ}$.								

^aThe four bond angles that make up this average value have been defined as per the numbering used in Figure 5.8, Chapter 5. ^bThis is the measurement of the Co(III) metal centre from the mean plane defined through the N_{eq} donors. A * indicates the Co(III) ion was found above the mean plane towards the β ligand. ^cTheoretical results obtained from a study conducted by Dolker *et al.*¹⁴¹ using the B3LYP method for the MeCbl model, [Benz–(Co(III)corrin)–CH₃] and AdoCbl model, [Benz–(Co(III)corrin)–CH₂THF]. ^{d,e}X-ray data for the MeCbl¹⁴⁹ and AdoCbl²⁹⁵ crystal structures, respectively.

Table 7.10: Average $N_{eq}-Co-C_{\beta}$ bond angles ($^{\circ}$), average angle of ring distortion (ω_{avg} / $^{\circ}$) and Co(III)- C_{β} BDEs (kcal mol $^{-1}$) for models A–D in both gas and solution phase

	Gas	H ₂ O	MeOH	Oct	DMSO	DCE	MeBut	Hex
E = [NH ₃ -(Co(III)cobaloxime)-CH ₃]								
^a ($N_{eq}-Co-C_{\beta}$) _{avg} / $^{\circ}$	89.3	89.2	89.2	89.2	89.2	89.2	89.2	89.2
^b Co(III) shift / \AA	0.023	0.027	0.027	0.028	0.025	0.027	0.027	0.027
ω_{avg} / $^{\circ}$	0.5	0.2	0.2	0.2	0.2	0.2	0.3	0.4
BDE /kcal mol $^{-1}$	41.06	40.73	41.41	41.78	42.23	41.48	41.83	42.13
BDE _{solv} /kcal mol $^{-1}$		40.35	41.76	42.11	43.73	41.94	43.34	43.26
F = [NH ₃ -(Co(III)corrole)-CH ₃]								
($N_{eq}-Co-C_{\beta}$) _{avg} / $^{\circ}$	91.2	90.6	90.7	90.8	90.7	90.8	90.9	91.0
Co(III) shift / \AA	0.037*	0.019*	0.022*	0.024*	0.022*	0.024*	0.026*	0.031*
ω_{avg} / $^{\circ}$	0.0	0.0	0.0	0.0	0.0	0.0	0.0	0.0
BDE /kcal mol $^{-1}$	35.24	33.44	34.42	34.94	35.11	34.5	34.99	35.67
BDE _{solv} /kcal mol $^{-1}$		31.38	33.51	34.54	34.94	33.78	34.67	36.37
G = [NH ₃ -(Co(III)corrin)-CH ₃]								
($N_{eq}-Co-C_{\beta}$) _{avg} / $^{\circ}$	90.3	90.3	90.4	90.3	90.4	90.3	90.3	90.3
Co(III) shift / \AA	0.007*	0.007*	0.010*	0.008*	0.010*	0.008*	0.007*	0.006*
ω_{avg} / $^{\circ}$	3.4	3.4	3.4	3.4	3.4	3.4	3.4	3.4
BDE /kcal mol $^{-1}$	32.85	32.39	33.12	33.43	33.81	33.18	33.41	33.63
BDE _{solv} /kcal mol $^{-1}$		32.75	33.38	33.98	34.26	33.87	34.22	34.91
H = [NH ₃ -(Co(III)porphyrin)-CH ₃]								
($N_{eq}-Co-C_{\beta}$) _{avg} / $^{\circ}$	90.7	90.4	90.5	90.5	90.5	90.5	90.5	90.6
Co(III) shift / \AA	0.025*	0.015*	0.018*	0.017*	0.016*	0.018*	0.018*	0.022*
ω_{avg} / $^{\circ}$	0.0	0.0	0.0	0.0	0.0	0.0	0.0	0.0
BDE /kcal mol $^{-1}$	33.28	31.61	32.79	33.3	33.7	32.85	33.25	33.74
BDE _{solv} /kcal mol $^{-1}$		28.64	30.75	31.85	32.77	30.72	32.07	32.55
^c ($N_{eq}-Co-C_{\beta}$) _{avg} value for MeCbl and AdoCbl ¹⁴¹ = 90.3 $^{\circ}$. ^{d,e} ($N_{eq}-Co-C_{\beta}$) _{avg} data for MeCbl ¹⁴⁹ = 89.5 $^{\circ}$ and AdoCbl ²⁹⁵ = 90.8 $^{\circ}$.								

^aThe four bond angles that make up this average value have been defined as per the numbering used in Figure 5.8, Chapter 5. ^bThis is the measurement of the Co(III) metal centre from the mean plane defined through the N_{eq} donors. A * indicates the Co(III) ion was found above the mean plane towards the β ligand. ^cTheoretical results obtained from a study conducted by Dolker *et al.*¹⁴¹ using the B3LYP method for the MeCbl model, [Benz-(Co(III)corrin)-CH₃] and AdoCbl model, [Benz-(Co(III)corrin)-CH₂THF]. ^{d,e}X-ray data for the MeCbl¹⁴⁹ and AdoCbl²⁹⁵ crystal structures, respectively.

When comparing the $N_{\text{eq}}\text{-Co-C}_{\beta}$ bond angles for models A–D with the experimental and theoretical values, a change of $< 3.5^{\circ}$ was observed for the average bond angles. In addition, what becomes evident when comparing models A–D with each other is that in most cases the $N_{\text{eq}}\text{-Co-C}_{\beta}$ bond angle's $> 90^{\circ}$ results in lower Co(III)-C_{β} BDEs (see **Table 7.9**, **Figure 7.13**).

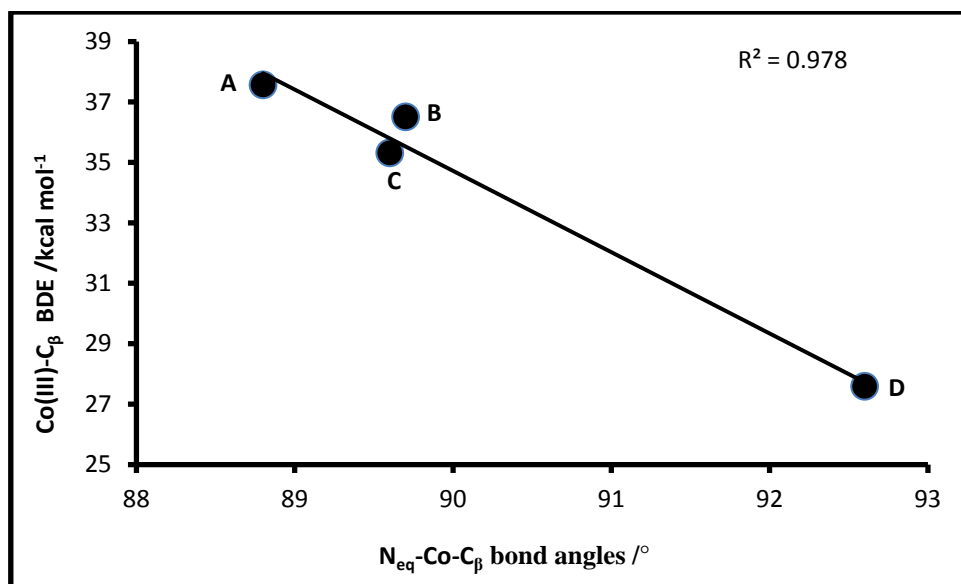


Figure 7.13: The $N_{\text{eq}}\text{-Co-C}_{\beta}$ bond angle versus Co(III)-C_{β} BDE for models A–D in the gas phase.

Although this observation suggests a weaker overlap may exist between the sp^3 and d orbital of the β ligand and Co metal centre respectively, producing lower Co(III)-C_{β} BDEs, the actual Co(III)-C_{β} bond strength continues to increase from models A–D (assessed by the ρ -value at the bcp, see **Table 7.2A**). Yet again it is observed that there is an inverse relationship between the strength of the Co(III)-C_{β} bond and its associated BDE, shown in **Figure 7.14**; as the bond of interest becomes stronger the BDE is observed to decrease.

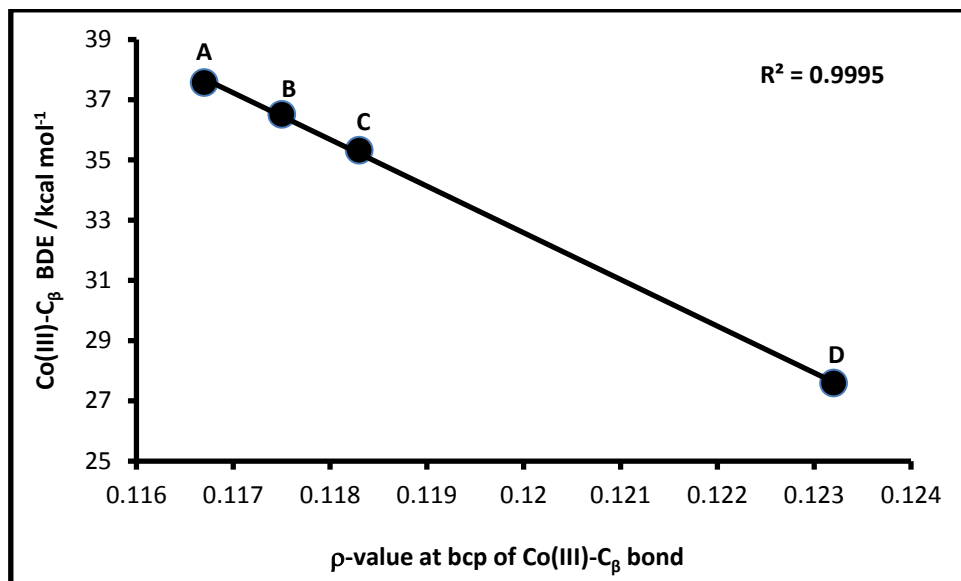


Figure 7.14: The change in the Co(III)–C $_{\beta}$ BDE as a function of the ρ -value at the bcp of the Co(III)–C $_{\beta}$ bond for models A–D in the gas phase.

In addition, it was also observed that the flatter the equatorial ligand (ω_{avg} for models F and H in **Table 7.10**), the stronger was the Co(III)–C $_{\beta}$ bond (ρ -value in **Table 7.2A**) and the greater the BDE for the homolysis of the Co(III)–C $_{\beta}$ bonds in models E–H, shown in **Figure 7.15**.

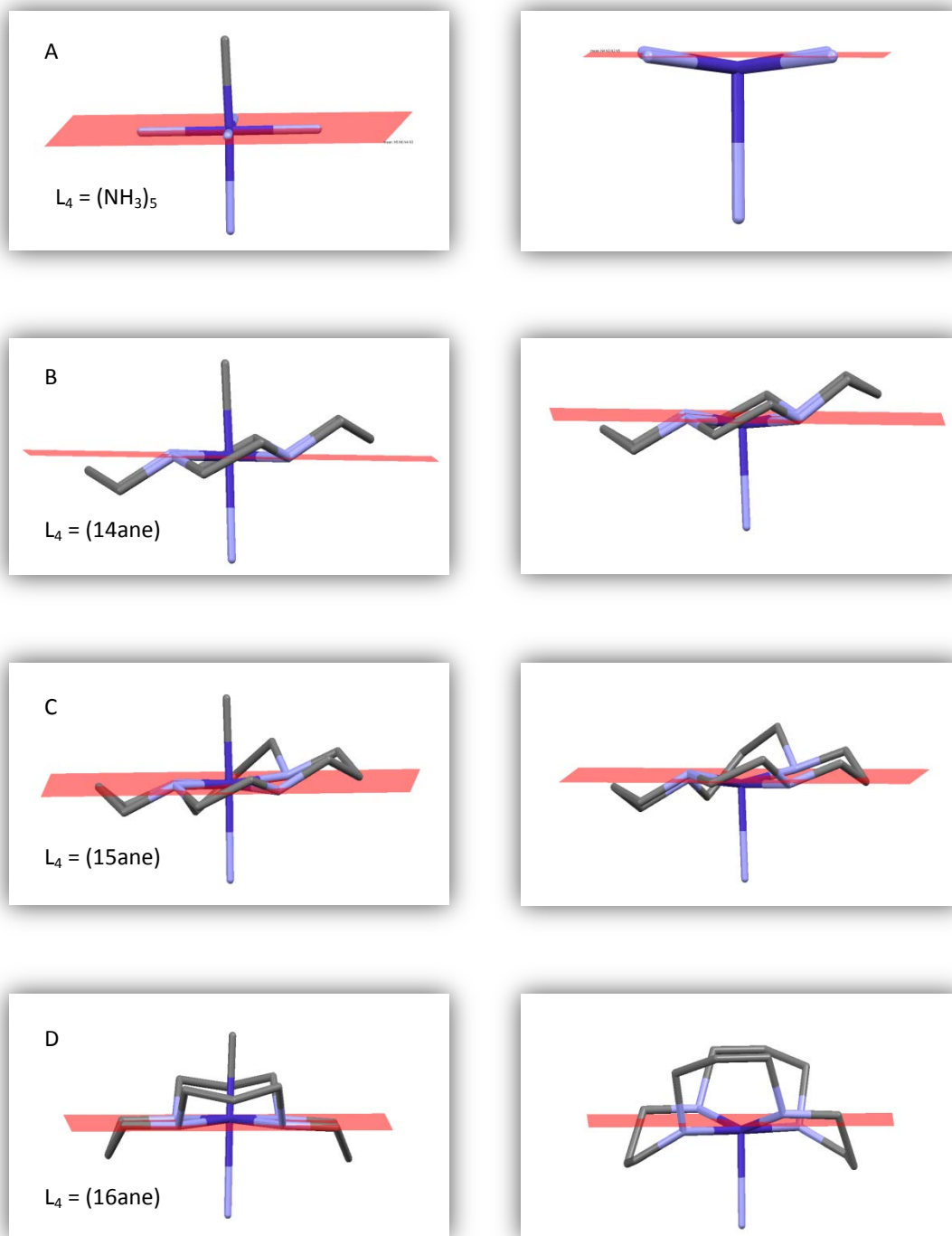


Figure 7.15: Movement of the equatorial ligand in the pre- (Co(III)) and post (Co(II)) homolysis complexes of the type $[\text{NH}_3-(\text{Co}(\text{III})(\text{L}_4)-\text{CH}_3)]^{n+}$ from the N_{eq} defined mean plane.

Model D is observed to have the greatest distortion of its $N_{\text{eq}}\text{-Co-C}_{\beta}$ bond angles, ranging from 92.5 to 92.9° and the lowest Co(III)-C_{β} BDE from the other models, A, B and C. In addition, it was observed, quite uniquely, that this model for both the gas and solution phase showed that the Co metal centre lay above the defined mean plane towards the β ligand. This provides evidence that a strong bond should exist between the β ligand and the Co metal centre as a result of a strong overlap of their orbitals at a closer distance. Moreover, this observation is further complemented by a decrease in the Co(III)-C_{β} bond length, shown in **Table 7.6**. However, the distortion of the $N_{\text{eq}}\text{-Co-C}_{\beta}$ bond angle counteracts both these effects and a lower BDE is obtained.

Undeniably, the size of the equatorial ligand is observed to play a role in this as well as a greater amount of flexibility was observed, (see **Figure 7.15D**), for model D, and progressively decreases to models C, B and then A as assessed by the $N_{\text{eq}}\text{-Co-C}_{\beta}$ bond angle. It can be concluded that as the macrocyclic ring gets smaller it becomes less flexible and more rigid, which is evidenced by the decrease in the $N_{\text{eq}}\text{-Co-C}_{\beta}$ bond angle and the decreasing shift of the Co(III) metal centre from the mean plane, leading to a subsequent higher Co(III)-C_{β} BDE for those models. The effect of the solvent is observed to suppress the shifting of the Co(III) metal centre from the defined mean plane for models A, B and C that contain larger surface accessible solvent areas while model D, with a smaller exposure of its surface area, shows the increasing shift of the Co(III) ion from the mean plane. This shift is in line with the increasing distortion of the $N_{\text{eq}}\text{-Co-C}_{\beta}$ bond angle.

On the other hand, models F–H (**Table 7.10**) which have a lower flexibility (see **Figure 7.16**) than models A–D, show no changes in the distortion of the macrocyclic ring (ω_{avg}) when comparing data from the gas to the solution phase. Model E (which has greater flexibility than models F and H shows a further flattening of the equatorial ligand as the Co(III) metal centre is observed to move closer to the α ligand from the gas to the solution phase. For the same model, with the exception of the water solvent, this observation is found to parallel the increase of the Co(III)-C_{β} BDE.

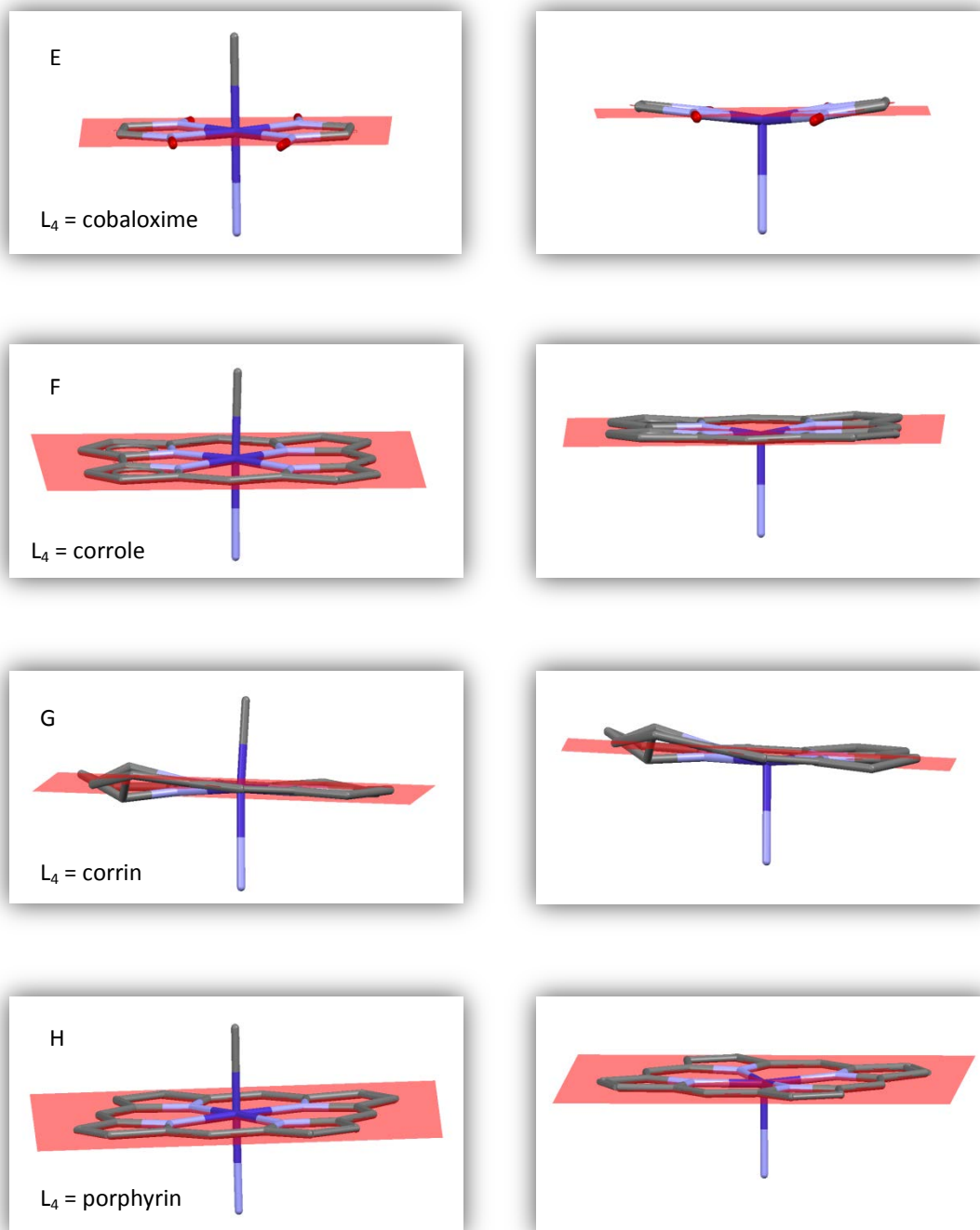


Figure 7.16: Movement of the equatorial ligand in the pre- (Co(III)) and post (Co(II)) homolysis complexes of the type $[\text{NH}_3-(\text{Co}(\text{III})(\text{L}_4))\text{CH}_3]^{n+}$ from the N_{eq} defined mean plane.

In addition, model E, which is observed to have the highest Co(III)–C_β BDE, contains two negatively charged oxygen atoms on the periphery of the equatorial ligand and because of intramolecular hydrogen bonding is greatly stabilised in the gas phase, and only slightly more so in the solution phase as a result of further intermolecular interactions, shown in **Figure 7.17**. Consequently, it is believed that the greater the stabilised equatorial ligand, the greater the *cis*-electronic influence on the upper axial ligand. Therefore, a stronger Co(III)–C_β bond forms and as a result high BDEs for the homolysis of the bond, > 40 kcal mol⁻¹, are obtained.

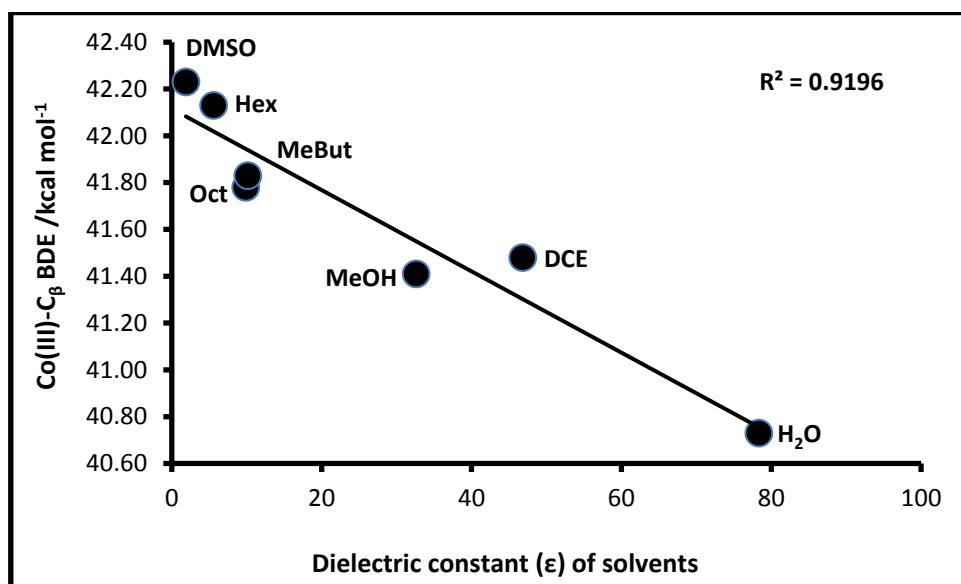


Figure 7.17: For model E, the Co(III)–C_β BDE (kcal mol⁻¹) is plotted as a function of the relative permittivities for polar aprotic, polar protic and non-polar solvents

Models F and H are similar in that they contain a planar equatorial framework but differ in the number of carbons to the macrocyclic ring, with model H having one extra methine group to its macrocyclic ring. The flatness of the equatorial ligand results in more solvent-accessible surfaces. The solvent effects are observed to have a stereo-electronic influence by increasingly suppressing the shift of the Co(III) metal centre from the gas phase to the solution phase, in other words by pushing it away

from the β ligand, as ε increases and the distortion of the $N_{\text{eq}}\text{-Co-C}_{\beta}$ bond angle increases. This results in a weaker Co(III)-C_{β} bond, observed to be much weaker for model H, and is shown to parallel the associated BDEs, as shown in **Figure 7.18**.

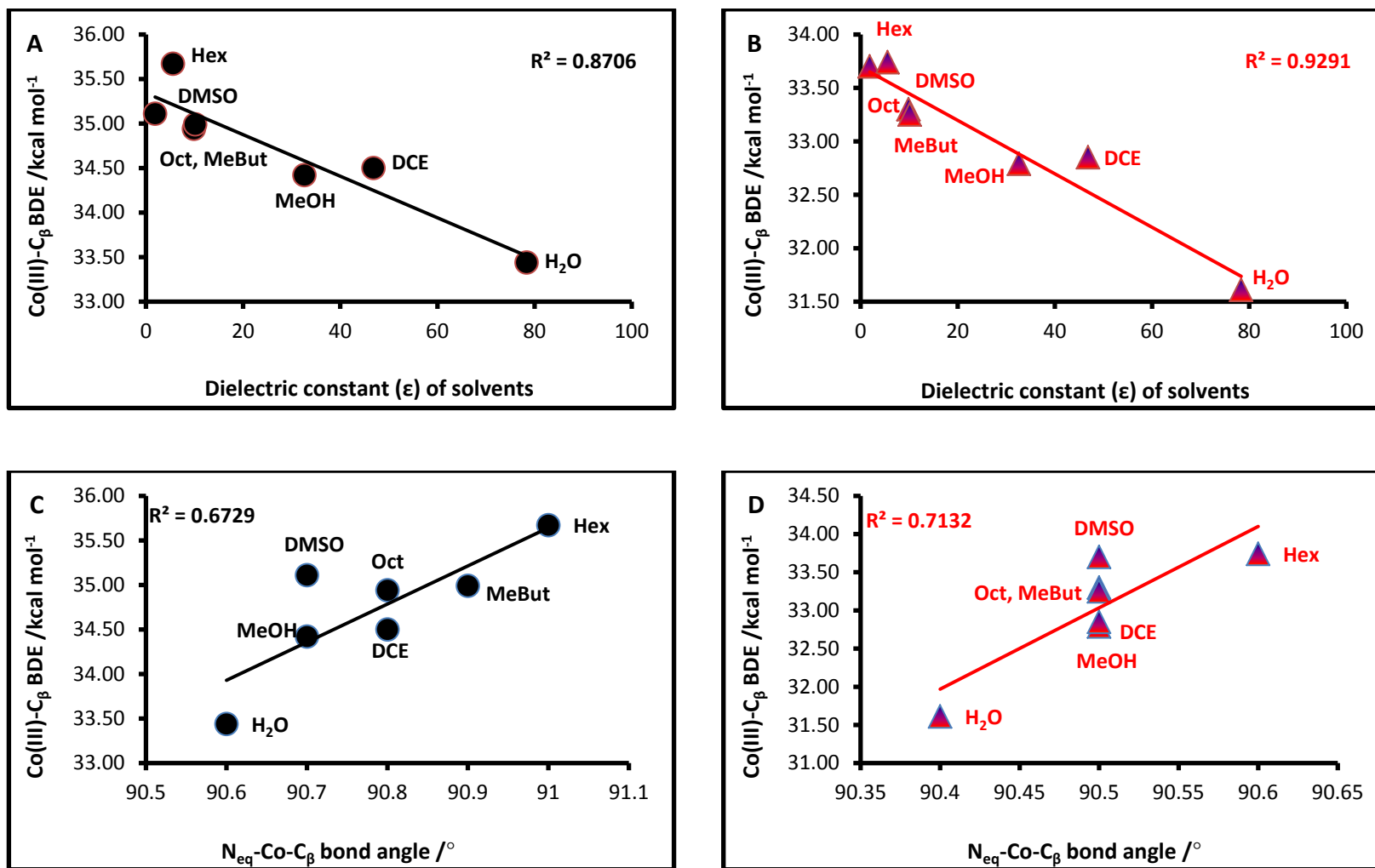


Figure 7.18: The change in the Co(III)-C_β BDE (kcal mol⁻¹) as a function of the the ε of the solvents and the distortion of the N_{eq}-Co-C_β (°) in models F (●) and H (▲).

Model G, $[\text{NH}_3\text{-(Co(III)corrin)-CH}_3]^+$, has an average ring distortion (ω_{avg}) of 3.4° in the gas and solution phase. This implies that the equatorial ligand is non-planar and therefore has a smaller surface area exposed to the solvent medium as compared to the other three models. Therefore, there is no significant change to the displacement of the Co(III) metal centre from the corrin plane (see **Figure 7.19A**), and from the gas to the solution phase; however, in comparison to models F and H, this model is observed to have the Co(III) ion furthest away from the β ligand. Consequently, the Co(III)- C_β bond is weak and a low BDE is obtained for the homolysis of this bond, shown in **Figure 7.19B**.

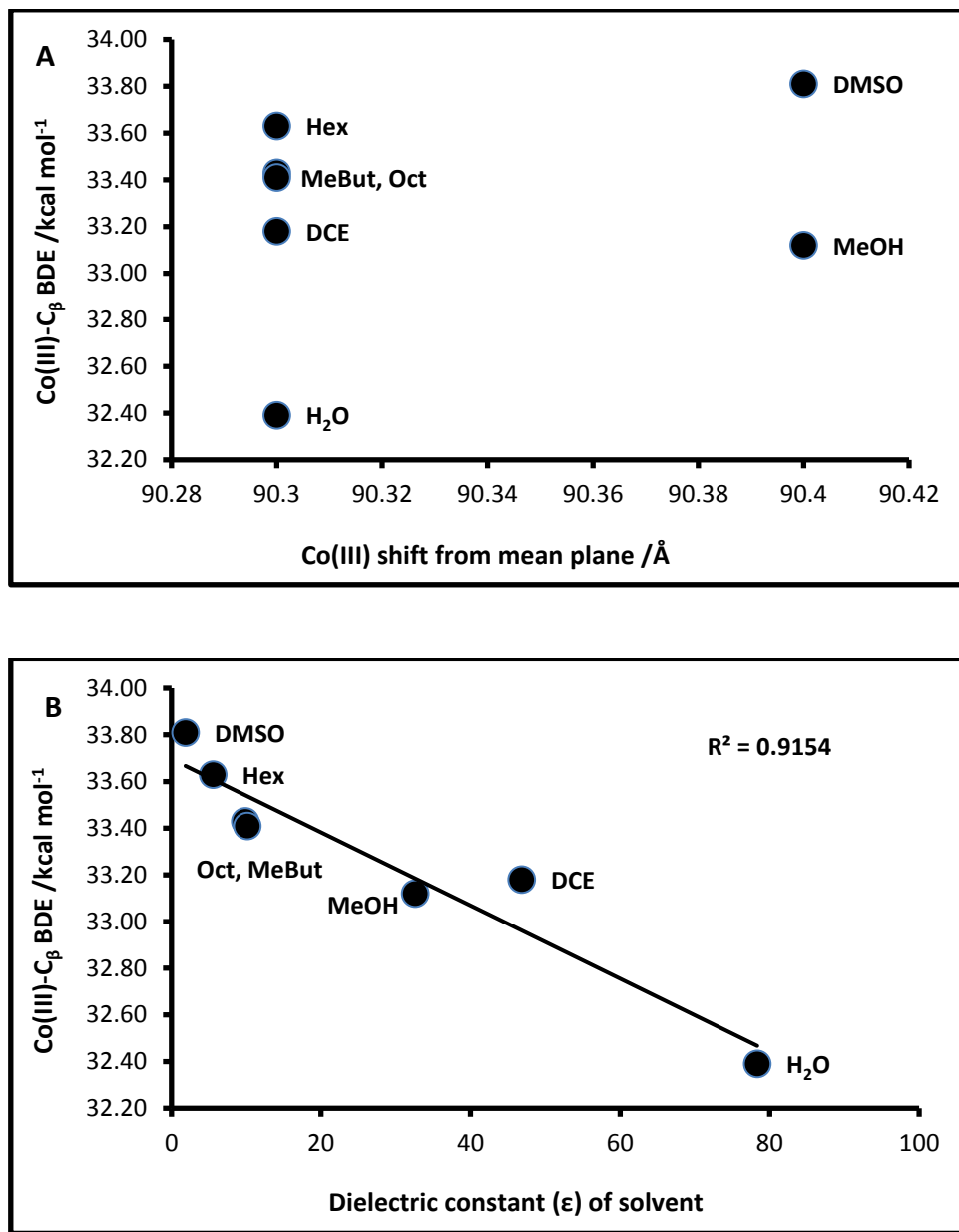


Figure 7.19: The change in the Co(III)-C_β BDE (kcal mol⁻¹) as a function of the A) Co(III) shift from the mean plane (Å) and B) the ε of the solvents in model G.

7.5 CONCLUSIONS

Calculations for models A–H (**Figure 7.1**) were conducted in both the gas and solution phase. These models differed from each other in the type of equatorial ligands incorporated into the model systems, which were either aliphatic, rich in π electrons or aromatic, and/or rich in π electron density.

The trend observed for the Co–alkyl models A–D, showed a decrease in BDE (and ΔG) as the equatorial ligand increased in the number of carbon atoms to the aliphatic macrocyclic ring. The larger equatorial macrocyclic ligand produced an increased flexibility of the macrocyclic ring as assessed by the measurement of the $N_{\text{eq}}\text{–Co–C}_\beta$ bond angles. These steric effects in the gas and solution phase were observed to have a direct influence on the homolysis of the Co(III)– C_β ΔG and BDEs. Furthermore, the introduction of environmental effects through the use of a variety of solvents led to the suppression of the shift of the Co(III) metal centre from the equatorial mean plane towards the β ligand, resulting in a reduced distortion of the $N_{\text{eq}}\text{–Co–C}_\beta$ bond angles. This suggests a better overlap of the Co d orbital with the C_β sp^3 orbital, resulting in higher BDEs for a stronger Co(III)– C_β bond in the order $A > B > C > D$.

Models E–H contained cobaloxime, corrole, porphyrin, and corrin respectively as their equatorial ligand. In both the gas and solution phases, the corrin model produced the lowest Co(III)– C_β BDE (and ΔG) with the BP86 functional, while the M06L functional described the porphyrin model as having the lowest BDE and ΔG . Notably, the differences in energy between these two models were small and ranged from $< 2 \text{ kcal mol}^{-1}$ for ΔG and $< 0.6 \text{ kcal mol}^{-1}$ for the BDEs in the gas phase.

By contrast to the models with the aliphatic equatorial ligands, the level of flexibility of the macrocyclic ring for these models were measured from the distortion of the equatorial ligand, ω_{avg} , and found to be in the order: corrin $>$ cobaloxime $>$ corrole = porphyrin. By excluding the results for the Co-cobaloxime complex, (because it

differs from the others in that it contains two negatively charged oxygens on its periphery), it was observed that the flexibility of the macrocyclic ligand does indeed affect the homolysis of the Co(III)–C β bond, similar to models A–D. In conjunction, the Co(III) metal centre was observed to be the furthest away from the β ligand in the Co-corrin model as compared to Co-corrole and -porphyrin. This of course directly affects the strength of the Co(III)–C β bond as is seen in the ρ -values at the bond critical point. The corrole and porphyrin models both share a planar framework of the equatorial ligand ($\omega_{\text{avg}} = 0$) and thus the significant difference between the two arose from the orbital overlap between the Co(III) metal centre and the β ligand together with the size of the equatorial ligand. The corrole complex exhibited a strong upper axial bond with the highest BDE of that bond.

What is evident so far from these results and others from the previous chapters, is that there is electronic communication and steric co-ordination between the axial ligands, Co metal centre and macrocyclic equatorial ligand, leading to a prime system for efficient Co(III)–C β bond homolysis.

CHAPTER 8

CIS INFLUENCE: SUBSTITUTION ON CORRIN'S

$C_{10}^{\dagger\dagger\dagger}$

8.1 INTRODUCTION

All calculations reported in Chapters 5–7 were based on a model structure of cobalamin with a corrin ring that contained only hydrogen atoms on its periphery (see **Figure 8.1A**). This chapter, however, will focus on the *cis* effects of the equatorial ligand once a substituent replaces the hydrogen atom at C_{10} on the corrin ring (see **Figure 8.1B**). Two types of substituent were used, either with an electron-donating or with electron-withdrawing character. The substituents were $-\text{NO}$, $-\text{NO}_2$, $-\text{CN}$, $-\text{COOH}$, $-\text{Br}$, $-\text{CH}_3$, $-\text{OH}$ and $-\text{NH}_2$.

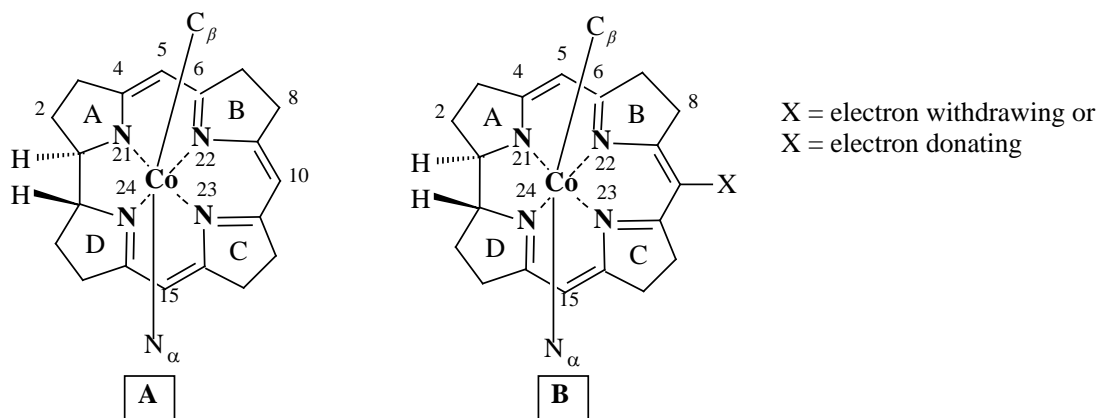



Figure 8.1: Representation of the corrin macrocycle used for calculations in complexes of the type, $[\text{NH}_3-(\text{Co}(\text{III})(\text{corrin-X}))-\text{CH}_3]^+$.

^{††††} Published manuscript: The *cis* influence of the corrin in vitamin B₁₂ models, Chemical Physics Letters, 550 (2012) 150-155

These substituents are quantified by the Hammett²⁹⁶ substituent parameter, σ_p , and are arranged in **Table 8.1** from low to high electron donor power.²⁹⁷

Table 8.1: Hammett substituent constant (σ_p) values^{297,298}

C ₁₀ – X	Hammett constant (σ_p)	electron donor power
NO	0.91	
NO ₂	0.78	
CN	0.66	
COOH	0.45	
Br/Cl	0.23	
H	0.00	
CH ₃ (Me)	-0.17	
OH	-0.37	
NH ₂	-0.66	

*The Hammett equation*²⁹⁸

Linear free energy relationships (LFER) were first studied in the 1930s by L.P. Hammett.²⁹⁸ The LFER was an attempt to develop a quantitative relationship between *structure* and *activity*. One such example of an LFER is the **rate** of base catalysed hydrolysis of a group of ethyl esters to form carboxylic acids and the **equilibrium** position of the ionisation in water of the corresponding group of acids, shown in equations 8.1 and 8.2 below.



An LFER was identified for these two processes, for a group of meta- and para-substituted benzoic acids ($\text{R} = -\text{C}_6\text{H}_5$) as a result of plotting $\log k$ for the reaction of esters against $\log K$ for the ionisation of acids (equation 8.3, **Figure 8.2**).

$$\log k = \rho \log K + C \quad 8.3$$

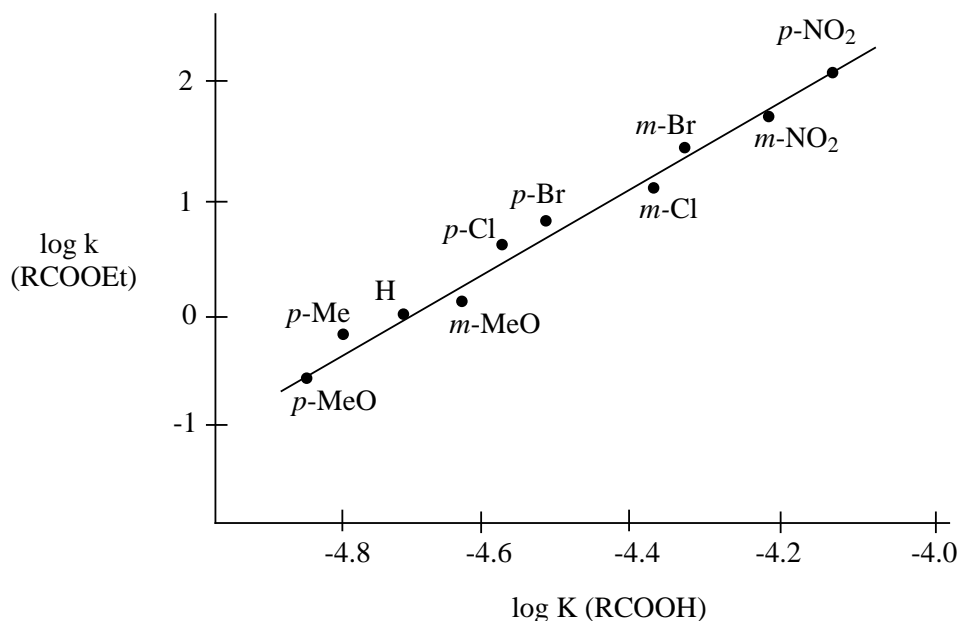


Figure 8.2: A linear relationship between log k vs log K is shown for a set of meta- and para-substituents on benzoic acids (redrawn from references 299 and 300).

Both the equilibrium constant (K) and rate constant (k) are linearly related to the free energy changes for the relevant reactions by the given equations 8.4 (ionisation in water) and 8.5 (activation for the ester reaction) below,^{299,300}

$$\log K = \frac{-\Delta G^\circ}{2.303RT} \quad 8.4$$

$$\log k = \frac{-\Delta G^\ddagger}{2.303RT} + \log \left[\frac{k'T}{h} \right] \quad 8.5$$

In 1937, Hammett²⁹⁸ presented the following kinetics and equilibria equations (referred to as the Hammett equations), respectively

$$\log \frac{k}{k_0} = \sigma\rho \quad 8.6$$

or

$$\log \frac{K}{K_0} = \sigma\rho \quad 8.7$$

where k and K are the rate and equilibrium constants for substituted systems while k_0 and K_0 are the rate and equilibrium constants for unsubstituted systems, that is, the substituent is hydrogen, σ is the Hammett substituent constant and ρ is the Hammett reaction constant.

The Hammett equation (equation 8.6 or 8.7) was derived from the difference between equation 8.3 (description of the relationship between the two reaction equations 8.1 and 8.2) and the standard reaction below (equation 8.8) for the unsubstituted carboxylic acid,

$$\log k_H = \rho \log K_H + C \quad 8.8$$

to give,

$$\log k - \log k_H = \rho (\log K - \log K_H) \quad 8.9$$

and finally providing,

$$\log \left(\frac{k}{k_H} \right) = \rho (pK_{a(H)} - pK_a) = \rho \cdot \sigma \quad 8.10$$

The term, $(pK_{a(H)} - pK_a)$, is given the symbol σ_m or σ_p for meta- and para-substituted benzoic acids and is known as the substitution constant. This constant can be calculated for any substituted benzoic acid for which the pK_a is given or can be measured.²⁹⁸ The Hammett relationship only applies to meta- or para- substituted aromatic systems attached to the reaction centre.

The Hammett substituent constant (σ)²⁹⁸

This constant is independent of the nature of the reaction site and is defined separately for meta- and para-substituents, that is, σ_m and σ_p , respectively. The σ is a

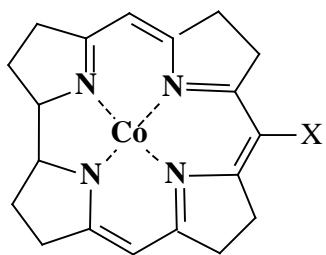
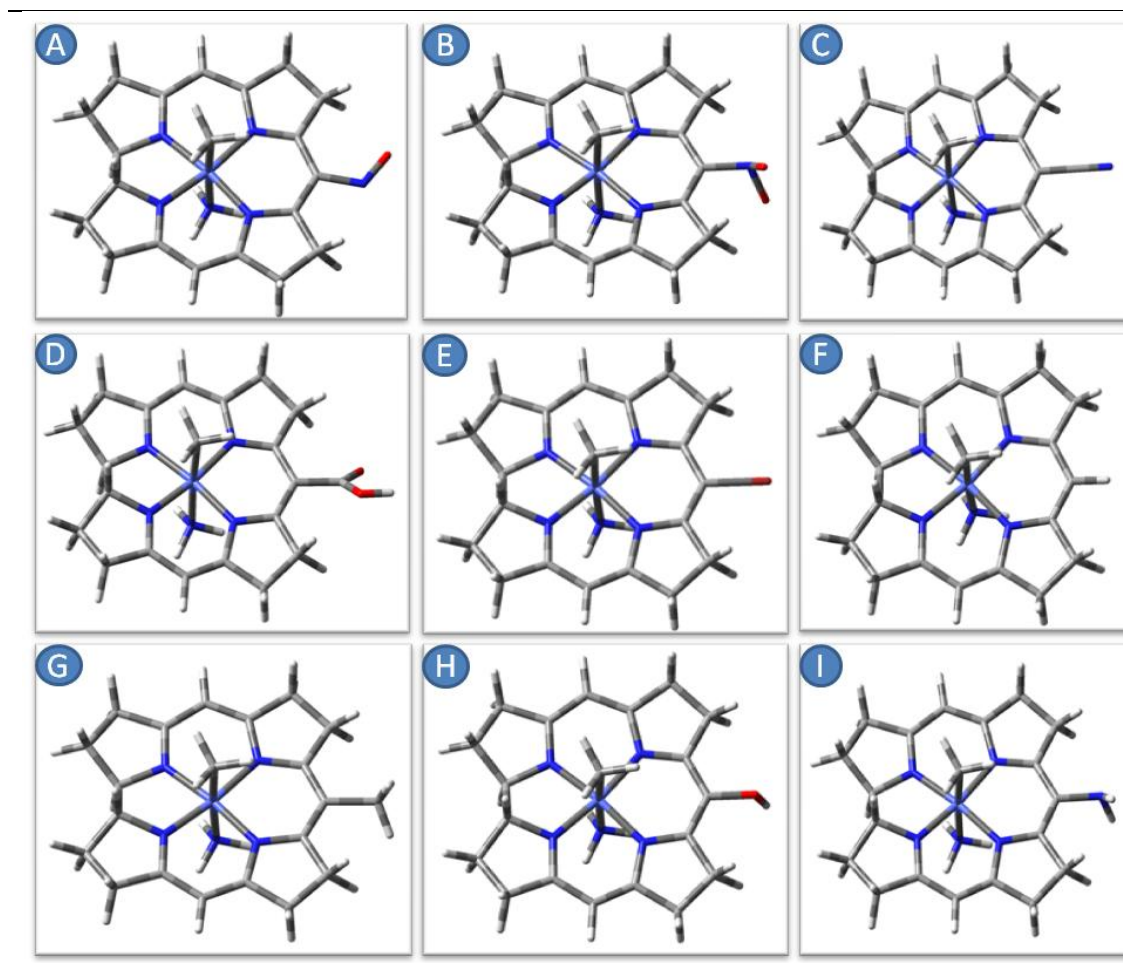
measure of the resonance and inductive effects of a substituent. It is a measure of how electron withdrawing or donating a substituent may be in its ability to supply or withdraw electrons to or from the reaction site.²⁹⁹ Evidently, the $\sigma_m > \sigma_p$ for an inductive electronic effect, as the substituent is closer to the reaction site while for a resonance effect the opposite is true due to a stronger conjugation for para-substituents. A $-\sigma$ and $+\sigma$ value will describe a substituent with electron-donating and $-\text{withdrawing}$ character, respectively.

*The Hammett reaction constant (ρ)*²⁹⁸

The reaction constant equals the slope of the line (**Figure 8.2**) correlating $\log k$ (or $\log K$) with the values of the Hammett substituents. The magnitude of the ρ value parallels the electronic effects of the substituents. A $+\rho$ is a result of an amassing of negative charge at the reaction centre in the transition state (ts) of the rate limiting step, where the rate is then accelerated by the presence of electron-withdrawing substituents, $-\sigma$. On the other hand, the reaction rate will be accelerated by electron-donating substituents when there is a build up of positive charge ($-\rho$) at the reaction centre in the ts of the rate limiting step.

8.2 MODEL STRUCTURES AND METHOD

The cobalamin models used, given in **Figure 8.3**, were adapted from a starting crystal structure of MeCbl retrieved from the CCSD.²¹² Modifications were made to the corrin ring by substituting different groups on C₁₀ of the corrin while only hydrogen occupied the other peripheral positions. The β and α -ligands comprised CH₃ and NH₃, respectively. All structures were geometry-optimised at the BP86/6-31+G(d,p) level of theory for all relevant spin states ($S = 0$ and 2 for Co(III) and $S = 1/2$ and $3/2$ for Co(II) complexes). Frequency calculations were performed to ensure all stationary points corresponded to stable minima. In addition, all of the energies reported included the correction to the zero-point energy.




A sketch of the cobalamin model of the type, $[\text{NH}_3\text{-[Co(III)(corrin-X)]-CH}_3]^+$. X represents the change in substituent at C₁₀ of the corrin macrocycle shown in models A — I above.

Figure 8.3: Cobalamin model of the type: $[\text{NH}_3\text{-(Co(III)(corrin-X))-CH}_3]^+$ where X in A=NO, B=NO₂, C=CN, D=COOH, E=Br, F=H, G = CH₃, H = OH and I=NH₂.

8.3 RESULTS AND DISCUSSION

(a) Energies, bond lengths and σ_p

An analysis of the data presented in **Table 8.2** shows a steady increase in the Co(III)–N _{α} bond length (see **Figure 8.4-A**) as the electron donor power, (quantified by the σ_p value), of the C₁₀ substituent increases. At the same time, the Co(III)–C _{β} bond length systematically decreases, although not by a significant amount. This behaviour is consistent with the increased orbital overlap of the Co metal centre with the β ligand (quantified by the shift of Co(III) from the mean plane, shown in **Table 8.2**) and is characteristic of a normal *trans* influence between the axial ligands (see **Figure 8.4-B**). In addition, the alteration of the C₁₀ substituents (*cis* ligand) is also observed to parallel the *trans* influence between these two axial ligands.

Table 8.2: Geometric parameters and ΔG and BDEs for the homolysis of the Co(III)–C $_{\beta}$ bond


C ₁₀ –X	σ_p	Bond lengths /Å				^d Co shift from mean plane /Å		^e ρ (bcp) /au		Bond Angle /°	Energies kcal mol ⁻¹	
		Co(III)–C $_{\beta}$	^a Co(III)–N $_{\alpha}$	^b Co(II)–N $_{\alpha}$	^c N $_{\Delta(5c-6c)}$	Co(III)	Co(II)	Co(III)–C $_{\beta}$	Co(III)–N $_{\alpha}$	N $_{\alpha}$ –Co(III)–C $_{\beta}$	^f ΔG	^g BDE
NO	0.91	1.986	2.199	2.187	-0.012	0.001*	0.137	0.1152	0.0560	176.39	21.39	34.00
NO ₂	0.78	1.985	2.214	2.194	-0.020	0.005	0.135	0.1156	0.0544	176.54	21.03	33.63
CN	0.66	1.985	2.214	2.194	-0.020	0.004	0.137	0.1157	0.0543	176.51	20.94	32.90
COOH	0.45	1.984	2.214	2.196	-0.018	0.006	0.132	0.1158	0.0542	176.49	21.08	33.68
Br	0.23	1.983	2.225	2.198	-0.027	0.007	0.134	0.1160	0.0530	176.34	20.95	32.89
H	0.00	1.982	2.220	2.196	-0.024	0.007	0.135	0.1162	0.0534	176.25	20.63	32.85
CH ₃	-0.17	1.982	2.224	2.198	-0.026	0.008	0.134	0.1163	0.0529	176.41	20.47	32.74
OH	-0.37	1.982	2.234	2.198	-0.036	0.009	0.137	0.1163	0.0519	176.55	20.60	32.55
NH ₂	-0.66	1.981	2.236	2.199	-0.037	0.009	0.138	0.1163	0.0516	176.59	20.54	32.41

^aThe axial bond length between Co(III) and N $_{\alpha}$ ligand in the 6 coordinate complex. ^bThe axial bond length between Co(II) and N $_{\alpha}$ ligand in the 5-coordinate complex. ^cThe difference in Co–N $_{\alpha}$ bond length between the 6 coordinate and 5 coordinate complex. ^dThe values given describe the shift of the Co atom from the mean corrin plane, defined through the N-donors, before and after homolysis has occurred, that is, the change from a 5-coordinate to a 6-coordinate complex. * Indicates that the Co metal centre was identified below the mean plane towards the α ligand. ^e1 au of $\rho = 6.7483 \text{ e } \text{\AA}^{-3}$. ^{f,g}Energies for the homolysis of the Co(III)–C $_{\beta}$ bond.

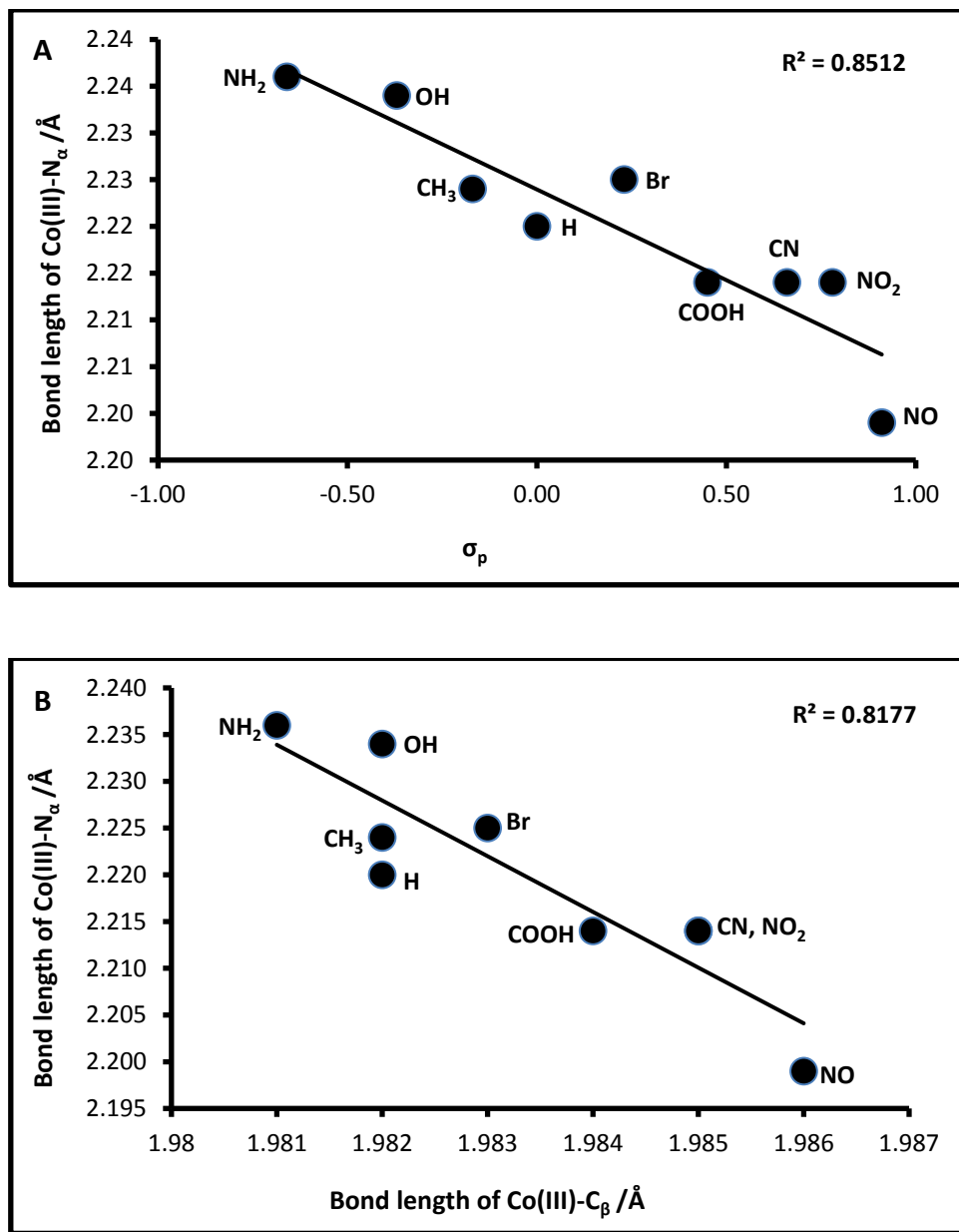


Figure 8.4: The Co(III)-N_α bond length is plotted as a function of the A) Hammett constant (σ_p) and B) Co(III)-C_β bond length (Å).

Although the Co(III)–C_β bond length was predicted to increase as the movement of electron density from the C₁₀ substituent to the equatorial ligand increased (introduction of an electronic repulsion effect between the Co atom and β ligand), in contrast, the Co(III)–C_β bond length decreased (**Figure 8.5**).

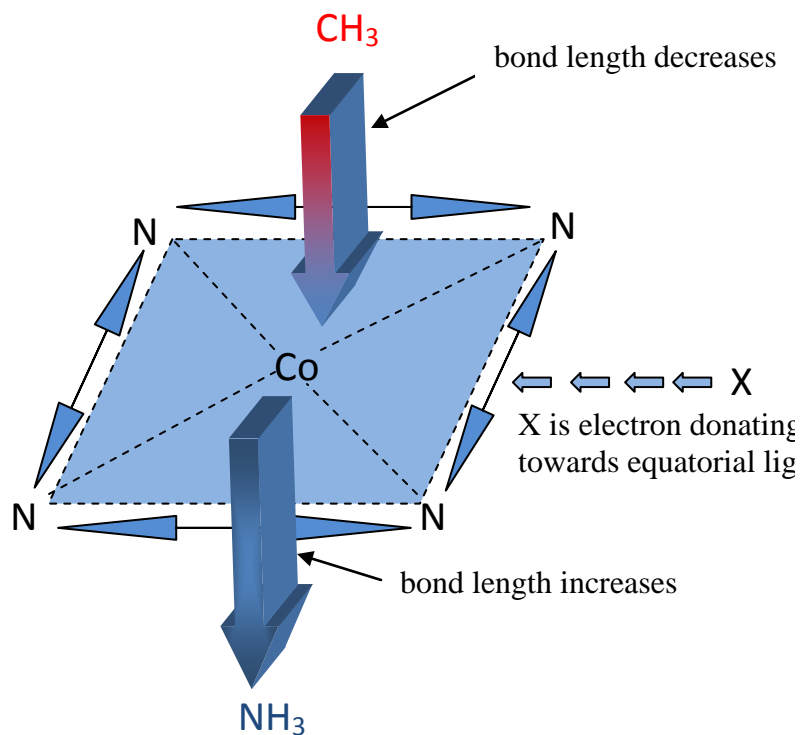


Figure 8.5: A schematic representation of the normal *trans* effect as a result of the electron donation increasing towards the macrocyclic equatorial ligand.

In addition, these results parallel those of the vibrational analysis; the Co–C stretching frequencies^{††††} move to higher wavenumbers and the C_β–H stretching frequencies are found to move to lower wavenumbers (shown in **Figure 8.6**) as the

^{††††}The Co(III)–CN stretch is not included in Figure 8.6 as it includes approximately four modes of vibrations.

donor power of the C₁₀ substituent increases. This trend confirms that the C_β-H bonds are weakened as the Co(III)-C_β bond strengthens (shortens) and the *cis* electron donation from the C₁₀ substituent increases.

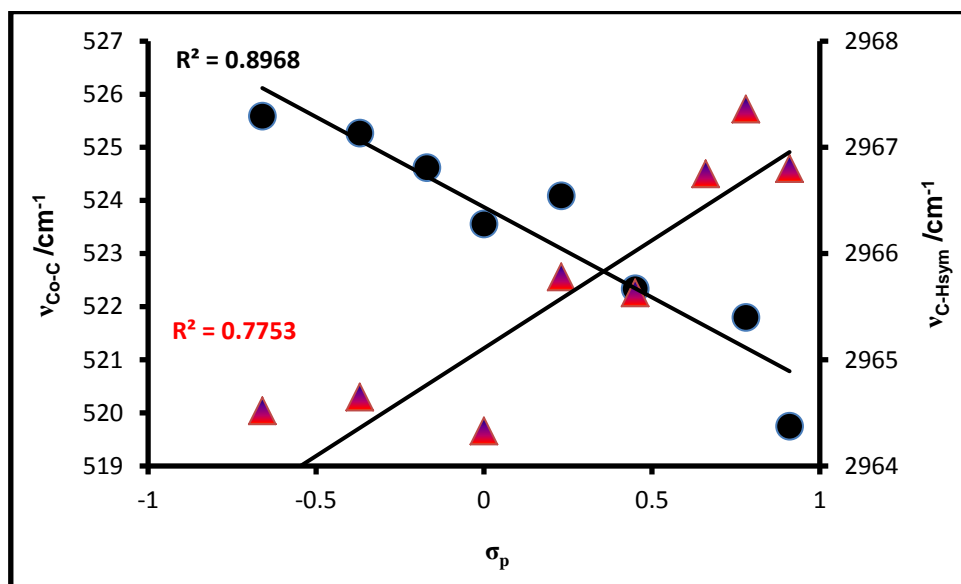


Figure 8.6: Vibrational analysis of the Co(III)-C_β bond (●) and C_β-H symmetric stretch (▲) against the Hammett constant (σ_p) of the C₁₀ substituent in the $[\text{NH}_3\text{-(Co(III)(corrin-X))}-\text{CH}_3]^{n+}$ complex.

These bond strengths are further affirmed by the ρ value at the bcp for both the axial ligands (see **Table 8.2**) where the ρ value at the bcp for the Co(III)-N_α bond decreases from 0.0560 to 0.0516 au as the *cis* donation from the C₁₀ substituent increases, while the Co(III)-C_β bond length subsequently strengthens (as assessed by its ρ value, 0.1152 to 0.1163 au). This reaffirms a normal *trans* influence relationship between the two axial ligands. Therefore, from the data given in **Table 8.2**, the Co(III)-C_β bond length is shown to strengthen as σ_p becomes more negative and as the Co metal centre deviates further away from the corrin mean plane towards the β ligand. As a result of the upper axial bond becoming stronger, an increase in both the BDE (and ΔG) for the homolysis of the Co(III)-C_β bond was expected. The opposite is true (see **Figure 8.7**).

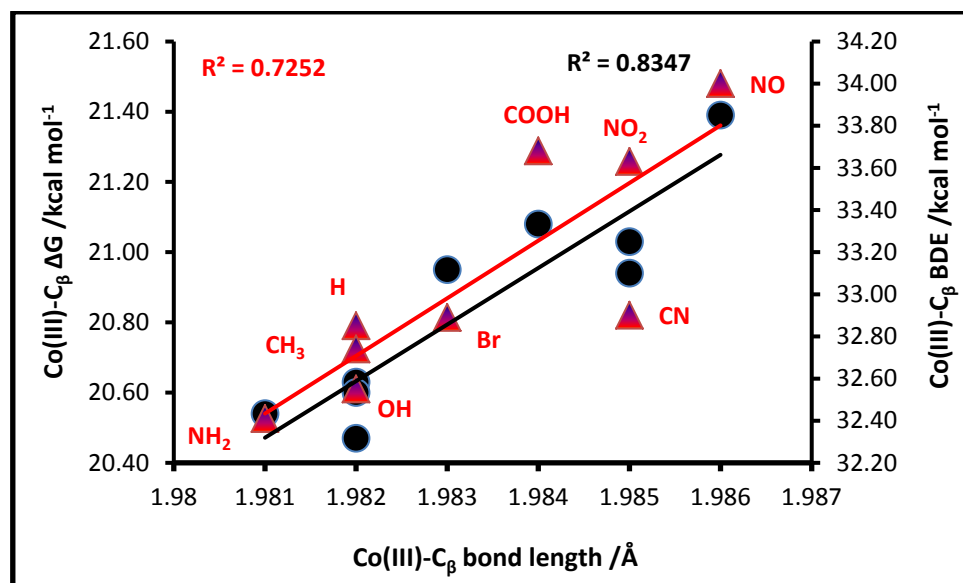


Figure 8.7: The Co(III)-C_β bond length (Å) is plotted as a function of the ΔG (●) and BDE (▲) (kcal mol⁻¹) for the homolysis of the Co(III)-C_β bond (Å).

In addition, an increase of 0.037 Å for the weaker Co(III)-N_α bond is observed as the electron density from the equatorial ligand increases as a result of changing the C₁₀ substituent (X = NO to NH₂), while at the same time the Co(III)-C_β bond length increases by only 0.005 Å. Under the same conditions, the Co(II)-N_α bond length (5-coordinate complex) changes by 0.012 Å. For the Co(II) complex, the decrease in bond length arises from the change in coordination number (from 6 to 5) of the cobalt ion and is found ~0.1 Å below the corrin plane towards the α ligand, resulting in an increase of the orbital overlap between the atoms.^{48,224} More importantly, this change in bond length (ΔCo-N_(5c-6c)) parallels the negative value of σ_p and the 5-coordinate complex is stabilised. This suggests that the BDE (and ΔG) for the homolysis of the Co(III)-C_β bond is influenced by the difference in the ΔCo-N_(5c-6c) bond length to the *trans* α ligand (shown in **Figure 8.8**).

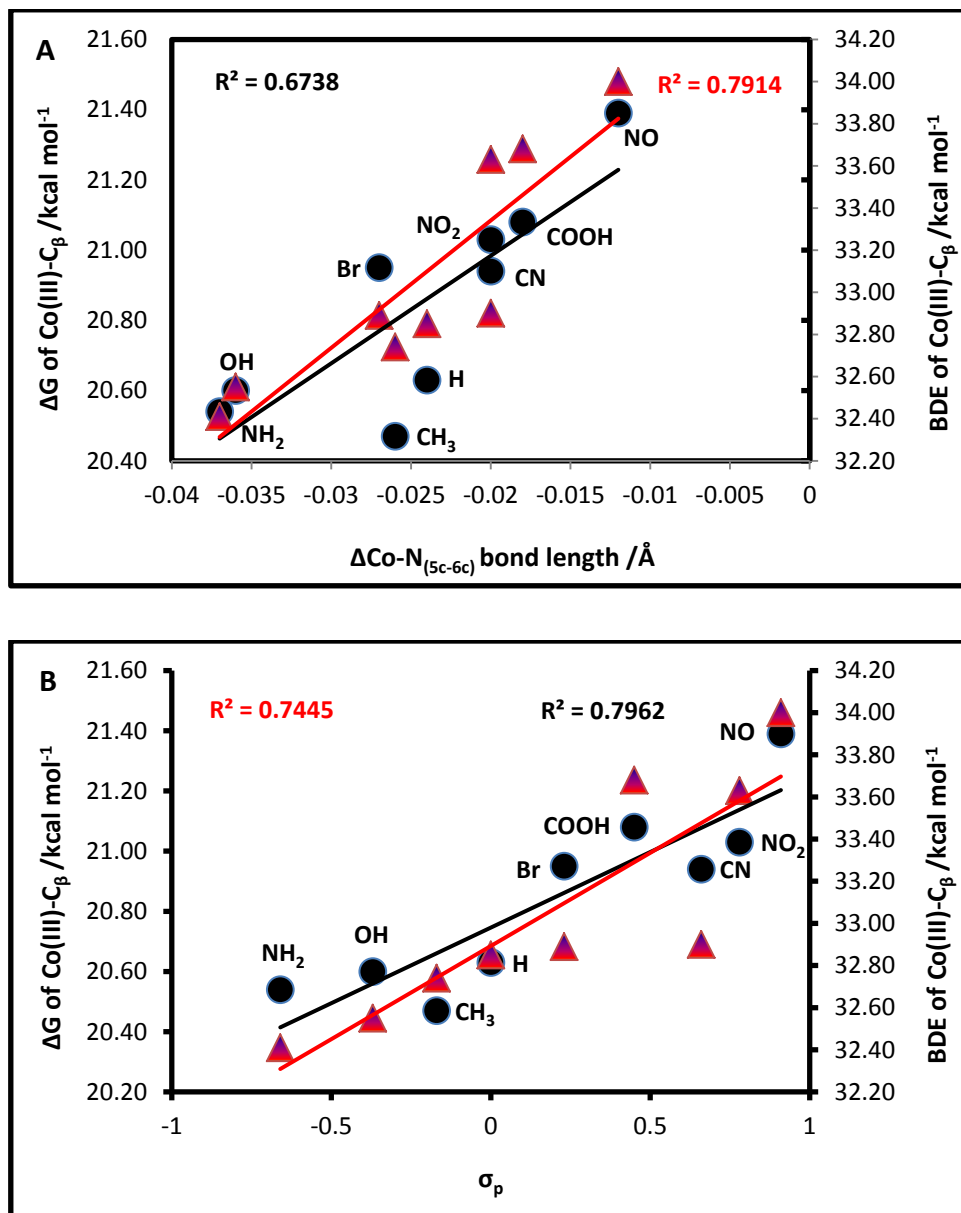


Figure 8.8: Trends in ΔG (●) and BDE (▲) (kcal mol $^{-1}$) for the homolysis of the Co(III)-C $_{\beta}$ bond in the $[\text{NH}_3-(\text{Co(III)}(\text{corrin-X})-\text{CH}_3)]^+$ complex as A) the Co-N $_{\alpha}$ bond length (Å) varies from the 6-coordinate to the 5-coordinate species and B) the σ_p of the C $_{10}$ substituent is varied.

(b) Partial charges and topological properties of the electron density

In this section the partial charges generated by the NBO³⁰¹ method (shown in **Table 8.3**) are reported while the QTAIM²¹⁸ method provided the topological properties of the electron density (see **Table 8.4**) of the model complexes.

The results presented in **Table 8.3** show that the positive charge on the Co atom marginally increases as the donor power of the C₁₀ substituent to the equatorial ligand increases. Consequently, the partial charge on the N_α becomes more negative while the charge on the carbon of the axial β ligand remains constant (see **Figure 8.9**). These small variations confirm that the C₁₀ substituent has little influence on the partial charges in the cobalamin models.

Table 8.3: NBO partial charges of atoms in the model complex, [NH₃–(Co(III)(corrin-X))–CH₃]⁺

C ₁₀ -X	σ _p	NBO						
		Co(III)	C _β	N _α	^a N ₁	^a N ₂	^a N ₃	^a N ₄
NO	0.91	0.187	-0.712	-1.044	-0.334	-0.367	-0.368	-0.330
NO ₂	0.78	0.187	-0.709	-1.047	-0.334	-0.368	-0.367	-0.332
CN	0.66	0.188	-0.708	-1.047	-0.335	-0.371	-0.369	-0.332
COOH	0.45	0.188	-0.711	-1.047	-0.337	-0.372	-0.371	-0.334
Br	0.23	0.190	-0.710	-1.049	-0.339	-0.368	-0.365	-0.335
H	0.00	0.190	-0.710	-1.048	-0.339	-0.378	-0.376	-0.336
CH ₃	-0.17	0.191	-0.711	-1.049	-0.340	-0.370	-0.369	-0.338
OH	-0.37	0.192	-0.710	-1.051	-0.343	-0.364	-0.361	-0.337
NH ₂	-0.66	0.193	-0.710	-1.051	-0.343	-0.361	-0.359	-0.341

^aNumbering format adopted from Figure 5.8, Chapter 5.

Table 8.4: Topological properties of the electron density of the Co(III)-C_β and Co(III)-N_α bonds

C ₁₀ -X	σ _p	Co(III)-C _β					
		ρ	∇ ² ρ	V(r)	G(r)	H(r)	V(r) /G(r)
NO	0.91	0.1152	0.0474	-0.1282	0.0700	-0.0582	1.8314
NO ₂	0.78	0.1156	0.0449	-0.1284	0.0698	-0.0586	1.8395
CN	0.66	0.1157	0.0456	-0.1286	0.0700	-0.0586	1.8371
COOH	0.45	0.1158	0.0473	-0.129	0.0704	-0.0586	1.8324
Br	0.23	0.1160	0.0462	-0.1292	0.0704	-0.0588	1.8352
H	0.00	0.1162	0.0483	-0.1296	0.0708	-0.0588	1.8305
CH ₃	-0.17	0.1163	0.0488	-0.1298	0.0710	-0.0588	1.8282
OH	-0.37	0.1163	0.0473	-0.1298	0.0708	-0.0590	1.8333
NH ₂	-0.66	0.1163	0.0474	-0.1298	0.0708	-0.0590	1.8333
Co(III)-N _α							
NO	0.91	0.0560	0.2120	-0.076	0.0645	-0.0115	1.1783
NO ₂	0.78	0.0544	0.2019	-0.0731	0.0618	-0.0113	1.1828
CN	0.66	0.0543	0.2015	-0.073	0.0617	-0.0113	1.1831
COOH	0.45	0.0542	0.2021	-0.0729	0.0617	-0.0112	1.1815
Br	0.23	0.0530	0.1945	-0.0708	0.0597	-0.0111	1.1859
H	0.00	0.0534	0.1981	-0.0717	0.0606	-0.0111	1.1832
CH ₃	-0.17	0.0529	0.1957	-0.0709	0.0599	-0.0110	1.1836
OH	-0.37	0.0519	0.1892	-0.0691	0.0582	-0.0109	1.1873
NH ₂	-0.66	0.0516	0.1877	-0.0685	0.0577	-0.0108	1.1872

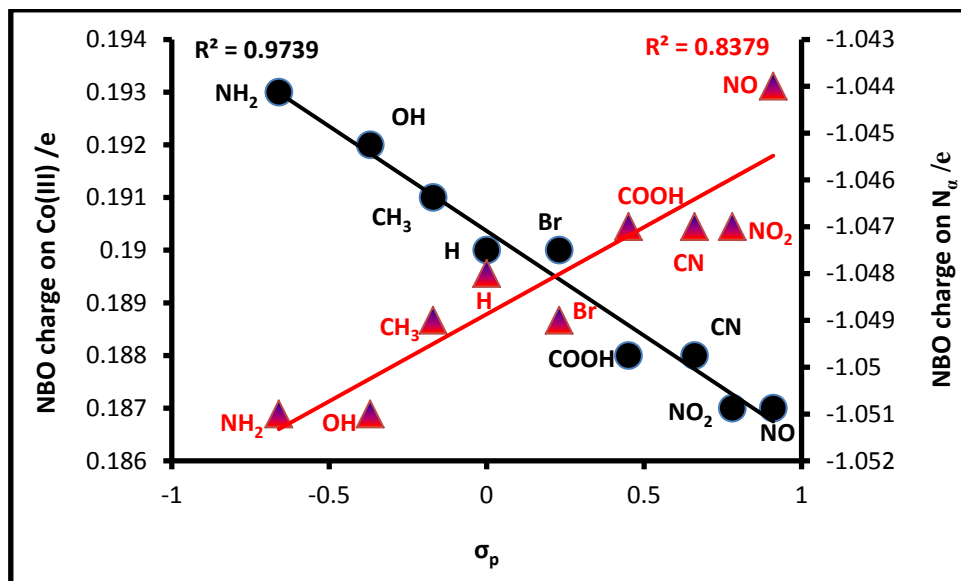


Figure 8.9: NBO partial charge on Co(III) (●) and N $_{\alpha}$ (▲) atoms as a function of the Hammett constant.

As a response to the variation of the partial charges on the atoms of the axial ligands, a normal *trans* influence of the axial bond lengths was confirmed; the Co(III)–N $_{\alpha}$ bond weakened as assessed by the decrease in the ρ value at the bcp and the ionicity of the same bond increased. This is further supported by the ratio of $|V(r)|/G(r)$ (shown in **Table 8.4**); this value can be used to characterise a bond.^{219,302} Clearly as seen in **Table 8.4** the $|V(r)|/G(r)$ value for the Co(III)–N $_{\alpha}$ bond (~ 1.2) describes it as being predominantly ionic in character while the nature of the Co(III)–C $_{\beta}$ bond (~ 1.8) is significantly covalent.

Finally, as the donor power of the C₁₀ substituent increases, the partial charge on the N_{eq} donors are observed to vary slightly; however, only a strong correlation is observed for the N₁ and N₄ atoms (see **Figure 8.10**). Unfortunately, there are no related observations that may suggest why the other donor atoms remain unaffected by the donor power of the C₁₀ substituents.

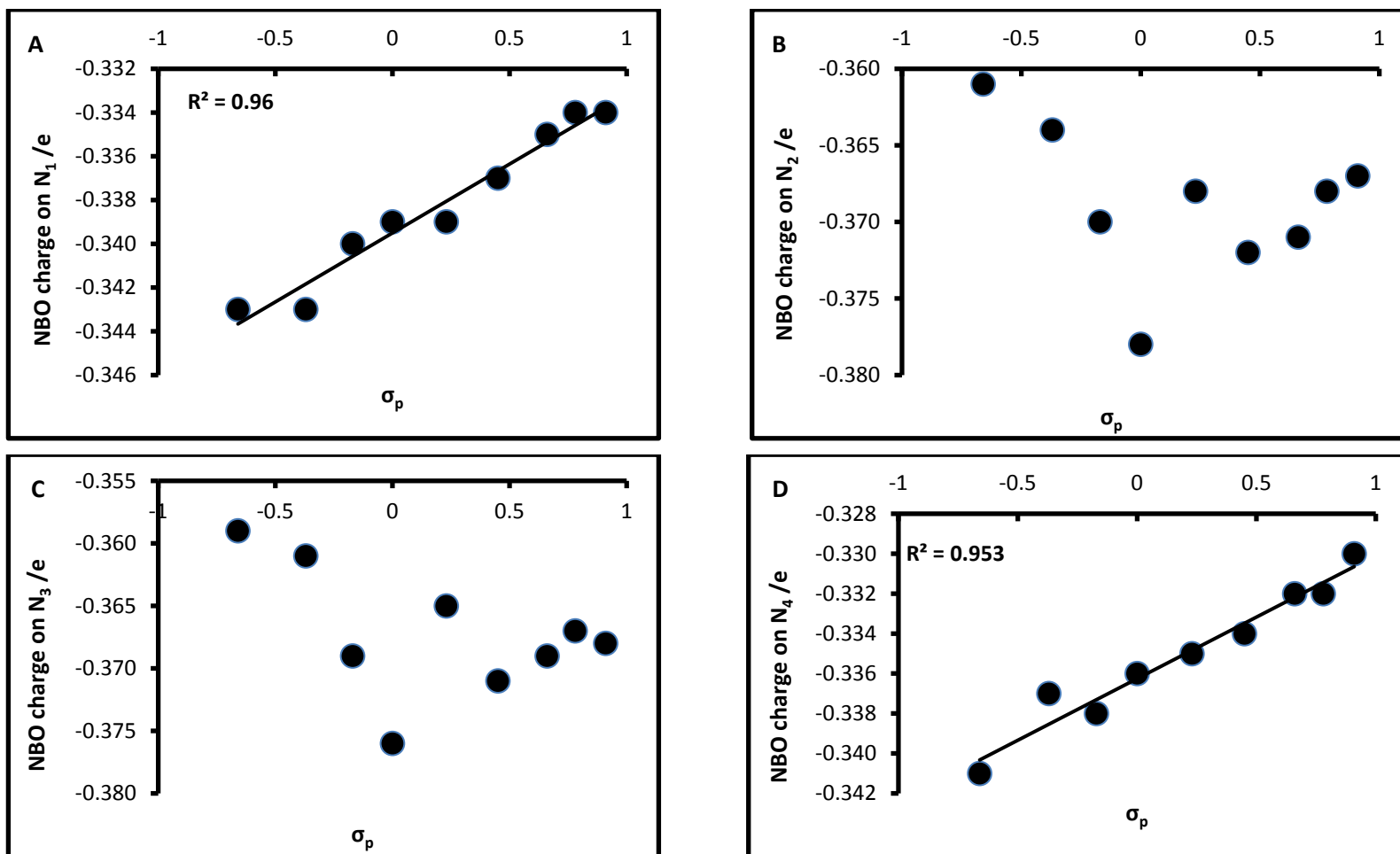


Figure 8.10: NBO partial charge on the equatorial N donors A) N_1 , B) N_2 , C) N_3 and D) N_4 as a function of the Hammett constant

8.4 CONCLUSIONS

In this chapter, groups of varying electron-donating and electron-withdrawing power replaced the hydrogen atom at the C₁₀ position of the corrin ring. The electron-donor power of the substituents was quantified by the Hammett function, σ_p . In other words, the more negative the value the greater is its donating ability. Surprisingly, it was found that the *cis* influence of this electron density enhanced further weakening of the Co(III)–N_α bond, while the Co(III)–C_β bond consequently strengthened, exhibiting a normal *trans* influence between the two axial ligands. The electron density at the bcps of the two axial bonds confirms the strengths of these bonds while the topological properties of the electron density shows the Co(III)–C_β bond to have a significantly more covalent character and the Co(III)–N_α bond to be of a dominant ionic character. Vibrational studies of the upper axial ligand further confirmed the strengthening and decrease of the Co(III)–C_β bond length.

Although it was still surprising to observe a decrease in ΔG and BDE as the Co(III)–C_β bond strengthened, it reaffirms that these parameters are not synonymous with each other, as the same trend was observed in Chapters 5 to 7. Evidently, once homolysis of the Co(III)–C_β bond occurred, the Co(II)–NH₃ bond was observed to shorten and paralleled the increase in electron donor power of the C₁₀ substituents. As a result of the increase in electron density from the C₁₀ substituent, the five-coordinate complex was better stabilised, and therefore lower BDEs (and ΔG) were obtained for the homolysis of the Co(III)–C_β bond. The ΔG and BDEs compared well with experimental values of actual complexes of MeCbl and AdoCbl. MeCbl^{145,146} is reported to have a BDE of 36–37 kcal mol⁻¹ and AdoCbl^{8,224,303} a range of 30–33 kcal mol⁻¹. For the complexes in this chapter, BP86 gave a BDE value ranging from 32–34 kcal mol⁻¹.

In order to gain better insight into the electronic influences caused by this *cis* perturbation of electron density, the NBO charges of the atoms in the models were assessed; however it was discovered that there was no strong *cis* influence from the C₁₀ substituent on the partial charges of the Co atom and axial α and β ligands.

CHAPTER 9

AN INVESTIGATION INTO THE CIS INFLUENCE IN COBALT CORRIN MODELS, [NH₃–(Co(III)(corrin))–R]ⁿ⁺, WHERE R = F, Cl, Br, SeCN OR CH₃ BY DFT AND TD-DFT STUDIES^{§§§§}

9.1 INTRODUCTION

In 1948 Karl Folkers *et al.* and E. Lester Smith and coworkers successfully isolated and purified the intensely red vitamin B₁₂ (cyanocobalamin).³⁰⁴ In the following year Ellis *et al.*³⁰⁵ recorded the UV-visible spectrum of vitamin B₁₂. The cobalamins were found to be interesting because of their ability to exhibit an array of colours as a consequence of their low-lying electronic excited state(s).^{56,306,307} Stich *et al.*¹¹⁷ highlighted the fact that most cobalamin absorption is similar as it is the corrin ligand itself that is responsible for the distinctive spectral features with all of the electronic transitions for the Co(III) cobalamins classified as having a $\pi \rightarrow \pi^*$ character.^{307,308}

The main absorption bands, α/β , D/E, γ and δ , appear in both metal-free corrin and in dicyanocobalamin, making it evident that the main absorption features of cobalamins

^{§§§§} In a recent manuscript (Cis Influence in Models of Cobalt Corrins by DFT and TD-DFT Studies, The Journal of Physical Chemistry B, (2012) 116(30):8836-45)) we reported on the cis influence in cobalt corrin models where both the α and β ligands were the same while the C₁₀-H was substituted by electron donating and –withdrawing substituents. In this Chapter, the cis influence of cobalt corrin models is investigated with a change to the β ligand while the C₁₀ substituent and α ligand is kept constant.

are attributed to the corrin macrocycle;³⁰⁸ this confirms the observation made by Stich *et al.*^{117,308}. The spectral changes of the cobalamins observed in UV-visible absorption spectra are usually characteristic of the oxidation state of Co, axial ligation and the surrounding environment.²⁸⁷

CNCbl and aquacobalamin (H_2OCbl^+), where the the β ligand is a cyanide and water molecule respectively, produce "typical" or normal absorption spectra, while the alkylcobalamins, MeCbl and AdoCbl, exhibit "atypical" (characterised as unique or anomalous) absorption spectra,¹⁰⁵ as shown in **Figure 9.1**. Cobalamins containing ligands such as I^- , NCSe^- and $\text{S}_2\text{O}_3^{2-}$ behave differently to cyanocobalamin, and are observed to exhibit "atypical" spectra (see **Figure 9.1**) similar to the alkylcobalamins such as methyl and vinyl cobalamin.¹⁰⁵ These "atypical" spectra have been noted for carbon ligands³⁰⁹⁻³¹¹ and certain, unspecified, sulfur containing compounds.^{312,313}

One way to discern the "atypical" from "typical" spectra is through identification of the γ band at lower wavelength with a reduced intensity, as well as the development of similar or stronger bands in the 300–350 nm range.¹⁰⁵ The β -band is also more prominent than the α -band.

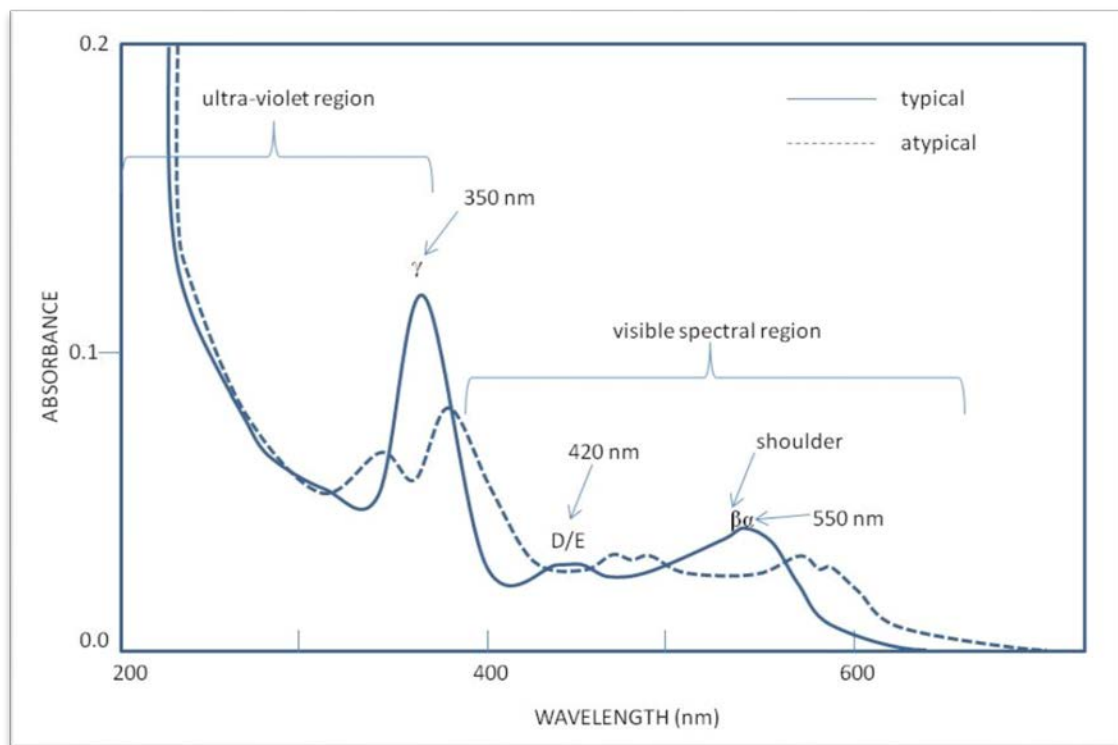


Figure 9.1: "Typical" (H_2OCbl^+) vs "atypical" (SCNCbl) absorption spectra of cobalamins.¹⁰⁶

In the spectrum above, the absorption bands due to corrin $\pi \rightarrow \pi^*$ transitions (denoted as α/β , around 450–600 nm) appear in the visible spectral region, while in the ultraviolet region one principal band (γ , around 340–370 nm) can be seen. In the α/β region of the electronic absorption spectrum several bands appear¹¹⁰ with the α band due to an electronic transition, while the β band is assumed (this is still under investigation) to originate from a vibrational mode¹⁰⁹ progression of the C=C stretching along the C_5 to C_{15} vector (see **Figure 9.2**).

In addition, it has been reported^{105,119,270,314,315} that the $\alpha\beta$ and γ bands experience a shift in wavelength when the donor atom of the axial ligands in the cobalamin is changed. Depending on the electronegativity of the donor atom, electron density is donated from the axial ligand *via* the σ -bond to the cobalt. In the complex, as the bond between the metal and ligand becomes more covalent, unpaired electrons from

the metal are spread over the ligand(s), leading to a reduction of interelectronic repulsion.³¹⁶ The decrease in the interelectronic repulsion is said to arise from the increased distance between the electrons plus the increased size of the orbitals (in other words, the cloud expanding). This increase is attributed to the formation of a large molecular orbital that results from the combination of orbitals from both the metal and ligand. This description is termed the nephelauxetic effect.^{317,318} Pratt and Thorpe¹⁰⁵ suggested the effect of the donor atom on the shift in wavelength to correlate with the nephelauxetic series: $\text{F}^- < \text{H}_2\text{O} < \text{urea(O)} < \text{NH}_3 < \text{en} < \frac{1}{2}\text{ox}^{2-} < \text{NCS}^- < \text{Cl}^- < \text{CN}^- < \text{Br}^- < \text{N}_3^- < \text{I}^- < \text{S}^{2-} < \text{Se}^{2-} < \text{Te}^{2-}$.^{265,318} As the electronegativity of donor atoms present in the axial ligand decreases, then the $\alpha\beta$ and γ bands are identified at longer wavelengths.^{106,270,314}

The nature of a ligand is also reported to affect the degree of d orbital crystal field splitting (Δ) which can be measured spectroscopically.^{318,319} A list of ligands was compiled to give what is known today as the spectrochemical series. The ligands are arranged from weak-field ligands to strong-field ligands: $\text{I}^- < \text{Br}^- < \text{S}^{2-} < \text{SCN}^- < \text{Cl}^- < \text{NO}_3^- < \text{F}^- < \text{OH}^- < \text{ox}^{2-} < \text{H}_2\text{O} < \text{NCS}^- < \text{CH}_3\text{CN} < \text{NH}_3 < \text{en} < \text{dipy} < \text{phen} < \text{NO}_2^- < \text{phosph} < \text{CN}^- < \text{CO}$.³¹⁸ The series shows an increase of Δ from left to right, with weak-field ligands show a small splitting of the d orbitals while strong-field ligands show a large splitting of the d orbitals.^{318,319} In a study¹¹⁹ conducted by Chemaly with cobalamins containing a variety of polarizable ligands a good correlation for band A (which is further defined later in this chapter) was found with the spectrochemical series rather than the nephelauxetic series. The cobalamin series is similar to the spectrochemical series in that P and C donor atoms are grouped together at the top of the series while I, Br, Cl, S and Se donor ligands are found at the bottom.

Absorption spectroscopy^{320,321} has been a particularly useful tool to experimentally probe the nature of excited states in cobalamins, however, a detailed understanding of the excited states remains elusive.¹⁰⁷ Consequently, several research groups have

started using TD-DFT,⁸⁵ a practical computational method that can be used consistently to study vertical excited states of complex molecules encompassing large structural frameworks. Moreover, the simulated absorption from TD-DFT calculations can be directly compared with those from experiment, since TD-DFT provides reliable estimates of the electronic excitation energies and transition dipole moments.¹⁰⁷ Notable, however, is the strong dependence of the simulated absorption on the type of functional used in the TD-DFT calculations. Consequently, in some cases, this led to poor quantitative and qualitative descriptions of the excited states where, for the lowest energy bands that appear in the α/β region, different assignments regarding the number of electronic transitions were made depending on whether hybrid or gradient-corrected functionals were used.^{55,107,110,117,322} Naturally, the question of how to select the appropriate functional arises. If the aim is to simulate an electronic spectrum, so that electronic transitions may be assigned accordingly, then the best functional may be judged on how well the simulated spectrum compares with the experimental one. It has been shown that for TD-DFT calculations in cobalamin chemistry, the BP86 functional appears to be the most reliable in reproducing the experimental absorption.¹⁰⁷ However, in a recent study³²³ on MeCbl, Kozłowski and co-workers showed that the TD-DFT calculation with GGA-type functional BP86 calculations correctly described the vis-NIR region of the absorption spectra, that is, the region common to the $\alpha\beta$ band as well as band A. The TD-DFT results were compared with the ab initio second-order multiconfigurational quasi-degenerate perturbation theory³²⁴ using complete active space self-consistent field orbitals³²⁵ (CASSCF/MC-XQDPT2) and the equation-of-motion coupled-cluster singles and doubles^{326,327} (EOM-CCSD) calculations.

9.2 MODEL STRUCTURES

A high-resolution crystal structure of CNCbl obtained from the CCSD was used as the source of the initial coordinates.²¹² CNCbl was modified by replacing the corrin side chains by H atoms and the α ligand was changed to imidazole (im) while the

β ligands comprised either F, Cl, Br, SeCN or CH_3 , as illustrated in **Figure 9.2**. The modified corrin ring of B_{12} cofactors have been demonstrated in previous studies as appropriate for exploring structural and electronic properties.⁶⁹ The iodide ion was not included in this study as the 6-31+G(d,p) basis set proved inadequate for describing the large iodo-cobalamin model.

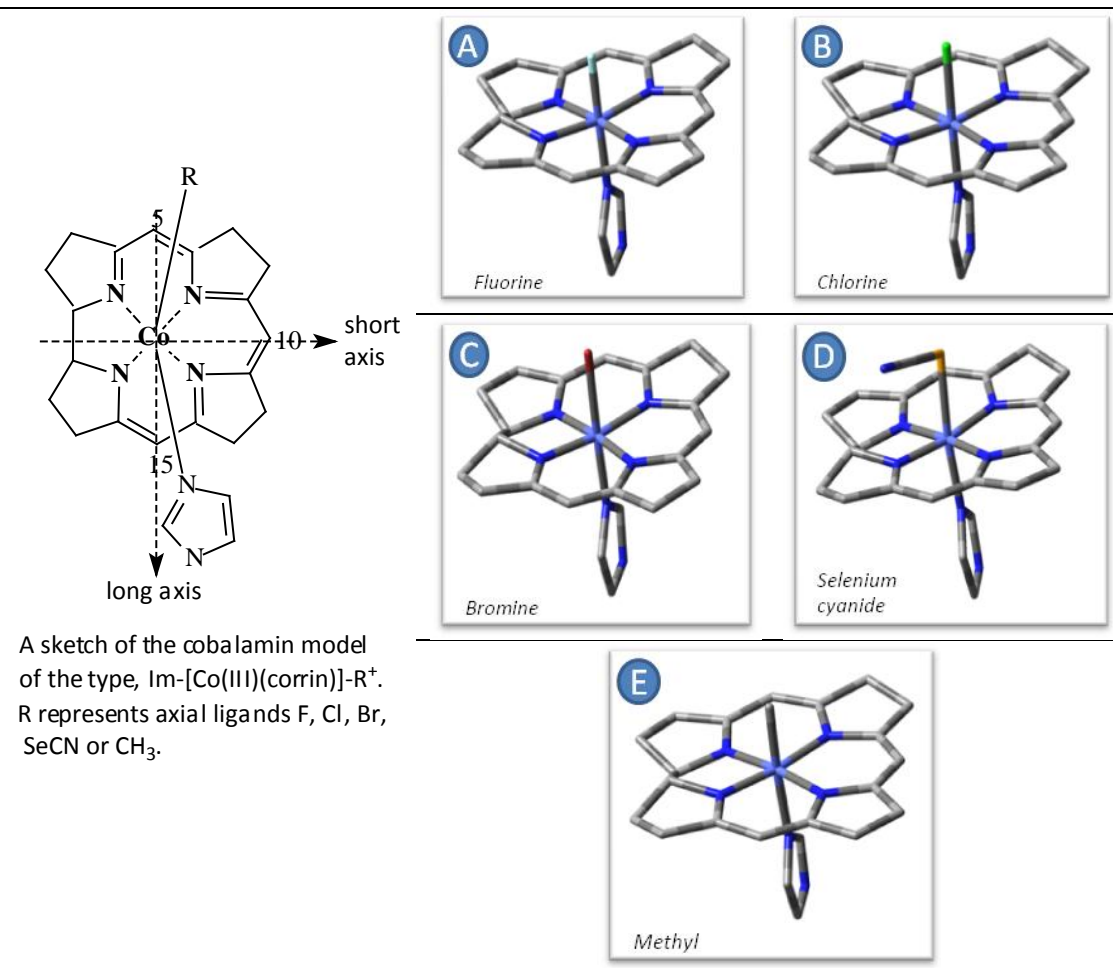


Figure 9.2: Models A–E of the type, $[\text{Im-(Co(III)(corrin))}\text{-R}]^n$, used in the DFT and TD-DFT calculations

9.3 METHOD

A full geometry optimisation was performed for structures A–E (**Figure 9.2**) employing the BP86 functional with the 6-31+G(d,p) basis set. For each optimised geometry, harmonic frequencies were calculated ensuring that a genuine minimum was reached for each of the structures. The TD-DFT vertical excitation energies together with the oscillator strengths were calculated for models A–E for the 30 lowest excited electronic states. These 30 excited states are not sufficient for reproducing the dominant features of the spectra of B₁₂ analogues for which experimental spectra are available but are enough to describe the high energy region of the spectra. These calculations were carried out for a single molecule in the gas phase without interaction from the environment, and for solvent effects the polarizable continuum model (PCM) from Tomasi³²⁸ was used as implemented in the Gaussian 09 software.²¹⁶ The absorption and circular dichroism spectra and molecular orbitals (MOs) were generated using the Chemcraft software.¹⁹⁷ For the description of the transition, the natural transition orbitals (NTOs) of Martin³²⁹ were calculated with the nancy_ex_NTO code³³⁰ from the nancy software.

9.4 RESULTS AND DISCUSSION

The TD-DFT absorption spectra, together with experimental absorption by Chemaly¹¹⁹ and Perry and Marques³¹⁵ are available for models A–C and D–E, respectively. Although the α ligands are different in the models used for the computational and experimental methods, that is, imidazole and dimethylbenzimidazole respectively, previous DFT calculations have reported a change in the lower axial ligand to have a minor influence on the calculated properties.^{48,331} Thus, when comparing the theoretical and experimental data, the computed absorption spectrum gives a fair representation of all of the salient features and trends observed experimentally.

In this chapter, the *cis* influence of the β axial ligand in cobalamin chemistry was examined by calculating and analysing the absorption spectra of model types $[\text{Im-(Co(III)(corrin))}\text{-R}]^{n+}$, where the β ligand is substituted by F, Cl, Br, SeCN or CH₃. This chapter reports on the electron distribution in the system and in the corrin as the nature of the β ligand is changed.

In addition, Chemaly¹¹⁹ obtained a number of experimental absorption spectra for a variety of cobalamins and discussed the existence of a broad absorption band (band A) appearing in the long wavelength region. Chemaly described band A as a ligand-to-metal charge transfer (LMCT) transition from a π orbital in the corrin ring to the Co(III) metal and showed a correlation of the shift of this band with the spectrochemical series.¹¹⁹ The calculations conducted in this chapter will be used to interpret the experimental results obtained by Chemaly. Kozłowski and co-workers³²³ concluded that the $S_0 \rightarrow S_1$ state transition of the MeCbl was a MLCT transition. Therefore, emphasis will be placed in describing the bands in the higher wavelength region.

While experimental data are only available for the models with F, Cl, Br, and SeCN as β ligands, both experimental and TD-DFT data for the model with MeCbl are readily available. Therefore, TD-DFT calculations were primarily conducted on MeCbl for validating the current method used in this chapter.

(a) [Imidazole-(Co(III)(corrin))-X]⁺ where X = F, Cl and Br

TD-DFT spectra in vacuo and methanol for models, **Figure 9.2, A-C**, were calculated. The solvent PCM calculations were performed so that the results could be reproduced closer to experimental conditions. It was found that the general shape of the spectra remained unchanged with or without the solvent but the oscillator strength of the transition of the α and β bands were stronger with the solvent. These spectral bands were also found to shift to the blue region of the spectra, shown in **Figure 9.3**, with solvent.

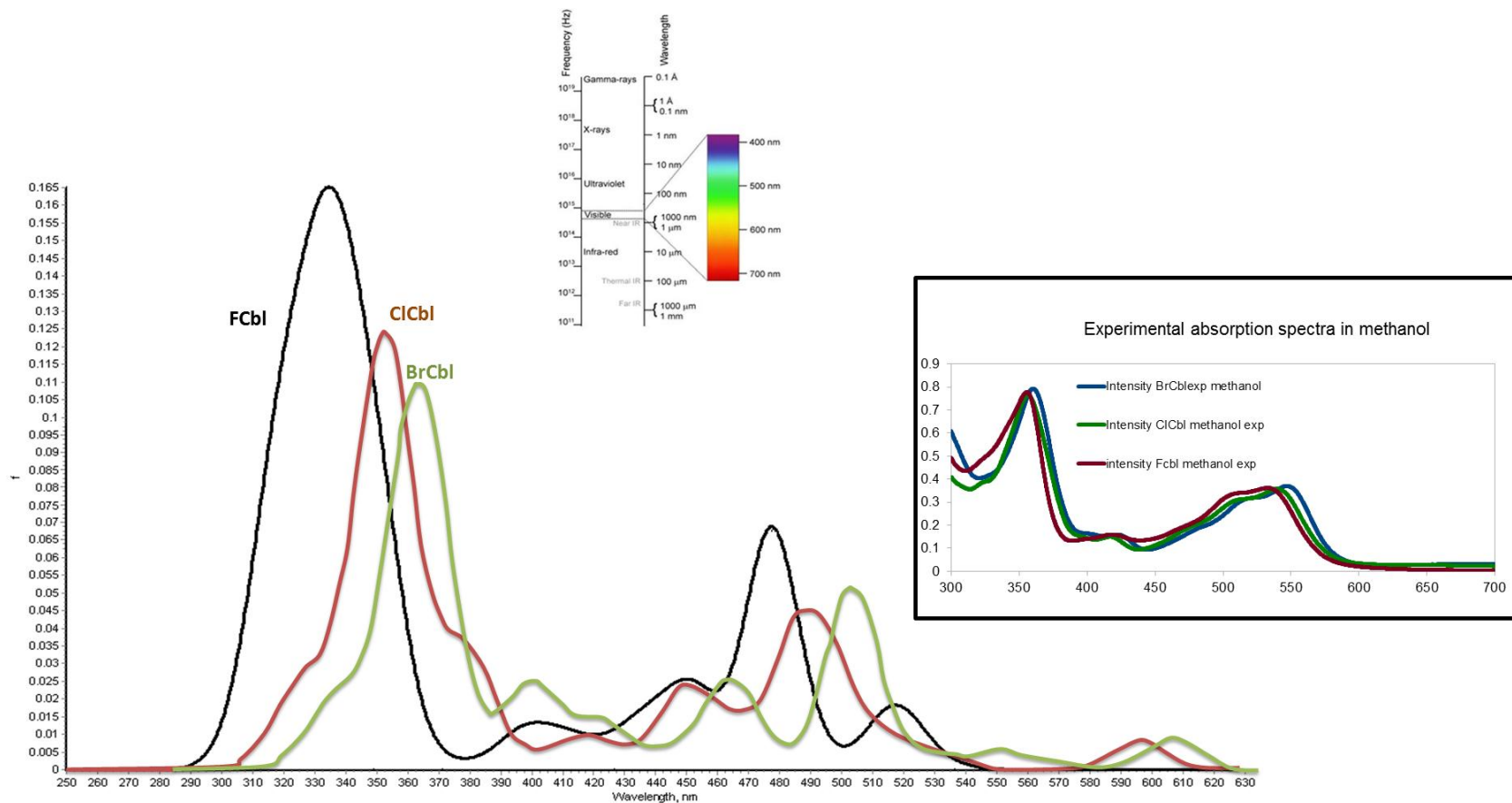


Figure 9.3: Comparisons of distinctive spectral features in simulated and experimental absorption spectra for models A, B and C in vacuo and methanol (insert). The electromagnetic spectrum was obtained from reference 332.

Although the gap between the α and γ band was not well reproduced, enough information was gathered from the TD-DFT calculations to interpret the experimental results.

The first transition state in ClCbl and BrCbl has a very small oscillator strength of 0.009 and 0.001 respectively, shown in **Tables 9.1** and **9.2**. This state corresponds to the band A described by Chémaly.¹¹⁹ The observation of the NTO (see **Figures 9.4** and **9.5**) of this state shows an electronic transfer from an electron on the π of the corrin, π on the halogen and the d_{xz} of the Co to the d_z^2 of the Co forming σ -antibonding orbital with the axial ligands.

In order to describe the polarization of the electronic transitions, the NTO involved in the transition is assessed and classed according to the symmetry with respect to the pseudo mirror plane orientated perpendicular to the $\text{C}_5\text{-C}_{15}$ axis and containing the Co-C_{10} axis. If the two NTOs have the same symmetry, the transition is said to be polarised along the Co-C_{10} vector, or else polarised along the $\text{C}_5\text{-C}_{15}$ vector. Therefore, the band A in BrCbl and ClCbl is polarised along the $\text{C}_5\text{-C}_{15}$ vector.

Table 9.1: TD-BP86 vertical electronic excitation energies (E), the corresponding oscillator strengths (f), and description of dominant configurations for the $[\text{Im-(Co(III)(corrin))}\text{-Cl}]^+$ complex

S_0 to State	Λ /nm	E (eV)	f	Coeff	Character
S ₁	599.30	2.0688	0.0085	0.6932	H ($d_{xz}/\pi_{xCl}/\pi_{cor}$) \rightarrow L ($d_z^2/n/\sigma_{Cl}^*/\sigma_{Na(im)}^*$)
S ₂	582.19	2.1296	0.0002	0.6901	H - 1 ($d_{yz}/\pi_{cor}/\pi_{yCl}$) \rightarrow L ($d_z^2/n/\sigma_{Cl}^*/\sigma_{Na(im)}^*$)
S ₃	542.55	2.2852	0.0002	0.6522	H - 2 (d_{xz}/π_{xCl}) \rightarrow L ($d_z^2/n/\sigma_{Cl}^*/\sigma_{Na(im)}^*$)
S ₄	535.71	2.3144	0.0038	0.5422	H - 2 (d_{xz}/π_{xCl}) \rightarrow L + 1 (d_{yz}/π_{cor}^*)
S ₅	519.13	2.3883	0.0085	0.5972	H - 1 ($d_{yz}/\pi_{cor}/\pi_{yCl}$) \rightarrow L + 1 (d_{yz}/π_{cor}^*)
S ₆	500.42	2.4776	0.0245	0.5194	H - 3 ($d_{yz}/\pi_{cor}/\pi_{yCl}$) \rightarrow L ($d_z^2/n/\sigma_{Cl}^*/\sigma_{Na(im)}^*$)
S ₇	488.01	2.5406	0.0351	0.4340	H - 3 ($d_{yz}/\pi_{cor}/\pi_{yCl}$) \rightarrow L ($d_z^2/n/\sigma_{Cl}^*/\sigma_{Na(im)}^*$)
S ₈	467.26	2.6534	0.0121	0.6436	H ($d_{xz}/\pi_{xCl}/\pi_{cor}$) \rightarrow L + 2 (d_{xy}/n)
S ₉	451.76	2.7444	0.0215	0.5692	H - 3 ($d_{yz}/\pi_{cor}/\pi_{yCl}$) \rightarrow L + 3 (d_{xz}/π_{cor}^*)
S ₁₀	435.96	2.8439	0.0013	0.5903	H - 1 ($d_{yz}/\pi_{cor}/\pi_{yCl}$) \rightarrow L + 2 (d_{xy}/n)
S ₁₁	424.40	2.9214	0.0070	0.5647	H - 2 (d_{xz}/π_{xCl}) \rightarrow L + 2 (d_{xy}/n)
S ₁₂	414.53	2.9909	0.0035	0.3760	H - 4 ($d_x^2 - y^2/\pi_{xCl}/\pi_{cor}$) \rightarrow L + 1 (d_{yz}/π_{cor}^*)
S ₁₃	410.58	3.0198	0.0011	0.4084	H - 5 ($d_{xz}/\pi_{xCl}/\pi_{cor}$) \rightarrow L ($d_z^2/n/\sigma_{Cl}^*/\sigma_{Na(im)}^*$)
S ₁₄	06.00	3.0538	0.0004	0.5552	H - 3 ($d_{yz}/\pi_{cor}/\pi_{yCl}$) \rightarrow L + 2 (d_{xy}/n)
S ₁₅	399.87	3.1006	0.0023	0.4545	H - 5 ($d_{xz}/\pi_{xCl}/\pi_{cor}$) \rightarrow L + 1 (d_{yz}/π_{cor}^*)
S ₁₆	384.01	3.2287	0.0154	0.4585	H - 2 (d_{xz}/π_{xCl}) \rightarrow L + 3 (d_{xz}/π_{cor}^*)
S ₁₇	380.39	3.2594	0.0197	0.3774	H - 2 (d_{xz}/π_{xCl}) \rightarrow L + 3 (d_{xz}/π_{cor}^*)
S ₁₈	365.76	3.3898	0.0009	0.6844	H - 6 ($\pi_{im}/3d_{yz}$) \rightarrow L ($d_z^2/n/\sigma_{Cl}^*/\sigma_{Na(im)}^*$)
S ₁₉	362.29	3.4223	0.0376	0.37667	H - 4 ($d_x^2 - y^2/\pi_{xCl}/\pi_{cor}$) \rightarrow L ($d_z^2/n/\sigma_{Cl}^*/\sigma_{Na(im)}^*$)
S ₂₀	359.24	3.4513	0.0011	0.6326	H - 4 ($d_x^2 - y^2/\pi_{xCl}/\pi_{cor}$) \rightarrow L + 2 (d_{xy}/n)
S ₂₁	354.77	3.4947	0.0702	0.3599	H ($d_{xz}/\pi_{xCl}/\pi_{cor}$) \rightarrow L + 3 (d_{xz}/π_{cor}^*)
S ₂₂	353.27	3.5096	0.0215	0.5517	H - 3 ($d_{yz}/\pi_{cor}/\pi_{yCl}$) \rightarrow L + 3 (d_{xz}/π_{cor}^*)
S ₂₃	347.56	3.5673	0.0059	0.4611	H - 7 ($d_{yz}/\pi_{C5/15\text{-cor}}/\pi_{yCl}$) \rightarrow L ($d_z^2/n/\sigma_{Cl}^*/\sigma_{Na(im)}^*$)
S ₂₄	346.74	3.5757	0.0065	0.5237	H - 6 (π_{im}/d_{yz}) \rightarrow L + 1 (d_{yz}/π_{cor}^*)
S ₂₅	336.00	3.6900	0.0052	0.5522	H ($d_{xz}/\pi_{xCl}/\pi_{cor}$) \rightarrow L + 4 (π_{cor}^*/π_{im}^*)
S ₂₆	332.72	3.7263	0.0039	0.4369	H - 8 ($d_{xz}/\pi_{xCl}/\pi_{cor}/\pi_{im}$) \rightarrow L ($d_z^2/n/\sigma_{Cl}^*/\sigma_{Na(im)}^*$)
S ₂₇	331.72	3.7376	0.0101	0.4838	H - 8 ($d_{xz}/\pi_{xCl}/\pi_{cor}/\pi_{im}$) \rightarrow L ($d_z^2/n/\sigma_{Cl}^*/\sigma_{Na(im)}^*$)
S ₂₈	329.33	3.7647	0.0031	0.4604	H - 5 ($d_{xz}/\pi_{xCl}/\pi_{cor}$) \rightarrow L + 2 (d_{xy}/n)
S ₂₉	322.57	3.8437	0.0063	0.6490	H - 2 (d_{xz}/π_{xCl}) \rightarrow L + 4 (π_{cor}^*/π_{im}^*)
S ₃₀	320.60	3.8672	0.0022	0.5697	H - 4 ($d_x^2 - y^2/\pi_{xCl}/\pi_{cor}$) \rightarrow L + 3 (d_{xz}/π_{cor}^*)
Experimental results ³¹⁵					Experimental results ¹¹⁹
$\alpha\beta$ - 514 nm					$\alpha\beta$ - 540 nm
γ - 353 nm					γ - 356 nm

Table 9.2: TD-BP86 vertical electronic excitation energies (E), the corresponding oscillator strengths (f), and description of dominant configurations for the $[\text{Im-(Co(III)(corrin))}\text{-Br}]^+$ complex

S_0 to State	Λ /nm	E (eV)	f	Coeff	Character
S ₁	602.31	2.0585	0.0009	0.6735	H ($d_{xz}/\pi_{\text{cor}}/\pi_{\text{xBr}}/\sigma_{\text{Na(im)}}$) → L ($d_z^2/\sigma_{\text{Br}}^*/\sigma_{\text{Na(im)}}^*/n$)
S ₂	587.86	2.1091	0.0004	0.6817	H - 1 ($d_{yz}/\pi_{\text{cor}}/\pi_{\text{yBr}}$) → L ($d_z^2/\sigma_{\text{Br}}^*/\sigma_{\text{Na(im)}}^*/n$)
S ₃	565.85	2.1911	0.0007	0.4093	H - 2 (d_{xz}/π_{xBr}) → L + 1 ($d_{yz}/\pi_{\text{cor}}^*$)
				0.4039	H - 2 (d_{xz}/π_{xBr}) → L ($d_z^2/\sigma_{\text{Br}}^*/\sigma_{\text{Na(im)}}^*/n$)
S ₄	561.00	2.2101	0.0018	0.5144	H - 2 (d_{xz}/π_{xBr}) → L ($d_z^2/\sigma_{\text{Br}}^*/\sigma_{\text{Na(im)}}^*/n$)
S ₅	546.14	2.2702	0.0050	0.5817	H - 1 ($d_{yz}/\pi_{\text{cor}}/\pi_{\text{yBr}}$) → L + 1 ($d_{yz}/\pi_{\text{cor}}^*$)
S ₆	524.58	2.3635	0.0051	0.6430	H - 3 ($d_{xz}/\pi_{\text{cor}}/\pi_{\text{yBr}}$) → L ($d_z^2/\sigma_{\text{Br}}^*/\sigma_{\text{Na(im)}}^*/n$)
S ₇	499.86	2.4804	0.0535	0.4684	H ($d_{xz}/\pi_{\text{cor}}/\pi_{\text{xBr}}/\sigma_{\text{Na(im)}}$) → L + 1 ($d_{yz}/\pi_{\text{cor}}^*$)
				0.4062	H - 2 (d_{xz}/π_{xBr}) → L + 1 ($d_{yz}/\pi_{\text{cor}}^*$)
S ₈	472.44	2.6243	0.0034	0.6365	H ($d_{xz}/\pi_{\text{cor}}/\pi_{\text{xBr}}/\sigma_{\text{Na(im)}}$) → L + 2 (d_{xy}/n)
S ₉	460.98	2.6896	0.0243	0.5348	H - 3 ($d_{xz}/\pi_{\text{cor}}/\pi_{\text{yBr}}$) → L + 1 ($d_{yz}/\pi_{\text{cor}}^*$)
S ₁₀	452.06	2.7426	0.0003	0.5648	H - 1 ($d_{yz}/\pi_{\text{cor}}/\pi_{\text{yBr}}$) → L + 2 ($d_{xy}/\sigma_{\text{cor}}^*$)
S ₁₁	443.10	2.7981	0.0052	0.6460	H - 2 (d_{xz}/π_{xBr}) → L + 2 ($d_{xy}/\sigma_{\text{cor}}^*$)
S ₁₂	428.15	2.8958	0.0012	0.4377	H - 4 ($d_x^2 - y^2/\pi_{\text{cor}}/\pi_{\text{xBr}}$) → L ($d_z^2/\sigma_{\text{Br}}^*/\sigma_{\text{Na(im)}}^*/n$)
S ₁₃	420.73	2.9469	0.0114	0.5707	H - 4 ($d_x^2 - y^2/\pi_{\text{cor}}/\pi_{\text{xBr}}$) → L + 1 ($d_{yz}/\pi_{\text{cor}}^*$)
S ₁₄	415.16	2.9864	0.0005	0.5024	H - 3 ($d_{xz}/\pi_{\text{cor}}/\pi_{\text{yBr}}$) → L + 2 ($d_{xy}/\sigma_{\text{cor}}^*$)
S ₁₅	410.43	3.0209	0.0031	0.4022	H - 1 ($d_{yz}/\pi_{\text{cor}}/\pi_{\text{yBr}}$) → L + 3 ($d_{xz}/\pi_{\text{cor}}^*$)
S ₁₆	399.84	3.1009	0.0118	0.4240	H - 2 (d_{xz}/π_{xBr}) → L + 3 ($d_{xz}/\pi_{\text{cor}}^*$)
S ₁₇	395.30	3.1365	0.0138	0.4173	H - 2 (d_{xz}/π_{xBr}) → L + 3 ($d_{xz}/\pi_{\text{cor}}^*$)
S ₁₈	370.52	3.3462	0.0242	0.4146	H - 5 ($d_x^2 - y^2/\pi_{\text{cor}}/\pi_{\text{xBr}}$) → L ($d_z^2/\sigma_{\text{Br}}^*/\sigma_{\text{Na(im)}}^*/n$)
S ₁₉	367.29	3.3757	0.0007	0.6909	H - 6 (π_{im}/d_{yz}) → L ($3d_z^2/\sigma_{\text{Br}}^*/\sigma_{\text{Na(im)}}^*/n$)
S ₂₀	363.41	3.4117	0.0128	0.5872	H - 3 ($d_{xz}/\pi_{\text{cor}}/\pi_{\text{yBr}}$) → L + 3 ($d_{xz}/\pi_{\text{cor}}^*$)
S ₂₁	362.32	3.4220	0.0494	0.3550	H - 4 ($d_x^2 - y^2/\pi_{\text{cor}}/\pi_{\text{xBr}}$) → L + 2 ($d_{xy}/\sigma_{\text{cor}}^*$)
S ₂₂	358.44	3.4590	0.0315	0.4321	H - 4 ($d_x^2 - y^2/\pi_{\text{cor}}/\pi_{\text{xBr}}$) → L + 2 ($d_{xy}/\sigma_{\text{cor}}^*$)
S ₂₃	353.98	3.5026	0.0079	0.4692	H - 7 ($d_{yz}/\pi_{\text{yBr}}/\pi_{\text{im}}/\pi_{\text{C5/15-cor}}$) → L ($d_z^2/\sigma_{\text{Br}}^*/\sigma_{\text{Na(im)}}^*/n$)
				0.4210	H - 5 ($d_x^2 - y^2/\pi_{\text{cor}}/\pi_{\text{xBr}}$) → L + 2 ($d_{xy}/\sigma_{\text{cor}}^*$)
S ₂₄	349.76	3.5449	0.0043	0.6474	H - 6 (π_{im}/d_{yz}) → L + 1 ($d_{yz}/\pi_{\text{cor}}^*$)
S ₂₅	339.34	3.6537	0.0058	0.5499	H ($d_{xz}/\pi_{\text{cor}}/\pi_{\text{xBr}}/\sigma_{\text{Na(im)}}$) → L + 4 ($\pi_{\text{cor}}^*/\pi_{\text{im}}^*$)
S ₂₆	337.13	3.6776	0.0074	0.6270	H - 1 ($d_{yz}/\pi_{\text{cor}}/\pi_{\text{yBr}}$) → L + 4 ($\pi_{\text{cor}}^*/\pi_{\text{im}}^*$)
S ₂₇	334.14	3.7105	0.0037	0.5175	H - 8 ($d_{xz}/\pi_{\text{xBr}}/\pi_{\text{cor}}/\pi_{\text{im}}$) → L ($d_z^2/\sigma_{\text{Br}}^*/\sigma_{\text{Na(im)}}^*/n$)
S ₂₈	332.99	3.7234	0.0016	0.4044	H - 8 ($d_{xz}/\pi_{\text{xBr}}/\pi_{\text{cor}}/\pi_{\text{im}}$) → L ($d_z^2/\sigma_{\text{Br}}^*/\sigma_{\text{Na(im)}}^*/n$)
				0.3622	H - 2 (d_{xz}/π_{xBr}) → L + 4 ($\pi_{\text{cor}}^*/\pi_{\text{im}}^*$)
S ₂₉	330.73	3.7488	0.0018	0.4255	H - 2 (d_{xz}/π_{xBr}) → L + 4 ($\pi_{\text{cor}}^*/\pi_{\text{im}}^*$)
S ₃₀	324.89	3.8162	0.0023	0.6131	H - 1 ($d_{yz}/\pi_{\text{cor}}/\pi_{\text{yBr}}$) → L + 5 ($\pi_{\text{cor}}^*/\pi_{\text{im}}^*$)
Experimental results ¹¹⁹				$\alpha\beta - 547 \text{ nm}$	$\gamma - 360 \text{ nm}$

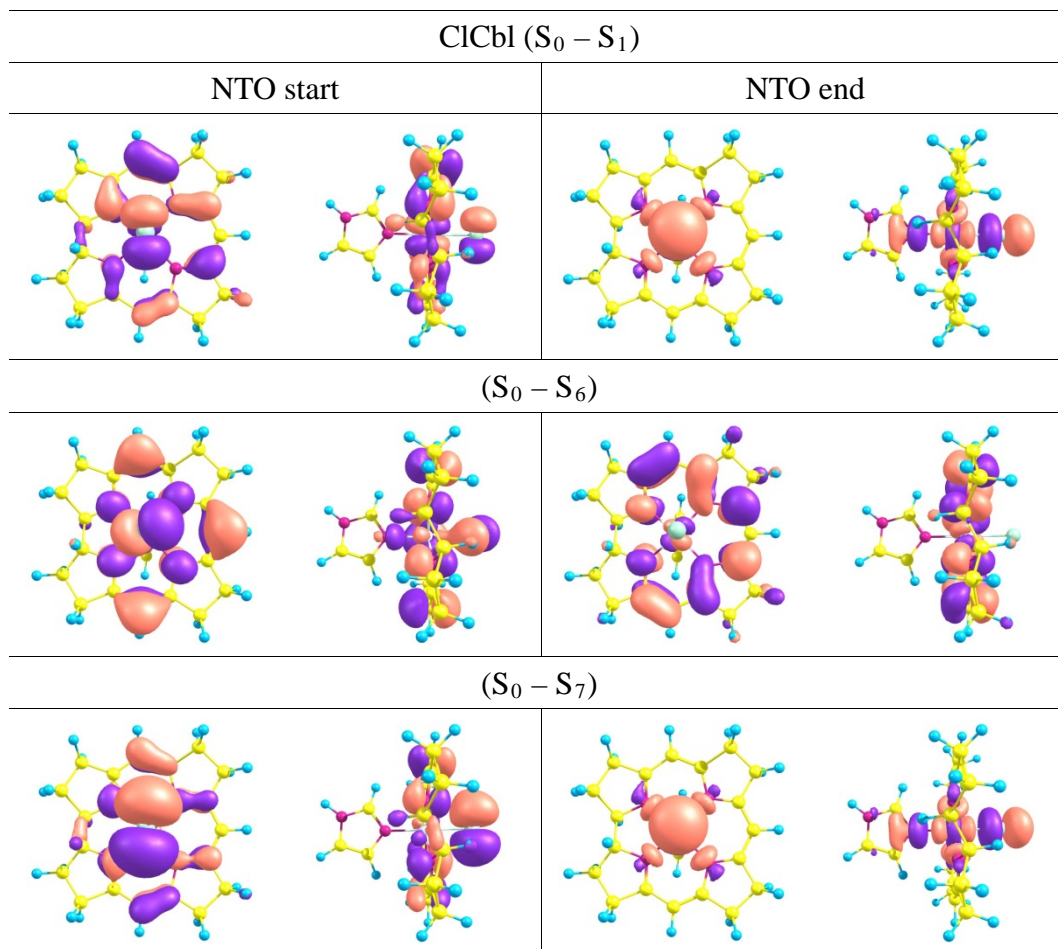


Figure 9.4: Natural Transition orbitals for the main transition bands α and band A for ClCbl in vacuo.

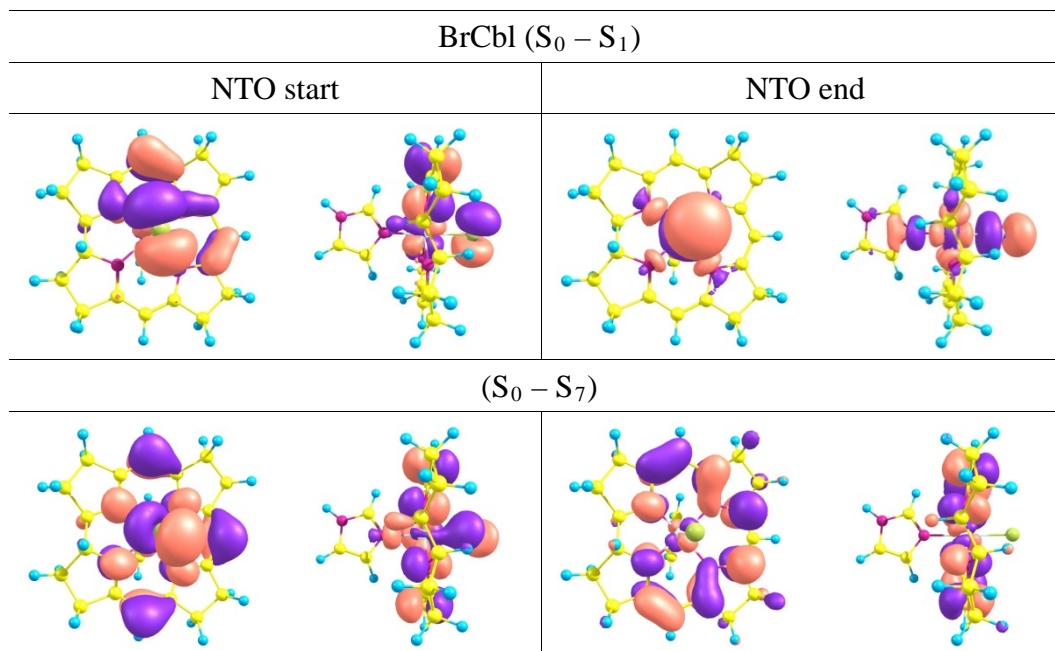


Figure 9.5: Natural Transition orbitals for the main transition bands α and band A for BrCbl in vacuo.

For the experimental result of FCbl, band A is not observed in the long wavelength region. In **Figure 9.3** the corresponding state for band A is state 3 (**Table 9.3**). This state has an oscillator strength of 0.007 (very close to that of ClCbl and BrCbl) and corresponds to the same character as the S_0-S_1 transition in ClCbl and BrCbl. The blue shift of this state brings the transition close to the next significant transition (state 6, $f = 0.068$). This transition does not appear in the experimental spectra as it already forms part of the α band.

Table 9.3: TD-BP86 vertical electronic excitation energies (E), the corresponding oscillator strengths (f), and description of dominant configurations for the $[\text{Im}[\text{Co(III)(corrin)}]\text{-F}^+]$ complex

S_0 to State	Λ /nm	E (eV)	f	Coeff	Character
S ₁	536.40	2.3114	0.0007	0.5658	H-1 (d_{xz}/π_{xF}) \rightarrow L ($\pi^*_{\text{cor}}/d_{yz}$)
S ₂	526.70	2.3540	0.0002	0.6815	H ($\pi_{\text{cor}}/d_{yz}/\pi_{yF}$) \rightarrow L + 1 ($\sigma^*_F/d_z^2/\sigma^*_{\text{im}}$)
S ₃	522.06	2.3749	0.0066	0.5271	H-1 ($\pi_{\text{cor}}/d_{xz}/\pi_{xF}$) \rightarrow L + 1 ($\sigma^*_F/d_z^2/\sigma^*_{\text{im}}$)
S ₄	514.93	2.4078	0.0129	0.4814	H ($\pi_{\text{cor}}/d_{yz}/\pi_{yF}$) \rightarrow L ($\pi^*_{\text{cor}}/d_{yz}$)
				0.4465	H-1 ($\pi_{\text{cor}}/d_{xz}/\pi_{xF}$) \rightarrow L + 1 ($\sigma^*_F/d_z^2/\sigma^*_{\text{im}}$)
S ₅	492.17	2.5191	0.0028	0.6206	H-2 (d_{xz}/π_{xF}) \rightarrow L + 1 ($\sigma^*_F/d_z^2/\sigma^*_{\text{im}}$)
S ₆	477.33	2.5974	0.0680	0.5275	H-1 ($\pi_{\text{cor}}/d_{xz}/\pi_{xF}$) \rightarrow L ($\pi^*_{\text{cor}}/d_{yz}$)
S ₇	451.67	2.7450	0.0222	0.6306	H-1 ($\pi_{\text{cor}}/d_{xz}/\pi_{xF}$) \rightarrow L + 2 ($\sigma^*_{\text{cor}}/d_{xy}$)
S ₈	436.59	2.8398	0.0120	0.5392	H-3 ($\pi_{\text{cor}}/d_{xy}/\pi_{yF}$) \rightarrow L ($\pi^*_{\text{cor}}/d_{yz}$)
S ₉	426.91	2.9042	0.0019	0.5094	H ($\pi_{\text{cor}}/d_{yz}/\pi_{yF}$) \rightarrow L + 2 ($\sigma^*_{\text{cor}}/d_{xy}$)
S ₁₀	421.49	2.9416	0.0024	0.5486	H-3 ($\pi_{\text{cor}}/d_{xy}/\pi_{yF}$) \rightarrow L + 1 ($\sigma^*_F/d_z^2/\sigma^*_{\text{im}}$)
S ₁₁	410.74	3.0186	0.0075	0.5226	H-4 ($\pi_{\text{cor}}/d_x^2\text{-}d_y^2/\pi_{yF}$) \rightarrow L ($\pi^*_{\text{cor}}/d_{yz}$)
S ₁₂	397.17	3.1217	0.0102	0.6593	H ($\pi_{\text{cor}}/d_{yz}/\pi_{yF}$) \rightarrow L + 3($\pi^*_{\text{cor}}/d_{xz}$)
S ₁₃	392.69	3.1573	0.0001	0.4865	H-2 (d_{xz}/π_{xF}) \rightarrow L + 2 ($\sigma^*_{\text{cor}}/d_{xy}$)
S ₁₄	378.06	3.2795	0.0011	0.6258	H-3 ($\pi_{\text{cor}}/d_{xy}/\pi_{yF}$) \rightarrow L + 2 ($\sigma^*_{\text{cor}}/d_{xy}$)
S ₁₅	371.27	3.3395	0.0010	0.6213	H-2 (d_{xz}/π_{xF}) \rightarrow L + 3 ($\pi^*_{\text{cor}}/d_{xz}$)
S ₁₆	357.34	3.4697	0.0050	0.6859	H-4 ($\pi_{\text{cor}}/d_x^2\text{-}d_y^2/\pi_{yF}$) \rightarrow L + 2 ($\sigma^*_{\text{cor}}/d_{xy}$)
S ₁₇	351.68	3.5255	0.0238	0.4892	H-5 ($\pi_{\text{cor}}/d_{xz}/\pi_{xF}$) \rightarrow L ($\pi^*_{\text{cor}}/3d_{yz}$)
S ₁₈	349.29	3.5496		0.5218	H-5($\pi_{\text{cor}}/d_{xz}/\pi_{xF}$) \rightarrow L + 1 ($\sigma^*_F/3d_z^2/\sigma^*_{\text{im}}$)
			0.0291		
S ₁₉	346.82	3.5749	0.0076	0.5841	H-6 (π_{im}) \rightarrow L ($\pi^*_{\text{cor}}/d_{yz}$)
S ₂₀	340.64	3.6398	0.0446	0.4628	H ($\pi_{\text{cor}}/d_{yz}/\pi_{yF}$) \rightarrow L + 4 ($\pi^*_{\text{im}}/\pi^*_{\text{cor}}$)
S ₂₁	337.43	3.6743	0.0044	0.5047	H-6 (π_{im}) \rightarrow L + 1 ($\sigma^*_F/d_z^2/\sigma^*_{\text{im}}$)
S ₂₂	336.59	3.6836	0.0114	0.4276	H-6 (π_{im}) \rightarrow L + 1 ($\sigma^*_F/3d_z^2/\sigma^*_{\text{im}}$)
S ₂₃	333.54	3.7172	0.0687	0.3666	H ($\pi_{\text{cor}}/d_{yz}/\pi_{yF}$) \rightarrow L + 4 ($\pi^*_{\text{im}}/\pi^*_{\text{cor}}$)
S ₂₄	328.51	3.7742		0.4661	H-4 ($\pi_{\text{cor}}/d_x^2\text{-}d_y^2/\pi_{yF}$) \rightarrow L + 1 ($\sigma^*_F/d_z^2/\sigma^*_{\text{im}}$)
			0.0069		
S ₂₅	327.11	3.7903	0.0246	0.4037	H-1 ($\pi_{\text{cor}}/d_{xz}/\pi_{xF}$) \rightarrow L + 4 ($\pi^*_{\text{im}}/\pi^*_{\text{cor}}$)
S ₂₆	320.67	3.8664	0.0152	0.6036	H-2 (d_{xz}/π_{xF}) \rightarrow L + 4 ($\pi^*_{\text{im}}/\pi^*_{\text{cor}}$)
S ₂₇	319.33	3.8827	0.0324	0.5643	H ($\pi_{\text{cor}}/d_{yz}/\pi_{yF}$) \rightarrow L + 5 ($\pi^*_{\text{im}}/\pi^*_{\text{cor}}$)
S ₂₈	316.29	3.9200	0.0154	0.5172	H-5 ($\pi_{\text{cor}}/d_{xz}/\pi_{xF}$) \rightarrow L + 2 ($\sigma^*_{\text{cor}}/d_{xy}$)
S ₂₉	314.87	3.9377	0.0092	0.4483	H-5 ($\pi_{\text{cor}}/d_{xz}/\pi_{xF}$) \rightarrow L + 2 ($\sigma^*_{\text{cor}}/d_{xy}$)
S ₃₀	308.65	4.0170	0.0096	0.5153	H-6 (π_{im}) \rightarrow L + 2 ($\sigma^*_{\text{cor}}/d_{xy}$)
Experimental results ¹¹⁹					
α/β – 532 nm γ – 355 nm (experimental gap between the 2 bands is 177 nm)					

This discrepancy of not observing band A in the spectrum of FCbl as compared to ClCbl and BrCbl can be explained by looking closely at the molecular orbitals of these complexes. **Figure 9.6** shows six orbital levels of the HOMO (H), H-1, H-2 and LUMO (L), L+1 and L+2 (for molecular orbital pictures see **Figures 9.7, 9.8 and 9.9**). The transition of the band A which consists of the H to L transition in BrCbl and ClCbl has the H-1 to L+1 character in FCbl. The final orbital (L in BrCbl and ClCbl and L+1 in FCbl) has a σ antibonding between the Co and the axial ligands. Its energy is much higher in the FCbl complex and therefore becomes the L+1 orbital. At the same time, the H in BrCbl and ClCbl, which has a d_{xz} character and π_x on the halogen, drops in energy to a lesser extent for FCbl. As a result, the band A blue shifts. The former observation confirms a LMCT of the band A, as stated by Chemaly.¹¹⁹

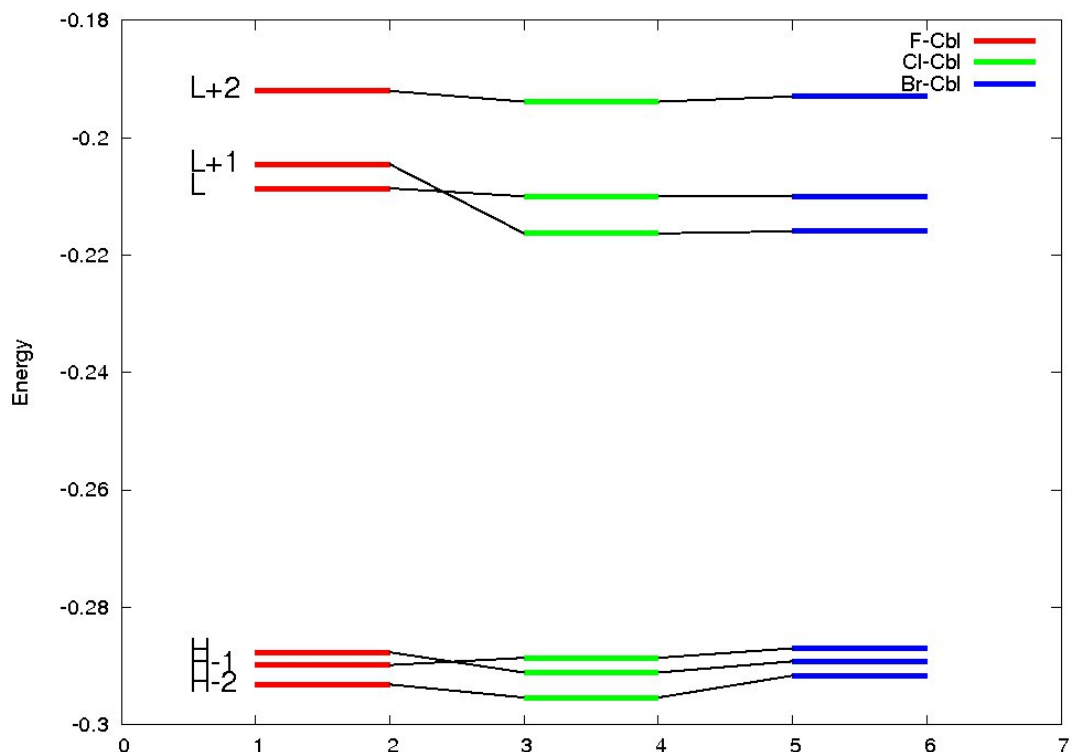


Figure 9.6: MO diagram of the 3 highest occupied orbitals and the 3 lowest unoccupied orbitals.

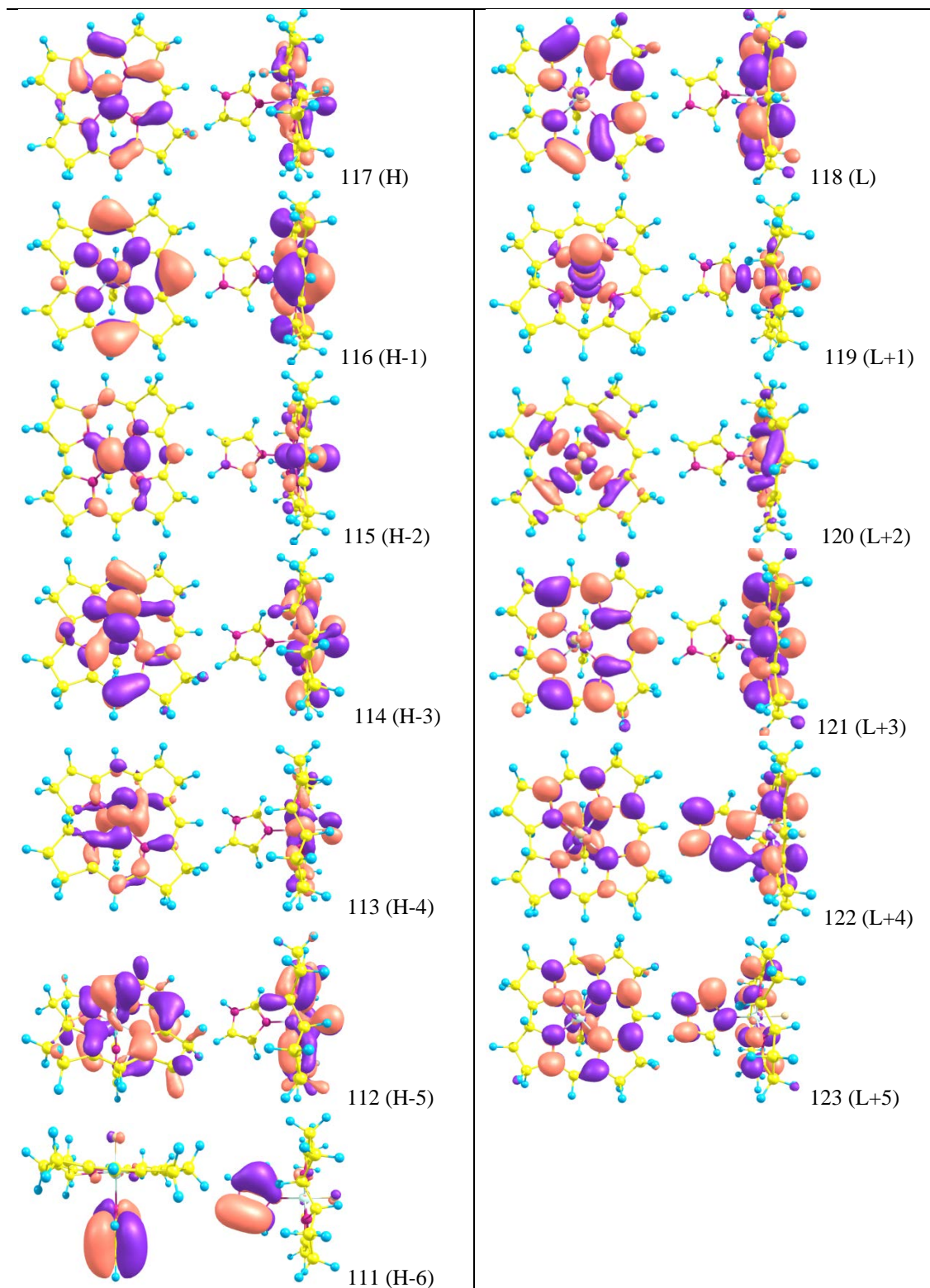


Figure 9.7: Isosurface plots for frontier molecular orbitals in the complex $[\text{Im-(Co(III)(corrin))-F}]^+$.

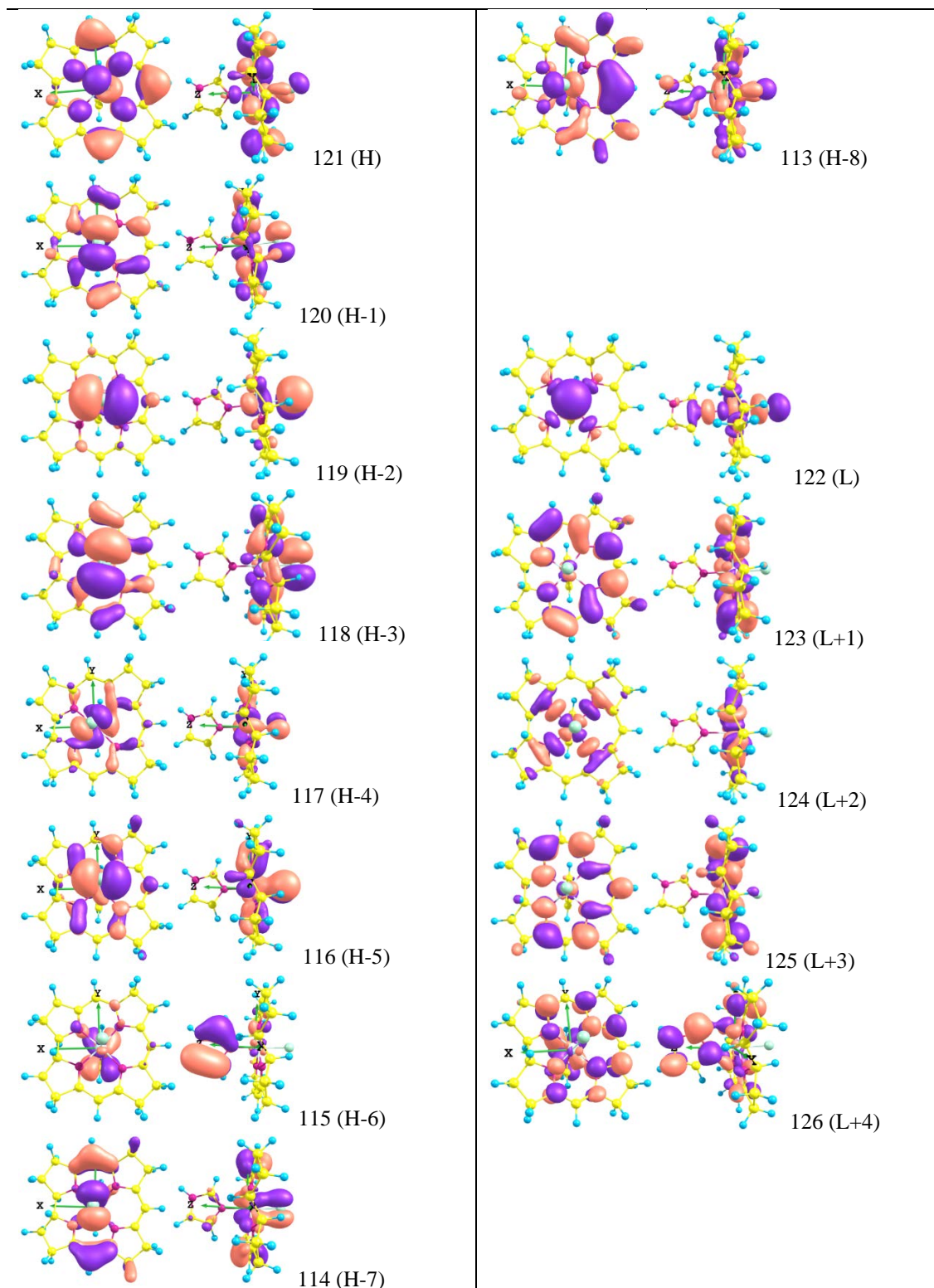


Figure 9.8: Isosurface plots for frontier molecular orbitals in the complex $[\text{Im-(Co(III)corrin)-Cl}]^+$.

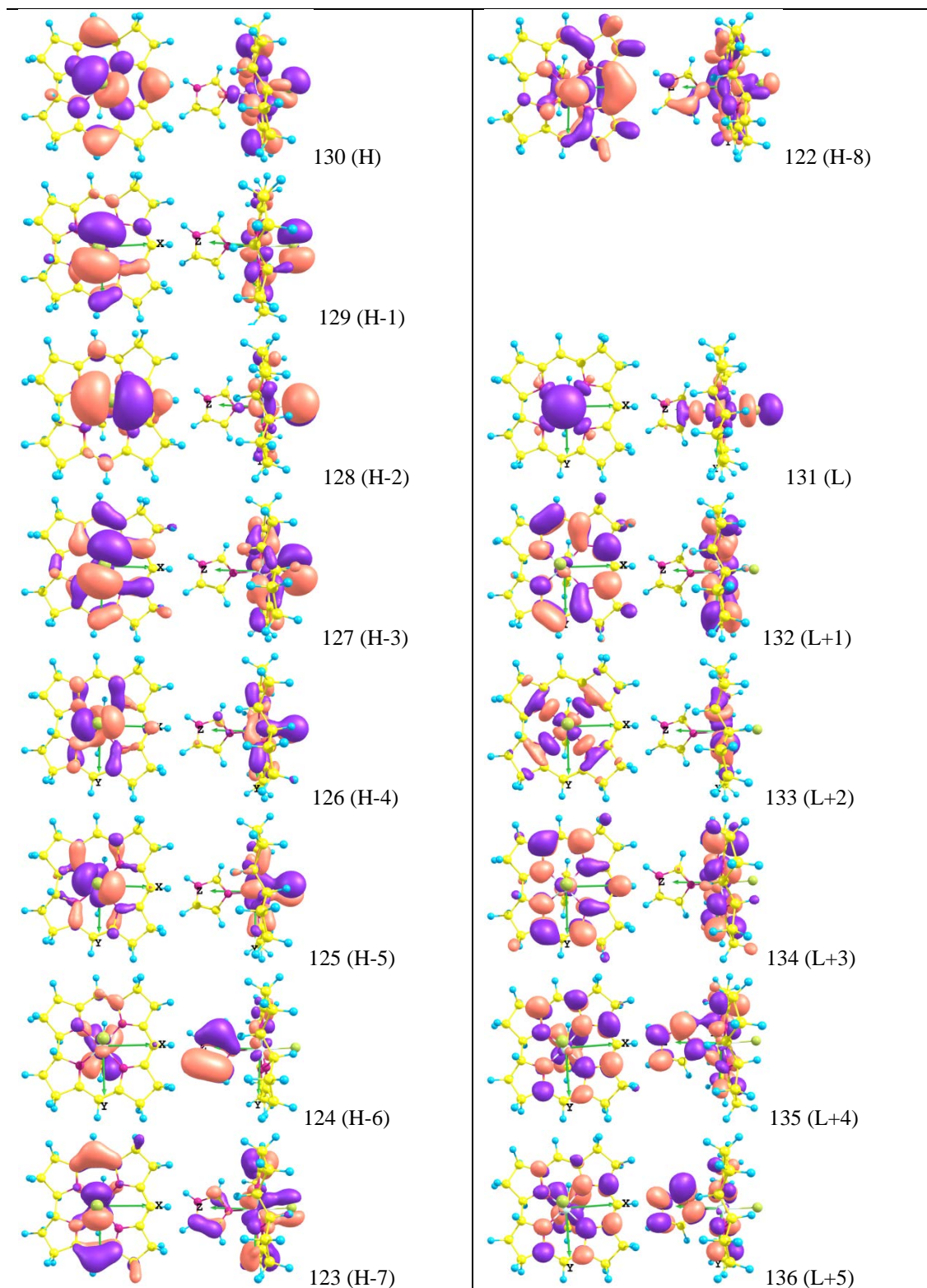


Figure 9.9: Isosurface plots for frontier molecular orbitals in the complex $[\text{Im-(Co(III)corrin)-Br}]^+$.

(b) [Imidazole-(Co(III)(corrin))-X]⁺ complex where X = SeCN or CH₃

The SeCNCbl spectrum (**Figure 9.10**) is interesting as it shows two bands before the α band ($S_0\text{-}S_5$ and $S_0\text{-}S_6$, see **Table 9.4**). The $S_0\text{-}S_1$ transition is red-shifted compared to the $S_0\text{-}S_1$ transition of the halo-cobalamins. The NTO analysis of this band (**Figure 9.11**) shows that it involves a charge transfer from the SeCN axial ligand to the π system of the corrin ring. The second transition $S_0\text{-}S_1$ is concentrated in the Co-SeCN system and does not show a strong electron transfer character. The $S_0\text{-}S_3$ transition has the LMCT character described for the band A of the halogen family. This shows that the band A, or the shoulder of the $\alpha\beta$ band can have different character, and attempting to find a relationship with the spectrochemical series may be very difficult.

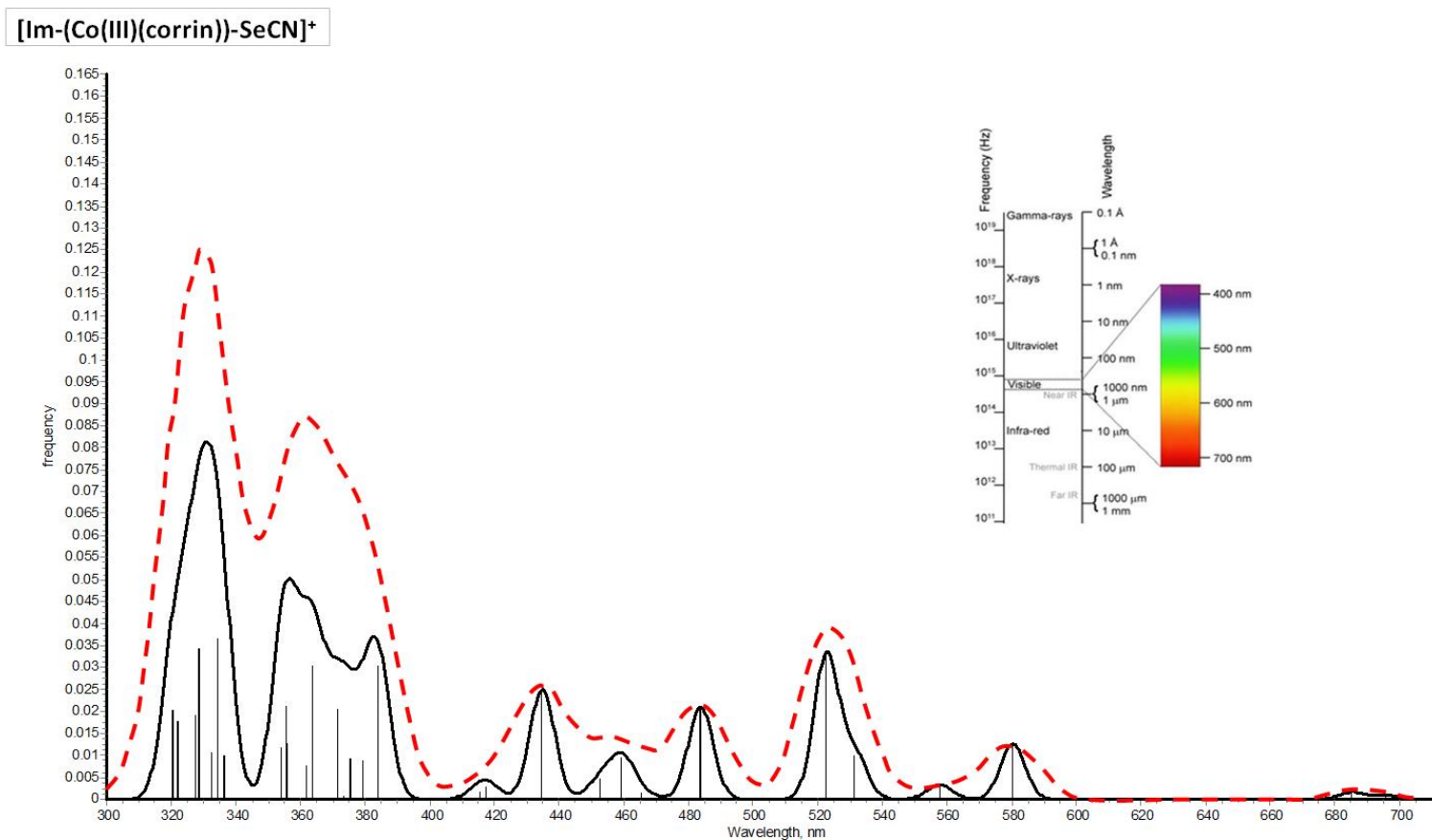


Figure 9.10: Simulated electronic absorption (black and red line) spectra of $[\text{Im}-(\text{Co(III)(corrin)})-\text{SeCN}]^+$ based on 30 first singlet excited states. The black and red line corresponds to a Doppler broadening with a width at half peak of 9 and 20 nm, respectively. The electromagnetic spectrum was obtained from reference 332.

Table 9.4: TD-BP86 vertical electronic excitation energies (E), the corresponding oscillator strengths (f), and description of dominant configurations for the $[\text{Im-(Co(III)(corrin))SeCN}]^+$ complex

S_0 to State	Λ /nm	E (eV)	f	Coeff	Character	
S ₁	695.75	1.7820	0.0008	0.6614	H ($d_{yz}/\pi_{y\text{SeCN}} \rightarrow L + 1(d_{xz}/\pi_{\text{cor}}^*)$)	
S ₂	685.37	1.8090	0.0016	0.6645	H ($d_{yz}/\pi_{y\text{SeCN}} \rightarrow L (d_z^2/\sigma_{\text{SeCN}}^*/\sigma_{\text{Na(im)}}^*/n)$)	
S ₃	580.36	2.1363	0.0125	0.6675	H - 1 ($d_{yz}/\pi_{y\text{SeCN}}/\pi_{\text{cor}}/\sigma_{\text{Na(im)}} \rightarrow L (d_z^2/\sigma_{\text{SeCN}}^*/\sigma_{\text{Na(im)}}^*/n)$)	
S ₄	557.73	2.2230	0.0032	0.6442	H - 2 ($d_{xz}/\pi_{\text{cor}} \rightarrow L (d_z^2/\sigma_{\text{SeCN}}^*/\sigma_{\text{Na(im)}}^*/n)$)	
S ₅	531.51	2.3327	0.0101	0.5746	H ($d_{yz}/\pi_{y\text{SeCN}} \rightarrow L + 2 (d_{x^2-y^2}/\sigma_{\text{cor}}^*)$)	
S ₆	522.69	2.3720	0.0328	0.5526	H - 1 ($d_{yz}/\pi_{y\text{SeCN}}/\pi_{\text{cor}}/\sigma_{\text{Na(im)}} \rightarrow L + 1 (d_{xz}/\pi_{\text{cor}}^*)$)	
S ₇	483.79	2.5628	0.0210	0.5630	H - 2 ($d_{xz}/\pi_{\text{cor}} \rightarrow L + 1 (d_{xz}/\pi_{\text{cor}}^*)$)	
S ₈	465.74	2.6621	0.0013	0.6451	H - 1 ($d_{yz}/\pi_{y\text{SeCN}}/\pi_{\text{cor}}/\sigma_{\text{Na(im)}} \rightarrow L + 2 (d_{x^2-y^2}/\sigma_{\text{cor}}^*)$)	
S ₉	459.50	2.6982	0.0094	0.5322	H ($d_{yz}/\pi_{y\text{SeCN}} \rightarrow L + 3 (d_{yz}/\pi_{\text{cor}}^*)$)	
S ₁₀	452.65	2.7391	0.0045	0.5937	H - 3 ($d_{xz}/\pi_{\text{cor}}/\pi_{y\text{SeCN}} \rightarrow L (d_z^2/\sigma_{\text{SeCN}}^*/\sigma_{\text{Na(im)}}^*/n)$)	
S ₁₁	434.80	2.8515	0.0250	0.6455	H - 3 ($d_{xz}/\pi_{\text{cor}}/\pi_{y\text{SeCN}} \rightarrow L + 1 (d_{xz}/\pi_{\text{cor}}^*)$)	
S ₁₂	417.84	2.9673	0.0028	0.5338	H - 4 ($d_{xy}/\pi_{\text{cor}}/\pi_{\text{SeCN}} \rightarrow L + 1 (d_{xz}/\pi_{\text{cor}}^*)$)	
S ₁₃	415.64	2.9830	0.0018	0.4966	H - 2 ($d_{xz}/\pi_{\text{cor}} \rightarrow L + 2 (d_{x^2-y^2}/\sigma_{\text{cor}}^*)$)	
S ₁₄	384.00	3.2287	0.0303	0.4369	H - 1 ($d_{yz}/\pi_{y\text{SeCN}}/\pi_{\text{cor}}/\sigma_{\text{Na(im)}} \rightarrow L + 3 (d_{yz}/\pi_{\text{cor}}^*)$)	
S ₁₅	379.57	3.2664	0.0090	0.4678	H ($d_{yz}/\pi_{y\text{SeCN}} \rightarrow L + 4(\pi_{\text{cor}}^*/\pi_{\text{im}}^*)$)	
S ₁₆	375.76	3.2996	0.0091	0.4206	H ($d_{yz}/\pi_{y\text{SeCN}} \rightarrow L + 4 (\pi_{\text{cor}}^*/\pi_{\text{im}}^*)$)	
S ₁₇	373.44	3.3200	0.0009	0.6457	H - 5($d_{xz}/\pi_{\text{im}} \rightarrow L (d_z^2/\sigma_{\text{SeCN}}^*/\sigma_{\text{Na(im)}}^*/n)$)	
S ₁₈	371.50	3.3374	0.0207	0.3328	H - 6($d_{xz}/\pi_{\text{im}}/\pi_{\text{SeCN}}/\pi_{\text{cor}} \rightarrow L (d_z^2/\sigma_{\text{SeCN}}^*/\sigma_{\text{Na(im)}}^*/n)$)	
S ₁₉	363.89	3.4072	0.0303	0.4110	H - 4 ($d_{xy}/\pi_{\text{cor}}/\pi_{\text{SeCN}} \rightarrow L (d_z^2/\sigma_{\text{SeCN}}^*/\sigma_{\text{Na(im)}}^*/n)$)	
S ₂₀	362.10	3.4241	0.0078	0.5693	H - 5($d_{xz}/\pi_{\text{im}} \rightarrow L + 1 (d_{xz}/\pi_{\text{cor}}^*)$)	
S ₂₁	356.09	3.4818	0.0126	0.4414	H - 4 ($d_{xy}/\pi_{\text{cor}}/\pi_{\text{SeCN}} \rightarrow L + 2 (d_{x^2-y^2}/\sigma_{\text{cor}}^*)$)	
S ₂₂	355.54	3.4872	0.0213	0.3764	H ($d_{yz}/\pi_{y\text{SeCN}} \rightarrow L + 5 (\pi_{\text{im}}^*)$)	
S ₂₃	354.13	3.5011	0.0118	0.5854	H ($d_{yz}/\pi_{y\text{SeCN}} \rightarrow L + 5 (\pi_{\text{im}}^*)$)	
S ₂₄	336.47	3.6849	0.0101	0.4181	H - 3 ($d_{xz}/\pi_{\text{cor}}/\pi_{y\text{SeCN}} \rightarrow L + 2 (d_{x^2-y^2}/\sigma_{\text{cor}}^*)$)	
S ₂₅	334.55	3.7060	0.0368	0.4302	H - 7($d_{yz}/\pi_{\text{cor}}/\pi_{\text{im}} \rightarrow L (d_z^2/\sigma_{\text{SeCN}}^*/\sigma_{\text{Na(im)}}^*/n)$)	
S ₂₆	332.69	3.7268	0.0106	0.5353	H - 1 ($d_{yz}/\pi_{y\text{SeCN}}/\pi_{\text{cor}}/\sigma_{\text{Na(im)}} \rightarrow L + 4 (\pi_{\text{cor}}^*/\pi_{\text{im}}^*)$)	
S ₂₇	328.89	3.7698	0.0344	0.3952	H - 7 ($d_{yz}/\pi_{\text{cor}}/\pi_{\text{im}} \rightarrow L (d_z^2/\sigma_{\text{SeCN}}^*/\sigma_{\text{Na(im)}}^*/n)$)	
S ₂₈	327.62	3.7844	0.0192	0.4043	H - 3 ($d_{xz}/\pi_{\text{cor}}/\pi_{y\text{SeCN}} \rightarrow L + 3 (d_{yz}/\pi_{\text{cor}}^*)$)	
S ₂₉	322.11	3.8491	0.0177	0.4192	H - 4 ($d_{xy}/\pi_{\text{cor}}/\pi_{\text{SeCN}} \rightarrow L + 3 (d_{yz}/\pi_{\text{cor}}^*)$)	
S ₃₀	320.57	3.8676	0.0203	0.5219	H - 1 ($d_{yz}/\pi_{y\text{SeCN}}/\pi_{\text{cor}}/\sigma_{\text{Na(im)}} \rightarrow L + 5 (\pi_{\text{im}}^*)$)	
Experimental data ³¹⁵					$\alpha/\beta - 516 \text{ nm}$	$\gamma - 355 \text{ nm}$
Experimental data ¹¹⁹					$\alpha/\beta - 539 \text{ nm}$	$\gamma - 330, 356, 370 \text{ nm}$ Band A - 684 nm

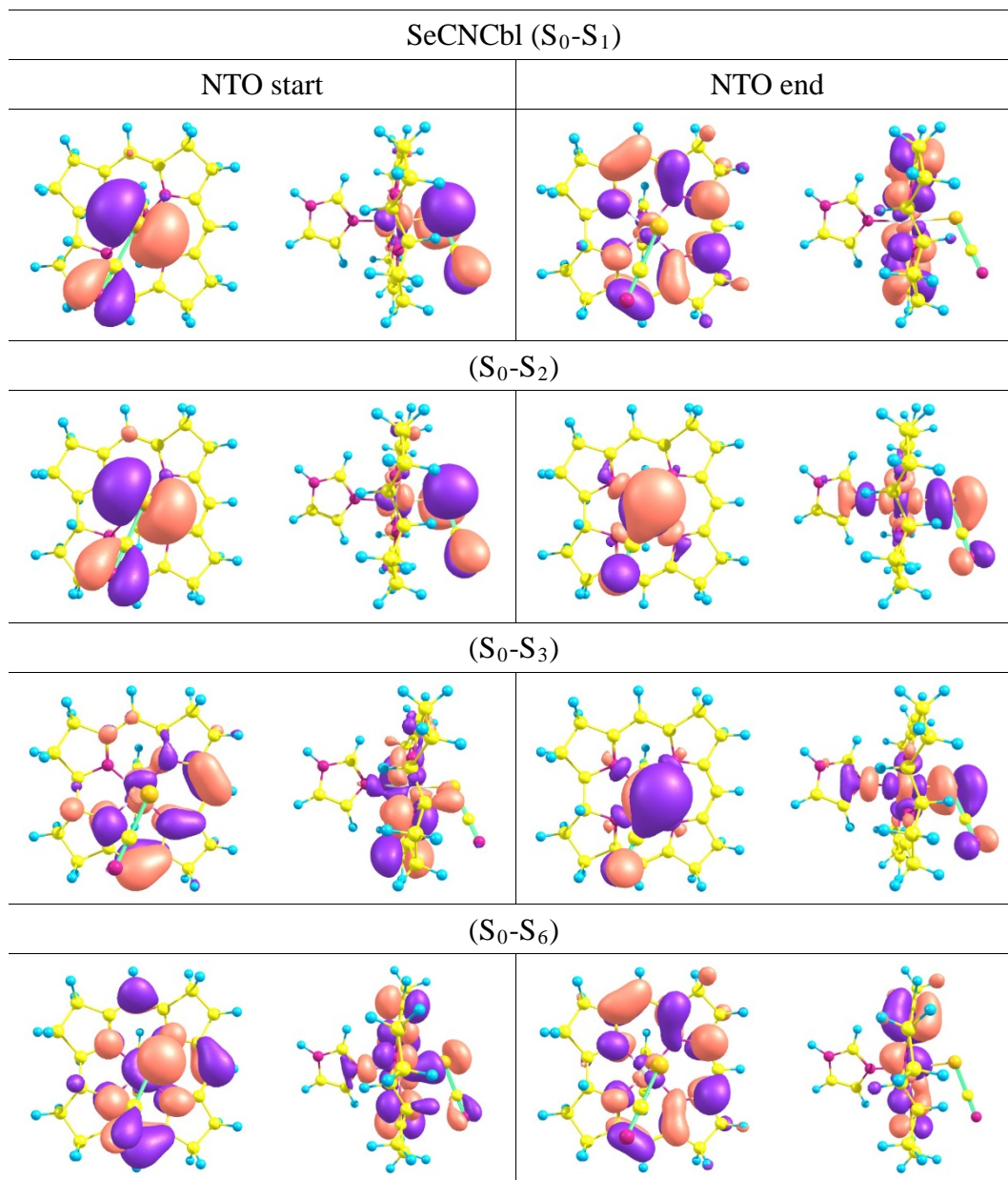


Figure 9.11: Natural Transition orbitals for the main transition bands α and band A for SeCNCbl in vacuo.

In MeCbl (**Figure 9.12**), the first $S_0\text{-}S_1$ transition is very close to states 2 and 3 at 553.7, 521.9 and 497.1 nm, respectively (**Table 9.5**). The main transition in this region is identified as the $S_0\text{-}S_3$ transition and is seen as the main transition of the $\alpha\beta$ band of the spectrum. Therefore, the $S_0\text{-}S_1$ transition is only 56.5 nm from the main transition and can be seen as part of the $\alpha\beta$ region. These three transitions show an outflow of electron density from Co to the corrin ring (**Figure 9.13**) and can thus be classified as a MLCT transition. While the first transition is observed as an $\alpha\beta$ shoulder, in the experimental spectrum it is completely part of the band. The deconvolution of the experimental absorption bands using Gaussian band analysis was predicted to be 3 Gaussian bands, consistent with the theoretical results.³¹⁵

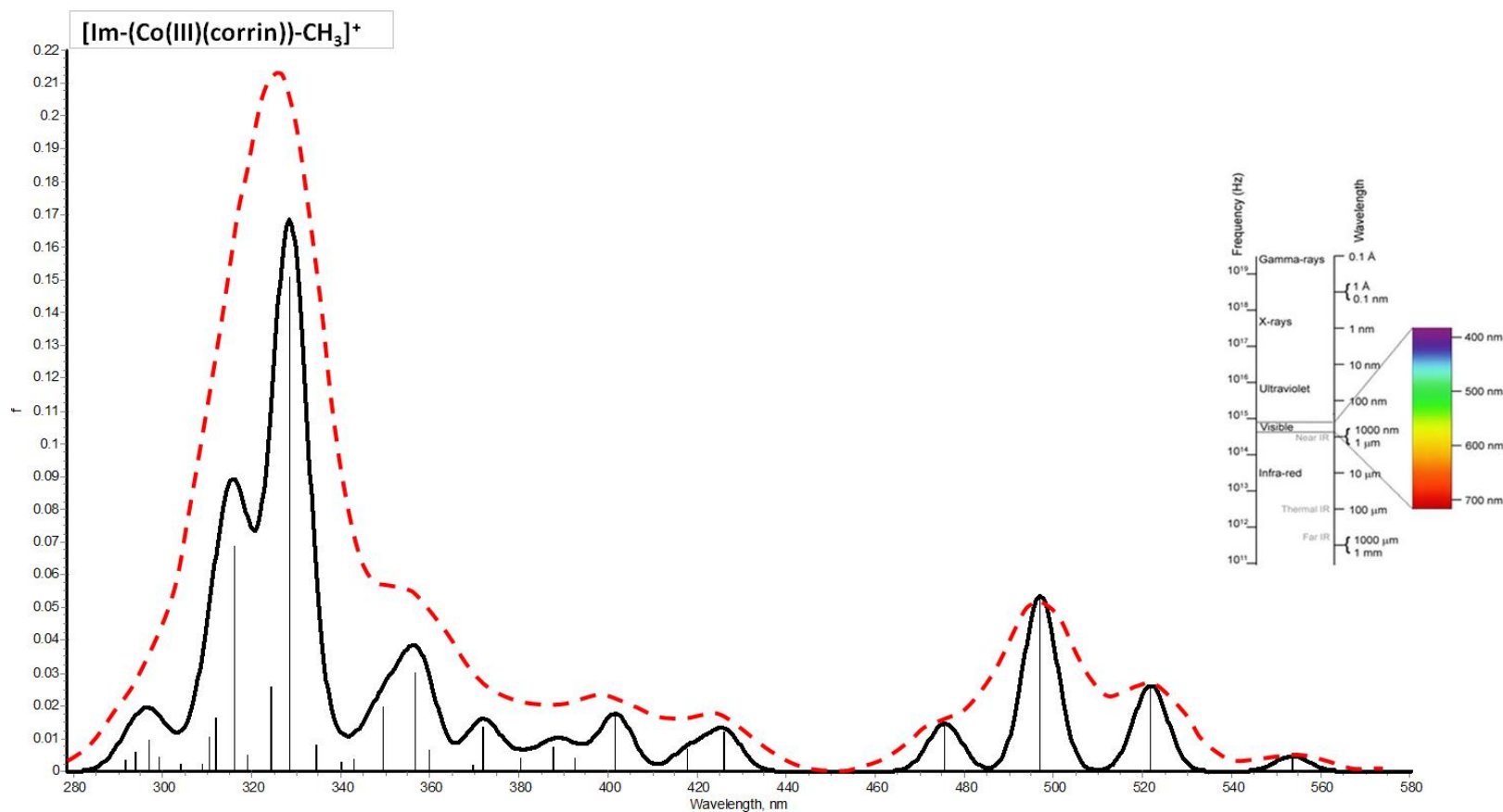


Figure 9.12: Simulated electronic absorption (black and red line) spectra of $[\text{Im}-(\text{Co(III)(corrin)})-\text{CH}_3]^+$ based on 30 first singlet excited states. The black and red line corresponds to a Doppler broadening with a width at half peak of 9 and 20 nm, respectively. The electromagnetic spectrum was obtained from reference 332.

Table 9.5: TD-BP86 vertical electronic excitation energies (E), the corresponding oscillator strengths (f), and description of dominant configurations for the $\text{Im-}[\text{Co(III)(corrin)}]\text{-CH}_3^+$ complex

S_0 to State	Λ /nm	E (eV)	f	Coeff	Character
S ₁	553.71	2.2391	0.0046	0.6000	H-1 ($\pi_{\text{cor}}/\text{d}_z^2/\sigma_{\text{Me}}/\sigma_{\text{im}}$) \rightarrow L ($\pi_{\text{cor}}^*/\text{d}_{yz}$)
S ₂	521.85	2.3759	0.0262	0.6591	H ($\pi_{\text{cor}}/\text{d}_{yz}$) \rightarrow L ($\pi_{\text{cor}}^*/\text{d}_{yz}$)
S ₃	497.07	2.4943	0.0535	0.5504	H-2 ($\pi_{\text{cor}}/\text{d}_{xz}$) \rightarrow L ($\pi_{\text{cor}}^*/\text{d}_{yz}$)
S ₄	475.68	2.6064	0.0145	0.6574	H-3 ($\pi_{\text{cor}}/\text{d}_x^2-\text{d}_y^2$) \rightarrow L ($\pi_{\text{cor}}^*/\text{d}_{yz}$)
S ₅	426.11	2.9096	0.0124	0.5020	H ($\pi_{\text{cor}}/\text{d}_{yz}$) \rightarrow L +1 ($\sigma_{\text{N-cor}}^*/\text{d}_{xy}$)
S ₆	418.18	2.9649	0.0068	0.5034	H-1 ($\pi_{\text{cor}}/\text{d}_z^2/\sigma_{\text{Me}}/\sigma_{\text{im}}$) \rightarrow L +1 ($\sigma_{\text{N-cor}}^*/\text{d}_{xy}$)
S ₇	401.82	3.0856	0.0173	0.6041	H ($\pi_{\text{cor}}/\text{d}_{yz}$) \rightarrow L +2 ($\pi_{\text{cor}}^*/\text{d}_{xy}$)
S ₈	392.82	3.1563	0.0042	0.4900	H ($\pi_{\text{cor}}/\text{d}_{yz}$) \rightarrow L+3 ($\sigma_{\text{Me}}^*/\sigma_{\text{im}}^*/\text{d}_z^2/\text{a}_n$)
S ₉	387.91	3.1963	0.0076	0.3696	H-4 ($\pi_{\text{im}}/\text{d}_{yz}$) \rightarrow L ($\pi_{\text{cor}}^*/\text{d}_{yz}$)
S ₁₀	380.54	3.2581	0.0042	0.6598	H-5 ($\pi_{\text{im}}/\text{d}_{yz}$) \rightarrow L ($\pi_{\text{cor}}^*/\text{d}_{yz}$)
S ₁₁	372.11	3.3319	0.0139	0.5613	H-1 ($\pi_{\text{cor}}/\text{d}_z^2/\sigma_{\text{Me}}/\sigma_{\text{im}}$) \rightarrow L+3 ($\sigma_{\text{Me}}^*/\sigma_{\text{im}}^*/\text{d}_z^2/\text{a}_n$)
S ₁₂	369.92	3.3516	0.0020	0.4724	H-3 ($\pi_{\text{cor}}/\text{d}_x^2-\text{d}_y^2$) \rightarrow L +1 ($\sigma_{\text{N-cor}}^*/\text{d}_{xy}$)
S ₁₃	359.96	3.4444	0.0066	0.5234	H-3 ($\pi_{\text{cor}}/\text{d}_x^2-\text{d}_y^2$) \rightarrow L +2 ($\pi_{\text{cor}}^*/\text{d}_{xy}$)
S ₁₄	356.84	3.4745	0.0303	0.4084	H-3 ($\pi_{\text{cor}}/\text{d}_x^2-\text{d}_y^2$) \rightarrow L +2 ($\pi_{\text{cor}}^*/\text{d}_{xy}$)
S ₁₅	349.70	3.5454	0.0200	0.3334	H-2 ($\pi_{\text{cor}}/\text{d}_{xz}$) \rightarrow L +2 ($\pi_{\text{cor}}^*/\text{d}_{xy}$)
S ₁₆	343.24	3.6121	0.0038	0.3792	H-2 ($\pi_{\text{cor}}/\text{d}_{xz}$) \rightarrow L+3 ($\sigma_{\text{Me}}^*/\sigma_{\text{im}}^*/\text{d}_z^2/\text{a}_n$)
S ₁₇	340.20	3.6445	0.0031	0.4828	H-6 ($\pi_{\text{C-10cor}}/\text{d}_z^2/\sigma_{\text{Me}}/\sigma_{\text{im}}$) \rightarrow L ($\pi_{\text{cor}}^*/\text{d}_{yz}$)
S ₁₈	334.81	3.7032	0.0082	0.4210	H ($\pi_{\text{cor}}/\text{d}_{yz}$) \rightarrow L+4 ($\pi_{\text{cor}}^*/\text{d}_{yz}$)
S ₁₉	328.90	3.7697	0.1512	0.3782	H ($\pi_{\text{cor}}/\text{d}_{yz}$) \rightarrow L+4 ($\pi_{\text{cor}}^*/\text{d}_{yz}$)
S ₂₀	324.47	3.8212	0.0261	0.4360	H-1 ($\pi_{\text{cor}}/\text{d}_z^2/\sigma_{\text{Me}}/\sigma_{\text{im}}$) \rightarrow L+4 ($\pi_{\text{cor}}^*/\text{d}_{yz}$)
S ₂₁	319.10	3.8854	0.0048	0.6829	H ($\pi_{\text{cor}}/\text{d}_{yz}$) \rightarrow L+5 (π_{im}^*)
S ₂₂	316.36	3.9190	0.0688	0.6384	H-2 ($\pi_{\text{cor}}/\text{d}_{xz}$) \rightarrow L+4 ($\pi_{\text{cor}}^*/\text{d}_{yz}$)
S ₂₃	312.20	3.9712	0.0164	0.3735	H-7 ($\pi_{\text{im}}/\text{d}_{xz}/\sigma_{\text{Me}}$) \rightarrow L ($\pi_{\text{cor}}^*/\text{d}_{yz}$)
S ₂₄	310.68	3.9907	0.0109	0.5750	H-1 ($\pi_{\text{cor}}/\text{d}_z^2/\sigma_{\text{Me}}/\sigma_{\text{im}}$) \rightarrow L+5 (π_{im}^*)
S ₂₅	309.14	4.0107	0.0023	0.6654	H-5 ($\pi_{\text{im}}/\text{d}_{yz}$) \rightarrow L +1 ($\sigma_{\text{N-cor}}^*/\text{d}_{xy}$)
S ₂₆	304.28	4.0747	0.0022	0.6848	H-3 ($\pi_{\text{cor}}/\text{d}_x^2-\text{d}_y^2$) \rightarrow L+4 ($\pi_{\text{cor}}^*/\text{d}_{yz}$)
S ₂₇	299.53	4.1393	0.0046	0.6088	H-5 ($\pi_{\text{im}}/\text{d}_{yz}$) \rightarrow L +2 ($\pi_{\text{cor}}^*/\text{d}_{xy}$)
S ₂₈	297.33	4.1699	0.0095	0.4442	H-3 ($\pi_{\text{cor}}/\text{d}_x^2-\text{d}_y^2$) \rightarrow L+3 ($\sigma_{\text{Me}}^*/\sigma_{\text{im}}^*/\text{d}_z^2/\text{a}_n$)
S ₂₉	294.11	4.2155	0.0061	0.5326	H-2 ($\pi_{\text{cor}}/\text{d}_{xz}$) \rightarrow L+5 (π_{im}^*)
S ₃₀	291.76	4.2496	0.0034	0.3670	H-4 ($\pi_{\text{im}}/\text{d}_{yz}$) \rightarrow L +1 ($\sigma_{\text{N-cor}}^*/\text{d}_{xy}$)
Experimental data ¹¹⁰		α – 527 nm (2.35 eV) β – 486 nm (2.55 eV)			
D – 429 nm (2.89 eV)		E – 401 nm (3.09 eV) γ – 378 nm (3.28 eV); 336 nm (3.69 eV); 316 nm (3.92 eV); 264 nm (4.70 eV)			
Experimental data ¹¹⁹		α/β – 522 nm γ – 343 nm			

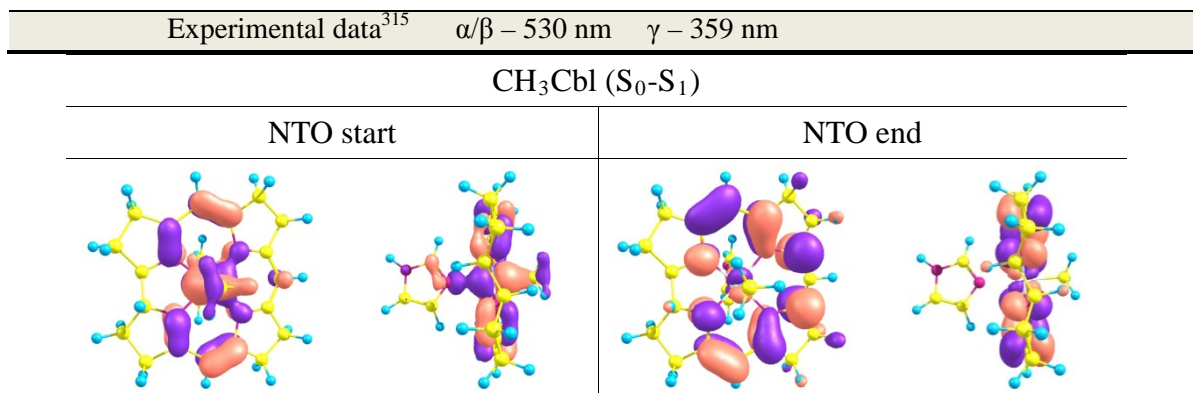


Figure 9.13: Natural Transition orbitals for the main transition bands α and band A for CH₃Cbl in vacuo.

9.5 CONCLUSIONS

TD-DFT calculations were successfully used to describe the first transition in MeCbl as MLCT, while band A in ClCbl and BrCbl exhibited LMCT. In FCbl, band A is hidden in the $\alpha\beta$ region, while in SeCNCbl the first transitions are located in the axial ligand.

CHAPTER 10

OVERALL CONCLUSIONS

The significance of the *trans* influence⁹ of the α -ligand has been the subject of considerable interest experimentally and theoretically since the discovery of the importance of B₁₂ analogues. Therefore, the effect of identity of this ligand on the various parameters of cobalamin models was investigated. In addition, the *cis* influence (which has been somewhat neglected in cobalamin chemistry) of the equatorial ligand and the substitution of hydrogen at C₁₀ of the corrin ring with electron donating and electron withdrawing substituents, as quantified by the Hammett function, was also explored.

For this study, four functionals were chosen and used based on an extensive literature review. The BP86 functional has been shown to perform well in predicting structural properties of B₁₂ analogues,^{18,69} Co(III)–C bond strength,^{14,57} reductive cleavage of the Co(III)–C bond in corrin complexes³³³ and electronically excited states.¹¹⁰ On the other hand, the results from the Truhlar M06L functional compared well with those from the BP86, while the hybrid functionals, B3LYP and PBE1PBE, gave much lower Co(III)–C _{β} BDE values in comparison to BP86 and M06L.

This study clearly demonstrated that there is no specific cause that promotes the labilisation of the Co(III)–C bond, but there is rather a manifold of factors that collectively work together to accomplish the easier scission of this important bond. These include the following.

The trans influence

In Chapter 5, a range of N-donor α ligands were used to explore the *trans* influence on the Co(III)–C BDE as well as the changes to the structural parameters of the model cobalamins. The α ligands were chosen so that the electronic (simple ligands with low to high proton affinities) and steric (neutral ligands with increasing bulk as assessed by the molar volumes) effects could be explored.

Calculations on $[Y-(\text{Co(III)}(\text{corrin}))-\text{CH}_3]^{n+}$ where $Y = \text{NH}_3, \text{NH}_2^-, \text{NH}^{2-}, \text{NH}_2\text{F}, \text{NHF}^-, \text{NF}^{2-}, \text{NH}_2\text{CH}_3$ or NHCH_3^- investigated the electronic effects. For each set of α ligands, for example $\text{NH}_3, \text{NH}_2^-$ and NH^{2-} , the E_{pa} (proton affinity) increased with the charge on the ligand. The Co(III)– N_α bond length decreased on going from the neutral to the charged ligands while the Co(III)– C_β bond elongated, revealing a normal *trans* influence. The Co(III)–C bond weakened. This weakening was confirmed by QTAIM studies where the decrease in electron density at the bond critical point (bcp) and the loss of covalency (characterised by the ratio of the potential and kinetic energies ($|V(r)|/G(r)$) at the bcp) of the organometallic bond was observed. Interactions with ($|V(r)|/G(r) > 2$) are classed as covalent, those with ($|V(r)|/G(r) < 1$) are typically ionic, and ($1 < |V(r)|/G(r) < 2$) is indicative of an interaction of intermediate character. It was found that the greater the contraction of the lower axial bond from the 5-coordinate to the 6-coordinate complex then the lower the BDE for the labilisation of the Co(III)–C bond would be. Therefore, the stability of the post-homolysis product has an important influence on the Co(III)– C_β BDE. To our knowledge, this fact has not been appreciated before.

Calculations on $[Y-(\text{Co(III)}(\text{corrin}))-\text{CH}_3]^{n+}$ where $Y = \text{NH}_3, \text{NH}_2\text{CH}_3, \text{NH}(\text{CH}_3)_2, \text{N}(\text{CH}_3)_3$ investigated the steric effects. These α ligands were progressively more bulky (as was assessed by the Tolman cone angle and molar volume) and basic (as assessed by the E_{pa} values). Results from these models immediately showed an inverse *trans* influence between the axial ligands, different from that noted above. As the Co(III)– N_α bond length increased so the Co(III)–C bond length also increased. In

order to confirm whether this influence was due to a steric effect, eight torsion angles were measured for these complexes. In the corrin complex no distortion of the corrin ring for those models carrying neutral α ligands ($\omega_{\text{avg}} = 3.3^\circ$) was observed, while small fluctuations were recorded for those with the charged ligands ($\omega_{\text{avg}} = 2.8^\circ - 3.7^\circ$). Therefore, no correlation could be drawn between the ring distortion and the thermodynamic parameters. As a result, further calculations for the same models $[\text{Y}-(\text{Co(III)}(\text{corrin}))-\text{CH}_3]^{n+}$ where $\text{Y} = \text{NH}_3, \text{NH}_2\text{CH}_3, \text{NH}(\text{CH}_3)_2$ were performed. This time the lower axial bond $\text{Co(III)}-\text{N}_\alpha$, was restricted from 1.9–2.5 Å so that the *trans* steric and *trans* inductive effect of the α ligands could be investigated. Keeping the α ligand constant and changing the lower axial bond length from 1.9 to 2.5 Å in 0.1 Å increments showed a normal *trans* influence between the two axial bonds and a negligible change to the thermodynamic data. The displacement of the Co metal centre from the defined mean plane complemented these observations. Conversely, as the α ligand increased in bulk and E_{pa} , with the $\text{Co(III)}-\text{N}_\alpha$ bond remaining constant, the $\text{Co(III)}-\text{C}$ bond length increased while the BDE decreased. It is suggested that with the increase in methyl groups on the α ligand, the electron density feeding into the corrin and axial ligand also increased. As a result, a *trans* inductive effect was applied to the upper axial ligand causing it to move away from the metal. The absence of ring distortion, calculations with restricted $\text{Co}-\text{N}_\alpha$ bond lengths and the $\text{N}_\alpha-\text{Co(III)}-\text{C}_\beta$ bond angles confirmed that there was no *trans* steric effect taking place for these models.

The partial charges on the atoms in these models were also calculated in order to assess any electronic effects. None of the methods, namely Mulliken, APT, NBO, or Bader, provided much insight. Moreover, a similar trend was also observed for these models where the contraction of the $\text{Co(III)}-\text{N}_\alpha$ bond from the pre- to the post homolysis complex paralleled both ΔG and BDE for the $\text{Co(III)}-\text{C}$ bond. The thermodynamic drive to form the more stable Co(II) complex resulted in lower bond dissociation energies.

The nature of the α ligand

In Chapter 6, models of the type $[\text{B}_\alpha\text{-(Co(III)(corrin))}\text{-CH}_3]^{n+}$ where B_α = methanethiol, dimethylsulfide, cysteine, methanethiolate, glycine, *p*-aminopyridine, imidazole, histidine, methanol, 2-propanol, serine, tyrosine and acetate were explored. These α ligands were examples of naturally occurring amino acids or models thereof and contained soft (S-), hard (O-) and intermediate (N-) donor atoms. The calculations revealed the nature of the α ligand to be the controlling factor in the homolytic cleavage of the organometallic bond rather than the variation of the Co(III)–C $_\beta$ bond length. From the three classes of α ligands, the Co(III)–C $_\beta$ bonds formed from the use of soft amino acids (cys) were much weaker when compared to the harder amino acids (asp) whose bonds were much stronger. On the other hand, N-donor ligands produced Co(III)–C $_\beta$ bonds of intermediate stability and therefore, presumably, of suitable catalytic character, reaffirming why nature chooses an N-donor ligand, particularly histidine or imidazole as a replacement for DMB.

The cis influence

In Chapter 5, model complexes of the form $[\text{NX}_3\text{-(Co(III)(L)}_4\text{)}\text{-CH}_3]^{n+}$, with neutral or charged α ligands (NH_3 , NH_2CH_3 , NHCH_3 , $\text{N}(\text{CH}_3)_3$ and NH_2^-) and various equatorial ligands ($(\text{L})_4$ = cobaloxime, corrole, corrin and porphyrin) were explored. At the very outset, the cobaloxime model proved a poor cobalamin model due to its extreme flexibility. Of the three remaining equatorial ligands, the corrole model exhibited the highest Co(III)–C $_\beta$ BDE irrespective of the type of α ligand attached, that is, neutral or charged in character. On the other hand, the porphyrin model with NH_2^- and the corrin model with NH_3 gave the lowest BDE values for the homolysis of the Co(III)–C $_\beta$ bond, respectively. It is suggested that the larger aromatic ring of porphyrin provides a greater stabilising environment for the charged ligand, resulting in a lower BDE for that model. Finally, the corrin model, although electron rich, contains a partially conjugated ring with one less carbon. In this corrin complex with NH_3 as the α ligand the Co metal centre was found closer to the defined mean plane.

This suggests that a poorer orbital overlap occurs between the metal and the β ligand, which in turn produces a weaker bond (as was confirmed by a QTAIM analysis), and therefore a lower BDE was observed for the cleavage of the Co(III)–C $_{\beta}$ bond.

The *cis* influence was further investigated in Chapter 7 with the α and β axial ligands kept constant as NH₃ and CH₃, respectively. The nature of the equatorial ligands incorporated into the cobalamin models were either aliphatic, aromatic or rich in π electrons. The calculations were conducted in the gas phase as well as an implicit solvent medium for a range of solvents. For the aliphatic equatorial ligands, the greater the ring size the greater was the flexibility of the ring, (as was assessed by the distortion of the N_{eq}–Co–C $_{\beta}$ bond angle) and consequently a lower Co(III)–C $_{\beta}$ BDE was obtained. In the solvent environment, the BDEs increased due to a better alignment of the orbitals (less distortion of the N_{eq}–Co–C $_{\beta}$ bond angle) with the upper ligand thus resulting in the formation of a stronger bond. For those ligands rich in π electrons, the corrin model was found to have the lowest BDE for the homolysis of the organometallic bond. The flexibility of the ring indirectly played a role in lowering the Co(III)–C $_{\beta}$ BDE. With the flexibility of the ring, the Co metal centre was found to shift either away or towards the β ligand. This shift paralleled the Co(III)–C $_{\beta}$ BDE. The environmental effects were negligible, as the homolytic reaction does not form charged fragments; therefore, as suggested by others, any changes to the BDEs possibly arose from cavitation, dispersion and repulsion energies.

In Chapter 8, the *cis* influence of the substitution of various electron donating and electron withdrawing groups on C₁₀ of the corrin ring with NH₃, CH₃ as the respective α , and β ligands, was calculated. The results revealed that the greater the electron density moving into the ring from the C₁₀ substituent the more covalent was the character of the Co(III)–C $_{\beta}$ bond. As this bond strengthened, both the ΔG and BDE of the said bond decreased, reaffirming that these parameters are not synonymous with each other. As was observed in some of the previous chapters, the

formation of the 5-coordinate complex was thermodynamically favourable. Here too, with an increase in electron donor power from the C₁₀ substituent the contraction of the Co–N_α increases from the 6-coordinate to the 5-coordinate complex, leading to low Co(III)–C_β BDEs.

The final investigation of the *cis* influence involved the prediction of the UV-vis spectra of various cobalamin models with a change to the β ligand. The central focus was to provide a molecular orbital picture of how the different β ligands would affect the main spectral bands (α and band A) and the excitations responsible for these defined bands. The β ligands differed from each other by their donor abilities in the following order: F[−] < Cl[−] < Br[−] < SeCN[−] < CH₃[−]. As the donor abilities of these ligands increased, so the spectra shifted from “typical” to “atypical” behaviour and the main spectral bands to longer wavelengths.

Recommendations for further studies

In Chapter 5 a range of anionic α ligands carrying different charges were used to explore the electronic effect to the Co(III)–C bond in the corrin model. It was observed that the corrin complex with anions carrying a -2 or -3 charge produced very low energies or failed to optimise to a stable ground state. A possible explanation for this occurrence may be a self-interaction error of the charge-bearing anionic α ligand with the corrin macrocycle. Therefore, it is proposed that the self-interaction error of these ligands should be explored in further detail.

In Chapters 5–8 a large number of trends have been recorded and discussed. Further value can be provided to these observations by exploring the electronic structural origin of the trends through the analysis of the relevant frontier molecular orbitals. The implications of these findings could be applied to exploring the mechanism of enzymatic Co–C bond activation. Other contributions such as investigating how hydrogen bonding to corrin side chains would affect the Co–C BDE could also lead to explanations for the unique Co–C bond activation observed in AdoCbl.

APPENDIX 1

DATA FOR CHAPTER 2

A1.1 The mathematical form of a normalized STO used in extended Hückel theory to represent valence orbitals.³

$$\varphi(r, \theta, \phi, \zeta, n, l, m) = \frac{(2\zeta)^{n+\frac{1}{2}}}{[(2n)!]^{\frac{1}{2}}} r^{n-1} e^{-\zeta r} Y_l^m(\theta, \phi)$$

ζ is an exponent chosen using Slater rules and is dependent on the atomic number.

n is the principle quantum number for the valence orbital.

r is the radial function.

$Y_l^m(\theta, \phi)$ are the spherical harmonic functions dependent on angular momentum quantum numbers, l and m .

The size of the secular determinant is dependent on the number of valence orbitals in the molecule.

A1.2 The general functional form of a normalized GTO in atom-centred Cartesian coordinates.³

$$\phi(x, y, z, \alpha, i, j, k) = \left(\frac{2\alpha}{\pi}\right)^{3/4} \left[\frac{(8\alpha)^{i+j+k} i! j! k!}{(2i)! (2j)! (2k)!} \right]^{1/2} x^i y^j z^k e^{-\alpha(x^2+y^2+z^2)}$$

α is the exponent describing the width of the GTO.

i , j , and k are non-negative integers. These integers (in a Cartesian manner) control the nature of the orbitals.

APPENDIX 2

DATA FOR CHAPTER 5

A2.1 Ligand steric effects measured by using the Tolman Cone Angle methodology²¹⁷ defined by the illustration below and calculated using the following equation.

$$\theta_{total} = \frac{2}{3} \sum_{i=1}^3 \theta_i$$

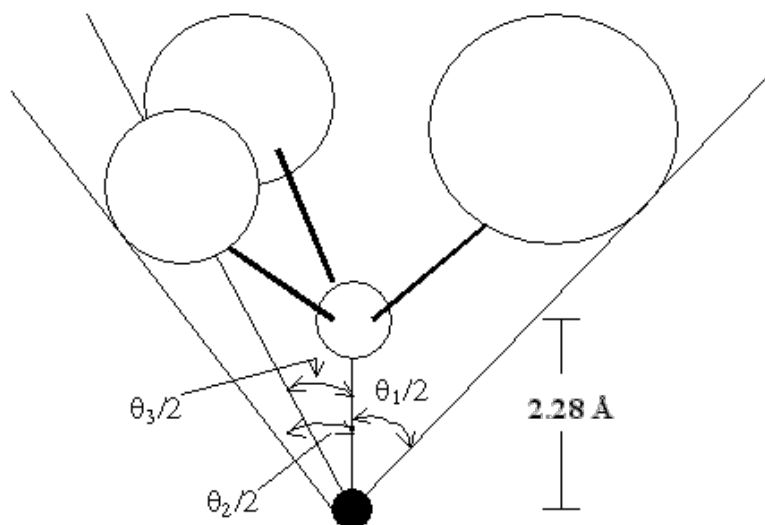


Table A2.1: Torsion angles (°) for Cobaloxime

	$[\text{NX}_3\text{Co(III)}(\text{L})_4\text{CH}_3]^{n+}$						$[\text{NX}_3\text{Co(II)}(\text{L})_4]^{n+}$					
	1	2	3	4	5	6	1	2	3	4	5	6
Cobaloxime												
ω_1	2.5	3.5	7.0	7.5	2.5	–	11.5	13.1	16.2	17.1	26.2	–
ω_2	-0.4	0.2	2.4	1.4	-0.4	–	0.2	0.3	2.1	2.0	-6.3	–
ω_3	0.1	-0.9	-2.9	-1.7	0.1	–	-0.2	-0.8	-2.5	-1.9	8.5	–
ω_4	-1.6	-1.6	-5.3	-3.6	-1.6	–	-10.4	-10.9	-13.8	-13.4	-20.8	–
ω_5	4.1	5.9	8.2	5.6	4.1	–	12.5	14.5	17.2	15.1	27.6	–
ω_6	-0.8	-1.0	2.7	1.7	-0.8	–	-0.4	-0.5	2.3	2.0	-6.5	–
ω_7	0.7	1.0	-2.5	-1.7	0.7	–	0.4	0.7	-2.1	-2.2	8.7	–
ω_8	-0.9	-0.3	-4.9	-6.2	-0.9	–	-10.4	-9.3	-13.7	-16.0	-20.2	–
ω_{avg}	0.5	0.8	0.6	0.4	0.1	–	0.4	0.9	0.7	0.3	2.2	–

In the table, 1–6 indicates the type of α ligand present in the complex where 1= NH_3 ; 2= NH_2CH_3 ; 3= $\text{NH}(\text{CH}_3)_2$, 4= $\text{N}(\text{CH}_3)_3$, 5= NH_2^- AND 6= NH^{2-} .

Table A2.2: Torsion angles (°) for Corrole

	$[\text{NX}_3\text{Co(III)}(\text{L})_4\text{CH}_3]^{n+}$						$[\text{NX}_3\text{Co(II)}(\text{L})_4]^{n+}$					
	1	2	3	4	5	6	1	2	3	4	5	6
Corrole												
ω_1	-3.1	-3.7	-4.9	-3.4	-0.7	–	5.0	4.9	4.2	5.5	8.9	–
ω_2	2.8	2.0	1.4	3.7	-0.3	–	-4.6	-4.9	-5.8	-3.6	-5.9	–
ω_3	-2.8	-2.2	-1.4	-4.0	-0.2	–	4.6	4.9	5.8	3.6	8.1	–
ω_4	2.9	3.8	4.9	5.7	0.9	–	-5.1	-4.8	-4.2	-5.5	-8.7	–
ω_5	-3.0	-3.7	-4.6	-5.3	-0.2	–	4.6	4.3	3.8	5.1	6.6	–
ω_6	1.4	1.5	1.7	3.0	0.4	–	-2.9	-3.0	-3.2	-3.5	-5.4	–
ω_7	-1.4	-1.6	-1.7	-3.1	-0.6	–	3.0	3.0	3.2	3.5	5.0	–
ω_8	3.2	3.7	4.6	3.6	0.7	–	-4.5	-4.4	-3.8	-5.1	-8.6	–
ω_{avg}	0.0	0.0	0.0	0.0	0.0	–	0.0	0.0	0.0	0.0	0.0	–

In the table, 1–6 indicates the type of α ligand present in the complex where 1= NH_3 ; 2= NH_2CH_3 ; 3= $\text{NH}(\text{CH}_3)_2$, 4= $\text{N}(\text{CH}_3)_3$, 5= NH_2^- AND 6= NH^{2-} .

Table A2.3: Torsion angles (°) for Corrin

	$[NX_3Co(III)(L)_4CH_3]^{n+}$						$[NX_3Co(II)(L)_4]^{+}$					
	1	2	3	4	5	6	1	2	3	4	5	6
Corrin												
ω_1	-10.4	-10.9	-11.7	-10.6	-7.5	-7.8	-3.1	-3.6	-4.3	-2.3	-1.4	10.2
ω_2	1.2	0.9	-1.2	4.6	-1.0	-0.2	-4.1	-4.5	-6.4	-2.0	-4.8	-6.2
ω_3	-1.4	-0.9	0.7	-4.8	0.5	0.9	2.9	3.9	5.7	0.3	4.3	-1.8
ω_4	-5.3	-5.2	-2.2	-4.4	-6.8	1.9	-12.0	-11.9	-9.4	-12.0	-12.7	-29.7
ω_5	5.2	5.0	1.8	5.4	4.5	-0.2	13.4	13.1	10.9	14.7	11.7	22.8
ω_6	-10.3	-10.4	-11.4	-8.8	-17.6	-18.9	-13.3	-13.4	-14.4	-12.4	-21.1	-28.0
ω_7	-15.0	-14.9	-14.1	-16.1	-9.0	-8.3	-11.8	-11.7	-11.0	-12.6	-4.9	5.6
ω_8	9.5	10.2	11.6	8.4	10.6	10.0	1.1	1.9	3.4	-1.7	4.9	-6.9
ω_{avg}	3.3	3.3	3.3	3.3	3.3	2.8	3.4	3.3	3.2	3.5	3.0	4.3

In the table, 1–6 indicates the type of α ligand present in the complex where 1= NH_3 ; 2= NH_2CH_3 ; 3= $NH(CH_3)_2$, 4= $N(CH_3)_3$, 5= NH_2^- AND 6= NH^2^- .

Table A2.4: Torsion angles (°) for Porphyrin

	$[NX_3Co(III)(L)_4CH_3]^{n+}$						$[NX_3Co(II)(L)_4]^{+}$					
	1	2	3	4	5	6	1	2	3	4	5	6
Porphyrin												
ω_1	-2.1	-6.6	4.6	-3.2	-0.4	–	4.2	1.6	9.2	3.9	7.0	–
ω_2	2.4	-2.5	8.5	2.6	0.4	–	-4.0	-6.9	0.4	-4.4	-7.4	–
ω_3	-2.2	2.3	-8.5	-2.8	-0.6	–	4.1	6.8	-0.4	4.3	3.7	–
ω_4	2.2	6.8	-4.6	1.7	-0.4	–	-4.1	-1.3	-9.3	-5.3	-8.6	–
ω_5	-2.3	-6.6	4.6	-1.2	0.1	–	4.1	1.3	9.3	5.9	8.1	–
ω_6	2.3	-2.2	8.5	0.9	-0.1	–	-4.1	-6.8	0.4	-6.1	-8.6	–
ω_7	-2.3	2.3	-8.5	-1.5	0.3	–	4.0	6.9	-0.4	5.4	9.0	–
ω_8	2.0	6.6	-4.6	3.4	0.6	–	-4.2	-1.6	-9.2	-3.8	-3.2	–
ω_{avg}	0.0	0.0	0.0	0.0	0.0	–	0.0	0.0	0.0	0.0	0.0	–

In the table, 1–6 indicates the type of α ligand present in the complex where 1= NH_3 ; 2= NH_2CH_3 ; 3= $NH(CH_3)_2$, 4= $N(CH_3)_3$, 5= NH_2^- AND 6= NH^2^- .

Table A2.5: Mulliken and APT partial charges (e) for cobaloxime at restricted Co–N_α bond lengths

α ligands	MULLIKEN							APT						
	1.9	2.0	2.1	2.2	2.3	2.4	2.5	1.9	2.0	2.1	2.2	2.3	2.4	2.5
Co(III)								Co(III)						
NH ₃	-1.121	-1.155	-1.168	-1.169	-1.163	-1.151	–	-0.173	-0.121	-0.075	-0.035	-0.001	0.028	–
NH ₂ CH ₃	-1.506	-1.548	-1.423	-1.374	-1.308	-1.252	-1.209	-0.189	-0.143	-0.100	-0.063	-0.031	-0.003	0.021
NH(CH ₃) ₂	-1.861	-1.775	-1.656	-1.526	-1.406	-1.311	-1.245	-0.183	-0.144	-0.108	-0.076	-0.048	-0.023	-0.002
N(CH ₃) ₃	-1.778	-1.596	-1.440	-1.328	-1.265	-1.244	-1.260	-0.174	-0.140	-0.108	-0.08	-0.056	-0.034	-0.015
C _β								C _β						
NH ₃	-0.336	-0.322	-0.314	-0.311	-0.311	-0.315	–	0.207	0.212	0.216	0.218	0.219	0.220	–
NH ₂ CH ₃	-0.198	-0.186	-0.185	-0.197	-0.218	-0.237	-0.255	0.193	0.200	0.205	0.209	-0.211	0.213	0.214
NH(CH ₃) ₂	-0.145	-0.140	-0.149	-0.167	-0.188	-0.209	-0.228	0.173	0.183	0.19	0.196	0.201	0.204	0.207
N(CH ₃) ₃	-0.077	-0.082	-0.097	-0.115	-0.131	-0.145	-0.155	0.161	0.173	0.182	0.190	0.196	0.200	0.204
N _α								N _α						
NH ₃	-0.922	-0.919	-0.915	-0.914	-0.918	-0.927	–	-0.080	-0.159	-0.214	-0.256	-0.287	-0.310	–
NH ₂ CH ₃	-0.616	-0.634	-0.648	-0.658	-0.669	-0.685	-0.703	-0.103	-0.164	-0.212	-0.247	-0.273	-0.292	-0.304
NH(CH ₃) ₂	-0.404	-0.415	-0.43	-0.446	-0.462	-0.477	-0.489	-0.154	-0.208	-0.248	-0.276	-0.295	-0.308	-0.316
N(CH ₃) ₃	-0.583	-0.593	-0.594	-0.584	-0.567	-0.546	-0.521	-0.205	-0.261	-0.300	-0.327	-0.345	-0.357	-0.365
N _{eq}								N _{eq}						
NH ₃	-0.252	-0.253	-0.256	-0.258	-0.258	-0.257	–	0.479	0.476	0.473	0.470	0.466	0.462	–
NH ₂ CH ₃	-0.211	-0.197	-0.221	-0.225	-0.231	-0.234	-0.234	0.473	0.471	0.468	0.465	0.463	0.461	0.458
NH(CH ₃) ₂	-0.217	-0.223	-0.232	-0.241	-0.248	-0.250	-0.248	0.462	0.460	0.458	0.456	0.455	0.454	0.452
N(CH ₃) ₃	-0.203	-0.218	-0.228	-0.229	-0.223	-0.212	-0.195	0.451	0.449	0.447	0.446	0.445	0.444	0.443

Table A2.6: Mulliken and APT partial charges (e) for corrole at restricted Co–N_α bond lengths

α ligands	MULLIKEN							APT						
	1.9	2.0	2.1	2.2	2.3	2.4	2.5	1.9	2.0	2.1	2.2	2.3	2.4	2.5
Co(III)								Co(III)						
NH ₃	-2.903	-2.850	-2.792	-2.747	-2.726	-2.727	–	0.258	0.279	0.293	0.301	0.302	0.298	–
NH ₂ CH ₃	–	-2.719	-2.623	-2.533	-2.471	-2.819	-2.465	–	0.280	0.294	0.303	0.307	0.306	0.299
NH(CH ₃) ₂	-2.869	-2.67	-2.475	-2.326	-2.217	-2.171	-2.179	0.265	0.287	0.302	0.312	0.316	0.315	0.310
N(CH ₃) ₃	-2.151	-1.757	-1.453	-1.262	-1.184	-1.21	-1.323	0.246	0.275	0.296	0.310	0.317	0.319	0.315
C _β								C _β						
NH ₃	-0.525	-0.514	-0.501	-0.483	-0.458	-0.429	–	0.105	0.118	0.129	0.140	0.149	0.157	–
NH ₂ CH ₃	–	-0.341	-0.354	-0.366	-0.374	-0.171	-0.369	–	0.100	0.113	0.124	0.134	0.144	0.152
NH(CH ₃) ₂	-0.262	-0.290	-0.342	-0.381	-0.41	-0.424	-0.424	0.083	0.095	0.107	0.118	0.129	0.138	0.146
N(CH ₃) ₃	-0.142	-0.191	-0.245	-0.29	-0.32	-0.333	-0.334	0.086	0.096	0.107	0.117	0.127	0.136	0.144
N _α								N _α						
NH ₃	-0.735	-0.745	-0.755	-0.772	-0.796	-0.830	–	-0.154	-0.216	-0.262	-0.294	-0.316	-0.330	–
NH ₂ CH ₃	–	-0.418	-0.433	-0.460	-0.500	-0.581	-0.607	–	-0.247	-0.292	-0.325	-0.35	-0.368	-0.380
NH(CH ₃) ₂	-0.127	-0.132	-0.146	-0.165	-0.196	-0.235	-0.278	-0.241	-0.301	-0.347	-0.381	-0.408	-0.430	-0.446
N(CH ₃) ₃	-0.697	-0.711	-0.707	-0.688	-0.660	-0.627	-0.592	-0.278	-0.351	-0.405	-0.446	-0.478	-0.503	-0.524
N _{eq}								N _{eq}						
NH ₃	0.402	0.393	0.389	0.391	0.400	0.415	–	-0.289	-0.287	-0.284	-0.282	-0.279	-0.276	–
NH ₂ CH ₃	–	0.367	0.352	0.345	0.347	0.380	0.381	–	-0.287	-0.286	-0.280	-0.277	-0.274	-0.270
NH(CH ₃) ₂	0.355	0.327	0.306	0.298	0.300	0.314	0.338	-0.293	-0.289	-0.286	-0.281	-0.277	-0.274	-0.270
N(CH ₃) ₃	0.259	0.217	0.189	0.177	0.182	0.203	0.237	-0.297	-0.293	-0.291	-0.287	-0.283	-0.279	-0.275

Table A2.7: Mulliken and APT partial charges (e) for porphyrin at restricted Co–N_α bond lengths

α ligands	MULLIKEN							APT						
	1.9	2.0	2.1	2.2	2.3	2.4	2.5	1.9	2.0	2.1	2.2	2.3	2.4	2.5
Co(III)								Co(III)						
NH ₃	-1.768	-1.757	-1.741	-1.735	-1.732	-1.742	–	0.335	0.349	0.358	0.360	0.365	0.364	–
NH ₂ CH ₃	-1.787	-1.765	-1.785	-1.685	-1.607	-1.563	-1.567	0.346	0.356	0.363	0.369	0.372	0.372	0.369
NH(CH ₃) ₂	-2.220	-2.002	-1.774	-1.589	-1.469	-1.409	-1.423	0.353	0.364	0.372	0.378	0.381	0.382	0.380
N(CH ₃) ₃	-1.636	-1.335	-1.123	-0.861	-0.755	-0.728	-0.823	0.342	0.359	0.370	0.379	0.383	0.385	0.384
C _β								C _β						
NH ₃	-0.525	-0.516	-0.503	-0.484	-0.469	-0.444	–	0.126	0.137	0.146	0.154	0.162	0.169	–
NH ₂ CH ₃	-0.334	-0.336	-0.351	-0.366	-0.379	-0.387	-0.389	0.111	0.122	0.131	0.140	0.148	0.155	0.162
NH(CH ₃) ₂	-0.226	-0.269	-0.319	-0.368	-0.406	-0.429	-0.436	0.104	0.115	0.124	0.132	0.141	0.147	0.154
N(CH ₃) ₃	-0.167	-0.208	-0.275	-0.298	-0.336	-0.360	-0.390	0.111	0.119	0.127	0.133	0.140	0.146	0.152
N _α								N _α						
NH ₃	-0.814	-0.821	-0.830	-0.846	-0.869	-0.901	–	-0.184	-0.232	-0.267	-0.291	-0.310	-0.321	–
NH ₂ CH ₃	-0.478	-0.492	-0.519	-0.550	-0.592	-0.640	-0.688	-0.216	-0.260	-0.291	-0.314	-0.331	-0.342	-0.350
NH(CH ₃) ₂	-0.128	-0.158	-0.202	-0.246	-0.287	-0.339	-0.379	-0.268	-0.309	-0.338	-0.360	-0.377	-0.390	-0.400
N(CH ₃) ₃	-0.687	-0.679	-0.679	-0.636	-0.621	-0.603	-0.586	-0.306	-0.356	-0.392	-0.418	-0.438	-0.454	-0.468
N _{eq}								N _{eq}						
NH ₃	0.308	0.304	0.303	0.309	0.316	0.330	–	-0.255	-0.252	-0.250	-0.246	-0.244	-0.241	–
NH ₂ CH ₃	0.300	0.294	0.299	0.288	0.289	0.297	0.315	-0.259	-0.254	-0.251	-0.248	-0.244	-0.241	-0.238
NH(CH ₃) ₂	0.311	0.289	0.273	0.266	0.271	0.284	0.307	-0.260	-0.256	-0.252	-0.248	-0.245	-0.242	-0.238
N(CH ₃) ₃	0.217	0.185	0.171	0.152	0.158	0.176	0.210	-0.263	-0.258	-0.254	-0.251	-0.247	-0.244	-0.241

APPENDIX 3

DATA FOR CHAPTER 6

Table A3.1: IP and EA values in kcal mol⁻¹

α ligand	Calculated values /kcal mol ⁻¹	
	IP	EA
Methanethiol	9.343	-0.471
Dimethylsulfide	8.566	-0.974
Cysteine	8.218	-0.097
Methanethiolate	1.909	-4.851
Glycine	9.392	-0.485
p-Aminopyridine	8.210	-0.564
Imidazole	8.774	-0.817
Histidine	8.776	-0.394
Methanol	10.470	-1.242
2-Propanol	9.588	-0.984
Serine	9.093	-0.193
Tyrosine	7.746	-0.190
Acetate	10.389	-0.780

APPENDIX 4

DATA FOR CHAPTER 7

Table A4.1: BP86 Thermochemical data for gas phase

Models	Energies /kcal mol ⁻¹			
	Sum of electronic and thermal free energies		Sum of electronic and zero-point energies	
	Low spin	High spin	Low spin	High spin
[MeCo(NH ₃) ₅] ²⁺	-1069888	-1069858	-1069863	-1069825
[MeCo(NH ₃) ₅] ^{•+}	-1044869	-1044863	-1044844	-1044844
[14-ane] N ₄ ²⁺	-1313433	-1313394	-1313406	-1313362
[14-ane]N ₄ ^{•+}	-1288416	-1288399	-1288388	-1288370
[15-ane]N ₄ ²⁺	-1338078	-1338043	-1338049	-1338009
[15-ane]N ₄ ^{•+}	-1313061	-1313051	-1313032	-1313020
[16-ane]N ₄ ²⁺	-1362718	-1362692	-1362688	-1362657
[16-ane]N ₄ ^{•+}	-1337709	-1337700	-1337679	-1337669
Methyl radical	-24993.9		-24981.5	

Table A4.2: M06L Thermochemical data for gas phase

Models	Energies /kcal mol ⁻¹			
	Sum of electronic and thermal free energies		Sum of electronic and zero-point energies	
	Low spin	High spin	Low spin	High spin
[MeCo(NH ₃) ₅] ²⁺	-1069690	-1069669	-1069665	-1069638
[MeCo(NH ₃) ₅] ^{•+}	-1044678	-1044682	-1044655	-1044655
[14-ane] N ₄ ²⁺	-1313205	-1313169	-1313178	-1313137
[14-ane]N ₄ ^{•+}	-1288189		-1288162	
[15-ane]N ₄ ²⁺	-1337849	-1337813	-1337821	-1337782
[15-ane]N ₄ ^{•+}	-1312835	-1312829	-1312806	-1312799
[16-ane]N ₄ ²⁺	-1362488	-1362464	-1362459	-1362431
[16-ane]N ₄ ^{•+}	-1337481	-1337479	-1337451	-1337448
Methyl radical	-24988.9		-24976.4	

Table A4.3: B3LYP Thermochemical data for gas phase

Models	Energies /kcal mol ⁻¹			
	Sum of electronic and thermal free energies		Sum of electronic and zero-point energies	
	Low spin	High spin	Low spin	High spin
[MeCo(NH ₃) ₅] ²⁺	-1069759	-1069757	-1069734	-1069724
[MeCo(NH ₃) ₅] ^{•+}	-1044753	-1044757	-1044727	-1044730
[14-ane] N ₄ ²⁺	-1313305	-1313282	-1313278	-1313250
[14-ane]N ₄ ^{•+}	-1288299	-1288295	-1288272	-1288267
[15-ane]N ₄ ²⁺	-1337951	-1337933	-1337923	-1337900
[15-ane]N ₄ ^{•+}	-1312947	-1312948	-1312918	-1312918
[16-ane]N ₄ ²⁺	-1362594	-1362584	-1362564	-1362550
[16-ane]N ₄ ^{•+}	-1337595	-1337598	-1337565	-1337567
Methyl radical	-24997.2		-24985.9	

Table A4.4: PBE1PBE Thermochemical data for gas phase

Models	Energies /kcal mol ⁻¹			
	Sum of electronic and thermal free energies		Sum of electronic and zero-point energies	
	Low spin	High spin	Low spin	High spin
[MeCo(NH ₃) ₅] ²⁺	-1069341	-1069342	-1069317	-1069309
[MeCo(NH ₃) ₅] ^{•+}	-1044370	-1044379	-1044345	-1044352
[14-ane] N ₄ ²⁺	-1312606	-1312585	-1312585	-1312553
[14-ane]N ₄ ^{•+}	-1287635	-1287635	-1287608	-1287606
[15-ane]N ₄ ²⁺	-1337221	-1337206	-1337194	-1337172
[15-ane]N ₄ ^{•+}	-1312252	-1312257	-1312223	-1312227
[16-ane]N ₄ ²⁺	-1361832	-1361826	-1361802	-1361791
[16-ane]N ₄ ^{•+}	-1336870	-1336876	-1336839	-1336846
Methyl radical	-24960.2		-24948.8	

Table A4.5(A): M06L: ΔG and BDE of Co(III)-C $_{\beta}$ bonds for models A – H in gas and solution phase

Models	Gas	H ₂ O	MeOH	Oct	DMSO	DCE	MeBut	Hex
	ΔG /kcal mol ⁻¹							
A	23.34	28.29	26.82	27.98	27.60	26.79	25.90	24.72
B	26.33	29.34	27.72	28.00	28.61	27.51	27.64	27.18
C	24.61	27.31	26.02	26.36	26.58	26.08	28.09	28.11
D	18.64	21.98	20.61	20.07	21.34	20.53	20.37	20.10
E	27.68	28.89	29.84	30.46	31.59	29.89	30.19	30.48
F	23.62	23.98	24.34	24.55	25.80	24.62	24.96	24.99
G	21.24	22.05	22.79	23.08	23.73	23.02	23.29	23.30
H	21.69	20.18	22.87	22.24	23.47	22.83	22.68	22.34
Models	BDE /kcal mol ⁻¹							
A	33.48	40.32	39.62	40.55	40.05	38.72	38.08	35.66
B	39.49	41.24	39.83	40.08	40.63	39.60	39.68	39.42
C	37.96	39.33	38.22	38.83	38.85	38.38	39.31	39.33
D	31.23	33.70	31.08	33.04	33.17	32.53	32.17	30.30
E	40.03	40.23	40.90	41.43	41.93	41.02	41.15	41.37
F	35.48	34.68	35.44	35.80	36.34	35.44	35.78	36.06
G	33.18	33.16	33.99	34.26	34.90	33.99	34.23	34.17
H	32.85	31.71	32.90	33.43	34.02	33.29	33.31	33.46

Table A4.5(B): M06L: Geometrical parameters for models A–H in gas and solution phase

	Gas	H ₂ O	MeOH	Oct	DMSO	DCE	MeBut	Hex
Models	Co(III)–C _β /Å							
A	1.966	1.966	1.964	1.962	1.963	1.962	1.963	1.963
B	1.963	1.970	1.969	1.967	1.970	1.967	1.965	1.961
C	1.960	1.966	1.966	1.963	1.966	1.964	1.961	1.958
D	1.935	1.946	1.945	1.943	1.946	1.944	1.940	1.938
E	1.980	1.986	1.986	1.985	1.984	1.985	1.983	1.981
F	1.957	1.965	1.966	1.964	1.966	1.965	1.964	1.959
G	1.964	1.968	1.968	1.966	1.968	1.967	1.966	1.964
H	1.956	1.962	1.962	1.960	1.962	1.962	1.960	1.957
	Co(III)–N _α /Å							
A	2.192	2.109	2.106	2.112	2.104	2.112	2.123	2.152
B	2.207	2.127	2.131	2.140	2.129	2.140	2.148	2.173
C	2.197	2.120	2.123	2.129	2.121	2.128	2.138	2.165
D	2.278	2.147	2.158	2.167	2.151	2.166	2.182	2.227
E	2.099	2.062	2.064	2.068	2.067	2.071	2.076	2.089
F	2.225	2.186	2.191	2.197	2.190	2.199	2.204	2.220
G	2.233	2.169	2.171	2.179	2.168	2.180	2.187	2.210
H	2.187	2.144	2.146	2.153	2.146	2.153	2.157	2.175
	Co(II)–N _α /Å							
A	2.244	2.115	2.106	2.110	2.123	2.127	2.122	2.134
B	2.298	2.240	2.242	2.243	2.240	2.243	2.247	2.266
C	2.288	2.232	2.288	2.241	2.233	2.240	2.249	2.262
D	2.268	2.132	2.203	2.213	2.217	2.214	2.214	2.236
E	2.141	2.141	2.112	2.115	2.116	2.119	2.123	2.132
F	2.284	2.307	2.297	2.291	2.295	2.293	2.288	2.284
G	2.264	2.250	2.248	2.248	2.246	2.248	2.249	2.253
H	2.233	2.230	2.227	2.226	2.224	2.229	2.231	2.232
	N _α –Co(III)–C _β /°							
A	177.29	179.14	177.45	177.85	177.37	177.78	179.58	178.38
B	178.41	179.23	179.10	178.68	179.17	178.69	178.42	178.09
C	176.74	176.85	176.80	176.35	176.83	176.41	176.10	176.13
D	178.89	178.79	178.87	179.41	179.18	179.34	179.77	179.51
E	179.61	179.75	179.59	179.52	179.14	179.15	179.23	179.33
F	177.90	177.72	177.68	177.64	177.70	177.73	177.69	177.76
G	176.85	176.74	177.20	177.20	177.45	177.39	177.27	177.09
H	178.97	178.26	179.24	178.88	178.88	179.00	178.98	179.22

Table A4.6(A): B3LYP: ΔG and BDE for Co(III)–C $_{\beta}$ bonds in models A–H in gas and solution phase

	Gas	H ₂ O	MeOH	Oct	DMSO	DCE	MeBut	Hex
Models	ΔG /kcal mol ⁻¹							
A	*4.37	*11.70	*10.42	*9.58	*10.02	*9.66	*10.73	*10.16
B	8.26	10.23	8.56	9.27	9.27	8.68	8.78	7.79
C	*5.60	*7.51	*2.06	*2.94	*2.86	*2.57	*2.70	*4.83
D	*-1.44	*5.18	*-14.74	*-3.33	*-15.35	*-5.07	*-4.13	*-1.94
E	15.66	16.46	17.31	18.13	16.89	17.82	17.49	17.48
F	10.25	8.86	10.21	10.31	10.98	10.15	10.58	11.37
G	7.33	7.51	8.04	8.27	9.38	8.03	8.26	8.5
H	8.86	6.89	7.25	7.81	9.31	8.12	8.75	10.12
Models	BDE /kcal mol ⁻¹							
A	*18.22	*24.66	*23.36	*23.18	*24.00	*22.86	*23.10	*23.33
B	20.12	22.22	20.98	21.46	21.17	20.92	21.00	20.05
C	*18.36	*16.23	*15.28	*16.17	*16.05	*15.74	*16.17	*17.96
D	*10.78	*10.30	*-7.11	*9.04	*-7.22	*7.89	*8.77	*10.32
E	27.22	27.65	28.22	28.55	28.68	28.25	28.40	28.54
F	21.43	20.11	21.05	21.48	21.80	21.06	21.49	22.05
G	18.58	18.93	19.63	19.86	20.64	19.53	19.71	19.62
H	18.79	17.83	18.51	18.93	19.71	18.85	19.23	19.42

*Energy calculated using the high spin state of the Co(II) species as it gave a lower energy than the low spin state; this is in accordance with previous reports on B3LYP calculations⁵⁰

Table A4.6(B): B3LYP: Geometrical parameters for models A–H in gas and solution phase

	Gas	H ₂ O	MeOH	Oct	DMSO	DCE	MeBut	Hex
Models	Co(III)–C _β /Å							
A	1.976	1.971	1.971	1.970	1.971	1.971	1.972	1.972
B	1.973	1.982	1.981	1.979	1.981	1.979	1.977	1.974
C	1.970	1.976	1.975	1.973	1.975	1.973	1.971	1.971
D	1.944	1.954	1.953	1.950	1.954	1.953	1.950	1.946
E	1.990	1.995	1.995	1.994	1.993	1.994	1.992	1.990
F	1.963	1.971	1.971	1.970	1.971	1.970	1.969	1.965
G	1.968	1.972	1.972	1.971	1.972	1.971	1.970	1.968
H	1.960	1.967	1.967	1.965	1.966	1.966	1.965	1.961
	Co(III)–N _α /Å							
A	2.207	2.105	2.109	2.116	2.107	2.116	2.122	2.154
B	2.240	2.133	2.138	2.149	2.136	2.149	2.161	2.192
C	2.222	2.128	2.132	2.136	2.130	2.136	2.144	2.183
D	2.349	2.165	2.174	2.192	2.171	2.192	2.214	2.270
E	2.097	2.062	2.063	2.068	2.066	2.070	2.076	2.088
F	2.240	2.202	2.205	2.213	2.202	2.215	2.221	2.237
G	2.250	2.174	2.175	2.184	2.172	2.186	2.195	2.223
H	2.194	2.146	2.149	2.156	2.147	2.157	2.164	2.182
	Co(II)–N _α /Å							
A	*2.132	*2.124	*2.175	*2.223	*2.225	*2.114	*2.116	*2.116
B	2.332	2.261	2.265	2.268	2.254	2.269	2.273	2.285
C	*2.191	*2.166	*2.249	*2.168	*2.246	*2.168	*2.167	*2.171
D	*2.178	*2.146	*2.282	*2.142	*2.284	*2.277	*2.172	*2.301
E	2.176	2.146	2.147	2.149	2.152	2.154	2.158	2.167
F	2.312	2.353	2.340	2.331	2.332	2.334	2.328	2.316
G	2.284	2.275	2.272	2.270	2.268	2.270	2.270	2.274
H	2.255	2.253	2.249	2.247	2.247	2.250	2.249	2.250
	N _α –Co(III)–C _β /°							
A	177.23	177.13	177.11	177.18	177.05	177.18	177.20	177.38
B	178.72	179.12	179.01	178.55	179.08	178.56	178.30	178.19
C	176.91	177.18	177.07	176.71	177.13	176.73	176.50	177.42
D	178.75	179.20	179.31	178.29	178.99	178.17	178.02	178.20
E	179.45	177.13	177.11	177.18	177.05	177.18	177.20	177.38
F	178.86	179.12	179.01	178.55	179.08	178.56	178.30	178.19
G	176.72	177.18	177.07	176.71	177.13	176.73	176.50	177.42
H	178.97	179.20	179.03	178.29	179.41	179.33	179.33	179.04

*High spin state of the Co(II) species was measured.

Table A4.7(A): PBE1PBE: ΔG and BDE for Co(III)–C $_{\beta}$ bonds in models A–H in gas and solution phase

	Gas	H ₂ O	MeOH	Oct	DMSO	DCE	MeBut	Hex
Models	ΔG /kcal mol ⁻¹							
A	*3.38	*5.63	*7.10	*9.00	*9.49	*5.07	*8.97	*6.09
B	10.99	14.09	10.00	11.77	10.81	11.29	11.23	10.23
C	*4.02	*1.71	*2.26	*0.90	*1.85	*1.23	*0.82	*3.86
D	*-4.69	*-5.08	*-5.49	*-6.15	*-4.99	*-8.45	*-5.64	*-6.01
E	19.11	19.31	21.40	20.66	22.04	20.53	20.51	20.18
F	12.97	12.21	14.28	13.23	14.22	13.19	13.24	14.03
G	9.64	10.08	11.82	10.99	12.05	10.64	11.02	10.93
H	9.83	7.87	8.60	9.03	8.40	7.70	8.17	10.00
Models	BDE /kcal mol ⁻¹							
A	*16.32	*19.46	*22.25	–	*23.12	*18.06	*21.67	*19.17
B	23.12	29.59	23.03	24.34	23.79	23.86	23.19	22.66
C	*17.19	*15.11	*14.43	*14.85	*15.10	*14.82	*14.84	*17.07
D	*7.57	*7.69	*6.45	*6.96	*7.17	*5.15	*6.50	*6.82
E	30.58	31.10	31.67	32.10	32.72	31.77	31.84	31.83
F	23.68	23.00	23.70	24.10	24.54	23.66	23.96	24.37
G	20.97	21.50	22.20	22.46	23.25	22.11	22.32	22.11
H	20.37	19.56	19.60	20.47	20.56	19.79	20.35	21.01

*Energy calculated using the high spin state of the Co(II) species as it gave a lower energy than the low spin state; this is in accordance with previous reports on B3LYP calculations.⁵⁰

Table A4.7(B): PBE1PBE: Geometrical parameters for models A–H in gas and solution phase

	Gas	H ₂ O	MeOH	Oct	DMSO	DCE	MeBut	Hex
Models	Co(III)–C _β /Å							
A	1.953	1.951	1.951	1.950	1.951	1.951	1.949	1.951
B	1.951	1.959	1.958	1.955	1.958	1.956	1.954	1.950
C	1.948	1.954	1.953	1.950	1.953	1.951	1.949	1.945
D	1.923	1.934	1.933	1.931	1.933	1.931	1.929	1.924
E	1.966	1.971	1.971	1.970	1.969	1.969	1.968	1.966
F	1.940	1.948	1.948	1.946	1.948	1.948	1.946	1.942
G	1.944	1.948	1.948	1.947	1.949	1.948	1.946	1.944
H	1.936	1.943	1.943	1.941	1.943	1.942	1.940	1.937
	Co(III)–N _α /Å							
A	2.151	2.066	2.069	2.076	2.067	2.076	2.083	2.109
B	2.166	2.089	2.093	2.102	2.091	2.102	2.111	2.138
C	2.158	2.086	2.089	2.095	2.087	2.095	2.103	2.125
D	2.245	2.117	2.121	2.130	2.119	2.145	2.149	2.200
E	2.053	2.025	2.026	2.030	2.029	2.032	2.037	2.046
F	2.161	2.131	2.134	2.139	2.132	2.140	2.146	2.157
G	2.175	2.118	2.119	2.127	2.117	2.128	2.135	2.155
H	2.136	2.097	2.100	2.106	2.099	2.107	2.112	2.127
	Co(II)–N _α /Å							
A	*2.116	2.198	#2.101	#2.192	#2.101	#2.127	#2.107	2.195
B	2.275	#4.302	#2.149	#2.144	#2.147	#2.143	#2.145	2.240
C	*2.165	#2.138	#2.139	#2.146	#2.139	#2.140	#2.148	#2.148
D	*2.154	#2.121	#2.120	#2.120	#2.129	2.121	#2.233	#2.142
E	2.140	2.119	2.120	2.122	2.125	2.126	2.129	2.135
F	2.249	2.278	2.272	2.264	2.270	2.268	2.260	2.249
G	2.233	2.227	2.226	2.224	2.223	2.225	2.224	2.227
H	2.206	2.209	#2.149	#2.150	#2.147	#2.152	#2.154	2.204
	N _α –Co(III)–C _β /°							
A	177.12	177.31	177.12	177.51	177.10	177.10	177.55	179.23
B	178.53	179.27	179.20	178.60	179.20	178.62	178.17	177.85
C	176.63	176.82	176.72	176.48	176.83	176.50	176.39	176.25
D	178.75	178.60	178.64	178.77	178.60	178.14	178.70	178.67
E	179.44	177.31	177.12	177.51	177.10	177.10	177.55	178.32
F	178.88	179.27	179.20	178.60	179.20	178.62	178.17	177.85
G	176.63	176.82	176.72	176.48	176.83	176.50	176.39	176.25
H	178.79	178.60	178.64	178.77	178.60	178.59	178.59	178.67

#high spin state measured

Table A4.8: $\Delta\Delta G_{\text{solv}}$ for BP86, M06L, B3LYP and PBE1PBE for models A–H

	$\Delta\Delta G_{\text{solv}} / \text{kcal mol}^{-1}$						
	H ₂ O	MeOH	Oct	DMSO	DCE	MeBut	Hex
BP86							
A	3.65	2.72	2.57	3.30	3.16	1.19	1.44
B	1.82	0.79	0.92	1.61	1.48	-0.01	-0.89
C	0.86	-0.39	-0.51	0.45	0.10	-1.33	0.48
D	4.42	2.34	-1.02	3.02	-0.76	0.91	0.20
E	-0.38	0.35	0.33	1.50	0.46	1.51	1.13
F	-2.06	-0.91	-0.40	-0.18	-0.71	-0.32	0.70
G	0.37	0.27	0.55	0.45	0.69	0.81	1.28
H	-2.97	-2.04	-1.44	-0.93	-2.13	-1.18	-1.20
M06L							
A	9.23	7.76	8.92	8.54	7.73	5.24	4.41
B	3.01	1.39	1.67	2.28	1.18	-0.30	-0.40
C	2.70	1.41	1.75	1.97	1.47	1.87	2.24
D	3.34	1.23	1.44	2.70	1.89	0.13	0.20
E	1.21	2.17	2.78	3.91	2.21	0.91	1.55
F	0.37	0.72	0.94	2.18	1.00	-0.26	0.12
G	0.81	1.54	1.84	2.49	1.78	0.44	0.80
H	-1.50	-4.81	0.56	1.78	1.14	-0.61	-0.60
B3LYP							
A	7.32	6.05	5.22	5.65	5.29	4.83	4.58
B	1.97	0.30	1.02	1.01	0.42	-1.01	-1.67
C	-2.54	-3.54	-2.66	-2.74	-3.03	-4.43	-1.98
D	1.63	-13.30	-1.89	-13.91	-3.63	-4.22	-1.71
E	-4.41	-1.05	2.47	1.23	2.16	0.30	0.61
F	-6.59	-2.74	0.06	0.73	-0.09	-1.20	-0.09
G	-5.03	-2.00	0.93	2.04	0.70	-0.60	-0.05
H	-7.17	-4.31	-1.05	0.46	-0.73	-1.64	0.05
PBE1PBE							
A	2.24	3.72	5.58	6.11	1.68	4.10	1.53
B	3.08	-0.99	0.78	-0.19	0.29	-1.25	-1.95
C	-2.32	-3.02	-3.12	-2.17	-2.80	-4.69	-1.35
D	-0.40	-2.06	-1.46	-0.31	-3.77	-2.44	-2.52
E	0.20	1.03	1.55	2.93	1.42	1.40	1.07
F	-0.76	0.04	0.26	1.24	0.21	0.26	1.06
G	0.44	0.92	1.35	2.41	1.01	1.38	1.30
H	-1.96	-11.77	-0.80	-1.42	-2.13	-1.66	0.17

Table A4.9: BDE_{solv} for BP86, M06L, B3LYP and PBE1PBE for models A–H for all solvents

Models	M06L						
	$BDE_{solv} / \text{kcal mol}^{-1}$						
	H ₂ O	MeOH	Oct	DMSO	DCE	MeBut	Hex
A	40.32	39.62	40.55	40.05	38.72	38.08	35.66
B	41.24	39.83	40.08	40.63	39.60	39.68	39.42
C	39.33	38.22	38.83	38.85	38.38	39.31	39.33
D	33.70	31.08	33.04	33.17	32.53	32.17	30.30
E	40.22	40.90	41.43	41.93	41.02	41.15	41.37
F	34.68	35.44	35.80	36.34	35.44	35.78	36.06
G	33.16	33.99	34.26	34.90	33.99	34.23	34.17
H	31.71	32.90	33.43	34.02	33.29	33.31	33.46
B3LYP							
A	17.33	17.31	17.97	18.36	17.57	18.28	18.75
B	20.26	20.68	20.45	20.16	20.51	22.02	21.72
C	18.77	18.82	18.83	18.79	18.77	20.59	19.93
D	8.67	6.19	10.93	6.69	11.52	12.99	12.04
E	32.06	29.27	26.08	27.45	26.08	28.09	27.93
F	26.70	23.79	21.42	21.08	21.16	22.69	22.14
G	23.96	21.63	18.92	18.60	18.83	20.31	19.67
H	25.00	22.82	19.97	19.25	19.58	20.86	19.37
PBE1PBE							
A	17.22	18.54	17.34	17.01	16.38	17.57	17.64
B	26.50	24.03	23.57	23.98	23.57	24.44	24.61
C	17.45	17.43	17.97	17.27	17.62	19.53	18.42
D	8.50	8.09	8.42	7.48	8.93	8.94	9.34
E	30.90	30.64	30.55	29.80	30.35	30.44	30.76
F	23.76	23.66	23.83	23.30	23.44	23.70	23.31
G	21.06	21.28	21.11	20.84	21.11	20.94	20.81
H	21.52	31.38	21.27	21.98	21.92	22.02	20.84

Table A4.10: N_{eq} -Co- C_β bond angles ($^\circ$) for models A–D in both gas and solution phase

	Gas	H ₂ O	MeOH	Oct	DMSO	DCE	MeBut	Hex	^a Theoretical value for MeCbl and AdoCbl ¹⁴¹	^b Experimental data for MeCbl ¹⁴⁹	^c Experimental data for AdoCbl ²⁹⁵
^d Bond angles	A = NH₃-[Co(III)(NH₃)₅]-CH₃										
N_{eq1} -Co- C_β	88.29	89.05	88.64	88.56	88.29	88.58	89.07	87.89	93.95	95.00	95.00
N_{eq2} -Co- C_β	88.00	89.09	89.19	88.86	89.49	88.87	90.83	88.24	87.76	86.00	86.00
N_{eq3} -Co- C_β	87.31	88.98	89.35	89.17	89.68	89.18	87.92	88.45	90.15	87.00	89.00
N_{eq4} -Co- C_β	91.64	92.70	92.64	92.54	92.42	92.56	91.14	92.13	89.52	90.00	93.00
	B = NH₃-[Co(III)(14-ane)N₄]-CH₃										
N_{eq1} -Co- C_β	87.12	87.48	92.61	92.59	92.63	92.61	87.25	92.46	93.95	95.00	95.00
N_{eq2} -Co- C_β	87.12	87.48	87.48	87.37	87.48	87.37	87.25	87.07	87.76	86.00	86.00
N_{eq3} -Co- C_β	92.19	92.65	87.48	87.38	87.48	87.37	92.57	87.07	90.15	87.00	89.00
N_{eq4} -Co- C_β	92.18	92.65	92.61	92.59	92.63	92.61	92.57	92.46	89.52	90.00	93.00
	C = NH₃-[Co(III)(15-ane)N₄]-CH₃										
N_{eq1} -Co- C_β	91.56	92.12	92.09	92.13	92.06	92.14	92.10	91.62	93.95	95.00	95.00
N_{eq2} -Co- C_β	85.78	86.05	86.02	85.80	86.10	85.84	85.67	85.50	87.76	86.00	86.00
N_{eq3} -Co- C_β	91.65	91.85	91.85	91.82	91.90	91.83	91.81	91.58	90.15	87.00	89.00
N_{eq4} -Co- C_β	89.56	89.95	89.90	89.88	89.87	89.88	89.83	89.56	89.52	90.00	93.00
	D = NH₃-[Co(III)(16-ane)N₄]-CH₃										
N_{eq1} -Co- C_β	90.88	91.48	91.51	91.19	91.48	91.14	91.32	91.19	93.95	95.00	95.00
N_{eq2} -Co- C_β	90.89	91.46	91.49	91.43	91.46	91.34	91.16	91.19	87.76	86.00	86.00
N_{eq3} -Co- C_β	94.22	94.37	94.27	93.96	94.34	94.05	94.74	94.47	90.15	87.00	89.00
N_{eq4} -Co- C_β	94.19	94.36	94.26	94.65	94.32	94.74	93.80	93.85	89.52	90.00	93.00

^a Theoretical results obtained from a study conducted by Dolker *et al.*¹⁴¹ using the B3LYP method for the MeCbl model, Benz-[Co(III)corrin]-CH₃ and AdoCbl model, Benz-[Co(III)corrin]-CH₂THF. ^{b,c} X-ray data for the MeCbl¹⁴⁹ and AdoCbl²⁹⁵ crystal structure, respectively. ^d These bond angles have been defined as per the numbering used in Figure 5.8, Chapter 5.

Table A4.11: Torsion angles (°) for models E–H in both the gas and solution phase

	Gas	H ₂ O	MeOH	Oct	DMSO	DCE	MeBut	Hex	^a Theoretical value for MeCbl ¹⁴¹	^b Experimental data for MeCbl ¹⁴⁹	^c Experimental data for AdoCbl ²⁹⁵
^d Bond angles /°	E = NH₃–[Co(III)cobaloxime]–CH₃										
N _{eq1} –Co–C _β	88.18	87.57	87.92	87.94	88.11	88.09	88.19	88.12	93.95	95.00	95.00
N _{eq2} –Co–C _β	87.44	87.82	87.53	87.51	87.69	87.61	87.52	87.52	87.76	86.00	86.00
N _{eq3} –Co–C _β	90.94	90.97	90.64	90.63	90.55	90.54	90.47	90.68	90.15	87.00	89.00
N _{eq4} –Co–C _β	90.67	90.39	90.63	90.57	90.58	90.55	90.57	90.47	89.52	90.00	93.00
	F = NH₃–[Co(III)corrole]–CH₃										
N _{eq1} –Co–C _β	92.22	91.59	91.77	91.86	91.51	91.91	91.87	92.19	93.95	95.00	95.00
N _{eq2} –Co–C _β	89.91	89.56	89.52	89.53	89.19	89.49	89.54	89.68	87.76	86.00	86.00
N _{eq3} –Co–C _β	90.13	89.67	89.72	89.71	90.02	89.70	89.85	89.84	90.15	87.00	89.00
N _{eq4} –Co–C _β	92.44	91.73	91.97	92.04	92.27	92.10	92.16	92.30	89.52	90.00	93.00
	G = NH₃–[Co(III)corrin]–CH₃										
N _{eq1} –Co–C _β	93.11	92.90	93.13	93.13	93.12	93.08	93.11	93.12	93.95	95.00	95.00
N _{eq2} –Co–C _β	87.37	87.15	87.53	87.50	87.58	87.50	87.50	87.47	87.76	86.00	86.00
N _{eq3} –Co–C _β	90.52	90.79	90.70	90.60	90.76	90.69	90.58	90.50	90.15	87.00	89.00
N _{eq4} –Co–C _β	90.10	90.32	90.07	90.00	90.01	90.00	89.94	89.94	89.52	90.00	93.00
	H = NH₃–[Co(III)porphyrin]–CH₃										
N _{eq1} –Co–C _β	92.12	91.43	91.43	91.92	91.90	91.96	91.96	92.13	93.95	95.00	95.00
N _{eq2} –Co–C _β	90.78	91.40	91.69	90.46	90.75	91.02	90.56	90.71	87.76	86.00	86.00
N _{eq3} –Co–C _β	89.22	89.60	89.61	89.08	89.08	89.06	89.09	89.07	90.15	87.00	89.00
N _{eq4} –Co–C _β	90.71	89.30	89.33	90.51	90.15	90.08	90.50	90.56	89.52	90.00	93.00

^a Theoretical results obtained from a study conducted by Dolker *et al.*¹⁴¹ using the B3LYP method for the MeCbl model, Benz–[Co(III)corrin]–CH₃ and AdoCbl model, Benz–[Co(III)corrin]–CH₂THF. ^{b,c} X-ray data for the MeCbl¹⁴⁹ and AdoCbl²⁹⁵ crystal structure, respectively. ^d These bond angles have been defined as per the numbering used in Figure 5.8, Chapter 5.

APPENDIX 5

DATA FOR CHAPTER 8

Table A5.1: GAS PHASE: Geometrical parameters and energies for M06L

M06L						
	σ_p	Bond length /Å			Energies /kcal mol ⁻¹	
		Co(III)-C β	Co(III)-N α	N α -Co(III)-C β	ΔG	BDE
NO	0.91	1.967	2.215	177.09	21.35	33.47
NO ₂	0.78	1.966	2.226	177.10	21.48	33.31
COOH	0.45	1.965	2.227	177.08	20.99	33.34
Cl	0.23	1.964	2.236	177.05	20.74	33.00
CH ₃	-0.17	1.964	2.237	177.03	21.06	32.98
OH	-0.37	1.963	2.246	177.11	21.19	33.05
NH ₂	-0.66	1.963	2.248	177.20	21.14	33.00

Table A5.2: GAS PHASE: Geometrical parameters and energies for B3LYP

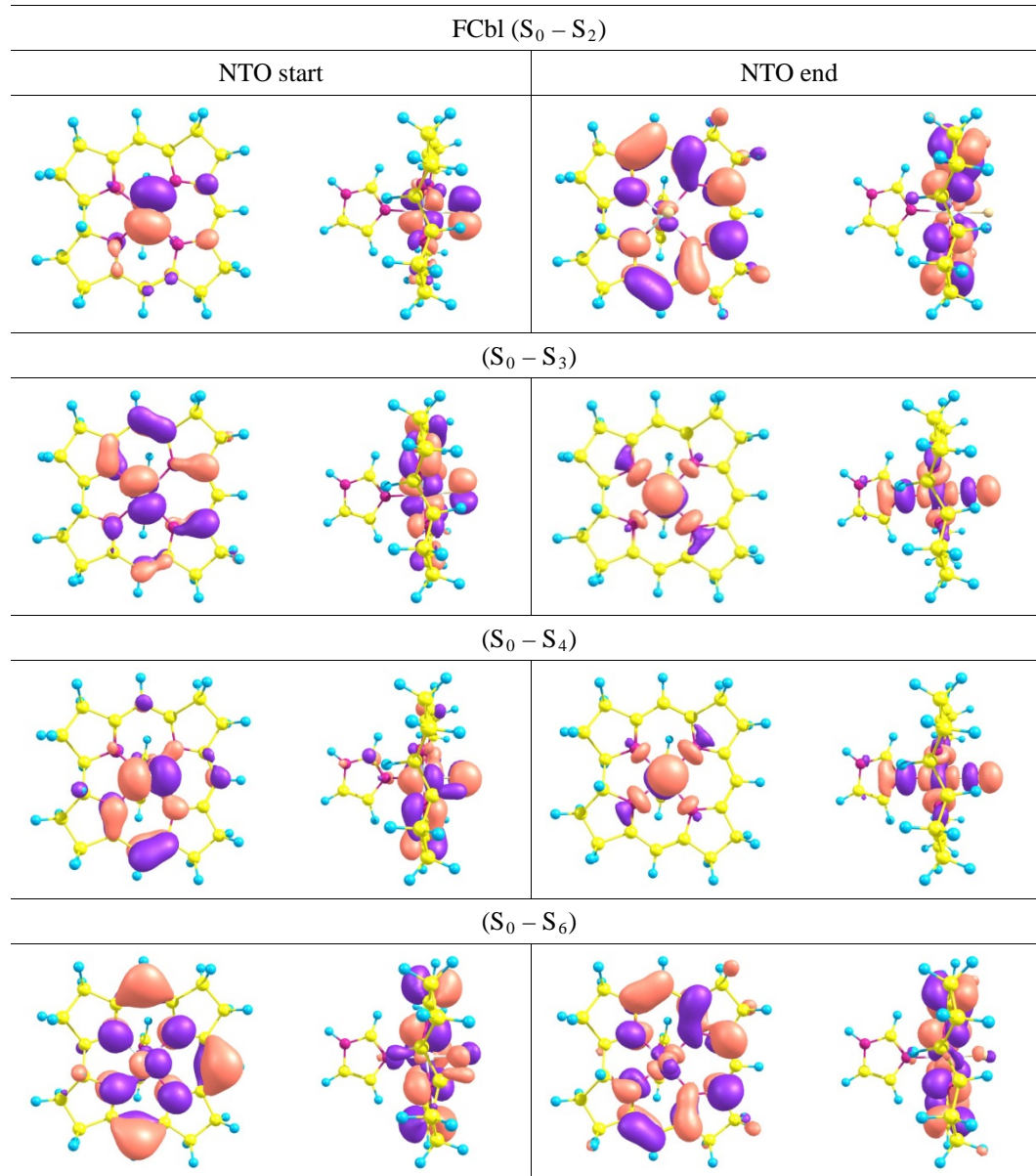
B3LYP						
	σ_p	Bond length /Å			Energies /kcal mol ⁻¹	
		Co(III)-C β	Co(III)-N α	N α -Co(III)-C β	ΔG	BDE
NO	0.91	1.972	2.228	176.84	8.00	18.99
NO ₂	0.78	1.971	2.242	176.89	7.76	18.75
COOH	0.45	1.970	2.242	176.86	7.84	18.84
Cl	0.23	1.969	2.255	176.81	7.59	18.55
CH ₃	-0.17	1.968	2.256	176.75	7.44	18.60
OH	-0.37	1.968	2.265	176.86	7.52	18.37
NH ₂	-0.66	1.967	2.269	176.85	7.48	18.45

Table A5.3: GAS PHASE: Geometrical parameters and energies for PBE1PBE

	PBE1PBE							
	σ_p	Bond length /Å			Bond Angle /°		Energies /kcal mol ⁻¹	
		Co(III)-C _β	Co(III)-N _α	N _α -Co(III)-C _β	ΔG	BDE		
NO	0.91	1.947	2.161	176.92	10.11	22.81		
NO ₂	0.78	1.946	2.169	176.95	9.99	21.10		
COOH	0.45	1.945	2.169	176.92	10.07	21.19		
Cl	0.23	1.944	2.178	176.86	9.71	20.84		
CH ₃	-0.17	1.943	2.178	176.74	9.49	20.88		
OH	-0.37	1.943	2.184	176.89	9.66	20.75		
NH ₂	-0.66	1.943	2.186	176.92	9.65	20.76		

APPENDIX 6

DATA FOR CHAPTER 9



REFERENCES

- (1) <http://chemistry.ncssm.edu/book/index.html>, last accessed 27/10/2009
- (2) http://en.wikipedia.org/wiki/Computational_chemistry, last accessed 27/10/2009
- (3) Cramer, C. J. *Essentials of Computational Chemistry*; 2 ed.; John Wiley and Sons: Chichester, 2004.
- (4) <http://www.shodor.org/chemviz/overview/ccbasics.html>, last accessed 28/10/2009.
- (5) Pathare, P. M.; Wilbur, D. S.; Heusser, S.; Quadros, E. V.; McLoughlin, P.; Morgan, A. C. *Bioconjugate Chem.* **1996**, *7*, 217-232.
- (6) Jensen, K. P.; Sauer, S. P. A.; Liljefors, T.; Norrby, P.-O. *Organometallics* **2001**, *20*, 550-556.
- (7) Zbik, D. R.; Jaworska, M.; Witko, M. *Struct. Chem.* **2004**, *15*, 431-435.
- (8) Hay, B. P.; Finke, R. G. *J. Am. Chem. Soc.* **1986**, *108*, 4820-4829.
- (9) Dölker, N.; Maseras, F.; Lledos, A. *J. Phys. Chem. B* **2001**, *105*, 7564-7571.
- (10) Hansen, L. M.; Kumar, P. N. V. P.; Marynick, D. S. *Inorg. Chem.* **1994**, *33*, 728-735.
- (11) Zbik, D. R.; Witko, M.; Stochel, G. *Theo. Chem. Acc.* **2008**, *120*, 411-419.
- (12) Banerjee, R. *Chem. Rev.* **2003**, *103*, 2083-2094.
- (13) Dölker, N.; Morreale, A.; Maseras, F. *J. Biol. Inorg. Chem.* **2005**, *10*, 509-517.
- (14) Kuta, J.; Patchkovskii, S.; Zgierski, M. Z.; Kozlowski, P. M. *J. Comp. Chem.* **2006**, *27*, 1429-1437.
- (15) Follett, A. D.; McNabb, K. A.; Peterson, A. A.; Scanion, J. D.; Cramer, C. J.; McNeill, K. *Inorg. Chem.* **2007**, *46*, 1645-1654.
- (16) Jensen, K. P.; Mikkelsen, K. V. *Inorg. Chim. Act.* **2001**, *323*, 5-15.

-
- (17) Liptak, M. D.; Brunold, T. C. *J. Am. Chem. Soc.* **2006**, *128*, 9144-9156.
- (18) Rovira, C.; Biarnes, X. *Inorg. Chem.* **2004**, *43*, 6628-6632.
- (19) Toraya, T. *Chem. Rev.* **2003**, *103*, 2095-2127.
- (20) Halpern, J.; Kim, S. H.; Leung, T. W. *J. Am. Chem. Soc.* **1984**, *106*, 8317-8319.
- (21) Mealli, C.; Sabat, M.; Marzilli, L. G. *J. Am. Chem. Soc.* **1987**, *109*, 1593-1594.
- (22) Silverman, R. B.; Dolphin, D. *J. Am. Chem. Soc.* **1976**, *98*, 4626-4633.
- (23) Kozłowski, P. M.; Andruniow, T.; Jarzecki, A. A.; Zgierski, M. Z.; Spiro, T. G. *Inorg. Chem.* **2006**, *45*, 5585-5590.
- (24) Matthews, R. G. *Acc. Chem. Res.* **2001**, *34*, 681-689.
- (25) Kozłowski, P. M. *Curr. Opin. Chem. Biol.* **2001**, *5*, 736-743.
- (26) Hay, B. P.; Finke, R. G. *J. Am. Chem. Soc.* **1987**, *109*, 8012-8018.
- (27) Garr, C. D.; Finke, R. G. *Inorg. Chem.* **1993**, *32*, 4414-4421.
- (28) Banerjee, R. *Chem. Bio.* **1997**, *4*, 175-186.
- (29) Marques, H. M.; Brown, K. L. *Inorg. Chem.* **1995**, *34*, 3733-3740.
- (30) Moore, R. E.; Woolard, F. X.; Bartolini, G. *J. Am. Chem. Soc.* **1980**, *102*, 7372-7373.
- (31) Freindorf, M.; Kozłowski, P. M. *J. Am. Chem. Soc.* **2004**, *126*, 1928-1929.
- (32) Brown, K. L. *Chem. Rev.* **2005**, *105*, 2075-2149.
- (33) Brown, K. L.; Marques, H. M. *J. Inorg. Biochem.* **2001**, *83*, 121-132.
- (34) Stewart, R. C.; Marzilli, L. G. *J. Am. Chem. Soc.* **1978**, *100*, 817-822.
- (35) Tavagnacco, C.; Balducci, G.; Costa, G.; Taschler, K.; von-Philipsborn, W. *Helv. Chim. Acta* **1990**, *73*, 1469-1480.
- (36) Charland, J. P.; Zangrando, E.; Bresciani-Pahor, N.; Randaccio, L.; Marzilli, L. G. *Inorg. Chem.* **1993**, *32*, 4256-4267.

-
- (37) Grate, J. H.; Schrauzer, G. N. *J. Am. Chem. Soc.* **1979**, *101*, 4601-4611.
- (38) Marsh, E. N. G.; Drennan, C. L. *Curr. Opin. Chem. Biol.* **2001**, *5*, 499-505.
- (39) Brown, K. L.; Zou, X. *J. Inorg. Biochem.* **1999**, *77*, 185-195.
- (40) Bresciani-Pahor, N.; Forcolin, M.; Marzilli, L. G.; Randaccio, L.; Summers, M. F.; Toscana, P. J. *Coord. Chem. Rev.* **1985**, *63*, 1-125.
- (41) Dong, S.; Padmakumar, R.; Banerjee, R.; Spiro, T. G. *J. Am. Chem. Soc.* **1999**, *121*, 7063-7070.
- (42) Vlasie, M. D.; Banerjee, R. *J. Am. Chem. Soc.* **2003**, *125*, 5431-5435.
- (43) Mancia, F.; Evans, P. R. *Struct.* **1998**, *6*, 711-720.
- (44) Scheuring, E.; Padmakumar, R.; Banerjee, R.; Chance, M. R. *J. Am. Chem. Soc.* **1997**, *119*, 12192-12200.
- (45) Tollinger, M.; Konrat, R.; Hilbert, B. H.; Marsh, E. N. G.; Krautler, B. *Struct.* **1998**, *6*, 1021-1033.
- (46) Siegbahn, P. E. M.; Blomberg, M. R. A. *Chem. Rev.* **2000**, *100*, 421-437.
- (47) Krautler, B.; Keller, W.; Kratky, C. *J. Am. Chem. Soc.* **1989**, *111*, 8936-8938.
- (48) Jensen, K. P.; Ryde, U. *J. Molec. Struct.: TheoChem* **2002**, *585*, 239-255.
- (49) Schafer, A.; Horn, H.; Alrichs, R. *J. Chem. Phys.* **1992**, *97*, 2571-2578.
- (50) Jensen, K. P.; Roos, B. O.; Ryde, U. *J. Chem. Phys.* **2007**, *126*, 014103.
- (51) Brunold, T. C.; Conrad, K. S.; Liptak, M. D.; Park, K. *Coord. Chem. Rev.* **2009**, *253*, 779-794.
- (52) Dölker, N.; Maseras, F.; Siegbahn, P. E. M. *Chem. Phys. Lett.* **2004**, *386*, 174-178.
- (53) Kohn, W.; Becke, A. D.; Parr, R. G. *J. Phys. Chem.* **1996**, *100*, 12974-12980.
- (54) Padmakumar, R.; Taoka, S.; Banerjee, R. *J. Am. Chem. Soc.* **1995**, *117*, 7033-7034.

-
- (55) Andruniow, T.; Jaworska, M.; Lodowski, P.; Zgierski, M. Z.; Dreos, R.; Randaccio, L.; Kozlowski, P. M. *J. Chem. Phys.* **2009**, *131*, 105105(1) - 105105(15).
- (56) Andruniow, T.; Kozlowski, P. M.; Zgierski, M. Z. *J. Chem. Phys.* **2001**, *115*, 7522-7533.
- (57) Jensen, K. P.; Ryde, U. *J. Phys. Chem. A* **2003**, *107*, 7539-7545.
- (58) Andruniow, T.; Zgierski, M. Z.; Kozlowski, P. M. *J. Phys. Chem. B* **2000**, *104*, 10921-10927.
- (59) Andruniow, T.; Zgierski, M. Z.; Kozlowski, P. M. *Chem. Phys. Lett.* **2000**, *331*, 509-512.
- (60) Andruniow, T.; Zgierski, M. Z.; Kozlowski, P. M. *J. Am. Chem. Soc.* **2001**, *123*, 2679-2680.
- (61) Rovira, C.; Kunc, K.; Hutter, J.; Parrinello, M. *Inorg. Chem.* **2001**, *40*, 11-17.
- (62) Hinchliffe, A. *Molecular Modelling for Beginners*; John Wiley and Sons: Chichester, 2003.
- (63) Foresman, J. B.; Frisch, A. *Exploring Chemistry with Electronic Structure Methods*; 2 ed.; Gaussian, Inc. Pittsburgh, PA, 1996.
- (64) Holtjie, H.-D.; Folkers, D. *Molecular Modelling: Basic Principles and Applications*; VCH Publishers, Inc.: Weinheim, 1996; Vol. 5.
- (65) Koch, W.; Holthausen, M. C. *A Chemist's Guide to Density Functional Theory*; 2 ed.; Wiley-VCH and John Wiley and Sons: Weinheim, 2001.
- (66) Atkins, W.; Friedman, R. S. *Molecular Quantum Mechanics*; Oxford University Press Inc., 1997.
- (67) Hehre, W. J.; Radom, L.; Schleyer, P. V. R.; Pople, J. A. *Ab initio molecular orbital theory*; John Wiley and Sons: New York, 1986.
- (68) Bisetty, K. PhD dissertation, University of Kwa-Zulu Natal, 2002.
- (69) Rovira, C.; Kozlowski, P. M. *J. Phys. Chem. B* **2007**, *111*, 3251-3257.
- (70) *Molecular Modelling: Principles and Applications*; Leach, A. R., Ed.; Addison Wesley Longman Ltd., 1998.

-
- (71) Jensen, F. *Introduction to Computational Chemistry*; 2 ed.; John Wiley and Sons: Chichester, 1999.
- (72) Marzilli, L. G.; Toscana, P. J.; Randaccio, L.; Bresciani-Pahor, N.; Calligaris, M. *J. Am. Chem. Soc.* **1979**, *101*, 6754-6756.
- (73) Kohn, W.; Sham, L. J. *Phys. Rev.* **1965**, *140*, A1133-A1138.
- (74) Hohenberg, P.; Kohn, W. *Phys. Rev.* **1964**, *136*, B864-B871.
- (75) Vosko, S. J.; Wilk, L.; Nusair, M. *Can. J. Phys.* **1980**, *58*, 1200-1211.
- (76) Perdew, J. P.; Wang, Y. *Phys. Rev. B* **1986**, *33*, 8800-8802.
- (77) Becke, A. D. *Phys. Rev. A* **1988**, *38*, 3098-3100.
- (78) Lee, C.; Yang, W.; Parr, R. G. *Phys. Rev. B* **1988**, *37*, 785-789.
- (79) Perdew, J. P. *Phys. Rev. B* **1986**, *33*, 8822-8824.
- (80) Perdew, J. P. *Phys. Rev. B* **1986**, *34*, 7406-7406.
- (81) Becke, A. D. *J. Chem. Phys.* **1993**, *98*, 1372-1378.
- (82) Young, D. *Computational Chemistry: A practical guide for applying techniques to real world problems*; John Wiley and Sons, Inc.: New York, 2001.
- (83) Casida, M. E.; Jamorski, C.; Casida, K. C.; Salahub, D. R. *J. Chem. Phys.* **1998**, *108*, 4439-4449.
- (84) Dhara, A. K.; Ghosh, S. K. *Phys. Rev. A* **1987**, *35*, 442-444.
- (85) Runge, E.; Gross, E. K. U. *Phys. Rev. Lett.* **1984**, *52*, 997-1000.
- (86) Mearns, D.; Kohn, W. *Phys. Rev. A* **1987**, *35*, 4796-4799.
- (87) Casida, M. In *Time Dependent Density Functional Response Theory for Molecules: In Recent Advances in Density Functional Methods*; Chong, D. P., Ed.; World Scientific: Singapore, 1995; Vol. 1.
- (88) Jamorski, C.; Casida, M.; Salahub, D. R. *J. Chem. Phys.* **1996**, *104*, 5134-5147.
- (89) Bauernschmitt, R.; Ahlrichs, R. *Chem. Phys. Lett.* **1996**, *256*, 454-464.

-
- (90) Marques, M. A. L.; Gross, E. K. U. *Annu. Rev. Phys. Chem.* **2004**, *55*, 427-455.
- (91) Maitra, N. T.; Burke, K.; Appel, H.; Gross, E. K. U.; van-Leeuwen, R. In *Reviews in Modern Quantum Chemistry: A Celebration of the Contributions of R.G. Parr*; Sen, K. D., Ed.; World Scientific: Singapore, 2002; Vol. 2.
- (92) Tozer, D. J.; Handy, N. C. *Phys. Chem. Chem. Phys.* **2000**, *2*, 2117-2121.
- (93) Petersilka, M.; Gossman, U. J.; Gross, E. K. U. *Phys. Rev. Lett* **1996**, *76*, 1212-1215.
- (94) Petersilka, M.; Gross, E. K. U. *Int. J. Quantum Chem. Symp.* **1996**, *30*, 181-186.
- (95) Bauernschmitt, R.; Ahlrichs, R.; Hennrich, F. H.; Kappes, M. M. *J. Am. Chem. Soc.* **1998**, *120*, 5052-5059.
- (96) van-Gisbergen, S. J. A.; Koostra, F.; Schipper, P. R. T.; Gritsenko, O. V.; Snijders, J. G.; Baerends, E. J. *Phys. Rev. A* **1998**, *57*, 2556-2571.
- (97) Stratmann, R. E.; Scuseria, G. E.; Frisch, M. J. *J. Chem. Phys.* **1998**, *109*, 8218-8225.
- (98) van-Gisbergen, S. J. A.; Rosa, A.; Ricciardi, G.; Baerends, E. J. *J. Chem. Phys.* **1999**, *111*, 2499-2507.
- (99) van-Gisbergen, S. J. A.; Groeneveld, J. A.; Rosa, A.; Snijders, J. G.; Baerends, E. J. *J. Phys. Chem. A* **1999**, *103*, 6835-6844.
- (100) Zhao, Y.; Truhlar, D. G. *Theo. Chem. Acc.* **2008**, *120*, 215-241.
- (101) Becke, A. D. *J. Chem. Phys.* **1993**, *98*, 5648-5652.
- (102) Perdew, J. P.; Burke, K.; Ernzerhof, M. *Phys. Rev. Lett* **1996**, *77*, 3865-3868.
- (103) Perdew, J. P.; Burke, K.; Ernzerhof, M. *Phys. Rev. Lett* **1997**, *78*, 1396-1396
- (104) Liptak, M. D.; Fleischhacker, A. S.; Matthews, R. G.; Telser, J.; Brunold, T. *C. J. Phys. Chem. B* **2009**, *113*, 5245-5254.
- (105) Pratt, J. M.; Thorpe, R. G. *Inorg. Phys. Theor.* **1966**, 187-191.
- (106) Firth, R. A.; Hill, H. A. O.; Pratt, J. M.; Williams, R. J. P.; Jackson, W. R. *Biochem.* **1967**, *6*, 2178-2189.

-
- (107) Solheim, H.; Kornobis, K.; Ruud, K.; Kozlowski, P. M. *J. Phys. Chem. B* **2011**, *115*, 737-748.
- (108) Harris, D. A.; Stickrath, A. B.; Carroll, E. C.; Sension, R. J. *J. Am. Chem. Soc.* **2007**, *129*, 7578-7585.
- (109) Lodowski, P.; Jaworska, M.; Andruniow, T.; Kumar, M.; Kozlowski, P. M. *J. Phys. Chem. B* **2009**, *113*, 6898-6909.
- (110) Andruniow, T.; Jaworska, M.; Lodowski, P.; Zgierski, M. Z.; Dreos, R.; Randaccio, L.; Kozlowski, P. M. *J. Chem. Phys.* **2008**, *129*, 085101.
- (111) Peng, J.; Tang, K. C.; McLoughlin, K.; Yang, Y.; Forgach, D.; Sension, R. J. *J. Phys. Chem. B* **2010**, *114*, 12398-12405.
- (112) Jaworska, M.; Lodowski, P. *J. Molec. Struct.: Theochem* **2003**, *631*, 209-223.
- (113) Kornobis, K.; Kumar, N.; Wong, B. M.; Lodowski, P.; Jaworska, M.; Andruniow, T.; Ruud, K.; Kozlowski, P. M. *J. Phys. Chem. A* **2011**, *115*, 1280-1292.
- (114) Brooks, A. J.; Vlasie, M.; Banerjee, R.; Brunold, T. C. *J. Am. Chem. Soc.* **2005**, *127*, 16522-16528.
- (115) Brooks, A. J.; Vlasie, M.; Banerjee, R.; Brunold, T. C. *J. Am. Chem. Soc.* **2004**, *126*, 8167-8180.
- (116) Sension, R. J.; Harris, D. A.; Stickrath, A.; Cole, A. G.; Fox, C. C.; Marsh, E. N. G. *J. Phys. Chem. B* **2005**, *109*, 18146-18152.
- (117) Stich, T. A.; Brooks, A. J.; Buan, N. R.; Brunold, T. C. *J. Am. Chem. Soc.* **2003**, *125*, 5897-5914.
- (118) Stich, T. A.; Buan, N. R.; Brunold, T. C. *J. Am. Chem. Soc.* **2004**, *126*, 9735-9749.
- (119) Chemaly, S. M. *Dalton Trans.* **2008**, 5766-5773.
- (120) Andruniow, T.; Kuta, J.; Zgierski, M. Z.; Kozlowski, P. M. *Chem. Phys. Lett.* **2005**, *410*, 410-416.
- (121) Jaworska, M.; Lodowski, P.; Andruniow, T.; Kozlowski, P. M. *J. Phys. Chem. B* **2007**, *111*, 2419-2422.
- (122) Zou, X.; Brown, K. L. *Inorg. Chim. Act.* **1998**, *267*, 305-308.

-
- (123) Zhu, L.; Kostic, N. M. *Inorg. Chem.* **1987**, *26*, 4194-4197.
- (124) Yoder, L. M.; Cole, A. G.; Walker, L. A.; Sension, R. J. *J. Phys. Chem. B* **2001**, *105*, 12180-12188.
- (125) Y. Shen; Ryde, U. *J. Inorg. Biochem.* **2004**, *98*, 878-895.
- (126) Wu, Q.; Voorhis, T. v. *J. Chem. Theo. Comput.* **2006**, *2*, 765-774.
- (127) Wood, J. M.; Kennedy, F. S.; Wolfe, R. S. *Biochem.* **1968**, *7*, 1707-1713.
- (128) Waddington, M. D.; Finke, R. G. *J. Am. Chem. Soc.* **1993**, *115*, 4629-4640.
- (129) Vogel, K. M.; Kozlowski, P. M.; Zgierski, M. Z.; Spiro, T. G. *Inorg. Chim. Act.* **2000**, *297*, 11-17.
- (130) Trommel, J. S.; Warncke, K.; Marzilli, L. G. *J. Am. Chem. Soc.* **2001**, *123*, 3358-3366.
- (131) Torrent, M.; Musaev, D. G.; Morokuma, K.; Ke, S. C.; Warncke, K. *J. Phys. Chem. B* **1999**, *103*, 8618-8627.
- (132) Toraya, T.; Krodel, E.; Mildvan, A. S.; Abeles, R. H. *Biochem.* **1979**, *18*, 417-426.
- (133) Stich, T. A.; Yamanishi, M.; Banerjee, R.; Brunold, T. C. *J. Am. Chem. Soc.* **2005**, *127*, 7660-7661.
- (134) Sorkin, A.; Iron, M. A.; Truhlar, D. G. *J. Chem. Theo. Comput.* **2008**, *4*, 307-315.
- (135) Sirovatka, J. M.; Rappe, A. K.; Finke, R. G. *Inorg. Chim. Act.* **1999**, *300-302*, 545-555.
- (136) Sirovatka, J. M.; Finke, R. G. *J. Am. Chem. Soc.* **1997**, *119*, 3057-3067.
- (137) Silverman, R. B.; Dolphin, D. *J. Am. Chem. Soc.* **1975**, *98*, 4633-4639.
- (138) Shiang, J. J.; Cole, A. G.; Sension, R. J.; Hang, K.; Weng, Y.; Trommel, J. S.; Marzilli, L. G.; Lian, T. *J. Am. Chem. Soc.* **2006**, *128*, 801-808.
- (139) Vogel, K. M.; Kozlowski, P. M.; Zgierski, M. Z.; Spiro, T. G. *J. Am. Chem. Soc.* **1999**, *121*, 9915-9921.

- (140) Ridder, D. J. A. D.; Zangrando, E.; Burgi, H.-B. *J. Molec. Struct.: Theochem* **1996**, *374*, 63-83.
- (141) Dölker, N.; Maseras, F.; Lleds, A. *J. Phys. Chem. B* **2003**, *107*, 306-315.
- (142) Hay, P. J.; Wadt, W. R. *J. Chem. Phys.* **1985**, *82*, 299-310.
- (143) Hehre, W. J.; Ditchfield, R.; Pople, J. A. *J. Chem. Phys.* **1972**, *56*, 2257-2261.
- (144) Hariharan, P. C.; Pople, J. A. *Theo. Chim. Acta* **1973**, *28*, 213-222.
- (145) Hung, R. R.; Grabowski, J. J. *J. Am. Chem. Soc.* **1999**, *121*, 1359-1364.
- (146) Martin, B. D.; Finke, R. G. *J. Am. Chem. Soc.* **1990**, *112*, 2419-2420.
- (147) Krautler, B.; Arigoni, D.; Golding, B. T. *Vitamin B₁₂ and B₁₂ proteins*; Wiley-VCH: Weinheim, Germany; New York, 1998.
- (148) Martin, B. D.; Finke, R. G. *J. Am. Chem. Soc.* **1992**, *114*, 585-592.
- (149) Rossi, M.; Glusker, J. P.; Randaccio, L.; Summers, M. F.; Toscano, P. J.; Marzilli, L. G. *J. Am. Chem. Soc.* **1985**, *107*, 1729-1738.
- (150) Savage, H. F. J.; Lindley, P. F.; Finney, J. L.; Timmins, P. A. *Acta Cryst. B* **1987**, *43*, 280-295.
- (151) Randaccio, L.; Pahor, N. B.; Zangrando, E.; Marzilli, L. G. *Chem. Soc. Rev.* **1989**, *18*, 225-250.
- (152) Randaccio, L.; Furlan, M.; Geremia, S.; Slouf, M.; Srnova, I.; Toffoli, D. *Inorg. Chem.* **2000**, *39*, 3403-3413.
- (153) Ouyang, L.; Rulis, P.; Ching, W. Y.; Nardin, G.; Randaccio, L. *Inorg. Chem.* **2004**, *43*, 1235-1241.
- (154) Ouyang, L.; Randaccio, L.; Rulisa, P.; Kurmaev, E. Z.; Moewes, A.; Chinga, W. Y. *J. Molec. Struct.: TheoChem* **2003**, *622*, 221-227.
- (155) Kurmaev, E. Z.; Moewes, A.; Ouyang, L.; Randaccio, L.; Rulis, P.; Ching, W. Y.; Bach, M.; Neumann, M. *Europhys. Lett.* **2003**, *62*, 582-587.
- (156) Ehlers, A. W.; Bohme, M.; Dapprich, S.; Gobbi, A.; Hollwarth, A.; Jonas, V.; Kohler, K. F.; Stegmann, R.; Veldkamp, A.; Frenking, G. *Chem. Phys. Lett.* **1993**, *208*, 111-114.

- (157) Hay, P. J.; Wadt, W. R. *J. Chem. Phys.* **1985**, *82*, 270-283.
- (158) Hay, P. J.; Wadt, W. R. *J. Chem. Phys.* **1985**, *82*, 284-298.
- (159) Ditchfield, R.; Hehre, W. J.; Pople, J. A. *J. Chem. Phys.* **1971**, *54*, 724-728.
- (160) Gordon, M. S. *Chem. Phys. Lett.* **1980**, *76*, 163-168.
- (161) Hariharan, P. C.; Pople, J. A. *Mol. Phys.* **1974**, *27*, 209-214.
- (162) Reiher, M.; Salomon, O.; Hess, B. A. *Theo. Chem. Acc.* **2001**, *107*, 48-55.
- (163) Zhao, Y.; Truhlar, D. G. *Acc. Chem. Res.* **2008**, *41*, 157-167.
- (164) Schultz, N.; Zhao, Y.; Truhlar, D. G. *J. Phys. Chem.* **2005**, *109*, 4388-4403.
- (165) Wodrich, M. D.; Corminboeuf, C.; Schleyer, P. v. R. *Org. Lett.* **2006**, *8*, 3631-3634.
- (166) Zhao, Y.; Truhlar, D. G. *Org. Lett.* **2006**, *8*, 5753-5755.
- (167) Valero, R.; Costa, R.; Morelra, I. D. P. R.; Truhlar, D. G.; Illas, F. *J. Chem. Phys.* **2008**, *128*, 114103(1)-(8).
- (168) Zhao, Y.; Lynch, B. J.; Truhlar, D. G. *J. Phys. Chem. A* **2004**, *108*, 2715-2719.
- (169) Zhao, Y.; Truhlar, D. G. *J. Phys. Chem. A* **2004**, *108*, 6908-6918.
- (170) Zhao, Y.; Truhlar, D. G. *J. Chem. Theo. Comput.* **2005**, *1*, 415-432.
- (171) Zhao, Y.; N.G-Garcia; Truhlar, D. G. *J. Phys. Chem. A* **2005**, *109*, 2012-2018.
- (172) Zhao, Y.; Truhlar, D. G. *J. Phys. Chem. A* **2005**, *109*, 5656-5667.
- (173) Voorhis, T. V.; Scuseria, G. E. *J. Chem. Phys.* **1998**, *109*, 400-410.
- (174) Becke, A. D. *J. Chem. Phys.* **1986**, *84*, 4524-4529.
- (175) Stoll, H.; Pavlidou, C. M. E.; Preuß, H. *Theo. Chim. Acta* **1978**, *49*, 143-149.
- (176) Zhao, Y.; Schultz, N. E.; Truhlar, D. G. *J. Chem. Phys.* **2005**, *123*, 161103(1)-(4).

- (177) Zhao, Y.; Schultz, N. E.; Truhlar, D. G. *J. Chem. Theo. Comput.* **2006**, *2*, 364-382.
- (178) Stephens, P. J.; Devlin, F. J.; Chabalowski, C. F.; Frisch, M. J. *J. Phys. Chem.* **1994**, *98*, 11623-11627.
- (179) Schmider, H. L.; Becke, A. D. *J. Chem. Phys.* **1998**, *108*, 9624-9631.
- (180) Jensen, K. P.; Ryde, U. *Coord. Chem. Rev.* **2009**, 769-778.
- (181) Himo, F.; Siegbahn, P. E. M. *Chem. Rev.* **2003**, *103*, 2421-2456.
- (182) Frenking, G.; Frhlich, N. *Chem. Rev.* **2000**, *100*, 717-774.
- (183) Siegbahn, P. E. M.; Blomberg, M. R. A. *Annu. Rev. Phys. Chem.* **1999**, *50*, 221-249.
- (184) Ziegler, T. *Chem. Rev.* **1991**, *91*, 651-667.
- (185) Ziegler, T. *Can. J. Chem.* **1995**, *73*, 743-761.
- (186) Harrison, J. F. *Chem. Rev.* **2000**, *100*, 679-716.
- (187) Neese, F. *J. Biol. Inorg. Chem.* **2006**, *11*, 702-711.
- (188) Kozłowski, P. M.; Kumar, M.; Piecuch, P.; Li, W.; Bauman, N. P.; Hansen, J. A.; Lodowski, P.; Jaworska, M. *J. Chem. Theo. Comput.* **2012**, *8*, 1870-1894.
- (189) Ryde, U.; Mata, R. A.; Grimme, S. *Dalton Trans.* **2011**, *40*, 11176-11183.
- (190) Siegbahn, P. E. M.; Blomberg, M. R. A.; Chen, S.-L. *J. Chem. Theo. Comput.* **2010**, *6*, 2040-2044.
- (191) Grimme, S.; Antony, J.; Ehrlich, S.; Krieg, H. *J. Chem. Phys.*, *132*, 154104.
- (192) Adamo, C.; Barone, V. *J. Chem. Phys.* **1999**, *110*, 6158-6169.
- (193) Rabuck, A. D.; Scuseria, G. E. *Theo. Chem. Acc.* **2000**, *104*, 439-444.
- (194) http://www.gaussian.com/g_tech/g_ur/m_citation.htm, last accessed 21/05/2012
- (195) GaussView; Dennington, R.; Keith, T.; Millam, J.; 5 ed.; Inc., S., Ed.: Shawnee Mission KS, 2009.

-
- (196) AIMALL, (ver 12.06.03); Keith, T. A.; TK Gristmill Software: Overland, Park KS, USA (aim.tkgristmill.com), 2011.
- (197) <http://www.chemcraftprog.com/index.html>, last accessed 21/05/2012.
- (198) <http://www.chpc.ac.za>, last accessed 21/05/2012.
- (199) Christianson, D. W.; Lipscomb, W. N. *J. Am. Chem. Soc.* **1985**, *107*, 2682-2686.
- (200) Randaccio, L. *Comments Inorg. Chem.* **1999**, *21*, 327-376.
- (201) Hansen, L. M.; Derecskei-Kovacs, A.; Marynick, D. S. *J. Molec. Struct.: Theochem* **1998**, *431*, 53-57.
- (202) Day, P. *Theo. Chim. Acta* **1967**, *7*, 328-341.
- (203) Jensen, M. P.; Halpern, J. *J. Am. Chem. Soc.* **1999**, *121*, 2181-2192.
- (204) Marques, H. M.; Warden, C.; Monye, M.; Shongwe, M. S.; Brown, K. L. *Inorg. Chem.* **1998**, *37*, 2578-2581.
- (205) Cini, R.; Moore, S. J.; Marzilli, L. G. *Inorg. Chem.* **1998**, *37*, 6890-6897.
- (206) Reed, A. E.; Weinstock, R. B.; Weinhold, F. *J. Chem. Phys.* **1985**, *83*, 735-746.
- (207) Cioslowski, J. *J. Am. Chem. Soc.* **1989**, *111*, 8333-8336.
- (208) De Proft, F.; Martin, J. M. L.; Geerlings, P. *Chem. Phys. Lett.* **1996**, *250*, 393-401.
- (209) Reed, A. E.; Curtiss, L. A.; Weinhold, F. *Chem. Rev.* **1988**, *88*, 899-926.
- (210) Bader, R. F. W. *Chem. Rev.* **1991**, *91*, 893-928.
- (211) Collins, J. B.; Streitwieser, A. *J. Comp. Chem.* **1980**, *1*, 81-87.
- (212) Allen, F. H. *Acta Cryst.* **2002**, *B58*, 380-388.
- (213) Hunter, E. P. L.; Lias, S. G. *J. Phys. Chem. Ref. Data* **1998**, *27*, 413-656.
- (214) Bartmess, J. E.; Scott, J. A.; McIver, R. T. *J. Am. Chem. Soc.* **1979**, *101*, 6046-6056.

- (215) http://en.wikipedia.org/wiki/Proton_affinity, last accessed 29/06/2012.
- (216) Frisch, M. J. T., G. W.; Schlegel, H. B.; Scuseria, G. E.; Robb, M. A.; Cheeseman, J. R.; J. A. Montgomery, J.; Vreven, T.; Kudin, K. N.; Burant, J. C.; Millam, J. M.; Iyengar, S. S.; Tomasi, J.; Barone, V.; Mennucci, B.; Cossi, M.; Scalmani, G.; Rega, N.; Petersson, G. A.; Nakatsuji, H.; Hada, M.; Ehara, M.; Toyota, K.; Fukuda, R.; Hasegawa, J.; Ishida, M.; Nakajima, T.; Honda, Y.; Kitao, O.; Nakai, H.; Klene, M.; Li, X.; Knox, J. E.; Hratchian, H. P.; Cross, J. B.; Adamo, C.; Jaramillo, J.; Gomperts, R.; Stratmann, R. E.; Yazyev, O.; Austin, A. J.; Cammi, R.; Pomelli, C.; Ochterski, J. W.; Ayala, P. Y.; Morokuma, K.; Voth, G. A.; Salvador, P.; Dannenberg, J. J.; Zakrzewski, V. G.; Dapprich, S.; Daniels, A. D.; Strain, M. C.; Farkas, O.; Malick, D. K.; Rabuck, A. D.; Raghavachari, K.; Foresman, J. B.; Ortiz, J. V.; Cui, Q.; Baboul, A. G.; Clifford, S.; Cioslowski, J.; Stefanov, B. B.; Liu, G.; Liashenko, A.; Piskorz, P.; Komaromi, I.; Martin, R. L.; Fox, D. J.; Keith, T.; Al-Laham, M. A.; Peng, C. Y.; Nanayakkara, A.; Challacombe, M.; Gill, P. M. W.; Johnson, B.; Chen, W.; Wong, M. W.; Gonzalez, C.; Pople, J. A. *Gaussian 09, Gaussian, Inc.: Wallingford CT 2009*.
- (217) Tolman, C. A. *Chem. Rev.* **1977**, 77, 313-348.
- (218) Bader, R. F. W. *Atoms in molecules: A quantum theory*; Cambridge University Press: Oxford, UK, 1990.
- (219) Mebs, S.; Henn, J.; Dittrich, B.; Paulmann, C.; Luger, P. *J. Phys. Chem. A* **2009**, 113, 8366-8378.
- (220) Macci, P.; Sironi, A. *Coord. Chem. Rev.* **2003**, 238-239, 383-412.
- (221) Espinosa, E.; Alkorta, I.; Elguero, J.; Molins, J. *J. Chem. Phys.* **2002**, 117, 5529-5542.
- (222) White, D.; Coville, N. *Adv. Organometal. Chem.* **1994**, 38, 95-159.
- (223) Wirt, M. D.; Sagi, I.; Chance, M. R. *Biophys.* **1992**, 63, 412-417.
- (224) Finke, R. G.; Hay, B. P. *Inorg. Chem.* **1984**, 23, 3041-3043.
- (225) Coe, B. J.; Glenwright, S. J. *Coord. Chem. Rev.* **2000**, 203, 5-80.
- (226) Kwiecien, R. A.; Rostkowski, M.; Dybala-Defratyka, A.; Paneth, P. *J. Inorg. Biochem.* **2004**, 98, 1078-1086.
- (227) Krautler, B.; Konrat, R.; Stupperich, E.; Farber, G.; Gruber, K.; Kratky, C. *Inorg. Chem.* **1994**, 33, 4128-4139.

- (228) Brink-Shoemaker, C.; Cruickshank, D. W. J.; Hodgkin, D. C.; Kamper, M. J.; Pilling, D. *Proc. Roy. Soc.* **1964**, A278, 1-26.
- (229) Grinberg, A. A. *Izv. Inst. Izucheniya Platiny* **1932**, 10, 47-58.
- (230) Nekrasov, B. V. *J. Gen. Chem. USSR* **1937**, 7, 1594-1598.
- (231) Syrkin, Y. K. *Izv. Akad. Nauk SSSR Otd. Khim. Nauk* **1948**, 69-73.
- (232) Chatt, J.; Duncanson, L. A.; Venanzi, L. M. *J. Chem. Soc.* **1955**, 4456-4460.
- (233) Orgel, L. E. *J. Inorg. Nucl. Chem.* **1956**, 2, 137-140.
- (234) Basolo, F.; Chatt, J.; Gray, H. B.; Pearson, R. G.; Shaw, B. L. *J. Chem. Soc.* **1961**, 2207-2215.
- (235) McWeeny, R.; Mason, R.; Towl, A. D. C. *Discuss. Far. Soc.* **1969**, 47, 20-26.
- (236) Mason, R.; Towl, A. D. C. *J. Chem. Soc. A: Inorg., Phys., Theo.* **1970**, 1601-1613.
- (237) Burdett, J. K.; Albright, T. A. *Inorg. Chem.* **1979**, 18, 2112-2120.
- (238) Bright, D.; Ibers, J. A. *Inorg. Chem.* **1969**, 8, 709-716.
- (239) Shustorovich, E. M.; Porai-Koshits, M. A.; Buslaev, Y. A. *Coord. Chem. Rev.* **1975**, 17, 1-98.
- (240) Stryer, L. *Biochemistry*; 4 ed.; Freeman: New York, 1995.
- (241) Murakami, Y.; Aoyama, Y.; Tokunaga, K. *J. Am. Chem. Soc.* **1980**, 102, 6736-6744.
- (242) Stolzenberg, A. M.; Stershic, M. T. *J. Am. Chem. Soc.* **1988**, 110, 6391-6402.
- (243) Ke, S. C.; Torrent, M.; Musaeu, D. G.; Morokuma, K.; Warncke, K. *Biochem.* **1999**, 38, 12681-12689.
- (244) Yamanishi, M.; Yamada, S.; Muguruma, H.; Murakami, Y.; Tobimatsu, T.; Ishida, A.; Yamauchi, J.; Toraya, T. *Biochem.* **1998**, 37, 4799-4803.
- (245) Shibata, N.; Masuda, J.; Tobimatsu, T.; Toraya, T.; Suto, K.; Morimoto, Y.; Yasuoka, N. *Struct.* **1999**, 7, 997-1008.

- (246) Lawrence, C. C.; Gerfen, G. J.; Samano, V.; Nitsche, R.; Robins, M.; Retey, J.; Stubbe, J. *J. Biol. Chem.* **1999**, *274*, 7039-7042.
- (247) Drennan, C. L.; Huang, S.; Drummond, J. T.; Matthews, R. G.; Ludwig, M. L. *Science* **1994**, *266*, 1669-1674.
- (248) Reitzer, R.; Gruber, K.; Jogl, G.; Wagner, U. G.; Bothe, H.; Buckel, W.; Kratky, C. *Struct.* **1999**, *7*, 891-902.
- (249) Liu, S.; Widom, J.; Kemp, C. W.; Crews, C. M.; Clardy, J. *Science* **1998**, *282*, 1324-1327.
- (250) Bewley, M. C.; Tam, B. M.; Grewal, J.; He, S.; Shewry, S.; Murphy, M. E.; Mason, A. B.; Woodworth, R. C.; Baker, E. N.; MacGillivray, R. T. *Biochem.* **1999**, *38*, 2535-2541.
- (251) Addlagatta, A.; Matthews, B. W. *Protein Sci.* **2006**, *15*, 1842-1848.
- (252) Moore, S. A.; Anderson, B. F.; Groom, C. R.; Haridas, M.; Baker, E. N. *J. Mol. Biol.* **1997**, *274*, 222-236.
- (253) Miyanaga, A.; Fushinobu, S.; Ito, K.; Wakagi, T. *Biochem. Biophys. Res. Commun.* **2001**, *288*, 1169-1174.
- (254) Rowland, P.; Blaney, F. E.; Smyth, M. G.; Jones, J. J.; Leydon, V. R.; Oxbrow, A. K.; Lewis, C. J.; Tennant, M. G.; Modi, S.; Eggleston, D. S.; Chenery, R. J.; Bridges, A. M. *J. Biol. Chem.* **2006**, *281*, 7614-7622.
- (255) Ng, F. T. T.; Rempel, G. L.; Halpern, J. *J. Am. Chem. Soc.* **1982**, *104*, 621-623.
- (256) Pearson, R. G. *Proc. natl. Acad. Sci. U.S.A.* **1986**, *83*, 8440-8441.
- (257) Parr, R. G.; Pearson, R. G. *J. Am. Chem. Soc.* **1983**, *105*, 7512-7516.
- (258) Sivasankar, C.; Sadhukhan, N.; Bera, J. K.; Samuelson, A. G. *New J. Chem.* **2007**, *31*, 385-393.
- (259) Basolo, F.; Pearson, R. G. *Prog. Inorg. Chem* **1962**, *4*, 381-453.
- (260) Pidcock, A.; Richards, R. E.; Venanzi, L. M. *J. Chem. Soc. A: Inorg., Phys., Theo.* **1966**, 1707-1710.
- (261) [http://en.mobile.wikipedia.org/wiki/Proton_affinity_\(data_page\)](http://en.mobile.wikipedia.org/wiki/Proton_affinity_(data_page)), last accessed 21/05/2012.

- (262) Zhan, C. G.; Nichols, J. A.; Dixon, D. A. *J. Phys. Chem. A* **2003**, *107*, 4184-4195.
- (263) Summers, M. F.; Marzilli, L. G.; Bresciani-Pahor, N.; Randaccio, L. *J. Am. Chem. Soc.* **1984**, *106*, 4478-4485.
- (264) Summers, M. F.; Toscana, P. J.; Bresciani-Pahor, N.; Nardin, G.; Randaccio, L.; Marzilli, L. G. *J. Am. Chem. Soc.* **1983**, *105*, 6259-6263.
- (265) Shriver, D. F.; Atkins, P. W.; Overton, T. L.; Rourke, J. P.; Weller, M. T.; Armstrong, F. A. *Inorganic Chemistry*; Oxford University Press: Oxford, 2006.
- (266) Mancia, F.; Keep, N. H.; Nakagawa, A.; Leadlay, P. F.; McSweeney, S.; Rasmussen, B.; Bösecke, P.; Diat, O.; Evans, P. R. *Struct.* **1996**, *4*, 339-350.
- (267) Pauling, L. *The Nature of the Chemical Bond*; 3 ed.; Cornell University Press: Ithaca, 1960.
- (268) Lenhert, P. G.; Hodgkin, C. D. *C. Nature* **1961**, *192*, 937-938.
- (269) Schrauzer, G. *Acc. Chem. Res.* **1968**, *1*, 97-103.
- (270) Pratt, J. M. *Inorganic Chemistry of Vitamin B₁₂*; Academic Press: New York, 1972.
- (271) Pratt, J. M.; Craig, P. J. *Adv. Organometal. Chem.* **1973**, *11*, 331-446.
- (272) Brown, D. G. *Prog. Inorg. Chem* **1973**, *18*, 177-286.
- (273) Roche, T. S.; Endicott, J. F. *Inorg. Chem.* **1974**, *13*, 1575-1580.
- (274) Roche, T. S.; Endicott, J. F. *J. Am. Chem. Soc.* **1972**, *94*, 8622-8623.
- (275) Roche, T. S.; Endicott, J. F. *Inorg. Chem.* **1974**, *13*, 1575-1580.
- (276) Mok, C. H.; Endicott, J. F. *J. Am. Chem. Soc.* **1978**, *100*, 123-129.
- (277) Bakac, A.; Espenson, J. H. *Inorg. Chem.* **1987**, *26*, 4353-4355.
- (278) Lee, S.; Espenson, J. H. *Inorg. Chem.* **1990**, *29*, 3442-3447.
- (279) Kofod, P. *Inorg. Chem.* **1995**, *34*, 2768-2770.
- (280) Lynch, B. J.; Truhlar, D. G. *J. Phys. Chem. A* **2001**, *105*, 2936-2941.

- (281) O'Brien, S. E.; Popelier, P. L. A. *Can. J. Chem.* **1999**, *77*, 28-36.
- (282) González, L.; Mó, O.; Yáñez, M.; Elguero, J. *J. Mol. Struct.* **1996**, *371*, 1-10.
- (283) Espinosa, E.; Souhassou, M.; Lachekar, H.; Lecomte, C. *Acta Cryst. B* **1999**, *55*, 563-572.
- (284) Howard, S. T.; Krygowski, T. M. *Can. J. Chem.* **1997**, *75*, 1174-1181.
- (285) Cramer, C. J.; Truhlar, D. G. *Chem. Rev.* **1999**, *99*, 2161-2200.
- (286) http://www.gaussian.com/g_tech/g_ur/k_scrf.htm, last accessed 21/05/2012.
- (287) Sension, R. J.; Harris, D. A.; Cole, A. G. *J. Phys. Chem. B* **2005**, *109*, 21954-21962.
- (288) Sharp, K. A. *Annu. Rev. Biophys. Biophys. Chem* **1990**, *19*, 301-332.
- (289) Honig, B. *Science* **1995**, *268*, 1144-1149.
- (290) Marenich, A. V.; Cramer, C. J.; Truhlar, D. G. *J. Phys. Chem. B* **2009**, *113*, 6378-6396.
- (291) Dolney, D. M.; Hawkins, G. D.; Winget, P.; Liotard, D. A.; Cramer, C. J.; Truhlar, D. G. *J. Comp. Chem.* **2000**, *21*, 340-366.
- (292) Tomasi, J.; Persico, M. *Chem. Rev.* **1994**, *94*, 2027-2094.
- (293) <http://en.wikipedia.org/wiki/Solvation>, last accessed 21/05/2012.
- (294) http://en.wikipedia.org/wiki/Gibbs_free_energy, last accessed 21/05/2012.
- (295) Lenhert, P. G. *Proc. R. Soc. London, Ser. A* **1968**, *303*, 45-84.
- (296) Seibles, L.; Deutsch, E. *Inorg. Chem.* **1977**, *16*, 2273-2278.
- (297) Hansch, C.; Leo, A.; Taft, R. W. *Chem. Rev.* **1991**, *91*, 165-195.
- (298) Hammett, L. P. *J. Am. Chem. Soc.* **1937**, *59*, 96-103.
- (299) www.joe-harrity.staff.shef.ac.uk/meetings/CurtinHammettreview.pdf, last accessed 12/07/2011.
- (300) www.ch.ic.ac.uk/local/organic/tutorial/db3.pdf, last accessed 11/07/2011.

- (301) Foster, J. P.; Weinhold, F. *J. Am. Chem. Soc.* **1980**, *102*, 7211-7218.
- (302) Abramov, Y. *Acta Cryst.* **1997**, *A53*, 264-272.
- (303) Hay, B. P.; Finke, R. G. *Polyhedron* **1988**, *7*, 1469-1481.
- (304) Folkers, K. *Vitamin B₁₂*: Berlin, 1979.
- (305) Ellis, B.; Petrow, V.; Snook, G. F. *J. Pharm. Pharm. Sci.* **1949**, *1*, 60-61.
- (306) Giannotti, C. *B₁₂*; Wiley Interscience: New York, 1982.
- (307) Pratt, J. M. In *Chemistry and Biochemistry of B₁₂*; Banerjee, R., Ed.; John Wiley and Sons: New York, 1999.
- (308) Toohey, J. I. *Proc. Natl. Acad. Sci. U.S.A.* **1965**, *54*, 934-942.
- (309) Hill, J. A.; Pratt, J. M.; Williams, R. J. P. *J. Chem. Soc.* **1964**, 5149-5153.
- (310) Johnson, A. W.; Mervyn, L.; Shaw, N.; Smith, E. L. *J. Chem. Soc.* **1963**, 4146-4156.
- (311) Muller, O.; Muller, G. *Biochem. Zeit.* **1962**, *336*, 299-313.
- (312) Hill, J. A.; Pratt, J. M.; Williams, R. J. P. *J. Theo. Biol.* **1962**, *3*, 423-425.
- (313) Dolphin, D.; Johnson, A. W. *J. Chem. Soc.* **1965**, 387, 2174-2181.
- (314) Pratt, J. M.; Thorpe, R. G. *Advances in Inorganic Chemistry and Radiochemistry*; Academic Press, New York, 1969; Vol. 12.
- (315) Perry, C. B.; Marques, H. M. S. *Afr. J. Chem.* **2005**, *58*, 9-15.
- (316) http://ww2.chemistry.gatech.edu/~wilkinson/Class_notes/CHEM_3111_6170/Electronic_spectra_of_TM_complexes.pdf, last accessed 08/09/2012.
- (317) Sharpe, A. G. *Inorganic Chemistry*; Longman Group Limited: New York, 1981.
- (318) Huheey, J. E. *Inorganic Chemistry: Principles of Structure and Reactivity*; 2nd ed.; Harper and Row, Publishers, Inc.: New York, 1978.
- (319) Chang, R. *Chemistry*; 5th ed.; McGraw-Hill, Inc.: United States of America, 1994.

- (320) Gillard, R. D. *Analyst* **1963**, 88, 825-828.
- (321) Fugate, R. D.; Chin, C. A.; Song, P. S. *Biochim. Biophys. Acta* **1976**, 421, 1-11.
- (322) Chemaly, S. M.; Brown, K. L.; Fernandes, M. A.; Munro, O. Q.; Grimmer, C.; Marques, H. M. *Inorg. Chem.* **2011**, 50, 8700-8718.
- (323) Kornobis, K.; Kumar, N.; Lodowski, P.; Jaworska, M.; Piecuch, P.; Lutz, J. J.; Wong, B.; Kozłowski, P. M. In *J. Comp. Chem.*, 2013, DOI: 10.1002/jcc.23204.
- (324) Nakano, H. *J. of Chem. Phys.* **1993**, 99, 7983-7992.
- (325) Andersson, K.; Malmqvist, P. A.; Roos, B. O.; Sadlej, A. J.; Wolinski, K. *J. Phys. Chem.* **1990**, 94, 5483-5488.
- (326) Stanton, J. F.; Bartlett, R. J. *J. Chem. Phys.* **1993**, 98, 7029-7039.
- (327) Geertsen, J.; Rittby, M.; Bartlett, R. J. *Chem. Phys. Lett.* **1989**, 164, 57-62.
- (328) Tomasi, J.; Mennucci, B.; Cammi, R. *Chem. Rev.* **2005**, 105, 2999-3094.
- (329) Martin, R. L. *J. Chem. Phys.*, 118, 4775-4777.
- (330) Assfeld, A. M.; Very, T. In *1.0.1*, 2011.
- (331) Kozłowski, P. M.; Zgierski, M. Z. *J. Phys. Chem. B* **2004**, 108, 14163-14170.
- (332) http://en.wikipedia.org/wiki/Electromagnetic_spectrum, last accessed 27/08/2012.
- (333) Kozłowski, P. M.; Kuta, J.; Galezowski, W. *J. Phys. Chem. B* **2007**, 111, 7638-7645.